1-1-2007

Postcollapse volcanism in the Valles Caldera, New Mexico: The transition from large volume explosive to small volume effusive eruptions

Kati Gibler
University of Nevada, Las Vegas

POSTCOLLAPSE VOLCANISM IN THE VALLES CALDERA, NEW MEXICO: THE TRANSITION FROM LARGE VOLUME EXPLOSIVE TO SMALL VOLUME EFFUSIVE ERUPTIONS

By

Kati Gibler

Bachelor of Science
University of Alaska
2004

A thesis in partial fulfillment
of the requirements for the

Master of Science Degree in Geoscience
Department of Geoscience
College of Sciences

Graduate College
University of Nevada, Las Vegas
August 2007

UNLV
UNIVERSITY OF NEVADA LAS VEGAS

UNIVERSITY OF NEVADA LAS VEGAS

Thesis Approval

The Graduate College
University of Nevada, Las Vegas

May 30, 2007

The Thesis prepared by

Kati I. Gibler

Entitled

Postcollapse Volcanism in the Valles Caldera, New Mexico: The Transition from Large Volume Explosive to Small Volume Effusive Eruptions

is approved in partial fulfillment of the requirements for the degree of

Master of Science

Andrews Dittan
Examination Committee Chair

Dean of the Graduate College

Examination Committee Member

Examination Committee Member

Graduate College Faculty Representative

ABSTRACT

Postcollapse volcanism in the Valles Caldera, New Mexico: The Transition from Large Volume Explosive to Small Volume Effusive Eruptions

By

Kati I. Gibler

Dr. Andrew Hanson, Examination Committee Chair
Associate Professor of Geology
University of Nevada, Las Vegas

Deer Canyon, Redondo Creek, and Del Medio rhyolites were erupted in the Valles Caldera within 54 ka following caldera collapse. Postcollapse rhyolites and Bandelier Tuff magmas are compositionally distinct, and Deer Canyon is heterogeneous between individual flows. $^{238}U/^{206}Pb$ zircon dating shows that Redondo Creek zircons were derived from the residual Bandelier Tuff crystal mush system whereas Deer Canyon zircons were derived from remelting of a pluton at depth. Electron microprobe analyses of feldspars reveal complex zonation caused by interactions between mafic magmas and silicic melts of residual crystal mush as well as between distinct melts from the crystal mush. Each postcollapse rhyolite was produced by independent melting events in the residual Bandelier Tuff crystal mush, interactions between these melts and heat-providing mafic magmas, and magma arriving from deeper in the crust. They are not comagmatic with each other, nor with the preceeding Bandelier Tuff magmas.

TABLE OF CONTENTS

LIST OF TABLES

LIST OF FIGURES

AKNOWLEDGEMENTS

This project was funded by the Graduate and Professional Student Association, Nevada Isotope and Geochronology Laboratory, Electron Microprobe Laboratory, and the Lilly and Wing Fong Geoscience Scholarship, University of Nevada, Las Vegas.

Many people were influential and invaluable in providing encouragement and assistance during this project. First, I would like to thank Dr. Terry Spell for his superb guidance, his dedication to perfection, his professionalism, and for his encouragement throughout this project. Second, I would like to thank Dr Terry Nauman for encouraging me to pursue higher education and for his mentoring and friendship. A special thank you to Dr. Andrew Hanson for his patience, assistance with petrographic work, and for editing this thesis; to Dr. Eugene Smith, for teaching me about igneous petrology and volcanology; to Dr. Rodney Metcalf for many positive conversations and for swapping teenage daughter stories; and to Dr Robert Fairhurst for assisting with electron microprobe analysis.

Most importantly, I would like to thank David Gibler, my young son, who remained unyieldingly supportive and positive while enduring the traumas of armed combat and serving our country as a member of the armed forces; Tracy Gibler, my teenaged daughter, for her positive attitude, and helpfulness at home; my mother for showing me that no matter how difficult a task is it should be attempted with a light heart; and my good friend, Susie Pinjuv, for her laughter and all of her kind words. Finally I would like to thank Chad and Tanika who went on long runs with me.

CHAPTER 1

INTRODUCTION

Although numerous investigations into the development and evolution of large silicic magma systems have been conducted, understanding of their temporal evolution and transition to, and from, large-scale caldera forming eruptions remains incomplete. A related debate over the origin, storage, and crustal residence times of voluminous high silicic rhyolite magma is also yet to be resolved. (Smith, 1979; Hildreth, 1981; Huppert and Sparks, 1988; Davies et al., 1989; Halliday, 1990; Mahood, 1990; Sparks et al., 1990; Reid et al., 1997; Davies and Halliday, 1998; Reid and Coath, 2000; Bindeman and Valley, 2001; Bachman et al., 2002, Bindeman et al., 2006).

The Geologic Problem

Previous work has produced two end member models for silicic magma generation that can be tested with the Valles caldera rhyolites. The first model suggests that high-silica rhyolites are derived from batholith sized magma chambers of substantial longevity, i.e. timescales approaching 1 Ma or more. These chambers exist in the mid to upper crust as thermally stable systems (Smith, 1979; Hildreth, 1981; Davies et al., 1989; Halliday, 1990; Reid et al., 1997; Davies and Halliday, 1998). Mafic magmas thermally sustain the silicic system over extended time periods. Tapping of this long-lived chamber

results in periodic eruptions of silicic magma including both large scale explosive and related small scale effusive eruptions.

In contrast, a second model suggests that independent batches of silicic magmas are rapidly generated and erupted on shorter time scales of < 100 ka (Huppert and Sparks, 1988; Sparks et al., 1990; Mahood, 1990; Reid and Coath, 2000; Bindeman and Valley, 2001; Bachman et al., 2002, Bindeman et al., 2006). In this model, basalt is injected into country rock and causes melting, producing silicic magmas. This melt may act as a density block trapping new basaltic intrusions. Continued melting occurs as a result, forming larger magma bodies. These silicic magmas rise into the shallow crust and erupt as rhyolites over a short time period.

A more recent hybrid model suggests that rhyolite magmas are produced from crystal mushes in time scales ranging from 10^4 to 10^5 years, erupting periodically as crystal rich ignimbrites when mafic magmas thermally rejuvenate them. This model considers fractional crystallization, crystal settling, compaction, crystal-liquid separation, and gas driven filter pressing, and suggests that the crystal mush system may be much more long lived, e.g. 10^6 years (Schmitt et al., 2002; Bachman and Bergantz, 2004).

If the long lived models apply to large silicic magma systems, then pre and post caldera eruptions would have to tap the same magma chamber. Debate related to these models has been the focus of numerous studies at Long Valley caldera, Yellowstone volcanic field, and at the Valles caldera complex (Smith, 1979; Hildreth, 1981; Huppert and Sparks, 1988; Halliday, 1990; Mahood, 1990; Sparks et al., 1990; Reid et al., 1997; Davies and Halliday, 1998; Reid and Coath, 2000; Bindeman and Valley, 2001; Bachman et al., 2002; Phillips, 2004; Bindeman et al., 2006).

Evidence for pre-caldera build up of large silicic magma systems is usually destroyed by caldera collapse. Thus, one approach to understand the evolution of silicic magma systems is to study the transition from caldera forming eruptions to the eruption of smaller post collapse domes and flows, which are often preserved.

Valles Caldera

The Valles caldera complex (Fig. 1.01) located in the Jemez volcanic field (JVF), is one of three large Quaternary silicic magma systems in North America, including the Long Valley and Yellowstone systems. Hundreds of cubic kilometers of high-silica rhyolite have been generated and erupted in the JVF over the past 2 Ma. In a major eruption at 1.26 Ma the Valles caldera volcano produced ~250 km^3 of ash forming the Bandelier Tuff. Immediately following collapse of the Valles caldera at 1.26 Ma (Phillips, 2004), the Deer Canyon, Redondo Creek and Del Medio rhyolites were erupted as numerous low volume domes and flows. The Valles caldera complex provides an ideal opportunity for studying the evolution of silicic magma systems because the caldera forming ignimbrite, the upper Bandelier Tuff, and postcollapse rhyolitic domes and flows are well exposed and preserved. These offer an excellent opportunity to study caldera forming magmatic systems and the transition from large volume explosive to small volume effusive eruptions, and to address questions of longevity of silicic magma systems.

This study is designed to test the hypothesis that postcollapse rhyolites in the Valles caldera were produced by independent, small volume magma batches and that they are unrelated to the preceeding upper Bandelier Tuff (Spell et al., 1993). This is in contrast to

early work by Smith (1979), which implied that the Upper Bandelier Tuff and post collapse rhyolites were the products of a large volume, long-lived magma chamber.

If the Redondo Creek, Deer Canyon, and Del Medio rhyolites are related to the upper Bandelier Tuff, then the first model, which favors long lived magma systems, would be supported. Alternatively, if these rhyolites are unrelated to the upper Bandelier Tuff, the second model which favors short lived magma generation, emplacement, and eruption would be supported. Finally, the petrographic, geochemical, and U/Pb zircon analyses obtained in this study will test the hypothesis that silicic magmas are derived from long lived crystal dominated mushes that are rapidly differentiated and erupted (Schmitt et al., 2002; Simon and Reid, 2005).

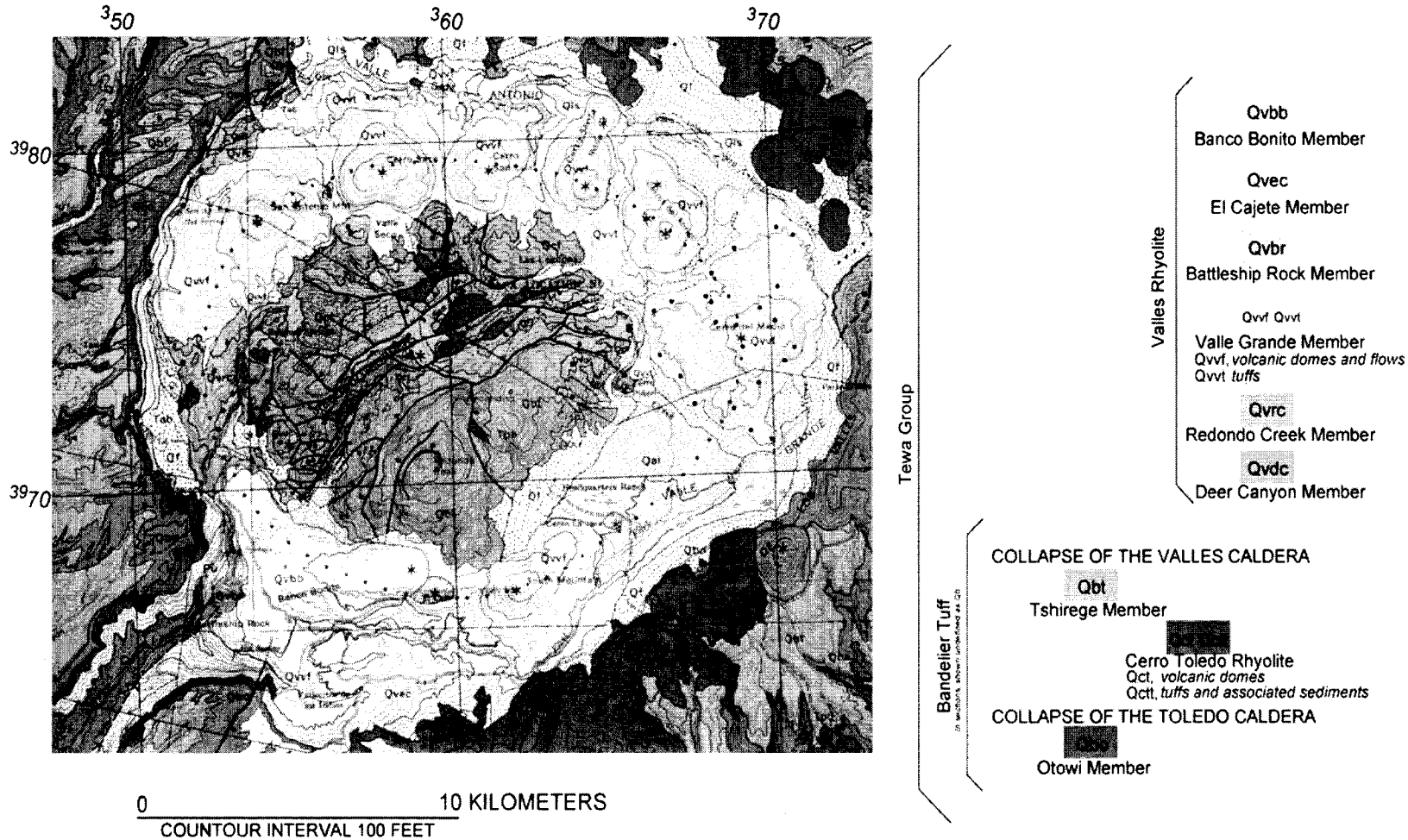

Figure 1.01. Valles Caldera geologic map modified from Smith et al. (1970).

Research Objectives

The following are the main objectives of this study.

(1) Test the hypothesis that postcollapse rhyolites in the Valles caldera were produced by independent, small volume magma batches and that they are unrelated to the preceeding Upper Bandelier Tuff.

Detailed petrography and geochemical composition obtained from EMPA, XRF, and ICPMS analyses of Deer Canyon, Redondo Creek, and Del Medio rhyolites are compared in order to constrain whether they represent multiple chemically distinct magma batches or whether they were erupted from a single evolving magma system. These data are compared to published analyses of upper Bandelier Tuff from Balsley (1988), and of Deer Canyon, Redondo Creek and Del Medio from Spell (1993) and from Phillips (2004) in order to understand the relationships among the postcollapse rhyolites and between the postcollaspe rhyolites and the upper Bandelier Tuff.

If the post collapse rhyolites are unrelated to the upper Bandelier Tuff then the models which favor short lived magma emplacement will be supported. On the other hand, the long lived magma system model is favored if the rhyolites are related to the upper Bandelier Tuff.

(2) *Document the origin, evolution, and magma storage time scales of the Del Medio, Redondo Creek, and Deer Canyon rhyolites.*

Recently determined $^{40}Ar/^{39}Ar$ dates (Phillips, 2004), establish reliable eruption age relationships on postcollapse rhyolites and the upper Bandelier Tuff and provide a chronological basis for geochemical and petrogenetic interpretations.

Detailed petrographic analyses are used to define petrogenetic relationships and to define a magmatic environment for crystallization of phenocrysts. Electron microprobe analysis (EMPA) is used to determine the major and trace element geochemical composition of selected phenocrysts which establish petrogenetic relationships and phenocryst affinities. X-ray fluorescence (XRF) and inductively coupled plasma mass spectroscopy (ICPMS) data is used to determine whole rock major and trace element chemistry in order to understand the petrogenetic evolution of these rhyolites. $^{206}Pb/^{238}U$ geochronology of zircons separated from Deer Canyon and Redondo Creek rhyolites are used to constrain magma residence times, recycling, and affinities of phenocrysts.

(3) Understand processes controlling the transition to and from large caldera forming eruptions.

Data obtained during this study is used to compare the Valles caldera postcollapse rhyolites to the Upper Bandelier Tuff. Petrogenetic relationships between these units define the processes that control the transition from large caldera forming eruptions to smaller postcollapse eruptions which in turn are used to constrain the processes that result in large caldera forming eruptions.

(4) Place constraints on the evolution of large caldera-forming magma systems in general.

The assessment of petrogenetic and geochronologic relationships among the Deer Canyon, Redondo Creek and Del Medio rhyolites is used to place constraints on the evolution of large caldera forming eruptions. The results from this study will define the temporal and geochemical transitions between large caldera forming eruptions and smaller post collapse eruptions in the Valles caldera. This will support either the long

lived or short lived silicic magma system model, and may have implications on the production, emplacement and storage of magma in other caldera forming systems.

CHAPTER 2

GEOLOGIC SETTING

The Jemez Volcanic Field (JVF) is situated at the intersection of the Jemez lineament, a NE-SW striking crustal feature marked by aligned volcanoes, and the Rio Grande rift, a N-S striking zone of Cenozoic extension composed of en-echelon sedimentary basins (Figure 2.01). The JVF is built upon upper Paleozoic sedimentary strata that overlies Proterozoic basement (Smith et al., 1970; Gardner et al., 1986) on the western margin of the Española Basin (Figure 2.01). Volcanoes along the Jemez lineament separate the Colorado Plateau from the Basin and Range Province and from the Rio Grande rift to the southeast. Strike slip faulting and extension related to both structures has played an important role in volcanism in the area (Aldrich, 1986). Recent seismic studies show a low velocity mantle to the north of the Jemez lineament and high velocity mantle to the south. This south dipping mantle boundary is interpreted as the Southern Yavapai-Mazatzal suture (Shaw and Karlstrom, 1999). The low velocity zone which is layered and extends from the Moho (40 to 50 km) to the base of the lithosphere (120 km) may be the source of magma for the JVF (Wolff et al., 2004).

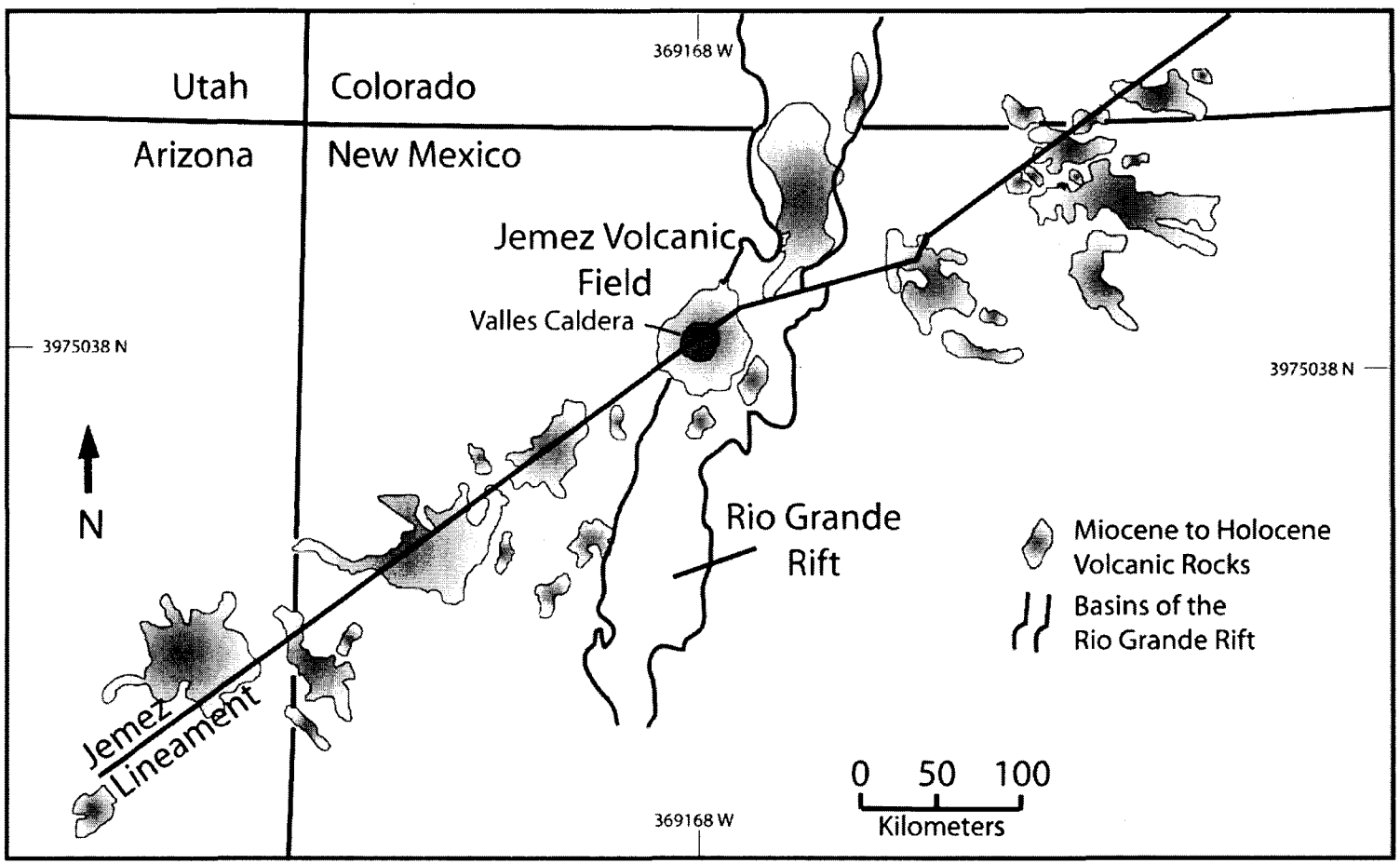

Figure 2.01. Regional tectonic map showing the relationship between the Jemez lineament, the Rio Grande rift, and the Jemez Volcanic Field. (after Baldridge et al., 1983; Gardner and Goff, 1984; Justet, 1999).

Basalts, andesites, dacites and rhyolites were all erupted within the JVF and represent varying degrees of interaction between mantle derived magmas and crustal melts (Aldrich, 1986). Magmatism, beginning as early as 15.5 Ma. (Justet and Spell, in preparation), was coeval with extension in the Rio Grande rift. Small volume volcanic activity began when alkali basalt erupted during deposition of rift fill sediments of the Santa Fe Group (Gardner and Goff, 1984). About half the volume of the JVF is composed of Paliza Canyon andesite which erupted between ~13 and 6 Ma. This interval was also characterized by minor eruptions of tholeiitic basalt, dacite, Canovas Canyon Rhyolite and Bearhead Rhyolite (Gardner et al., 1986; Justet and Spell 2001; Justet, 2004). These units are collectively referred to as the Keres Group and are exposed in the southern part of the volcanic field (Table 2.01) (Gardner et al., 1986; Justet, 1999).

Polvadera Group rocks are exposed in the northern part of the JVF and include the Lobato basalt (~11 to 8 Ma), Tshicoma Formation andesite, dacite and rhyodacite (~6.9 to 2.2 Ma), and the Puye Formation (Gardner et al., 1986). The volcanic activity that formed these rocks coincided with the last eruptions of the Keres Group rocks in the south.

The youngest volcanic suite in the JVF, the Tewa Group, began with the large-volume (250 to 400 km^3 dense rock equivalent, DRE) eruptions of the Bandelier Tuff (Smith and Bailey, 1966; Spell et al., 1996). Volcanism in the JVF culminated in formation of two nested calderas, the Toledo and Valles calderas. The first eruption occurred at 1.61 Ma with the Otowi member (lower) Bandelier Tuff (Spell et al., 1996). Resulting collapse produced the Toledo caldera which was followed by eruptions of the Cerro Toledo intracaldera rhyolites. The second, Tshirege member (upper) Bandelier

Tuff erupted at 1.26 Ma (Phillips, 2004), forming the Valles caldera in approximately the same location and destroying most of the Toledo caldera. This event was followed by resurgence and renewed rhyolite dome formation (Smith et al., 1966). Following the convention of Smith et al. (1966), the Otowi and Tshirege members are referred to as the lower Bandelier Tuff and upper Bandelier Tuff respectively in the remainder of this thesis. Inside the Valles caldera the Deer Canyon, Redondo Creek and nine ring fracture domes referred to as the Valle Grande member were erupted.

The Valles Caldera

The Valles caldera complex is the type locality for large ignimbrite eruptions and caldera collapse followed by resurgence, as originally described by Smith and Bailey (1968). A number of stages occur in the development of a typical caldera (Lipman, 2000). (1) Pre-caldera volcanism is accompanied by tumescence and small dome eruptions, which is often the only record of magma accumulation at shallow crustal levels. (2) The geologic record of this volcanism is frequently destroyed by large scale ignimbrite eruptions and the associated caldera collapse. This stage of caldera development may begin with a central vent phase evolving to a ring vent phase (Cole et al., 2004). (3) Resurgence and continued post-collapse magmatism may be localized along structural trends, such as ring fractures, and renewed magma emplacement may produce uplift in the center of the caldera forming a resurgent dome. (4) Hydrothermal activity and mineralization occurs throughout the life of the caldera, but is often the dominant volcanic activity late in the caldera forming cycle. This is a general model applicable to the Valles caldera.

The Valles caldera is a semicircular depression ranging from 90 to 650 meters in depth and is 23 km east to west and 19 km north to south in diameter. Redondo Peak, a resurgent dome, rises 3,430 meters above sea level and has over 950 meters of local relief. Between the caldera rim and this central dome and along ring fracture vents there are 15 rhyolite domes, flows and associated pyroclastic rocks that erupted after caldera collapse.

Post Collapse Volcanism

The Del Medio, Redondo Creek, and Deer Canyon rhyolites comprise numerous domes and flows formed immediately after collapse of the Valles caldera and are the focus of this study (Smith et al., 1970). The Del Medio dome complex is situated near the eastern caldera wall. The Redondo Creek and Deer Canyon rhyolites are centrally located in the caldera upon and around the resurgent dome (Figure. 2.02).

The eruption of the upper Bandelier tuff, at 1.26 Ma, and formation of the Valles caldera mark the lower time constraint on resurgence. The upper time constraint, 1.23 ± 0.02 Ma, $^{40}Ar/^{39}Ar$ ages, (Phillips, 2004), is marked by the eruption and emplacement of Del Medio, which is the oldest ring fracture dome emplaced following resurgence. The Deer Canyon rhyolites averaging 1.26 ± 0.12 Ma and the Redondo Creek rhyolites averaging 1.22 ± 0.02 Ma, were erupted between the upper Bandelier Tuff and the Del Medio rhyolite (Phillips, 2004). The Deer canyon member erupted prior to resurgence and is overlain by caldera fill sediments. The Redondo Creek member erupted during resurgence and is faulted and tilted due to continued uplift following its emplacement (Bailey et al., 1969; Smith et al., 1970; Gardner et al., 1986).

In all, nine Valle Grande member rhyolitic domes ranging in age from ~1.23 Ma to 0.52 Ma were formed along the ring fracture, which acted as a magma conduit, following the collapse of the Valles caldera. The Valle Grande member rhyolites get progressively younger in a counter clockwise direction. From oldest to youngest they are Cerro del Medio, Cerros del Abrigo, Cerro Santa Rosa, San Luis, Cero Seco, San Antonio Mountain, and South Mountain (Figure 2.02). The most recent volcanic eruptions produced the Banco Bonito, Battleship Rock, VC1, and El Cajete member rhyolites at about 50 to 60 ka (Reneau et al., 1996). Age relations of JVF rocks are summarized in Table 2.01.

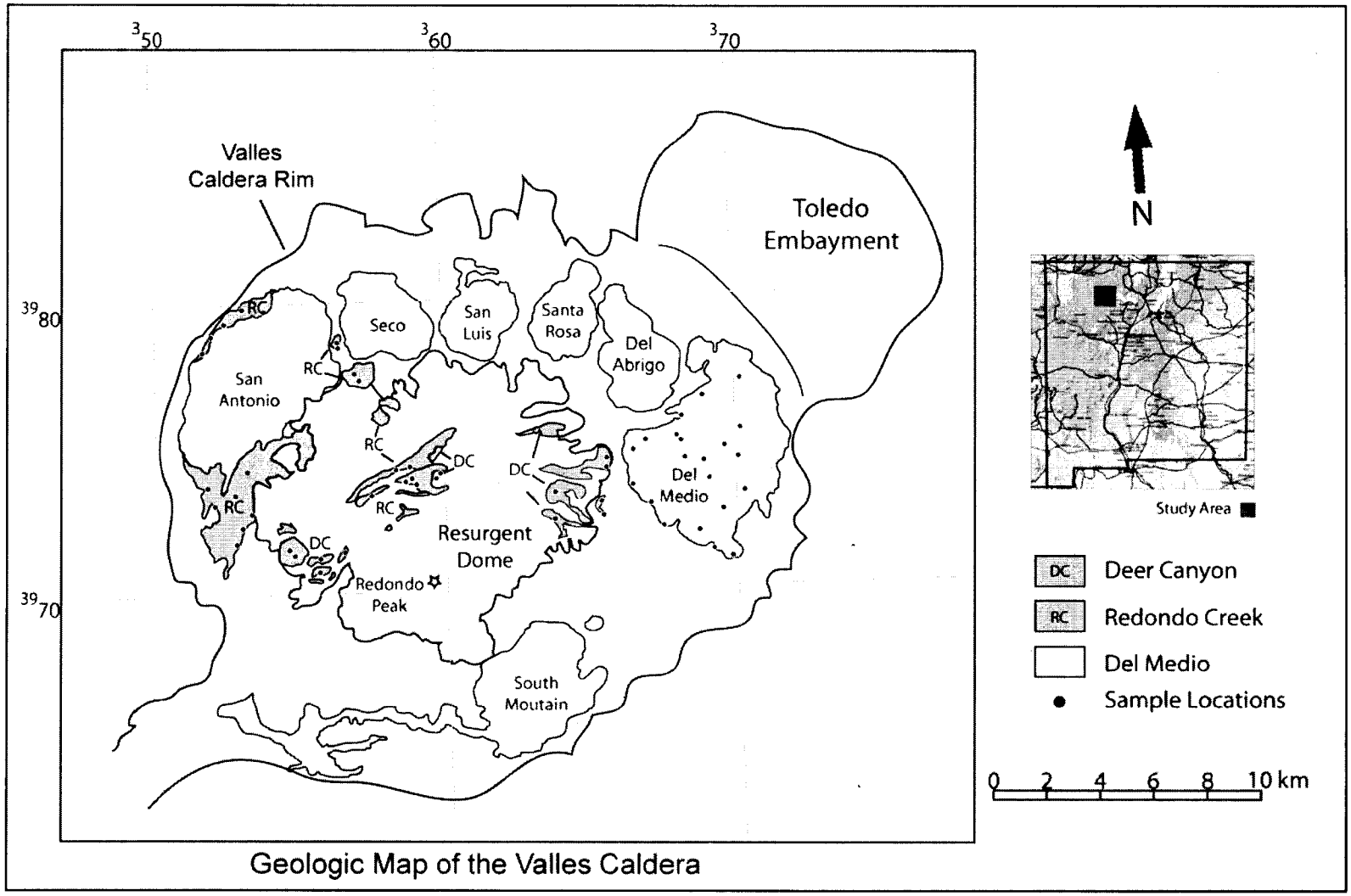

Figure 2.02: Generalized geologic map of the Valles Caldera. Modified from Smith et al. 1970. UTM coordinates are shown at the top and left side of the map.

Table 2.01: Stratigraphy and age relations of Jemez volcanic rocks

Group		Member	Unit	Age
Tewa Group 1.85 Ma-60 ka		Banco Bonito		50-60 ka
		VC1 Rhyolite		50-60 ka
		Battleship Rock		50-60 ka
		El Cajete		50-60 ka
	Valles Rhyolites	Valle Grande	La Jara	523 ka
			South Mountain	521 ka
			San Antonio	557 ka
			Santa Rosa II	787 ka
			San Luis	800 ka
			Seco	800 ka
			Santa Rosa I	915 ka
			Del Abrigo	973 ka
			Del Medio	1.23 Ma
	Bandelier Tuff	Redondo Creek		1.22 Ma
		Deer Canyon		1.26 Ma
		Tshirege/Upper BT		1.26 Ma
		Cerro Toledo Rhyolite		1.59 Ma
		Otowi/Lower BT		1.61 Ma
Polvadera Group 11.0-2.2 Ma		Cerros del Rio	Puye Fm	1.85 Ma
		El Alto		2.8 Ma
		Santa Anna		2.8 Ma
			Tschicoma Fm	6.9 Ma
			Lobato Basalt	11.0 Ma
Keres Group 15.5–6.0 Ma		Bearhead Rhyolite		7.0Ma
		Canovas Canyon		12.5 Ma
		Paliza Canyon		13.0 Ma

Modified from Spell et al., (1993), with data from Spell and Harrison, (1993), Spell et al., (1996), Reneau et al., (1996), Justet and Spell, (2001), and Phillips, (2004). The ages of Deer Canyon, Redondo Creek and Del Medio rhyolites are based on average $^{40}Ar/^{39}Ar$ ages from Phillips, 2004. Note BT = Bandelier Tuff.

CHAPTER 3

PREVIOUS WORK

R.A. Bailey, C.S. Ross, and R.L. Smith were the first to work in the Valles caldera complex (Smith et al., 1961; Smith and Bailey, 1968, Bailey et al, 1969; Smith et al 1970). As a result of their efforts the Valles Caldera is known today as a "type" resurgent caldera. Chronological data on the Valles rhyolites were first provided by Doell et al. (1968) using the K-Ar isotopic dating method. Relative ages were assigned to various hydrothermally altered units based on stratigraphy, and volcanic rocks of the Jemez Mountains were formally put into three groups; the Keres Group, the Polvadera Group, and the Tewa group (Doell et al., 1968; Bailey et al., 1969) (Fig. 3.01 and Table 2.01).

Doell et al. (1968) were the first to point out that the Valles Grande member rhyolites were petrographically heterogenous. This was later confirmed and elaborated on by Bailey et al. (1969) who suggested that progressive changes in phenocryst type with time was an indication that the Valle Grande Member consisted of a petrologically related group of domes. Gardner et al. (1986) noted that the Valles rhyolite could be divided into two groups based on chemistry, with the Deer Canyon, Redondo Creek and Valle Grande Member rhyolites belonging to an older, higher silica group and the El Cajete, Battleship

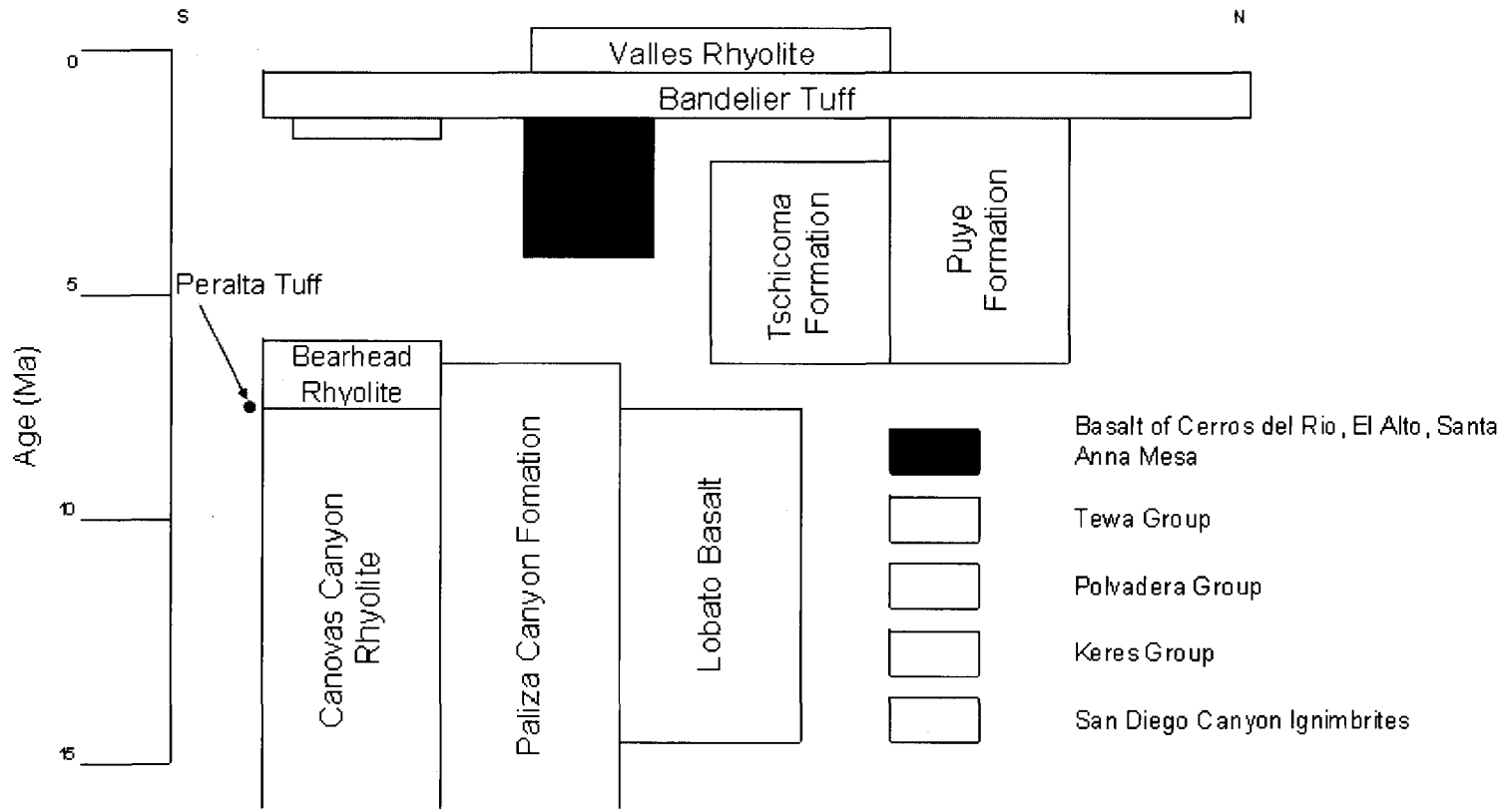

Figure 3.01: Temporal and spatial distribution of units found in the Jemez Volcanic Field (Modified from Gardner and Goff 1984; Gardner 1985; Spell, 1987; Justet, 1999).

Rock, silica and higher Fe, Mg, Ca, Ti and P. Interpretations of major and trace element geochemistry suggested that the Valle Grande member rhyolites consisted of at least 3 separate magma batches generated and erupted on short time scales <100,000 years (Spell, 1997; Spell et al., 1993)

Upper Bandelier Tuff

Previous work on the Upper Bandelier Tuff is relevant to this study because the geochemical, and temporal evolution of the tuff is necessary for comparison with the subsequent Redondo Creek, Deer Canyon and Del Medio rhyolites in order to understand the transition between the large silicic magma system from which the Bandelier Tuff was erupted and post collapse domes and flows. The term Bandelier Tuff was first used by H.T.U Smith (1938). Griggs (1964) formally designated the names Guaje pumice beds for the Plinian deposit underlying the lower Bandelier Tuff and the names Otowi and Tshirege for the lower and upper member respectively. Bailey et al. (1969) formally named the Plinian deposit at the base of the Tshirege as the Tsankawi Pumice bed. Many ideas regarding physical volcanology of ash flow tuffs as well as the concept of compositionally zoned magma chambers are based on studies of the Bandelier Tuff. Smith and Bailey (1966) showed that zonations in trace elements of the Upper Bandelier Tuff reflected variations in a compositionally stratified magma chamber. Smith (1979) later proposed a long-lived continuously fractionating silicic magma chamber for the formation of the Valles caldera. Balsley (1988) used major and trace element chemistry to determine the relationship between upper and lower Bandelier Tuffs. On the basis of incompatible trace element variations Balsley concluded that the Upper Bandelier Tuff

formed by either mixing or from contamination of a high Yb/Th dacite with a low Yb/Th magma and that it was not the product of residual lower Bandelier magma. Instead he suggested that the Upper Bandelier Tuff represents individually generated magma batches from a region of high heat flux in the crust. Further investigation of the Bandelier tuff showed that $^{87}Sr/^{86}Sr$ and $^{87}Rb/^{86}Sr$ on single sanidines were positively correlated. This suggested that magmas producing the Bandelier tuff could have resulted from in situ aging in a closed system or from a single long lived magma chamber (Wolff et al., 1999). However, later studies reported large Pb isotope variations in single sanidine crystals, which were attributed to open system processes, supporting the model for rapid magma production and eruption (Wolff et al., 2005).

Deer Canyon, Redondo Creek and Del Medio Rhyolites

The Deer Canyon, Redondo Creek and Del Medio rhyolites were first described by Bailey et al. (1969) and later mapped (Fig 2.02) to provide stratigraphic relationships (Smith et al., 1970). Relative age relations indicated that Deer Canyon is older than Redondo Creek rhyolite and that the Del Medio rhyolite dome is complex consisting of three independent flows. However, most of the previous work and data gathered on the Deer Canyon, Redondo Creek and Del Medio rhyolites has provided insufficient evidence to fully support current models for magma genesis of Valles caldera size and longevity. Anomalously high K-Ar ages attributed to alteration were calculated by Doell et al. (1968) for the Deer Canyon and Redondo Creek rhyolites. Detailed stratigraphy of the Redondo Creek dome was presented based on samples drilled from wells (Nielson and Hulen, 1984).

A study by Spell et al. (1993), focused on the Valle Grande member, suggested that post collapse domes and flows are heterogeneous petrographically, geochemically and isotopically and thus are the products of small independent magma batches, rapidly produced and erupted on time scales of <100 ka and that the rhyolite domes and flows evolved from a series of temporally and spatially separated magma chambers. The petrogenetic model proposed was one in which discrete episodes of parental melts were most likely produced by basalt-induced fusion events in the deep crust resulting in magma emplacement in the upper crust and differentiation to high silica rhyolites.

High $^{87}Sr/^{86}Sr$ and low $^{143}Nd/^{144}Nd$ suggests that Del Medio rhyolites were produced by crustal contamination of residual upper Bandelier magma (Spell et al., 1993). However, evidence for a crustal contamination model is inconclusive. A mixing model for the Upper Bandelier Tuff and an upper crustal end member yield Del Medio isotopic compositions with additions of 20-25% crustal Nd and 5-10% crustal Sr. For this to occur the $^{87}Sr/^{86}Sr$ of the upper crust must be <0.720 or large quantities of upper crustal wall rock must be incorporated into the magma. Twenty to twenty-five percent assimilation of crust is difficult to imagine based on thermal budget arguments. The Del Medio rhyolites were found to have lower $^{87}Sr/^{86}Sr$ than either model allows, which suggest that they were produced by a source distinct from the Upper Bandelier Tuff (Spell et al., 1993). There have been no isotope studies on the Deer Canyon or Redondo Creek rhyolites.

$^{40}Ar/^{39}Ar$ ages of 1.26 Ma, 1.22 Ma, 1.23 Ma and 1.26 Ma respectively were gathered on Deer Canyon, Redondo Creek and Del Medio rhyolites and on the Tshirege member of the Upper Bandelier Tuff in order to determine a rate of resurgence (~3.7 cm/yr) after the formation of the Valle Caldera (Phillips, 2004). Petrographic descriptions by Spell

(1987) and Phillips (2004) indicate that the Deer Canyon rhyolite consists of a wide variety of rock types all containing similar phenocryst assemblages, Redondo Creek rhyolite is porphyritic and glomeroporphyritic with perlitic texture and contains abundant sanidine and plagioclase, and Del Medio rhyolite is crystal poor and pumicious. Phillips (2004) also concluded that the Deer Canyon and Redondo Creek rhyolites were related to the Upper Bandelier Tuff and that they may have been parts of a residual zoned magma chamber based on a limited number of major and trace element analysis.

CHAPTER 4

SAMPLE STRATEGY AND ANALYTICAL METHODS

Sample Collection

Fieldwork for this project was completed during July and August 2005. Locations for sample collection were based on mapping by Smith et al., (1970) and on GPS coordinates from Phillips (2004). Several samples were collected from each of the Redondo Creek, Deer Canyon and Del Medio 1, 2 and 3 units. The UTM coordinates are listed in Appendix A. Samples chosen for isotope and geochemical analyses showed no flow banding, little to no alteration and as little devitrification as possible. Limited outcrops in some areas resulted in the collection of samples from boulder sized float. Each sample was trimmed of weathering rinds and areas of alteration in the field.

Sample Preparation

Hand samples were set aside and thin section billets ~22 x 44 x 15 mm were cut using a rock saw. Twenty one thin section billets were sent to Quality Thin Sections for final preparation. These were later used for petrographic analysis and to determine sample suitability for geochemical analyses and $^{238}U/^{206}Pb$ zircon dating. Each hand sample was then broken into small ~10 cm diameter chips using a hammer and steel plate.

Rock powders for XRF/ICPMS were prepared by first inspecting each chip for signs of alteration. Altered pieces were discarded leaving only fresh clean chips. Samples were then crushed using a jaw crusher. All surfaces coming in contact with the rock chips were cleaned with compressed air and a wet paper towel between each sample. Samples were then powdered using a tungsten carbide shatter-box. As before, surfaces coming into contact with powders were cleaned between each sample. Individual powders were sealed and stored in plastic containers.

Samples chosen for $^{238}U/^{206}Pb$ zircon analyses were crushed using a jaw crusher to ~2 cm diameter pieces and placed in an 850 μm sieve which was stacked on 417, 223, and 53 μm sieves. These were placed in a Ro-tap for 10 minutes at a time. Each fraction was stored in separate containers. All lab equipment was cleaned with compressed air and a wire brush between samples. Mineral separates of zircon were extracted from the 53-223 μm sieved fraction using the heavy liquid separation technique. Methylene iodide liquid was filtered by pouring it through filter paper and into a separation flask. Approximately 3 cm^3 of sieved sample was added to the flask and stirred. This was allowed to settle for 30 minutes. With the heavy minerals resting on the bottom of the separation flask, the valve was opened for ~1 second allowing the heavy minerals and some liquid to fall into a funnel lined with filter paper. The filter paper and minerals were washed with acetone and allowed to dry several times to remove remaining methylene iodide. Magnetite phenocrysts were removed by passing a magnet over the minerals. Zircons were then hand picked using a binocular microscope. The complete process was repeated several times, in order to gather 30 to 50 zircons for each sample.

Petrography

Hand samples were examined in order to describe their overall texture, color, and grain size, and to make preliminary identification of the major minerals. Twenty one thin sections were examined using a petrographic microscope to determine sample suitability for EMPA, XRF, ICPMS, and $^{238}U/^{206}Pb$ zircon analysis (Appendix A).

Microstructures, textures, phenocryst assemblage, and abundances were noted in order to identify major, minor, and accessory minerals as well as provide a detailed petrographic description for each sample. Alteration, inclusions, reaction rims, and intergrowths were also observed and noted in sample petrographic descriptions. In addition, point counts of approximately 600 points per thin section were conducted on representative samples to calculate proportions of phenocrysts and groundmass (Tables 5.01, 5.02, and 5.03).

Electron Microprobe Analysis

Prepared thin sections from six samples, DC03, DC08, DM2-02, DM2-10, RC07, and RC12, were polished using 1μm diamond polishing paste and sanding paper on a mechanical grinder and cleaned to remove all traces of oil and any polishing debris. The thin sections were then metallic carbon coated to ensure that the electron charge deposited on the sample during analysis would be uniformly conducted to ground. Twenty to thirty micron thick carbon coating was deposited on each thin section by first placing it face upwards in a bell jar which was evacuated to less than 10^{-5} torr. Current passed through carbon electrodes caused the carbon to vaporize and be deposited on the thin sections.

One hundred twelve Backscatter electron images with 2.4 μm resolution were taken of each thin section using a JXA-8900 SuperProbe (EMPA) at the Electron Microanalysis and Imaging Laboratory (UNLV). Backscatter electron images were spliced together producing 5 μm resolution images and used to pinpoint locations for major element analysis of sanidine, plagioclase, biotite, and pyroxene phenocrysts. Major element analysis was first done at individual points on selected phenocrysts. Patchy and zoned surfaces were analyzed in both light and dark areas. This point data along with petrographic analyses was used to pick phenocrysts suitable for line traverses. Line traverses were used to identify zonation in sanidine and in plagioclase and to look for it in other phenocrysts. A 1μm resolution backscatter image and K, Si, Ca, and Mg element maps were produced across two resorped plagioclase crystals that had brown glass inclusions. Major element analysis of these inclusions was not completed due to time constraints and problems in the electron microprobe lab. However line traverses across the same phenocrysts indicate distinctly different major element chemistry. Analyzed standards are reported with EMPA data (Appendixes B, C, and D).

Loss on Ignition

Loss on ignition (LOI) calculations, included with XRF and ICPMS data (Appendix E) were conducted to measure the amount of water and other volatiles in each sample. Ceramic crucibles were cleaned, labeled and weighed to ± 0.00005g. Approximately 15 ± 0.00005g of sample was added to the crucible. The combined weight of crucible + sample was recorded. Each crucible was then placed in a 110°C oven for 2 hours. The crucible was then removed and allowed to cool to room temperature. After cooling, the sample +

crucible were reweighed in order to measure the weight percent H_2O^- lost. The LOI for 110°C was calculated by dividing the weight loss by the original sample weight and multiplying the result by 100. The sample and crucible were then heated to 1050°C for 2 hours, cooled on a heat resistant surface and reweighed to ± 0.00005g. LOI calculations for 1050°C were performed by the same methods as 110°C calculations. This represents the percent H_2O^+ lost. The total loss on ignition was calculated by adding both values for H_2O^- and H_2O^+.

XRF/ICPMS Analysis

Approximately 15 grams of powdered sample from each unit was sealed in Pyrex vials and sent to the Washington State University Geo Analytical lab (http://www.wsu.edu/~geolab/) to measure major, trace and rare earth elements. Further sample preparation and analytical procedures at Washington State University Analytical lab followed the methods presented by Johnson et al. (1999) for XRF and by Knaack et al. (1994) for ICPMS. Analytical precision and instrumentation accuracy are reported in Appendix E.

$^{238}U/^{206}Pb$ Zircon Analysis

Prepared zircons were transported to the UCLA SIMS laboratory where they were screened and hand picked under a binocular microscope. Sample zircons and AS3 zircon standards (Paces et al., 1993; Schmitz et al., 2003) were positioned in rows on double-sided tape. Epoxy in a mixture of 5 parts resin and 1 part hardener was poured over the zircons into a 1 cm diameter mold and allowed to cure for ~8 hours. The grain mount was

then sectioned and polished with diamond sanding paper, in order to expose the zircon cores and to produce flat surfaces for $^{238}U/^{206}Pb$ measurements. The mount was then rinsed with de-ionized water and cleaned in an ultrasonic HCL bath to reduce common Pb contamination. A thin ~20 nm gold coating was applied to the prepared grain mount. The zircon mount was then placed in a vacuum chamber in the CAMECA IMS 1270 ion microprobe, where it was allowed to de-gas for eight hours. Ion microprobe measurements were begun after running five AS3 zircon standards (Paces et al., 1993; Schmitz et al., 2003), each giving an age of ~ 1 Ga. AS3 zircon standards were measured after every fifth Redondo Creek RC07 or Deer Canyon DC03 zircon. Twenty-four spots were measured on RC07 zircons and twenty-seven spots were measured on DC03 zircons.

Zircon Imaging

Cathodoluminescence (CL) Scanning Electron Microscope (SEM) and Backscatter (BSE) imaging of representative RC07 and DC03 zircons were prepared at the UNLV Electron Microanalysis and Imaging Laboratory (EMIL). Following ion microprobe measurements the gold coating was removed from zircon samples. Carbon coating was applied to the zircons and BSE, SEM and CL images were produced. SEM images were used to define $^{238}U/^{206}Pb$ measurement locations. In order to identify structures, zonation, overgrowths, and disequilibrium textures within zircon, CL images were produced. These images are critical in the interpretation of crystal growth history.

CHAPTER 5

PETROGRAPHY

A total of 57 samples representative of Deer Canyon, Redondo Creek, and Del Medio rhyolites were gathered in the field and later examined macroscopically in order to select a subset of suitable samples for petrographic analysis. Sample descriptions and a complete table of UTM locations are listed in Appendix A.

The lithologies of Redondo Creek, Del Medio and Deer Canyon rhyolites are highly variable with textures ranging from porphyritic and devitrified in Deer Canyon rhyolites, to glassy, perlitic and spherulitic in Redondo Creek rhyolites, and to aphyric in Del Medio rhyolites (Figure 5.01). Phenocryst assemblages for the three units include sanidine, plagioclase, quartz, biotite, clinopyroxene, orthopyroxene, apatite, zircon and oxides.

Petrography of the Deer Canyon Rhyolite

The Deer Canyon rhyolites are variable in character but they are generally porphyritic with a devitrified groundmass. Some samples are flow banded (DC12) or vesicular (DC08 and DC09). These rocks can be broken into two groups, type A and type B, based on texture and phenocryst assemblages.

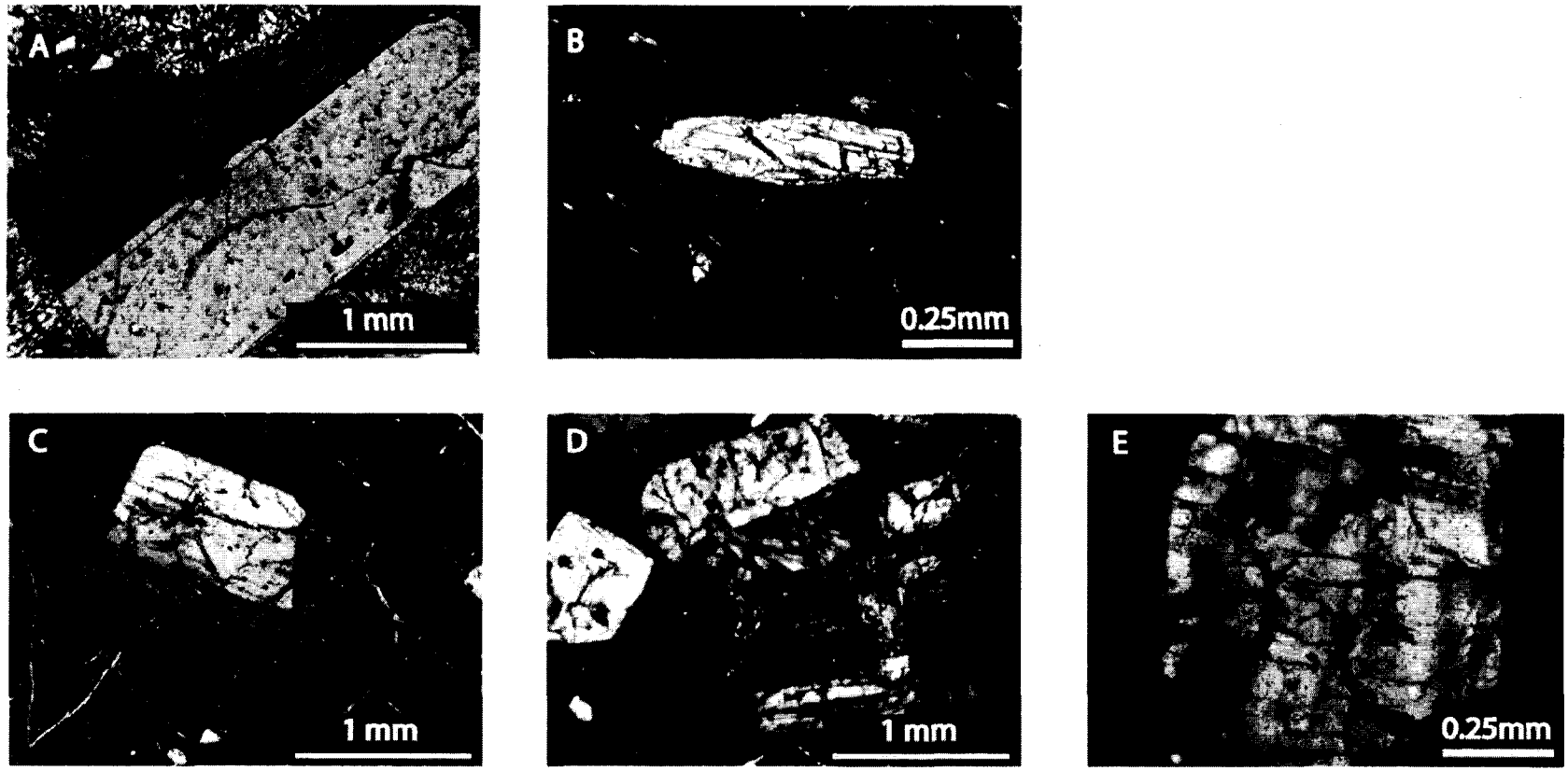

Figure 5.01. Photomicrographs in cross polarized light of various textures and phenocrysts found in Deer Canyon, Redondo Creek and Del Medio rhyolites. Sanidine with Carlsbad twins in a devitrified and spherulitic groundmass from Deer Canyon (A). Clinopyroxene in a glassy groundmass from Del Medio (B). Plagioclase with a sanidine rim, and biotite in a glassy, perlitic groundmass from Redondo Creek (C). Zoned plagioclase with tartan (a feature of plutonic alkali feldspars) and albite twinning, sanidine rimmed plagioclase, right and top, biotite, bottom, and spherulite, center, in a glassy groundmass from Redondo Creek (D). Patchy zoned sanidine with blue dispersion colors in a glassy groundmass from Redondo Creek (E).

Type A (DC01, DC03) is sparsely porphyritic to aphyric with 2 and 6 % phenocrysts respectively. The dominant minerals present are sanidine with a modal abundances of 49-100 % and plagioclase with modal abundances of 0-34 %. The groundmass is glassy with minor devitrification (Table 5.01, Figure 5.02A). Type A contains little to no quartz.

The total percentage of phenocrysts in type B (DC08, DC09, and DC12) Deer Canyon rhyolites ranges from 20-23 %. Type B has modal abundances of 55-76 % quartz, 5-32 % sanidine, and 7-13 % plagioclase (Table 5.01, Figure 5.02B). Pyroxene and oxides are also present in small abundances of less than 2 %. The groundmass in type B samples ranges from glassy to devitrified and has minor vesicles.

Euhedral to subhedral sanidine was found as singular phenocrysts and in glomerocrysts with quartz and oxides. Blue dispersion and Carlsbad twins are seen in many of the more euhedral sanidine phenocrysts (Figure 5.02B). Sanidine often exhibits patchy or concentric zonation, averages 0.5 mm in diameter in type A Deer Canyon rhyolites and ~ 1.4 mm diameter in type B. The range of sizes in sanidine is from 0.3-2.5 mm for both types. Plagioclase is euhedral to subhedral and often resorbed, and ranges in size from 1.7-3.0 mm and averages ~ 2.4 mm diameter in type A Deer Canyon rhyolite (Figure 5.02A and Figure 5.03A). Type B plagioclase ranges in size from 0.5-2.1 mm and averages ~ 1.5 mm in diameter. Quartz is subhedral, fractured, embayed and resorbed, ranges in size from 0.4-1.8 mm and averages ~ 1.1 mm in diameter. It is abundant in type B Deer Canyon rhyolite where it is found in glomerocrysts with sanidine and plagioclase (Figure 5.03B). Oxides are anhedral to subhedral, often exhibiting hexagonal crystal form.

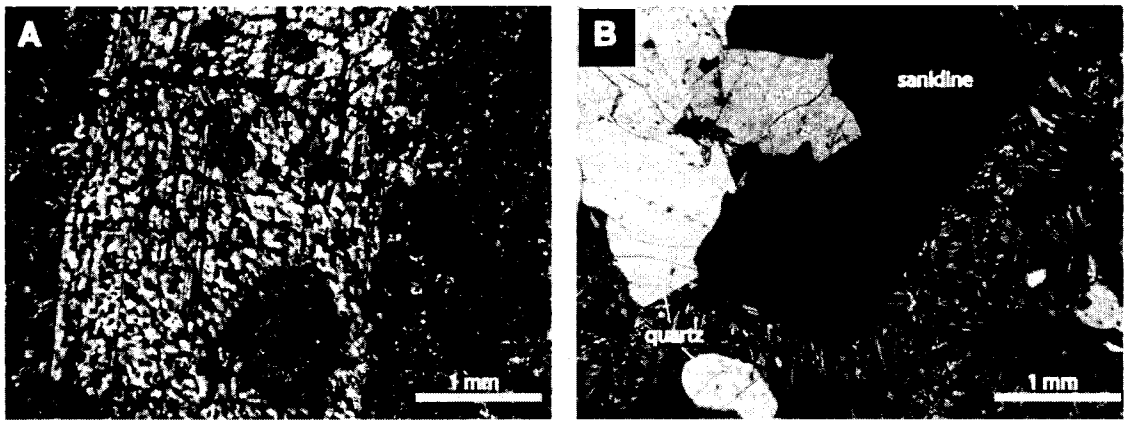

Figure 5.02: Photomicrograph in cross polarized light of resorbed plagioclase phenocryst from sparsely porphyritic type A Deer Canyon rhyolite (A) and of sanidine and quartz in a devitrified groundmass from porphyritic type B Deer Canyon rhyolite (B). The plagioclase in figure A was also analyzed by electron microprobe (see Chapter 6).

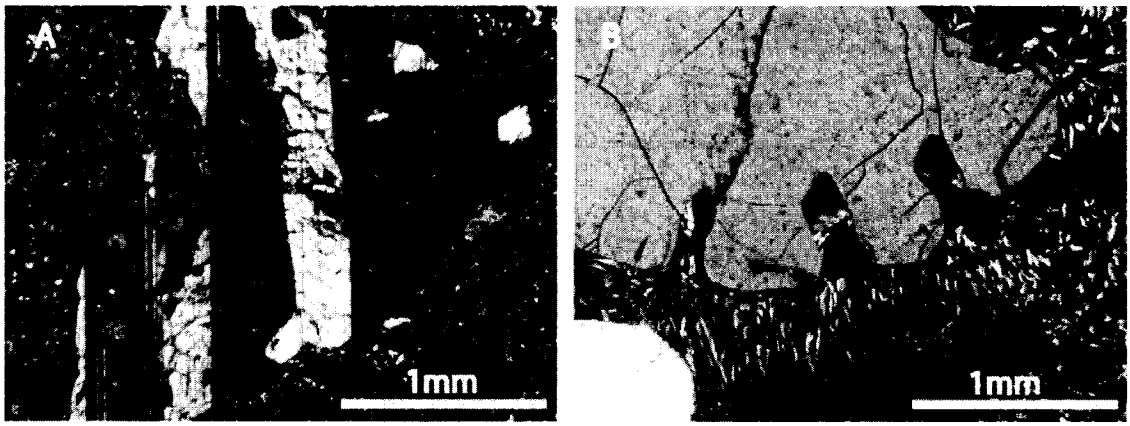

Figure 5.03. Photomicrograph in cross polarized light of a plagioclase in sample DC03, showing albite and Carlsbad twins (A). Photomicrograph of fractured and embayed quartz in a devitrified and vesicular groundmass found in sample DC08 (B).

Zircon microphenocrysts found in DC03 type A Deer Canyon rhyolite are green and reddish in plain light and variable in length to width ratio. Most are subhedral, but some are more euhedral with sharp pyramid and tetragonal faces. Zircons average 102 μm in length and range from 160-50 μm length (Figure 5.04).

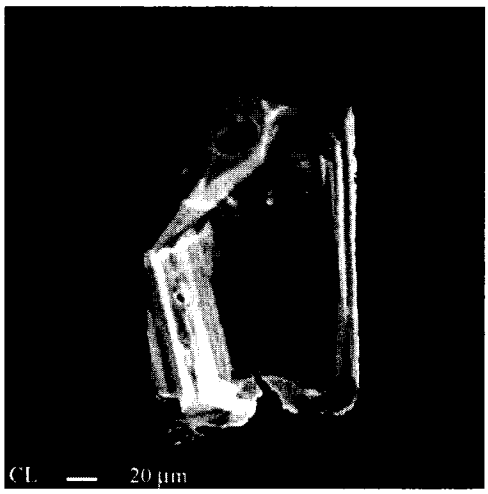

Figure 5.04. Cathodoluminescence image of a zircon from sample DC03, approximately 135 μm long with euhedral crystal form and a pyramidal termination. Oscillatory zoning is be discussed in Chapter 8, $^{238}U/^{206}Pb$ Zircon Analyses.

Petrography of the Redondo Creek Rhyolite

The Redondo Creek rhyolite is porphyritic to glomeroporphyritic and sometimes flow banded. The groundmass is glassy in all samples. Samples RC07, RC09, and RC12 exhibit pervasive perlitic texture (Figure 5.01C) and RC09 and RC07 have spherulitic devitrification (Figure 5.01D). In RC02 alteration to clay is found in the groundmass and in some of the sanidines. Samples RC02, RC03, RC12, and RC18 are pumiceous, with numerous vesicles. The phenocryst assemblage consists of sanidine, plagioclase, biotite, clinopyroxene, orthopyroxene, quartz, oxides, zircon and apatite. The total phenocryst

percentages range from 14-20 % (Table 5.02). Modal abundances of phenocrysts are from 40-72 % sanidine, from 15-46 % plagioclase, from 5-17 % biotite, from 0-4 % clinopyroxene, from 0-4 % quartz, and from 0-2 % orthopyroxene. The groundmass is glassy with minor vesicles and devitrification

Sanidine occurs both as an overgrowth on plagioclase and individually as euhedral to subhedral phenocrysts. It ranges in size from 0.25-1.90 mm and averages ~ 0.79 mm in diameter and often exhibits patchy or concentric zonation, resorption, blue dispersion and Carlsbad twinning (Figure 5.01E). Plagioclase phenocrysts are euhedral to subhedral and range in size from 0.2-2.0 mm and average ~ 0.7 mm in diameter. They are found both alone and as glomerocrysts. The plagioclase is resorbed, embayed and displays antirapikivi texture with sanidine overgrowth rims (Figure 5.01D, Figure 5.05). Some phenocrysts display patchy, concentric or oscillatory zonation. Albite and pericline twinning is common (Figures 5.01D, 5.04, 5.05, and 5.06). Highly resorbed plagioclase found in RC12 is filled with brown glass inclusions (Figure 5.06).

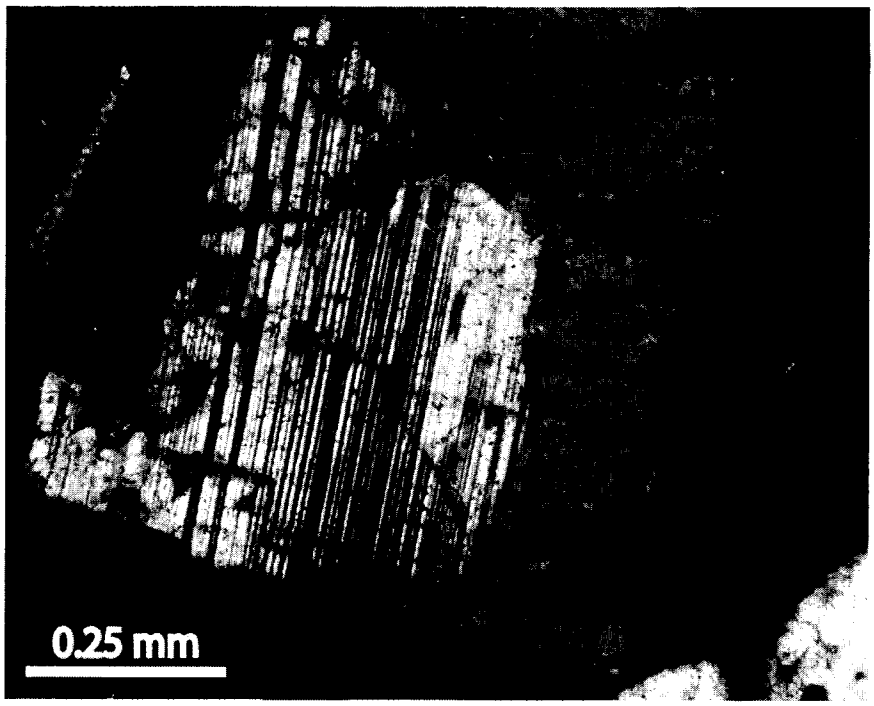

Figure 5.05. Photomicrograph with cross polarized light of a sanidine rimmed plagioclase from sample RC07. The plagioclase shows albite twins. The sanidine rim is subhedral and shows patchy zonation.

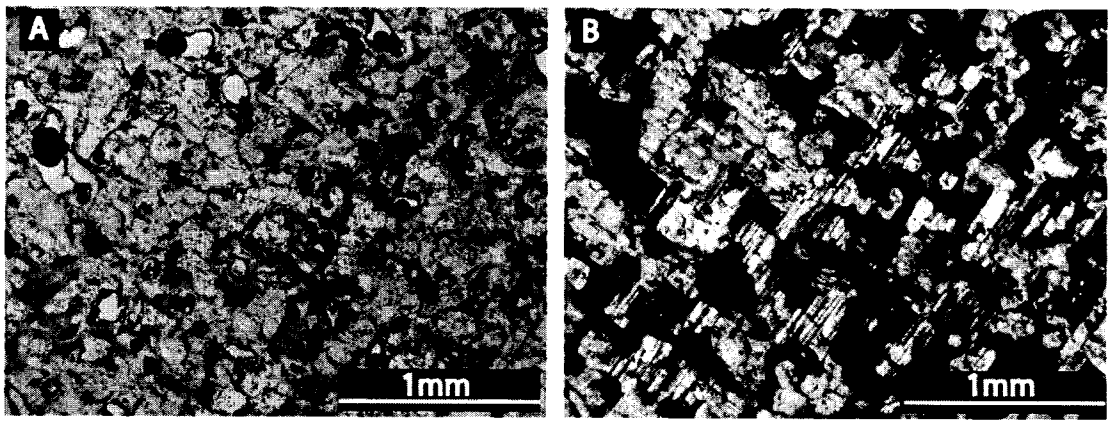

Figure 5.06. Photomicrograph in plain polarized light (A) and in cross polarized light (B) of resorbed plagioclase with brown glass inclusions from sample RC12.

Reddish brown to brown biotite is euhedral and range in size from 0.1-1.5 mm and average ~ 0.4 mm in diameter (Figure 5.07). They are strongly pleochroic and show typical bird's eye extinction under cross polarized light. Biotites are generally fresh and unaltered, although some phenocrysts are fractured. They are often found in glomerocrysts with sanidine and plagioclase and are occasionally found as inclusions in sanidine.

Clinopyroxene found in RC07 and RC12 is subhedral to anhedral and shows cleavage at ~ 90 degrees. It is pale green pleochroic and fractured. It has inclined extinction, exhibits second order interference colors and ranges from 0.4-0.80 mm and averages ~ 0.6 mm in diameter (Figure 5.08). Orthopyroxene is pale green, generally anhedral, fractured and altered. Only one orthopyroxene was measured and it was 0.3 mm in diameter. Oxides average ~0.2 mm and are anhedral to subhedral. They occur both as isolated phenocrysts and as inclusions within clinopyroxene (Figure 5.08), biotite, sanidine and plagioclase. Redondo Creek rhyolite is generally devoid of quartz, but embayed and resorbed quartz was found in sample RC02.

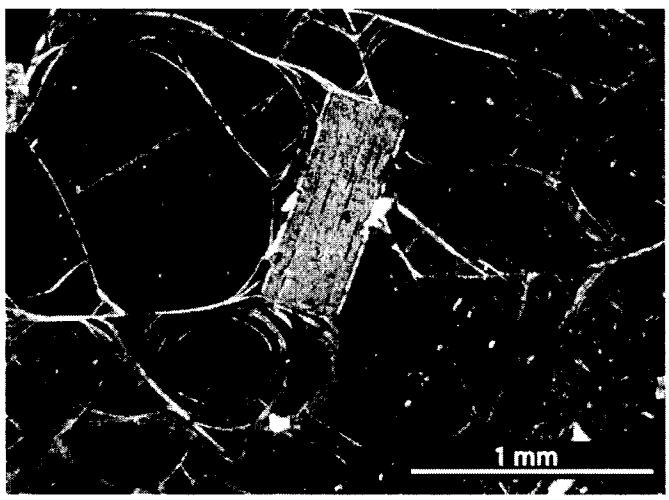

Figure 5.07. Photomicrograph in cross polarized light of a euhedral, reddish brown biotite from RC07 with a slightly mottled appearance. The glassy groundmass exhibits well developed perlitic texture.

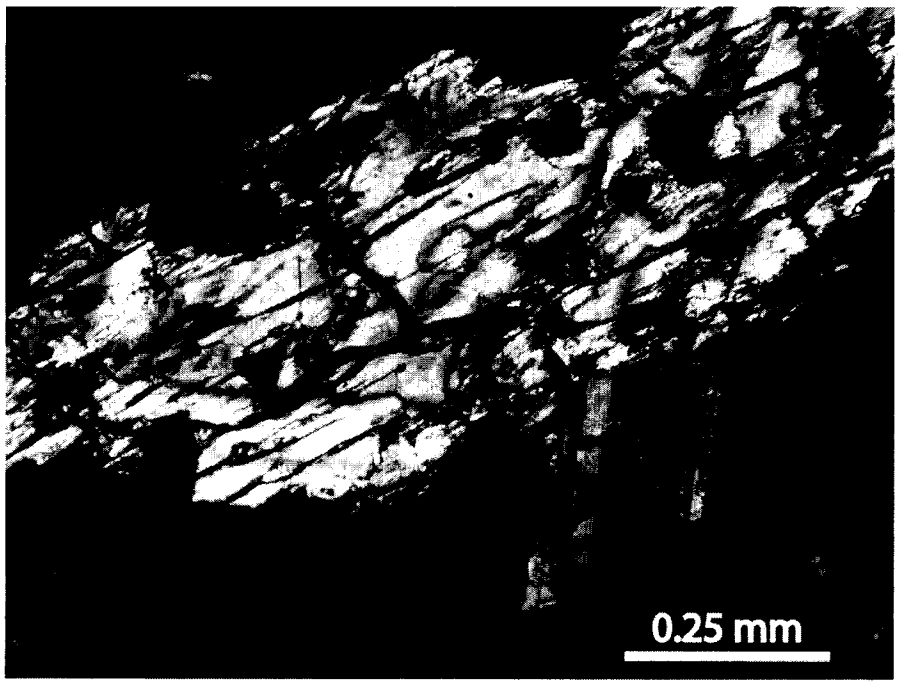

Figure 5.08. Photomicrograph in cross polarized light of clinopyroxene found in Redondo Creek rhyolite sample RC07. Also seen are oxide inclusions within the pyroxene and a slightly zoned sanidine near the bottom of the photograph.

Apatite in the form of transparent, hexagonal, euhedral phenocrysts is rare. It was only seen as microphenocrysts associated with oxides and zircon. Zircons are greenish, translucent, euhedral to subhedral microphenocrysts with pyramidal terminations. They show resorption along their edges and are often fractured. Zircons range in size from 50-130 μm long and average ~74 μm in width (Figure 5.09).

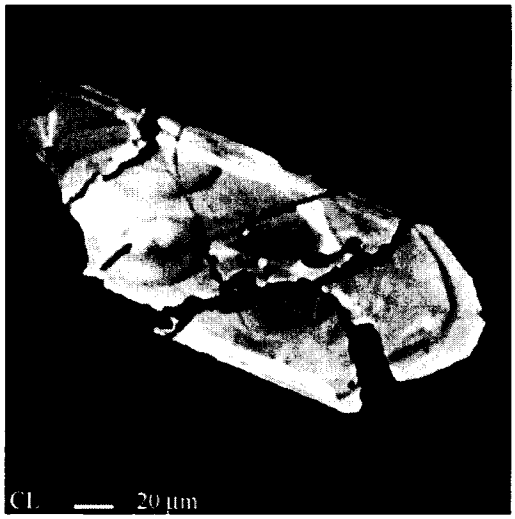

Figure 5.09. Cathodoluminescence image of a fractured zircon (RC07) approximately 120 µm in diameter with acicular, subhedral crystal form.

Petrography of Del Medio Rhyolites

Del Medio rhyolites are composed of three distinct units DM1, DM2, and DM3 based on previous mapping (Smith et al, 1970). The base of Del Medio is composed of DM1 overlain by DM2 making these units the oldest of the three. Both DM1 and DM2 are more aphyric than DM3 which lies stratigraphically above them. DM1 is devitrified and vesicular and contains less than 3% phenocrysts. DM2 and DM3 rhyolites contain up to 6% phenocrysts (Table 5.03). All three units are composed of sparsely porphyritic pumiceous rocks with mostly glassy groundmass. The phenocrysts assemblages consist of sanidine, plagioclase, clinopyroxene, quartz, and oxides. One of the DM1 samples is aphyric, while the other is sparsely porphyritic. The sparsely porphyritic sample DM1-04 has a modal abundance of 86 % clinopyroxene and 13 % plagioclase. DM1 groundmass is glassy, often pumiceous and shows minor devitrification in the form of spherulites. Of the three units DM2 is the most variable in phenocryst type and in modal abundances with phenocryst percentages ranging from 0-6 %. Sanidine has a modal abundance of 56-

76 %. Plagioclase is between 0-18 % and clinopyroxene is between 0-18 %. The groundmass for this unit has a range of textures from glassy to devitrified and contains up to 23 % vesicles. DM3 is composed of 1-5 % phenocrysts with modal abundances of 30-100 % for sanidine and 0-10 % for quartz. The groundmass is glassy with minor vesicles.

Sanidine is commonly resorbed and a few pheoncrysts show incipient alteration to sericite. It is euhedral to subhedral, ranges in size from 0.2-1.8 mm and averages ~ 0.6 mm in diameter. Sanidine displays patchy zonation with blue dispersion colors (Figure 5.10A). Plagioclase exhibits skeletal resorption and is in some cases incipient alteration to sericite. Plagioclase ranges in size from 0.8-2.0 mm and averages ~ 1.4 mm in diameter (Figure 5.10B). Clinopyroxene is subhedral and fractured, ranges in size from 0.3-0.9 mm and averages 0.6 mm. Oxides are anhedral. Quartz is seen only in DM3-03.

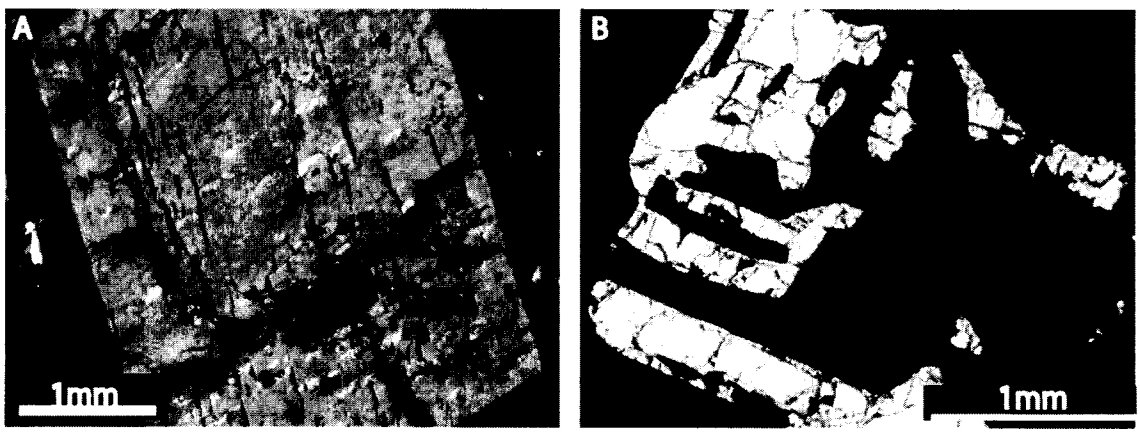

Figure 5.10 Photomicrographs in cross polarized light of patchy zoned sanidine showing sericite alteration and blue dispersion from Del Medio sample DM2-10 (A) and skeletal resorbed plagioclase from Del Medio sample DM2-02 (B). The sanidine in Figure A was also analyzed by electron microprobe (see Chapter 6).

Table 5.01. Point count results of selected Deer Canyon samples.

Sample	DC-01	DC-03	DC-08	DC-09	DC-12
Quartz	0	0	101	76	73
Plagioclase	0	12	9	18	8
Sanidine	11	17	7	41	38
Biotite	0	0	0	0	0
Clinopyroxene	0	0	0	2	0
Orthopyroxene	0	0	0	0	0
Oxides	0	0	0	0	0
Unknown	0	6	16	0	0
Vesicles	0	14	99	24	2
Glassy Groundmass	572	551	22	376	358
Devitrified Groundmass	17	0	346	63	121
Total Points	**600**	**600**	**600**	**600**	**600**
Modal Abundance					
Quartz	0.00	0.00	75.94	55.47	61.34
Plagioclase	0.00	34.29	6.77	13.14	6.72
Sanidine	100.00	48.57	5.26	29.93	31.93
Biotite	0.00	0.00	0.00	0.00	0.00
Clinopyroxene	0.00	0.00	0.00	1.46	0.00
Orthopyroxene	0.00	0.00	0.00	0.00	0.00
Oxides	0.00	0.00	0.00	0.00	0.00
UnKnown	0.00	17.14	12.03	0.00	0.00
% Phenocrysts	**1.83**	**5.83**	**22.17**	**22.83**	**19.83**
% Groundmass					
Glassy	95.33	91.83	3.67	62.67	59.67
Devitrified	2.83	0.00	57.67	10.50	20.17
Vesicles	0.00	2.33	16.50	4.00	0.33
Groundmass Counted	**98.17**	**94.17**	**77.83**	**77.17**	**80.17**

Note: DC01 and DC03 are Type A, DC08, DC09, DC12 are Type B.

Table 5.02. Point count results of selected Redondo Creek samples.

Sample	RC-02	RC-03	RC-07	RC-09
Quartz	5	0	0	0
Plagioclase	20	50	19	21
Sanidine	66	44	60	47
Biotite	17	12	14	15
Clinopyroxene	0	0	4	0
Orthopyroxene	0	0	3	2
Oxides	0	0	0	0
Unknown	10	3	6	4
Vesicles	0	74	18	18
Glassy Groundmass	453	416	476	470
Devitrified Groundmass	21	1	0	23
Total Points	**592**	**600**	**600**	**600**
Modal Abundance				
Quartz	4.24	0.00	0.00	0.00
Plagioclase	16.95	45.87	17.92	23.60
Sanidine	55.93	40.37	56.60	52.81
Biotite	14.41	11.01	13.21	16.85
Clinopyroxene	0.00	0.00	3.77	0.00
Orthopyroxene	0.00	0.00	2.83	2.25
Oxides	0.00	0.00	0.00	0.00
Unknown	8.47	2.75	5.66	4.49
% Phenocrysts	**19.93**	**18.17**	**17.67**	**14.83**
% Groundmass				
Glassy	76.52	69.33	79.33	78.33
Devitrified	3.55	0.17	0.00	3.83
Vesicles	0.00	12.33	3.00	3.00
Groundmass Counted	**80.07**	**81.83**	**82.33**	**85.17**

Table 5.02. Point count results of selected Redondo Creek samples (cont.).

Sample	RC-10	RC-12	RC-18
Quartz	0	0	0
Plagioclase	20	23	12
Sanidine	37	58	58
Biotite	12	5	7
Clinopyroxene	3	0	0
Orthopyroxene	0	0	0
Oxides	0	0	0
Unknown	12	9	4
Vesicles	12	37	64
Glassy Groundmass	503	464	455
Devitrified Groundmass	1	4	0
Total Points	**600**	**600**	**600**
Modal Abundance			
Quartz	0.00	0.00	0.00
Plagioclase	23.81	24.21	14.81
Sanidine	44.05	61.05	71.60
Biotite	14.29	5.26	8.64
Clinopyroxene	3.57	0.00	0.00
Orthopyroxene	0.00	0.00	0.00
Oxides	0.00	0.00	0.00
Unknown	14.29	9.47	4.94
% Phenocrysts	**14.00**	**15.83**	**13.50**
% Groundmass			
Glassy	83.83	77.33	75.83
Devitrified	0.17	0.67	0.00
Vesicles	2.00	6.17	10.67
Groundmass Counted	**86.00**	**84.17**	**86.50**

Table 5.03. Point count results of selected Del Medio samples.

Sample	DMI-01	DMI-04	DM2-02	DM2-07	DM2-09
Quartz	0	0	0	0	0
Plagioclase	0	2	2	0	0
Sanidine	0	0	7	0	0
Biotite	0	0	0	0	0
Clinopyroxene	0	13	2	0	0
Orthopyroxene	0	0	0	0	0
Oxides	0	0	0	0	0
Unknown	0	0	0	0	0
Vesicles	155	35	105	138	48
Glassy Groundmass	445	527	460	458	537
Devitrified Groundmass	0	23	24	4	15
Total Points	**600**	**600**	**600**	**600**	**600**
Modal Abundance					
Quartz	0.00	0.00	0.00	0.00	0.00
Plagioclase	0.00	13.33	18.18	0.00	0.00
Sanidine	0.00	0.00	63.64	0.00	0.00
Biotite	0.00	0.00	0.00	0.00	0.00
Clinopyroxene	0.00	86.67	18.18	0.00	0.00
Orthopyroxene	0.00	0.00	0.00	0.00	0.00
Oxides	0.00	0.00	0.00	0.00	0.00
Unknown	0.00	0.00	0.00	0.00	0.00
% Phenocrysts	**0.00**	**2.50**	**1.83**	**0.00**	**0.00**
% Groundmass					
Glassy	74.17	87.83	76.67	76.33	89.50
Devitrified	0.00	3.83	4.00	0.67	2.50
Vesicles	25.83	5.83	17.50	23.00	8.00
Groundmass Counted	**100.00**	**97.50**	**98.17**	**100.00**	**100.00**

Table 5.03. Point count results of selected Del Medio samples (cont.).

Sample	DM2-10	DM2-11	DM3-01	DM3-03	DM3-05
Quartz	0	0	0	1	0
Plagioclase	2	0	0	0	15
Sanidine	19	13	6	3	12
Biotite	0	0	0	0	0
Clinopyroxene	0	0	0	0	0
Orthopyroxene	0	0	0	0	0
Oxides	0	0	0	0	0
Unknown	13	4	0	6	3
Vesicles	114	46	92	44	88
Glassy Groundmass	450	94	494	546	481
Devitrified Groundmass	2	443	8	0	1
Total Points	**600**	**600**	**600**	**600**	**600**
Modal Abundance					
Quartz	0.00	0.00	0.00	10.00	0.00
Plagioclase	5.88	0.00	0.00	0.00	50.00
Sanidine	55.88	76.47	100.00	30.00	40.00
Biotite	0.00	0.00	0.00	0.00	0.00
Clinopyroxene	0.00	0.00	0.00	0.00	0.00
Orthopyroxene	0.00	0.00	0.00	0.00	0.00
Oxides	0.00	0.00	0.00	0.00	0.00
	38.24	23.53	0.00	60.00	10.00
% Phenocrysts	**5.67**	**2.83**	**1.00**	**1.67**	**5.00**
% Groundmass					
Glassy	75.00	15.67	82.33	91.00	80.17
Devitrified	0.33	73.83	1.33	0.00	0.17
Vesicles	19.00	7.67	15.33	7.33	14.67
Groundmass Counted	**94.33**	**97.17**	**99.00**	**98.33**	**95.00**

CHAPTER 6

EMPA MINERAL CHEMISTRY

Electron microprobe analyses (EMPA) were used to determine phenocryst composition and to measure chemical variations within phenocryst phases. Feldspar, pyroxene, and biotite were first viewed with backscatter images in order to detect variations in the mean atomic number (Z) within phenocrysts, i.e. to identify zoning. Phenocrysts with large Z such as iron oxides produce images that are brighter, while those with lower Z such as quartz produce darker images. Because electrons are charged particles they can be accelerated with electron static lenses and focused onto a sample surface. As electrons hit the sample they produce high energy backscattered electrons that rebound from the sample surface. The quantity of electrons backscattered is proportional to the mean atomic number of the spot being analyzed, thus a high Z spot will produce more backscattered electrons than a low Z spot. Backscattered electrons are counted as they hit a detector and an image is produced. In Figure 6.01 the brightest areas are biotite, that contain high Z Fe. The next brightest area is sanidine that contains Fe, but also lower Z elements such as Si and Al. The darkest grey areas are plagioclase feldspar and glassy groundmass.

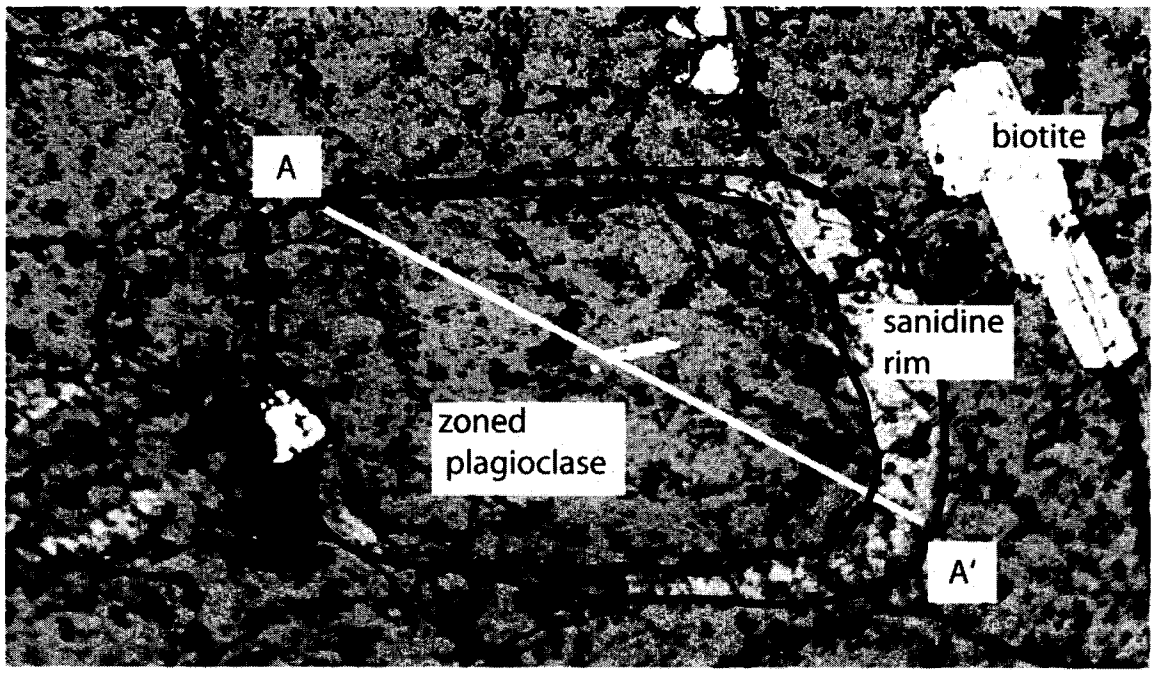

Figure 6.01. Electron microprobe backscatter image of sample RC12-4, showing a zoned plagioclase phenocryst with a sanidine overgrowth. A corresponding petrographic image is shown in Figure 6.05. The phenocryst is approximately 800 μm by 500 μm. A line traverse from A to A' shows distinct chemical variation (see text).

Representative phenocrysts were picked for analyses using 112 images at 2.4 micron resolution for each of two thin sections from each rhyolite unit, DC03, DC08, RC07, RC12, DM2-02, and DM2-10. Chemical composition data was gathered in suitable locations, at least 10 μm away from cracks and obvious imperfections and in the cores and on the rims of representative feldspar, pyroxene, and biotite. Using these data along with backscatter images, phenocrysts were selected for more detailed line traverse analyses. Line traverse analyses were used to measure chemical composition and to constrain the presence or absence of zoning. Nomenclature of phenocrysts analyzed by EMPA includes the rhyolite unit, sample number and a phenocryst number, e.g. DC03-1. Line traverses are referred to in the same manner as phenocrysts except when more than one traverse was analyzed, in which case a letter is also assigned, e.g. RC12-2A. All

chemical analyses were recalculated using mineral chemistry spreadsheets from the website http://www.abdn.ac.uk/geology/profiles/analysis/software.htm at the University of Aberdeen Department of Geology and Petroleum Geology (Preston, 2002).

Feldspars

The composition of feldspars analyzed by individual points in Deer Canyon rhyolites record two separate feldspar types, andesine and sanidine (Figure 6.02A, Appendix B). Andesine ranges from $An_{45}Ab_{51}Or_4$ to $An_{32}Ab_{63}Or_5$ and sanidine ranges from $An_1Ab_{42}Or_{57}$ to $An_6Ab_{40}Or_{54}$. Analyses along line traverses record even higher variability and chemical zonation within the Deer Canyon feldspars. Alkali feldspars range from sanidine to anorthoclase and plagioclase feldspars range from oligoclase to labradorite (Figure 6.02B, Appendix B). Phenocryst DC03-1 is a zoned and resorbed andesine with two overgrowths. A rim to rim line traverse from A to A' (Figure 6.03A) reveals a systematic and alternating pattern of An content. The core with An_{38-39} is overgrown by plagioclase An_{36-24}, which is overgrown by rims, An_{38-42}. A line traverse along a sanidine phenocryst, DC08-1, shows patchy zonation with the compositions ranging from $An_1Ab_{55}Or_{44}$ to $An_2Ab_{61}Or_{37}$. In this case An content remains almost constant while Ab and Or content vary by more than 10% (Figure 6.03B). Phenocryst DC08-4 displays antirapikivi texture with the composition along a line traverse ranging from anorthoclase between 0 and 630 microns to oligoclase between 660 and 1080 microns to anorthoclase between 1140 to 1740 microns (Figure 6.03C). A line analysis point that plots as labradorite, An_{58}, in figure 6.02B is not part of a systematic trend, rather it appears to be an isolated area located within resorbed plagioclase DC03-2 (Appendix B).

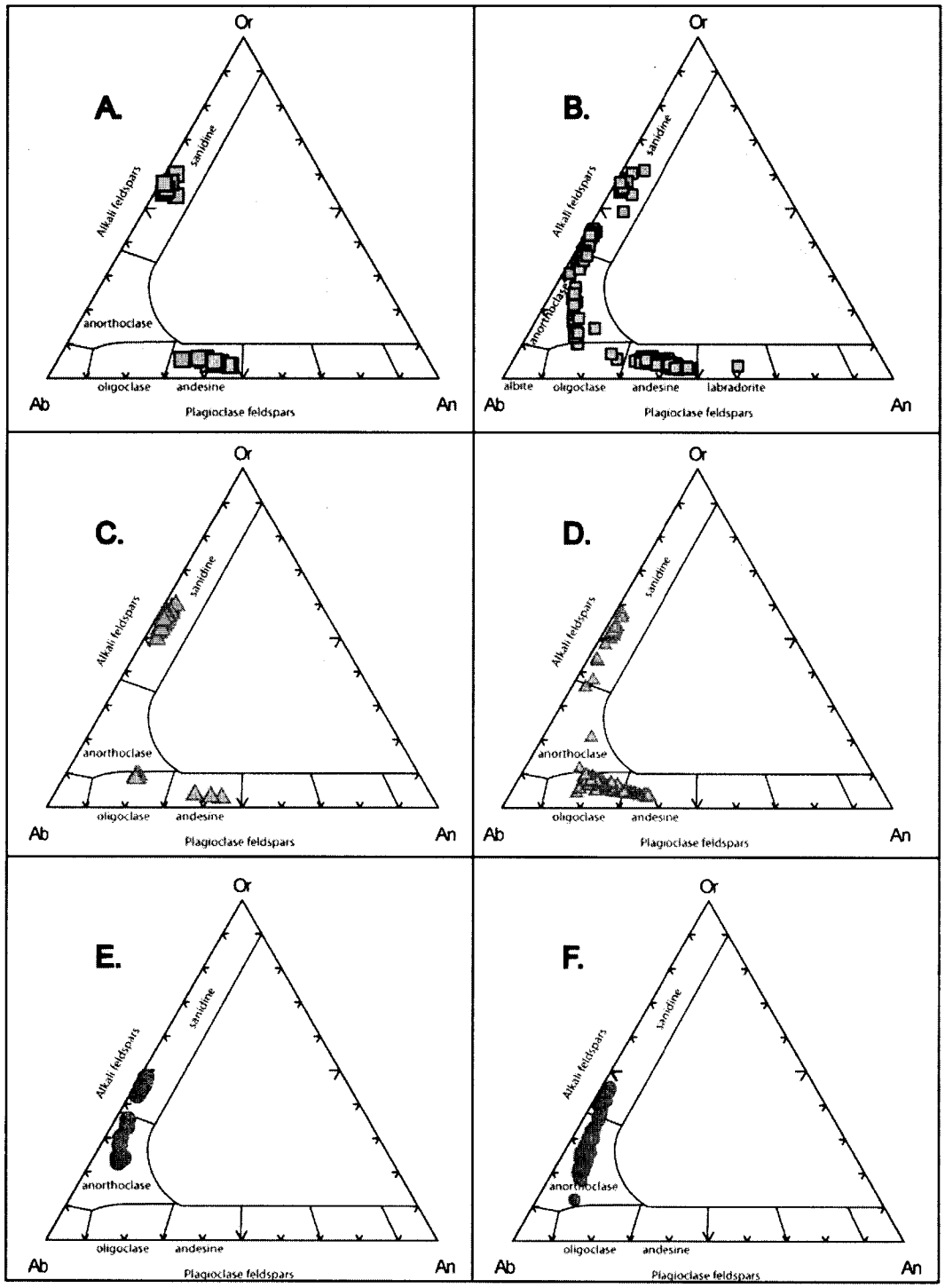

Figure 6.02. EMPA results from Deer Canyon point (A) and line traverse (B), Redondo Creek point (C) and line traverse (D) and Del Medio point (E) and line traverse (F) feldspar analyses. All analyses were recalculated on the basis of 32 oxygen and restated in terms of molecular percentages of albite (Ab), anorthite (An), and orthoclase (Or) end members.

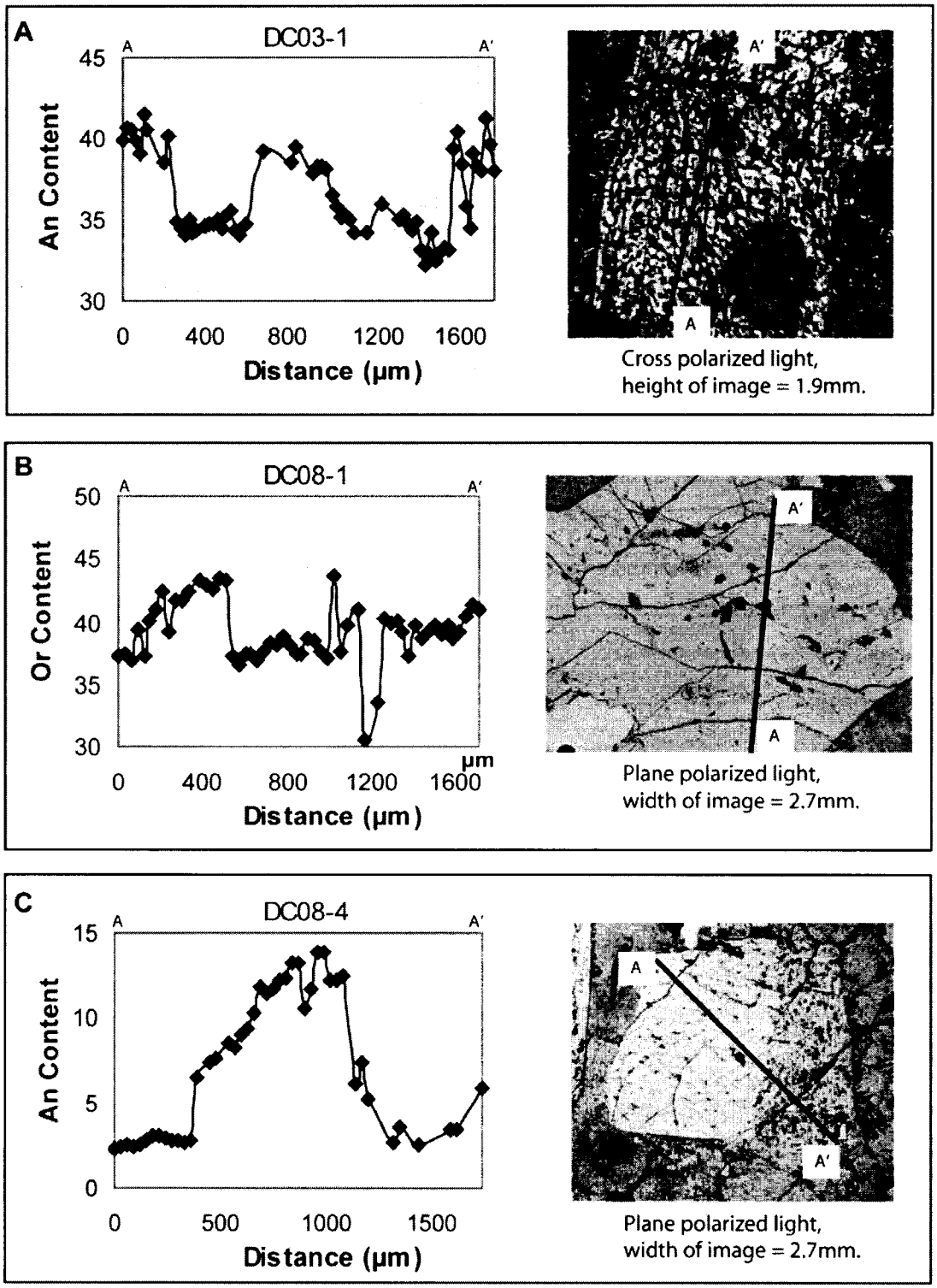

Figure 6.03A, B, and C. Graphs of line traverses and corresponding photomicrographs of selected phenocrysts from Deer Canyon samples.

Feldspar compositions in Redondo Creek rhyolites consist of sanidine, oligoclase and andesine. Point analyses of RC07 phenocrysts are sanidine, ranging from $An_3Ab_{37}Or_{60}$ to $An_2Ab_{44}Or_{54}$. Analyses of points from RC12 include sanidine ranging from $An_2Ab_{40}Or_{57}$ to $An_3Ab_{47}Or_{50}$, and oligoclase and andesine ranging from $An_{43}Ab_{54}Or_3$ to $An_{18}Ab_{73}Or_9$ (Figure 6.02C, Appendix B). A more detailed characterization of Redondo Creek feldspars was acquired with analyses along line traverses, which showed systematic variability in chemistry and zonation within phenocrysts. Line traverses along phenocrysts from both samples, RC07 and RC12, generally consist of plagioclase in the core with sanidine overgrowths on the rims. Plagioclase in the cores of three phenocrysts (RC07-12, RC12-2, and RC12-4) varies between andesine and oligoclase (Figure 6.04, Figure 6.05, Appendix B). RC07-12 was the most homogenous feldspar analyzed with an oligoclase core and sanidine rim (Figure 6.04A). RC12-2 and RC12-4 feldspars show distinctive patterns in which variable An content is observed. RC12-2 has an oligoclase core, An_{23-29}, with more sodic overgrowths, An_{14-22}, followed by sanidine rims, An_2 (Figure 6.04). Phenocryst RC12-4 has a distinct pattern of successive overgrowths with andesine composition An_{30-37} in the core, oligoclase overgrowths, An_{17-24} followed by sanidine overgrowths at the rims, An_{2-3} (Figure 6.05). Phenocryst RC12-14 is a resorbed plagioclase feldspar with brown glass inclusions. A photomicrograph is shown in Figure 5.06. A rim to rim line traverse shows variable chemistry between oligoclase $An_{17}Ab_{74}Or_9$ to $An_{22}Ab_{72}Or_6$ and patchy anorthoclase $An_5Ab_{57}Or_{38}$ to $An_4Ab_{61}Or_{35}$ in the core with overgrowth rims of sanidine $An_2Ab_{45}Or_{53}$ to $An_3Ab_{41}Or_{56}$. The brown glass inclusions were not analyzed in this study.

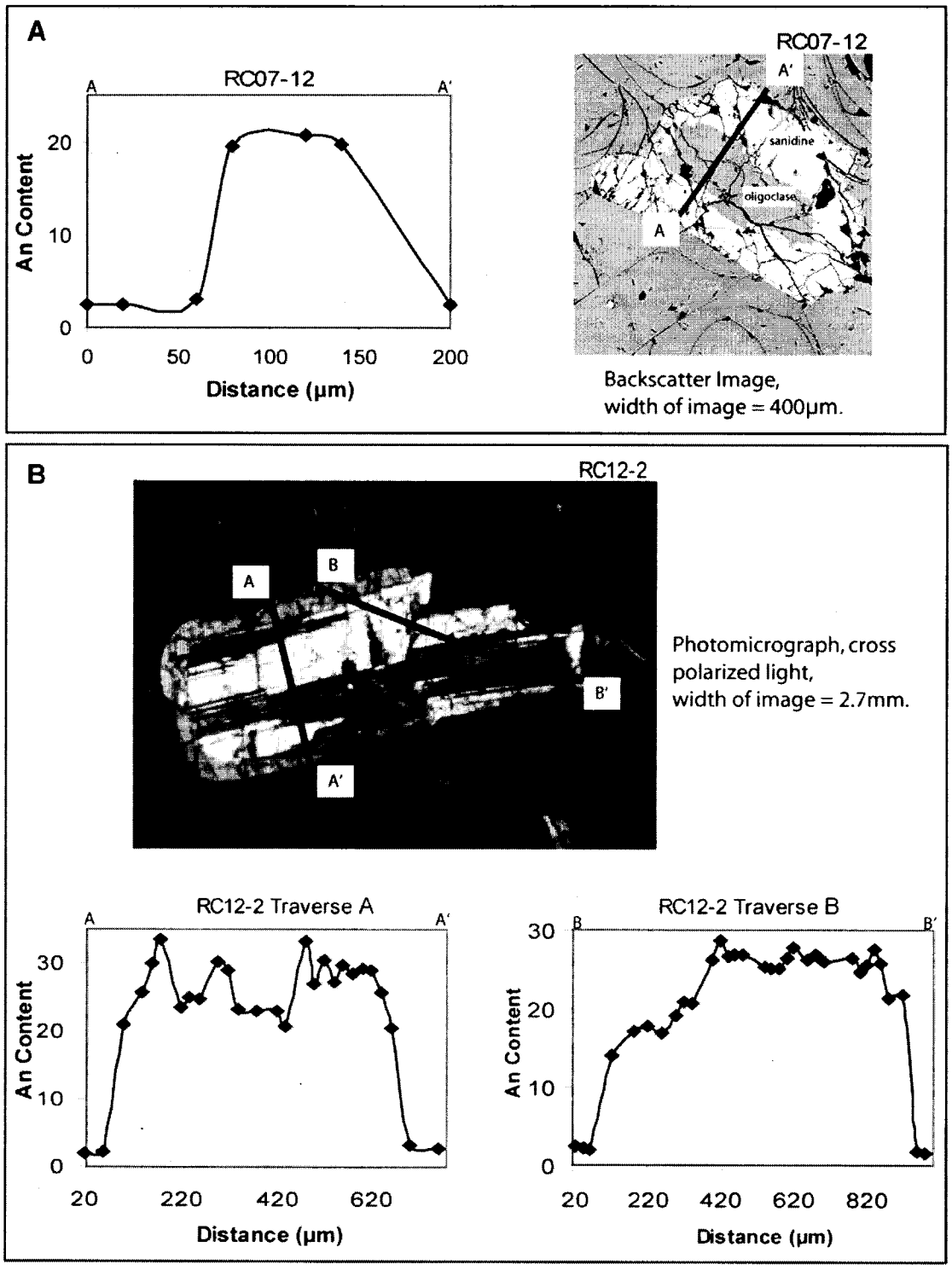

Figure 6.04 A and B. Line traverse graph and corresponding backscatter image of phenocryst RC07-12 showing oligoclase with sanidine rims(A). Line traverse graphs and photomicrograph of phenocryst RC12-2 showing patchy zoned oligoclase core, with more sodic overgrowths, rimmed by sanidine (B).

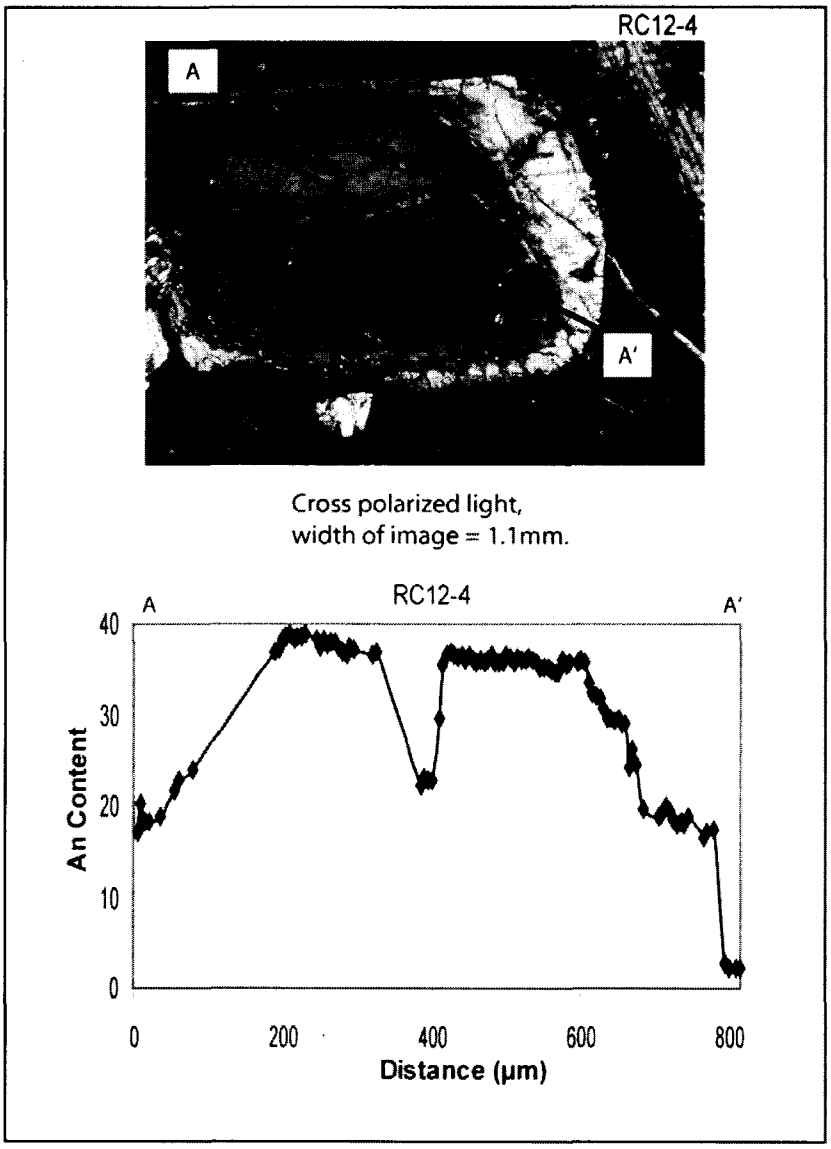

Figure 6.05. Photomicrograph and line traverse graph of phenocryst RC12-4, a normally zoned plagioclase, with an andesine core, oligoclase overgrowth, and sanidine rim. The decrease in An content in the center of the graph is due to an oligoclase inclusion.

Del Medio feldspars are composed of anorthoclase and sanidine (Figures 6.02E, 6.02F, 6.06A and 6.06B). In contrast with Deer Canyon and Redondo Creek feldspars, this group of feldspars exhibit patchy core to rim zoning when present and rare

overgrowths. Analyzed points range from $An_2Ab_{51}Or_{47}$ to $An_7Ab_{69}Or_{24}$. Line traverses show a larger range of compositions with patchy zonation in most phenocrysts. Phenocryst DM2-10-3 has an anorthoclase core, Or_{23-25}, with sanidine rims, Or_{41-44}, (Figure 6.06A, Appendix C). A anorthoclase phenocryst, DM2-10-2, has patchy zonation with a core composition of Or_{24-27} and rim compositions of Or_{20-24} (Figure 6.06B, Appendix B).

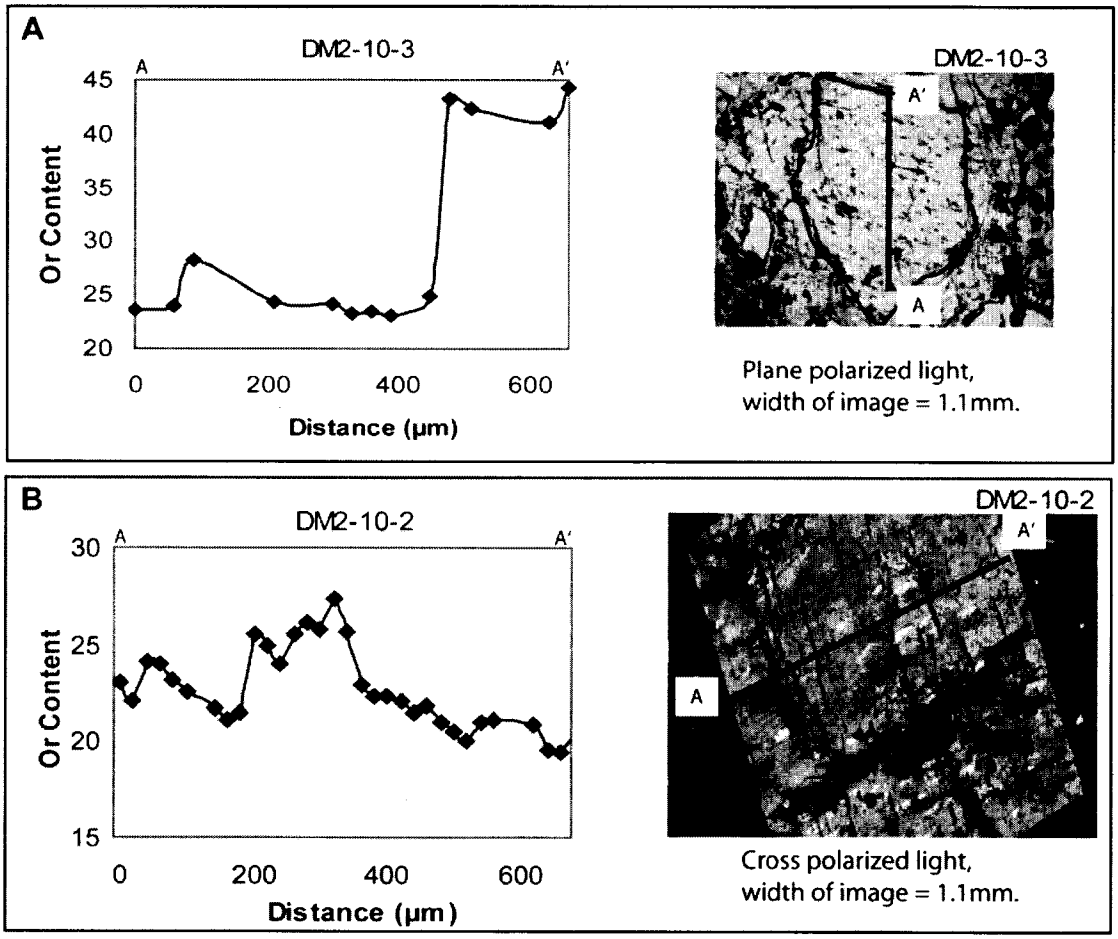

Figure 6.06A and B. Line traverse graphs and photomicrographs of Or content versus distance of anorthoclase with a sanidine overgrowth rim (A) and of a patchy zoned anorthoclase (B).

Biotite

Biotites were analyzed only from Redondo Creek rhyolite as they are not present in other units. The phenocrysts are a homogenous chemically unzoned group with only small variations in composition. Analyses were obtained from individual points within the phenocrysts, and along line traverses (Appendix C). On a cation plot of Fe/(Fe +Mg) versus Al^{IV} showing ideal end members, analyses yield Al^{IV} from 2.19 to 2.45 and Fe/(Fe +Mg) from 0.41 to 0.46 (Figure 6.07). This is about half way between phlogopite and annite end member compositions.

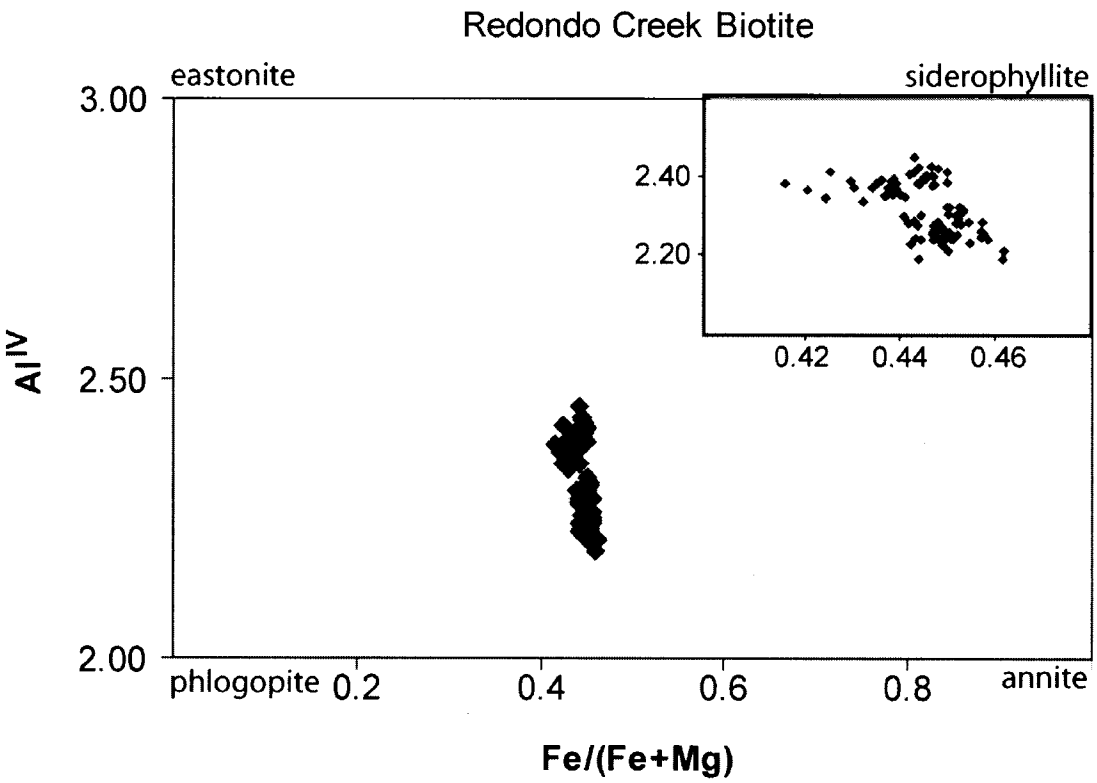

Figure 6.07. Cation plot of Fe/(Fe +Mg) versus Al^{IV} showing ideal end members from EMPA analyses of biotite. The inset shows a close up of the data plotted in the larger chart.

Pyroxene

Pyroxenes were analyzed from Redondo Creek and Del Medio samples. Point analyses are nearly identical to line traverse analyses (Appendix D). When plotted on a standard Wo-En-Fs ternary diagram analyzed phenocrysts plot as clinopyroxene. Those from Redondo Creek are augite with line traverse compositions ranging from $Wo_{42}En_{42}Fs_{14}Ac_2$ to $Wo_{44}En_{40}Fs_{14}Ac_2$, whereas those from Del Medio are augite to salite with line traverse compositions ranging from $Wo_{42}En_{34}Fs_{22}Ac_2$ to $Wo_{46}En_{33}Fs_{19}Ac_2$ (Figures 6.08, and 6.09).

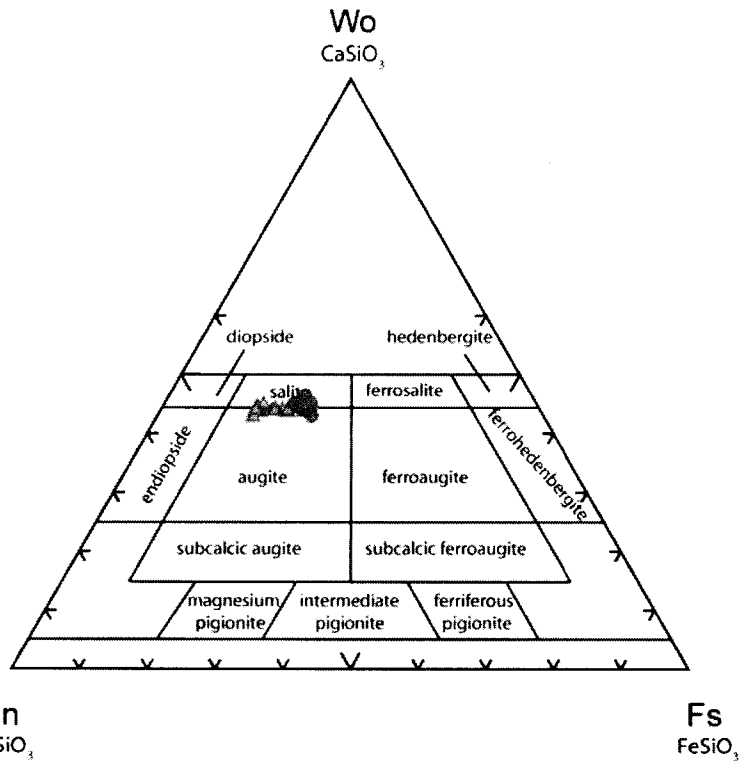

Figure 6.08: Wo-En-Fs classification diagram of pyroxene phenocrysts analyzed from Redondo Creek (green triangles) and Del Medio (red dots) rhyolites. Analyses recalculated on the basis of 6 oxygen and restated in terms of molecular percentages of enstatite (En), ferrosilite (Fs), wollastonite (Wo), and acmite (Ac) end members. Ac accounts for less than 3 wt % and is not depicted on the diagram.

Line traverse analyses exhibit minor chemical variability. Phenocrysts RC07-20 varies in Wo content from Wo_{42} to Wo_{44}, but shows no systematic trends (Figure 6.09, Appendix D).

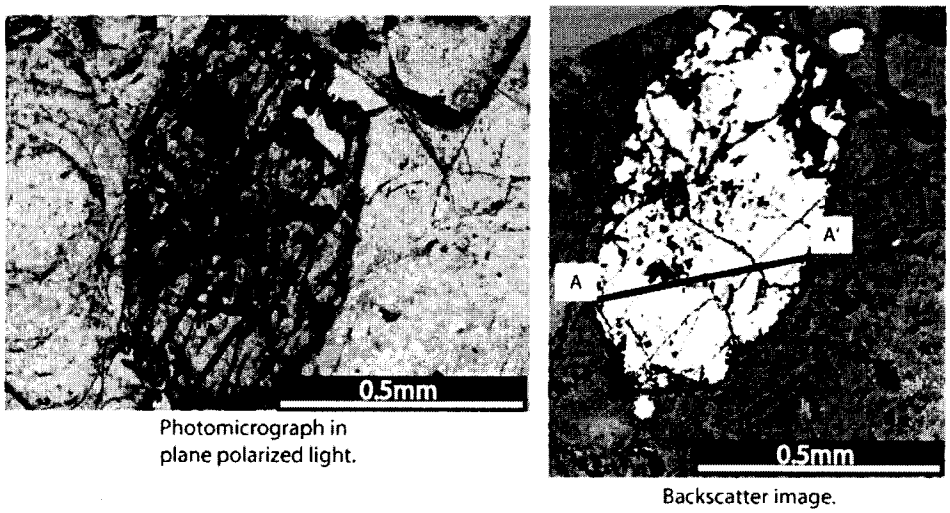

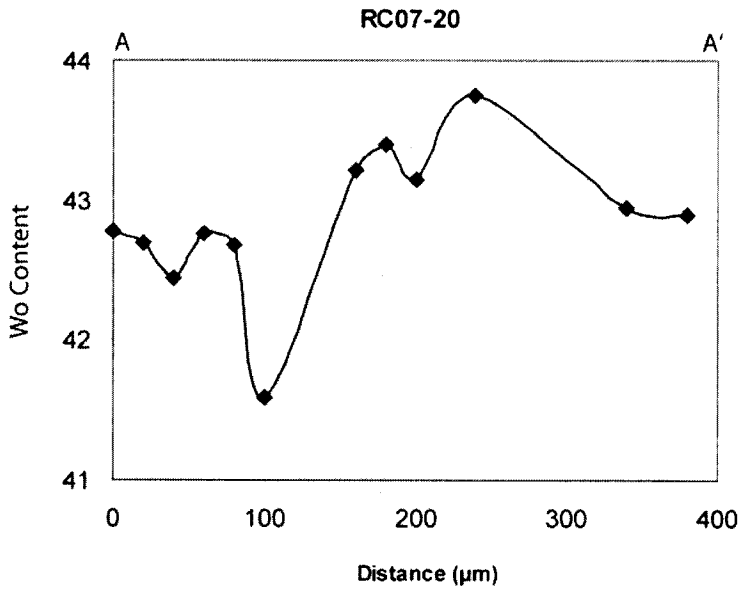

Figure 6.09. Photomicrograph, corresponding backscatter image and line traverse graph of clinopyroxene RC07-20, showing variation in wollastonite composition through the crystal.

Del Medio clinopyroxenes have restricted MgO concentrations between 11.09 and 12.77 wt% and do not show trends on plots of CaO and FeO. In contrast, Redondo Creek clinopyroxenes have highly variable MgO content between 11.74 and 15.14 wt%. CaO shows little variation with increasing MgO whereas FeO shows a distinct inverse trend with increasing MgO (Figure 6.10, Appendix D).

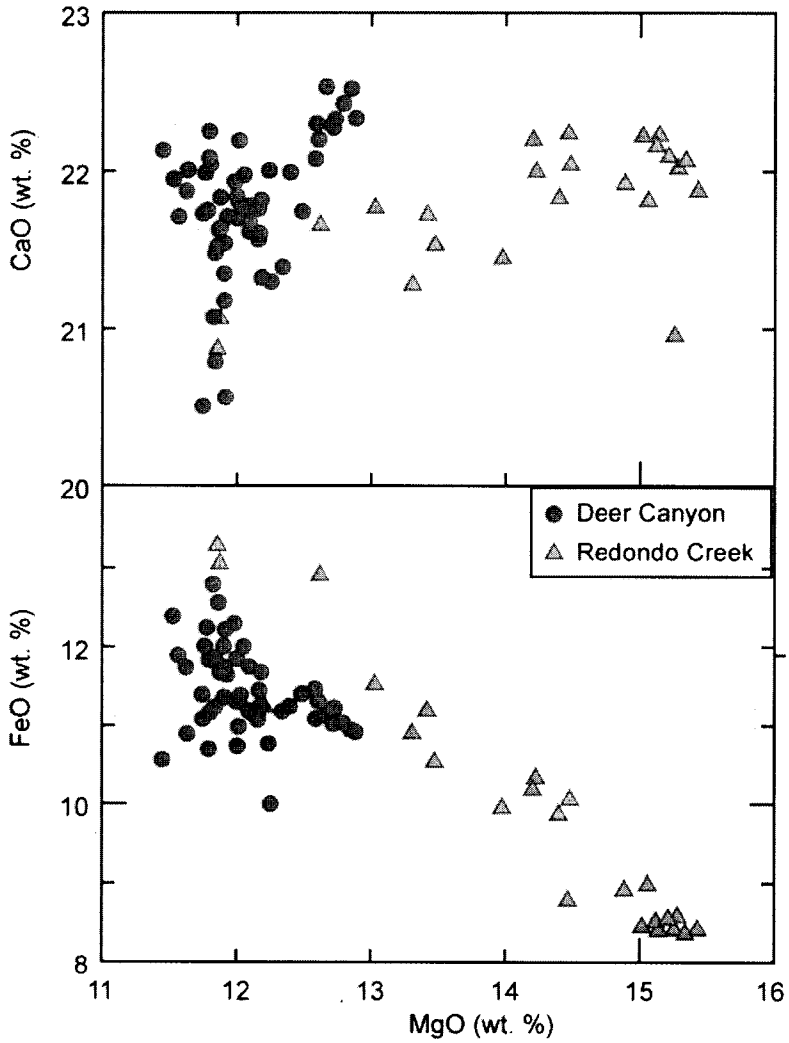

Figure 6.10. Diagrams of FeO and CaO versus MgO of pyroxene phenocrysts from Redondo Creek and Del Medio rhyolites.

CHAPTER 7

GEOCHEMISTRY

Whole rock major and trace element results and instrumental precision from XRF and ICPMS analyses of representative samples from Deer Canyon, Redondo Creek and Del Medio rhyolites are listed in Appendix E. LOI values (Appendix E) included in XRF results were calculated based on procedures described in Chapter 4. All major elements on plots are normalized to 100% anhydrous and expressed in wt.%.

Major Element Chemistry

Using the classification of LeBas et al. (1986) samples from Del Medio are classified as high silica rhyolites, whereas those from Redondo Creek are classified as rhyolites (Figure 7.01). Deer Canyon samples vary in SiO_2 with both rhyolite and high silica rhyolite types. Sample DC01 plots in the rhyolite range (74.8 wt. % SiO_2) and sample DC03 plots as a high silica rhyolite (77.1 wt. % SiO_2). Two samples from Deer Canyon DC08 and DC12 (79.73 and 81.25 wt. % SiO_2 respectively) do not fall on the LeBas classification plot. The X axis was extended in Figure 7.01 in order to show these two samples which may have been hydrothermally altered. Each unit is compositionally distinct with Deer Canyon exhibiting the most widely varying major element chemistry, Del Medio exhibiting tightly clustered major element chemistry, and Redondo Creek exhibiting loosely clustered trends in major element chemistry (Figures 7.02 and 7.03).

Deer Canyon rhyolite has very high abundances of SiO_2, with normalized average of ~78 wt.%. Redondo Creek has the lowest abundances of SiO_2, and Del Medio is intermediate between the other two units. With the exception of Na_2O Redondo Creek samples are higher in oxide abundances than either Deer Canyon or Del Medio samples. Del Medio samples have the lowest MgO, FeO and P_2O_5, the highest Na_2O and intermediate concentrations of all other major elements. Deer Canyon samples vary significantly in major element abundances and overlap with both of the other units.

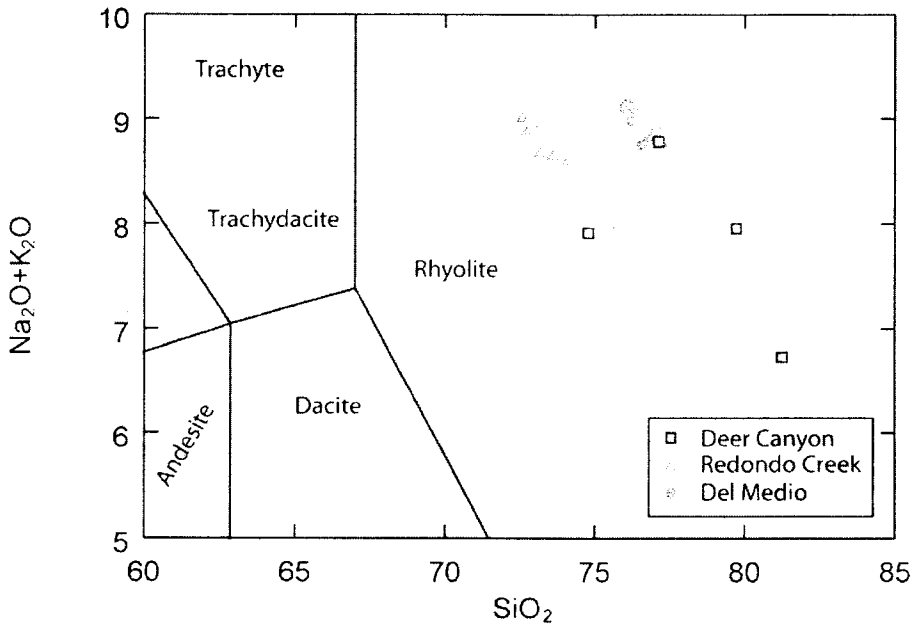

Figure 7.01. Total alkalies ($Na_2O + K_2O$) versus SiO_2 classification diagram of Deer Canyon, Redondo Creek, and Del Medio rhyolites. Diagram after LeBas et al., 1986.

All three units show some correlation between major elements and SiO_2, but correlation between Redondo Creek rhyolite major elements and SiO_2 is the most well defined (Figures 7.02 and 7.03). Plots of Al_2O_3, CaO and TiO_2 versus SiO_2 show the most

well defined tends and deceases in value with increasing SiO_2. Na_2O and P_2O_5 also decrease, but the results are somewhat scattered for Deer Canyon samples. K_2O increases in Redondo Creek while it decreases in Del Medio and is scattered in Deer Canyon samples. FeO and MgO exhibit no real trends with increasing SiO_2 in Redondo Creek and Del Medio samples, but show a slight decrease for Deer Canyon samples. For all oxides, sample DC01 plots along with the tightly grouped Del Medio samples, and with the exception of K_2O and MgO, sample DC03 plots with or very near Redondo Creek samples.

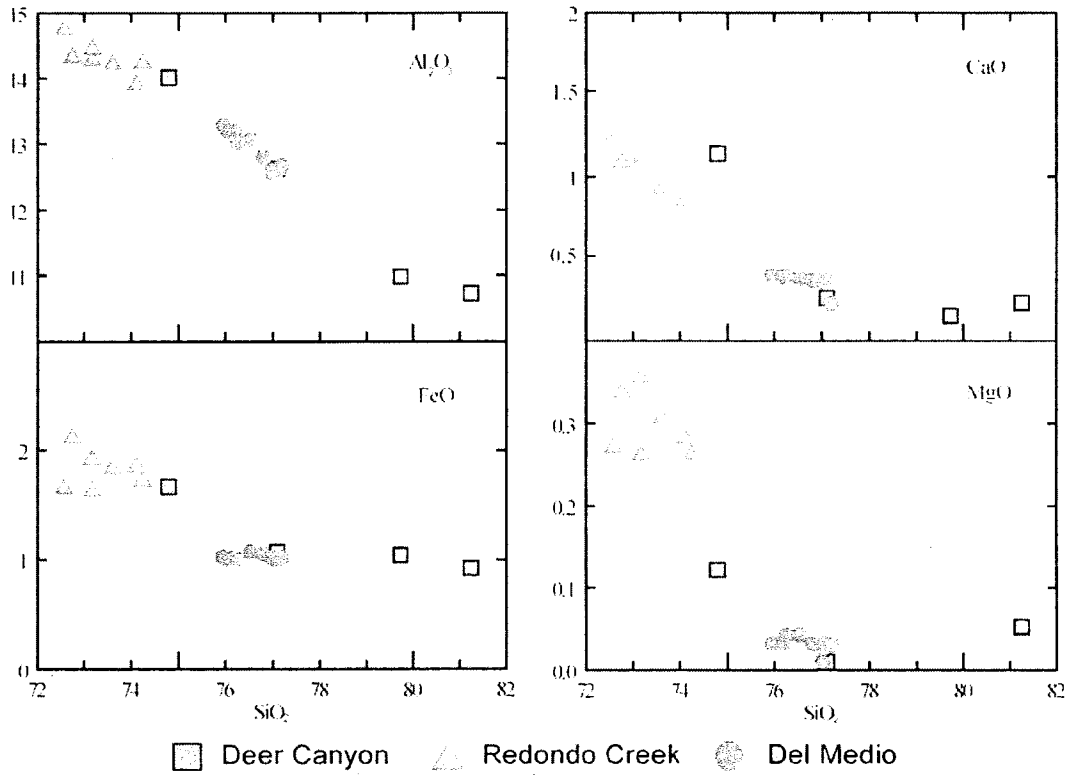

Figure 7.02. Harker variation diagrams plotting SiO_2 vs. Al_2O_3, FeO (total Fe as FeO), CaO, and MgO.

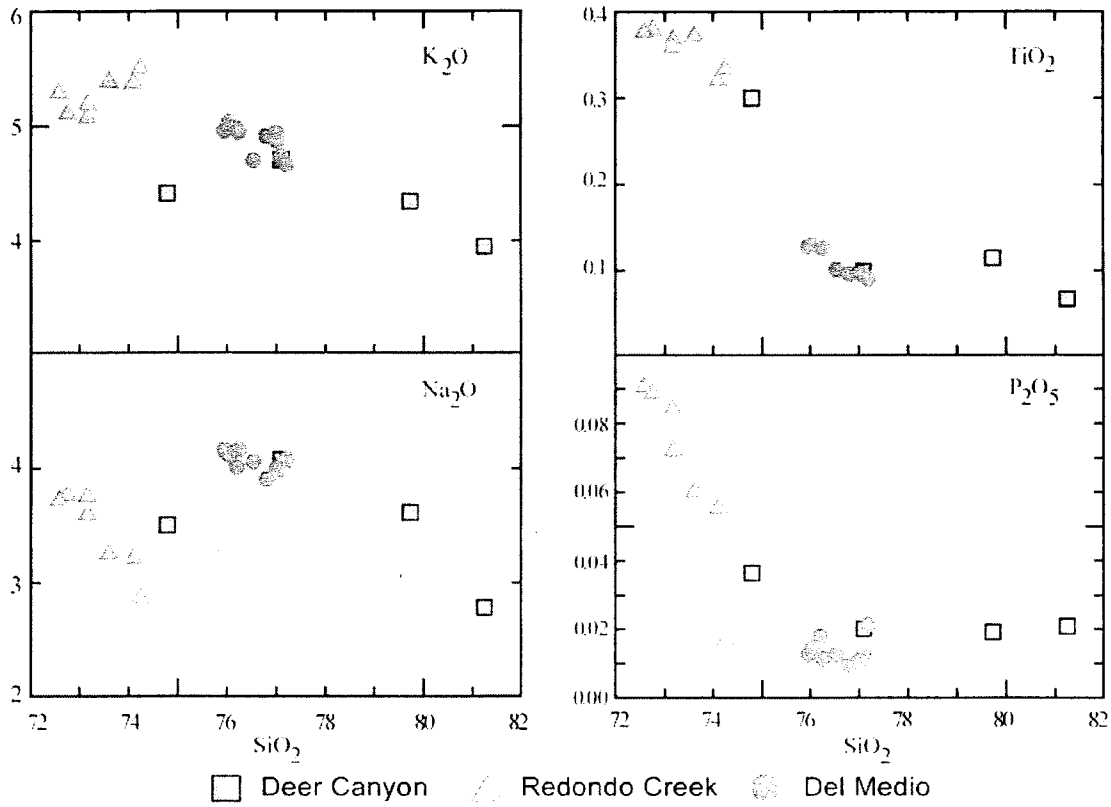

Figure 7.03. Harker variation diagrams plotting SiO_2 vs. K_2O, Na_2O, TiO_2, and P_2O_5.

Trace Element Chemistry

Variations in trace element composition are shown on Figures 7.04, 7.05 and 7.06. A suitable index of differentiation must be an incompatible and immobile trace element that is accurately measured. An incompatible element is chosen because the latest stages of evolution in rhyolitic magmas, at ~750 °C, occurs in the upper crust where it is surrounded by wall rock, at ~200-300 °C. The dominant differentiation mechanism in this situation is likely to be fractional crystallization, thus an incompatible element will show the effects of differentiation. Trace elements Cs, Rb, and Nb all have good analytical

precision, and are highly incompatible during fractional crystallization. Nb was chosen because it is the least mobile.

Data on plots of Nb versus other trace elements were divided into four groups, those that increase with increasing Nb, those that decrease with increasing Nb, those that show invariant trends that do not vary with Nb, and those that have scattered data sets (Table 5.04). When plotted against increasing Nb, Deer Canyon rhyolite has the most variable trace element abundances of the three units, Redondo Creek shows the most increasing or decreasing trace element trends, and Del Medio has the most invariant trace elements. Deer Canyon has variable Nb concentrations, Redondo Creek has low Nb concentrations and Del Medio rhyolite has high Nb values. One Deer Canyon sample is identical to the Del Medio samples in some plots (Figure 7.04, 7.05, and 7.06) Deer Canyon samples show increasing trends in Hf, Tb, Lu, Ta, Y, Yb, Gd, Dy, Ho, Er, and Tm, decreasing trends in Sc, Ba, Sr, and Eu, and scattered trends in Zn, Nd, Rb, La, Cs, U, Sm, Ce, and Th with increasing Nb. Redondo Creek samples show increasing trends in Ta, Rb, U, and, Th, decreasing trends in Y, Ba, Sr, Eu, Ho, and scattered or invariant trends in all the remaining trace elements. Del Medio samples show increasing trends in Ta, Ce, Yb, Th, and , Er, decresing trends in Lu, Y, Gd, and, Ho, and scattered or invariant trends in the remaining trace elements with increasing Nb (Figures 7.04, 7.05 and 7.06).

The relative abundances of trace elements among the three units were divided into two groups, those with highest trace element abundances and those with lowest trace element abundances. Deer Canyon often exhibits a range of trace element abundances that spans from low to high. Redondo Creek samples form a cohesive group, with all trace elements loosely clustered together. Most Del Medio samples are closely grouped,

but one sample, DM2-11, has lower abundances of Lu, Zn, Y, Nd, La, Cs, Sm, Ce, Yb, Gd, Dy, Ho, Er, and Tm than all of the other samples from the Del Medio rhyolite.

Table 7.01. Summary of trace elements with increasing Nb.

Samples	Deer Canyon	Redondo Creek	Del Medio
Increasing Trend	Hf, Tb, Lu, Ta, Y, Yb, Gd, Dy, Ho, Er, Tm	Ta, Rb, U, Th	Ta, Ce, Yb, Th, Er
Decreasing Trend	Sc, Ba, Sr, Eu	Y, Ba, Sr, Eu, Ho	Lu, Y, Gd, Ho
Scattered	Zn, Nd, Rb, La, Cs, U, Sm, Ce, Th	Hf, Sc, Tb, Zn, Nd, La, Cs, Sm, Ce, Dy, Er, Tm	Hf, Rb, Cs, U, Tm
Invarient		Lu, Yb	Sc, Tb, Zn, Ba, Nd, La, Sr, Sm, Eu, Dy

Table 7.02. Comparison chart of trace element concentrations.

Samples	Deer Canyon	Redondo Creek	Del Medio
Highest Abundance	Cs	Hf, Sc, Ba, Nd, La, Sr, Ce, Eu	Lu, Zn, Ta, Y, Rb, U, Yb, Th, Er, Tm
Lowest Abundance	Zn, La, Ce	Lu, Ta, Y, Rb, U, Yb, Th, Er, Tm	Hf, Sc, Ba, Nd, Sr, Eu

Note: Sc, Tb, Lu,Ta, Y, Rb, U, Sr, Sm, Yb, Gd, Dy, Ho, Er, and Tm were ignored for Deer Canyon rhyolite, since in these cases they are scattered from lowest to highest abundances.

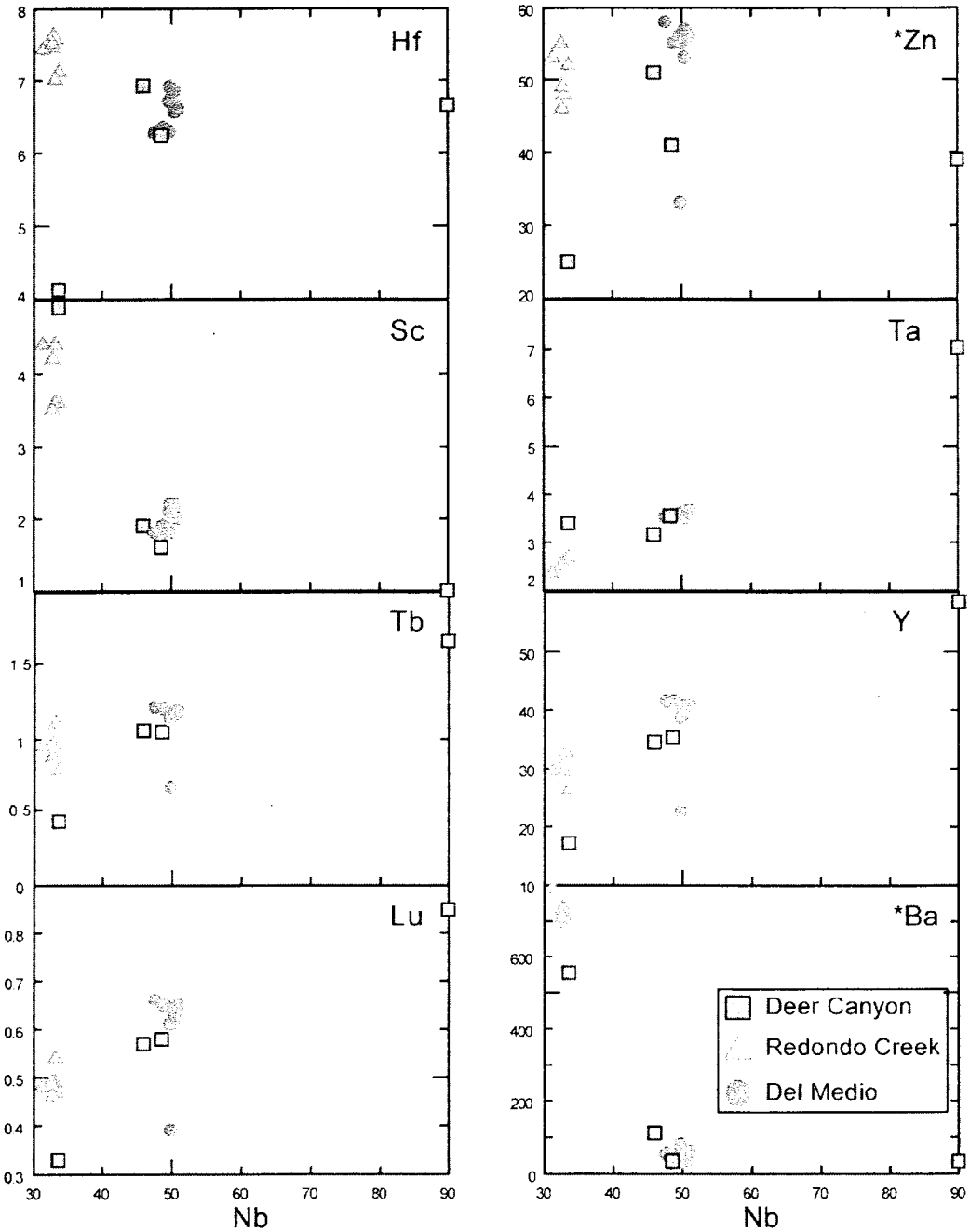

Figure 7.04: Plots of Nb versus trace elements. All elements are in ppm. Elements with * were analyzed by XRF, others by ICPMS.

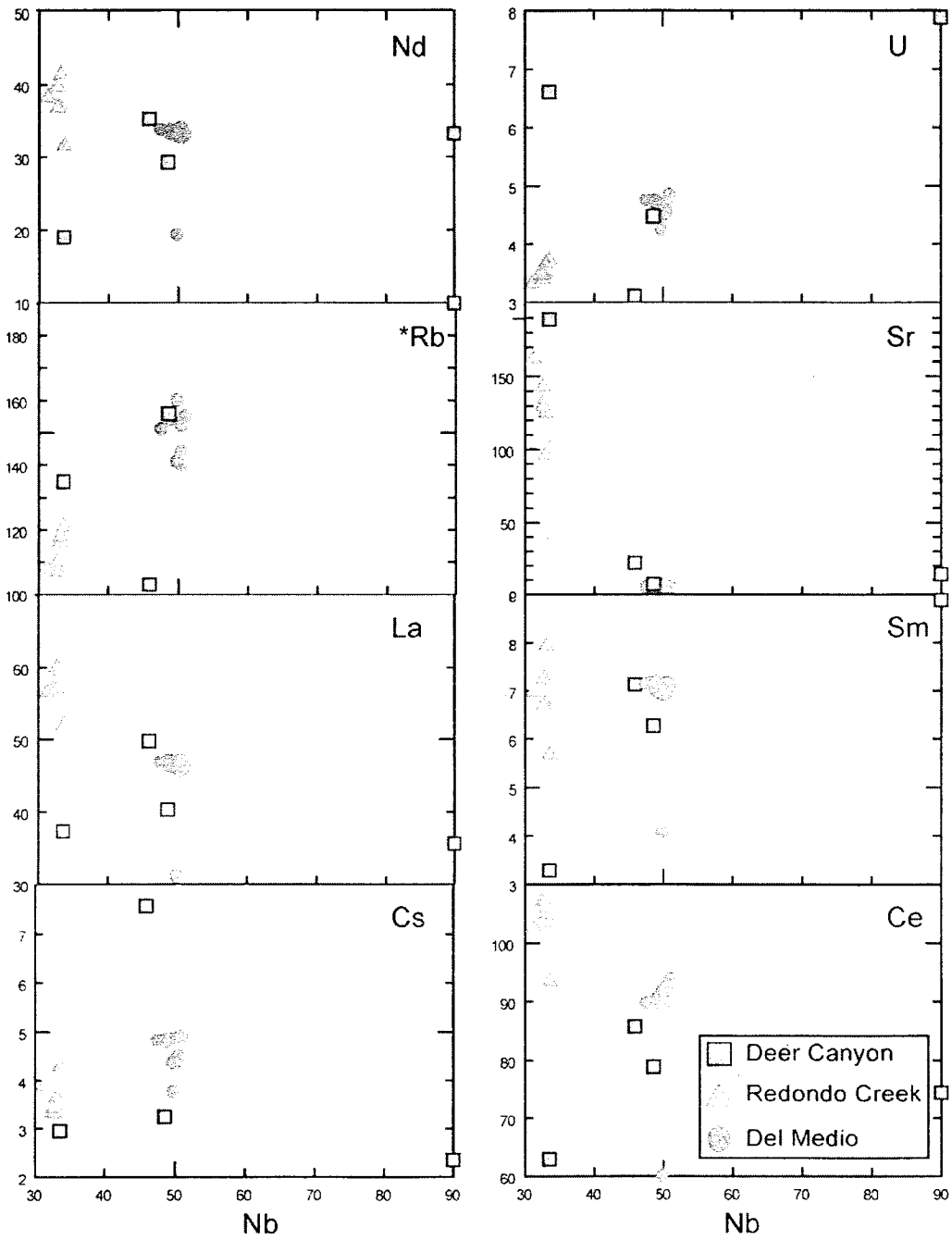

Figure 7.05: Plots of Nb versus trace elements. All elements are in ppm. Elements with * were analyzed by XRF, others by ICPMS.

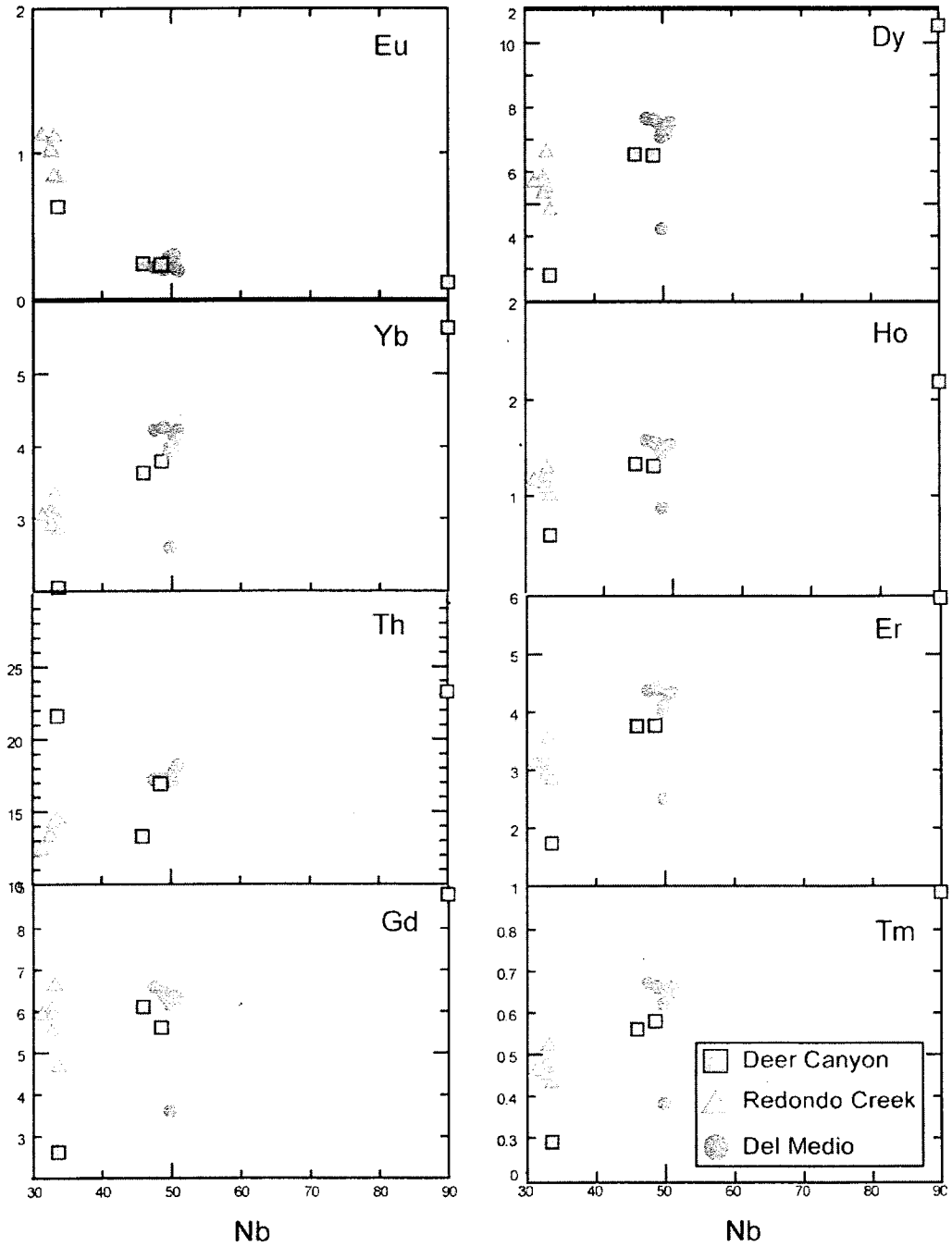

Figure 7.06: Plots of Nb versus trace elements. All elements are in ppm. Elements with * were analyzed by XRF, others by ICPMS.

Ratios of Incompatible Trace Elements

Rocks that form in the mid to lower crust display distinct incompatible element ratios that remain relatively unchanged throughout normal magma evolution. Ratios of incompatible trace elements are unaffected by upper crustal processes such as fractional crystallization, because the crystallizing minerals remove little of these trace elements and their relative concentrations essentially remain constant. Thus incompatible trace element ratios potentially provide a record of the composition of the original magma. Plots of incompatible trace element ratios versus Nb were used to define relationships among Deer Canyon, Redondo Creek and Del Medio rhyolites. In general Deer Canyon samples are scattered, while Redondo Creek and Del Medio samples cluster together.

Differences among Deer Canyon samples are exhibited by their relative locations on plots of Y/Yb, Ta/Yb, Th/Nb, and Th/Yb versus Nb (Figures 7.07 and 7.08). Two Deer Canyon samples plot together with Del Medio samples showing similar trace element ratios. One Deer Canyon sample has similar Nb but higher or lower Y-axis ratios than the Redondo Creek rhyolites. These observations are also seen in plots of individual trace elements versus Nb, described previously. Redondo Creek trace element ratios are loosely clustered together, showing similar trace element ratios for all samples. Del Medio samples are tightly clustered. One exception is sample DM2-11 which, in the plot of Y/Yb versus Nb is located below the other samples and in plots of Ta/Yb, and Th/Yb versus Nb, is located above the other samples (Figures 7.07 and 7.08. In individual trace element plots this sample often was found with lower abundances of trace elements than all other Del Medio samples.

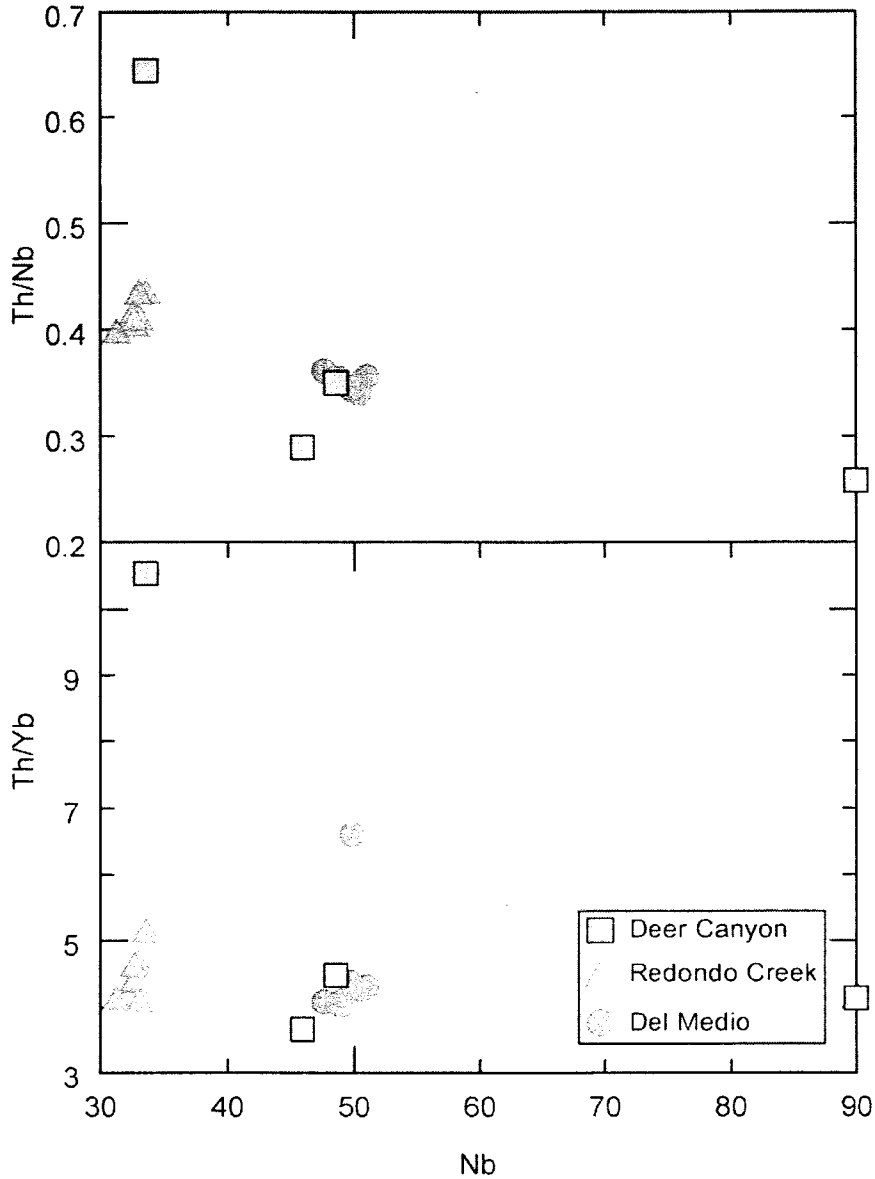

Figure 7.07. Nb versus ratios of incompatible trace elements. Abundances expressed in ppm.

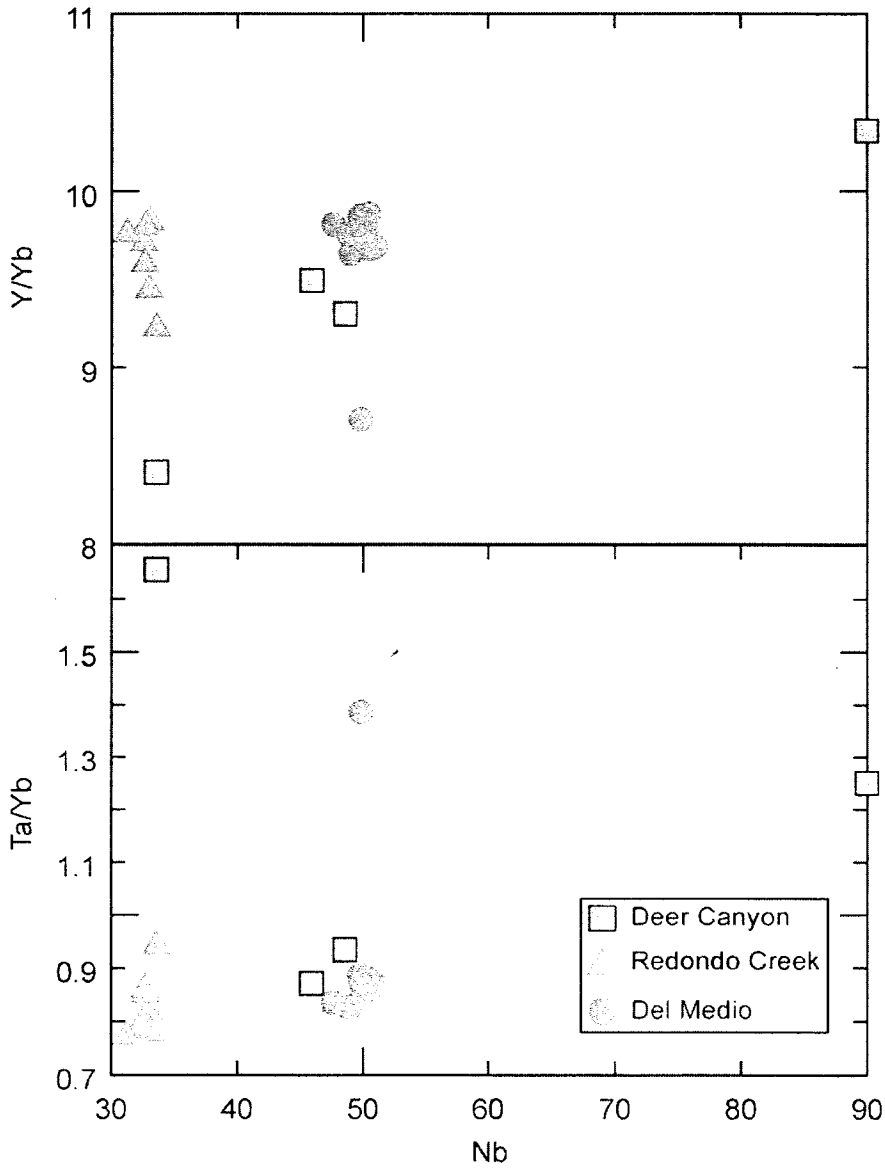

Figure 7.08. Nb versus ratios of incompatible trace elements. Abundances expressed in ppm.

REE Chondrite Diagrams

Chondrite normalized REE plots also show differences and some similarities among Deer Canyon, Redondo Creek, and Del Medio rhyolites. Each rhyolite exhibits a Eu anomaly, but the magnitude varies among them (Figures 7.09, 7.10 and 7.11). Each

rhyolite exhibits enriched LREE patterns with negative slopes and relatively flat HREE patterns.

Deer Canyon has a variable and shallow to deep negative Eu anomalies. A steep negative LREE slope contrasts with an almost flat, slightly negative HREE slope (Figure 7.09). Two Deer Canyon samples plot closely together, while the other two are different. One Deer Canyon sample has a shallow Eu anomaly similar to Redondo Creek samples (Figures 7.09 and 7.10). Redondo Creek has a shallow Eu anomaly with a steeply dipping negative LREE slope and a gently dipping negative HREE slope. Samples from Redondo Creek are tightly grouped (Figure 7.10). The REE diagram for Del Medio is similar to Redondo Creek, but has a deeper Eu anomaly (Figures 7.10 and 7.11). One Del Medio sample plots lower than the other Del Medio samples (Figure 7.11).

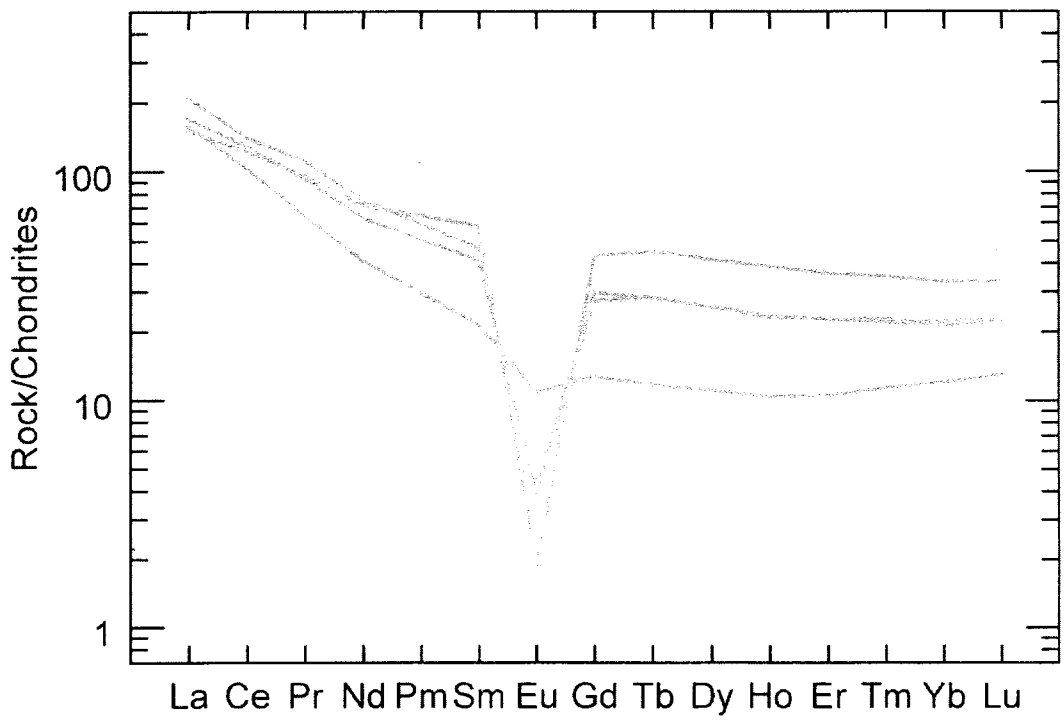

Figure 7.09. REE plot of Deer Canyon rhyolite samples. Chondrite values from Sun and McDonald (1989).

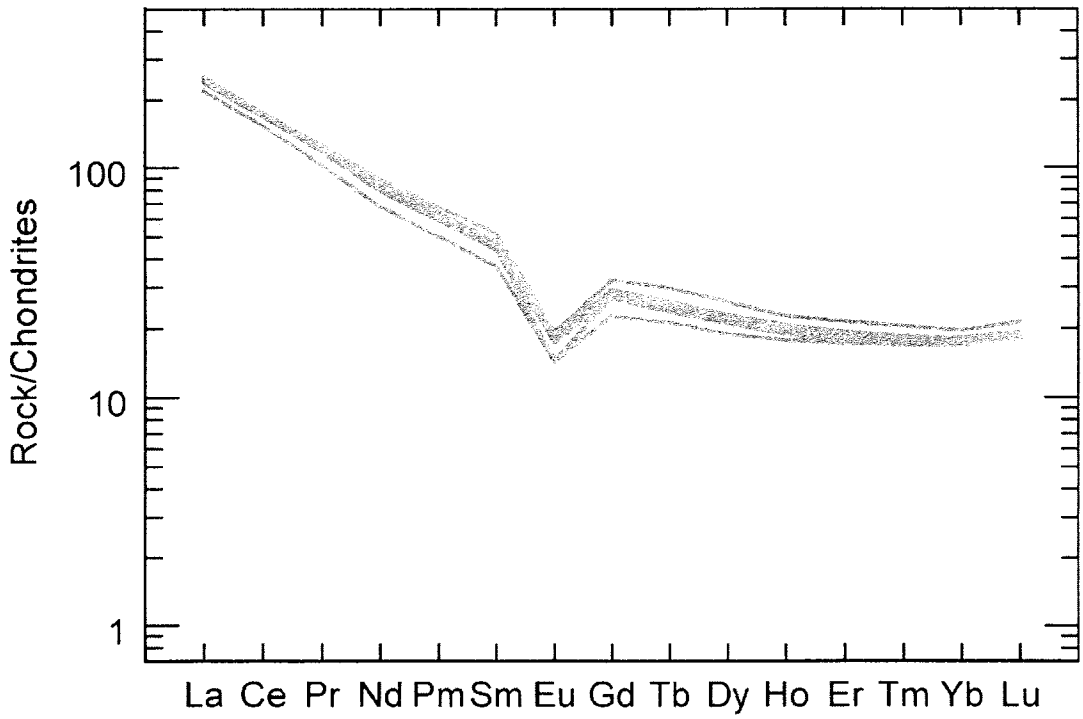

Figure 7.10. REE plot of Redondo Creek rhyolite samples. Chondrite values from Sun and McDonald (1989).

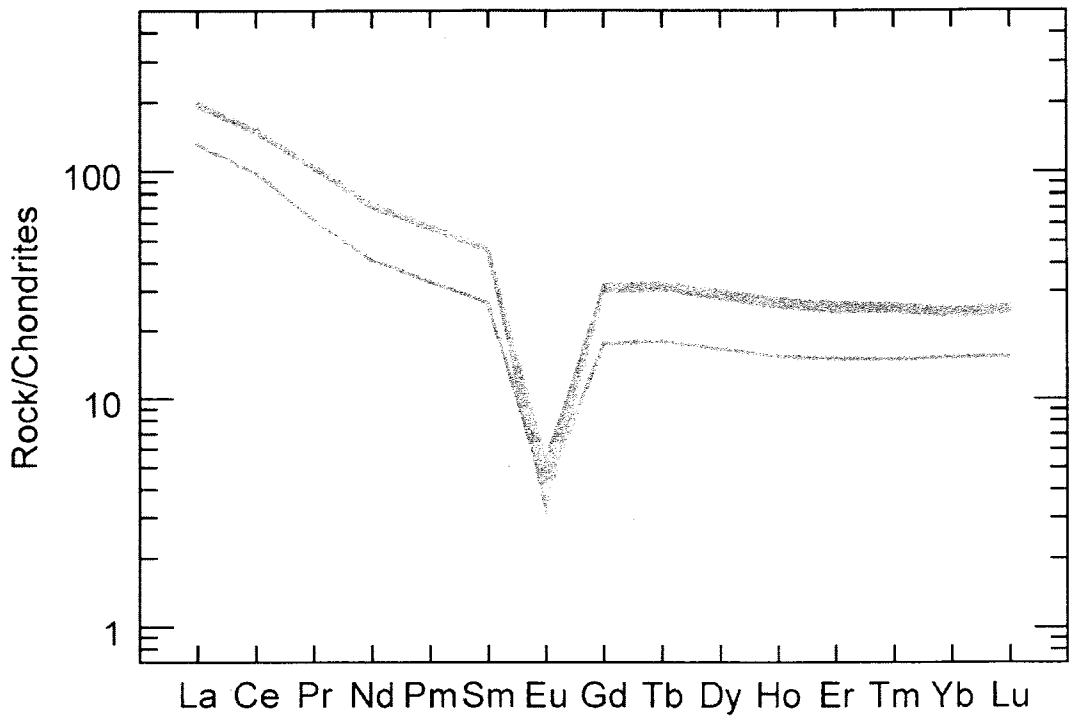

Figure 7.11. REE plot of Del Medio rhyolite samples. Chondrite values from Sun and McDonald (1989).

CHAPTER 8

U/PB ZIRCON ANALYSES

Sample preparation, previously discussed, yielded twenty-five zircons from Deer Canyon sample DC03 and thirty zircons from Redondo Creek sample RC07. No zircons were recovered from the Del Medio rhyolite. DC03 and RC07 epoxy mounted zircons were analyzed for their $^{206}Pb/^{238}U$ compositions using the University of California Los Angeles CAMECA ims 1270 ion microprobe. AS3 zircon standards (Paces et al., 1993; Schmitz et al., 2003) were analyzed between every five Deer Canyon or Redondo Creek analysis (Appendix F). In addition to ion microprobe spot analyses, cathodoluminescence (CL) imaging was used in order to examine selected zircons for internal zonation (Figures 5.31 and 5.34).

The $^{238}U/^{206}Pb$ ages obtained in this study are disequilibrium corrected ages (Schmitt et al., 2002). This is because for young samples such as the Deer Canyon and Redondo Creek rhyolites, the interval before secular equilibrium (~350 ka) is established is significant and must be corrected for. A total of 48 individual $^{238}U/^{206}Pb$ spot ages, 27 from Deer Canyon and 20 from Redondo Creek, were measured.

Weighted mean zircon crystallization ages were calculated using Isoplot software from the Berkley Geochronology Center (Ludwig, 2003). In addition, possible age spans

of zircon crystallization were calculated by grouping 4 of the youngest ages and 4 of the oldest ages for each unit and recalculating their weighted means. All uncertainties are reported as 1σ.

Deer Canyon Rhyolite

Deer Canyon zircons are ~100 μm long, generally euhedral and have visible cores surrounded by concentrically zoned overgrowths, which can be seen with cathodoluminescence images (Figure 8.01). Core and rim analyses were performed both singularly and as pairs on individual zircons in order to determine the ages of the innermost and outermost zones respectively. $^{206}Pb/^{238}U$ ages are older in the cores and younger on the rims in every core-rim analyses pair (Figure 8.01). Ages range from 4.83 ± 0.16 Ma to 5.58 ± 0.12 Ma and average 5.27 ±0.25 Ma (Appendix F). These zircon ages are significantly older than the $^{40}Ar/^{39}Ar$ eruptive age of 1.26 ± 0.02 Ma measured on sanidine phenocrysts by Phillips (2004) (Figure 8.02).

The Mean Square of Weighted Deviates (MSWD) for the 27 analyses performed on sample DC03 exceeds the 1.68 MSWD for a single population (Wendt and Carl, 1985). Thus, in order to provide an estimate of pre-eruptive crystallization ages, zircons with the highest weighted residuals were sequentially excluded until the MSWD value was acceptable for a single population. A weighted mean crystallization age of 5.17 ± 0.09 Ma and associated MSWD value of 1.5 was calculated using 23 of the 27 $^{206}Pb/^{238}U$ ages (Figure 8.03, Table 8.01). Deer canyon zircons range in age between weighted mean minimum age of 4.90 ± 0.14 Ma (MSWD = 0.02) and maximum age of 5.45 ± 0.160 Ma (MSWD = 0.87). Both minimum and maximum ages were calculated using the youngest

4 and oldest four ages from the coherent group of 23 used to calculate the mean crystallization age.

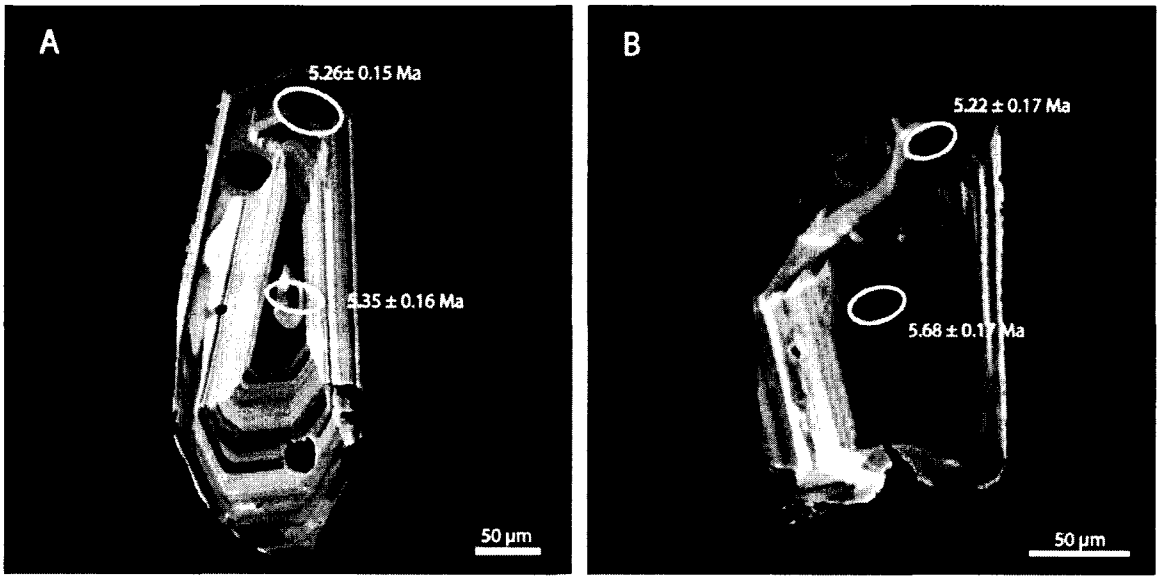

Figure 8.01 A and B. Cathodoluminescence images of representative DC03 zircons showing core and rim ages obtained by ion microprobe. Ellipses represent the locations of individual analyses. Concentric core to rim zoning on these euhedral zircons is seen by the light and dark rings. Figure 8.01A suggests an ~100 ka difference in age from core to rim. Figure 8.01B shows an ~ 460 ka difference in age from core to rim. Note that these zircons are ~3.6 to 4.3 Ma older than the eruption age of the Deer Canyon rhyolite (see text).

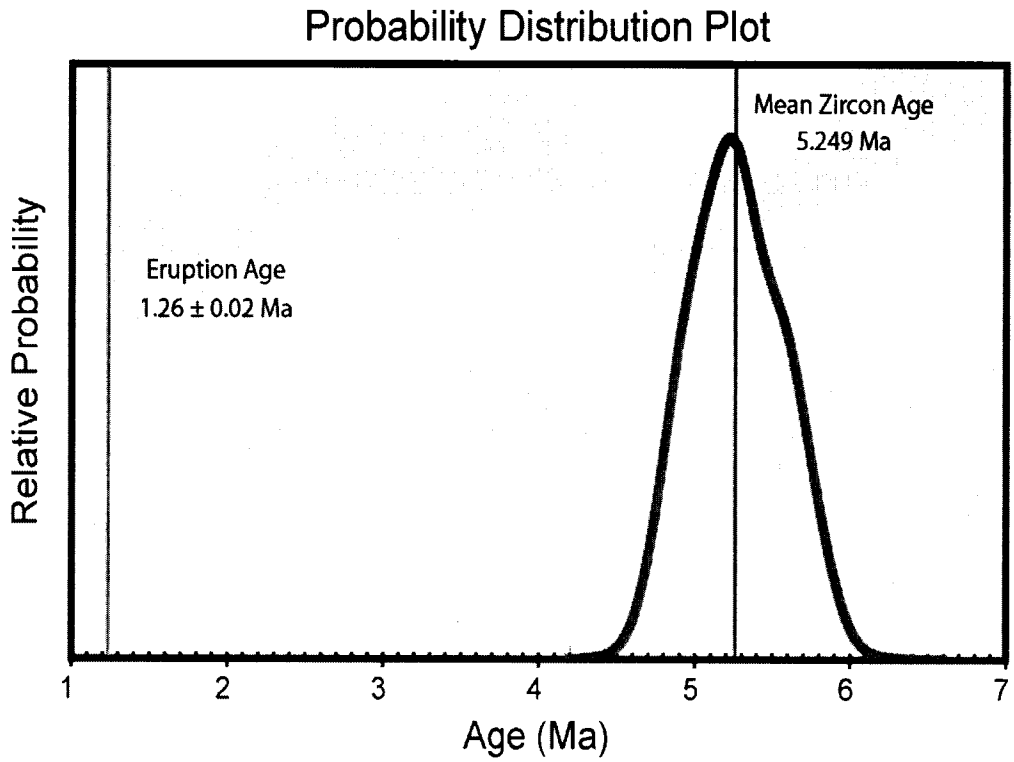

Figure 8.02. Probability distribution plot of the Deer Canyon DC03 zircon population. Eruption age indicated with red bar on the left was reported by Phillips (2004). Mean zircon age of 5.25 Ma is indicated by the blue vertical line.

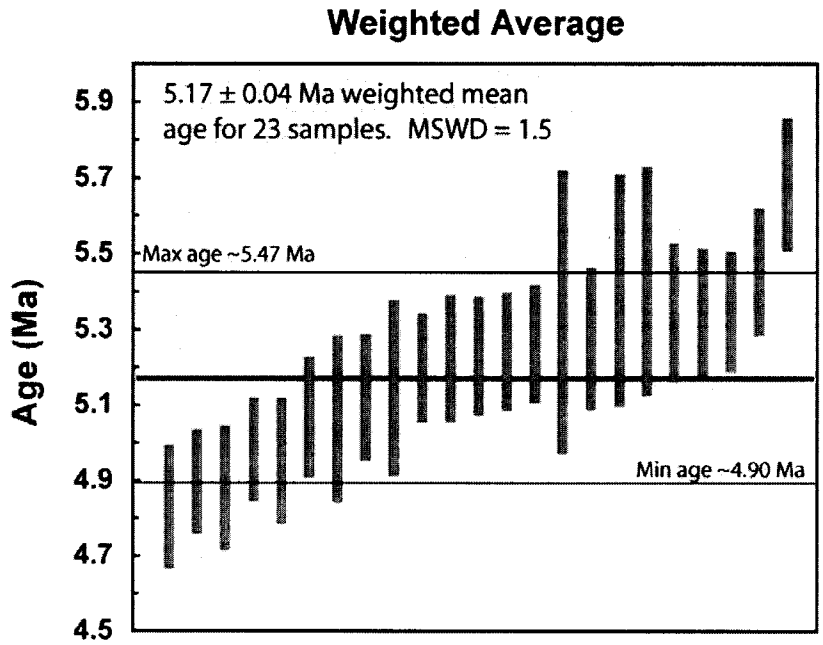

Figure 8.03. Plot showing the weighted Deer Canyon DC03 rhyolite average of 23 $^{238}U/^{206}Pb$ zircon crystallization ages. Boxes heights are 1σ.The maximum age possible is 5.45 ± 0.16 Ma and the minimum age possible is 4.90 ± 0.14 Ma. The green line represents the weighted mean of 5.17 ± 0.04 Ma.

Redondo Creek Rhyolite

Redondo Creek zircons are subhedral to anhedral, fractured and have rounded cores surrounded by slightly zoned overgrowths (Figure 8.04). A range of $^{238}U/^{206}Pb$ ages, from 0.97 ± 0.24 to 1.60 ± 0.35 Ma, were calculated from a near Gaussian distribution for Redondo Creek zircons from 19 of the 20 analyses (Figure 8.05). The mean of these ages is 1.29 ± 0.15 Ma. An anomalously old age (23.17 ± 1.34 Ma) from a xenocrystic zircon was obtained, but was excluded from the data set. A weighted mean zircon crystallization age of 1.29 ± 0.04 Ma (MSWD = 0.51) was obtained. This MSWD is within the limits of acceptable values for the 19 spots analyzed and is thus representative of a single population of ages (Figure 8.06, Table 8.01). RC07 zircons range in age between weighted mean minimum age of 1.10 ± 0.22 Ma (MSWD = 0.17) and maximum age of 1.44 ± 0.28 (MSWD = 0.13). Within uncertainty, Redondo Creek zircon ages range from 1.61 Ma the eruption age of the Lower Bandelier Tuff to 1.23 Ma the eruption age of the Del Medio rhyolite. Redondo Creek's weighted mean zircon crystallization age of 1.29 ± 0.04 Ma is 70 ka older than the eruption age of 1.22 Ma reported for this unit (Phillips, 2004).

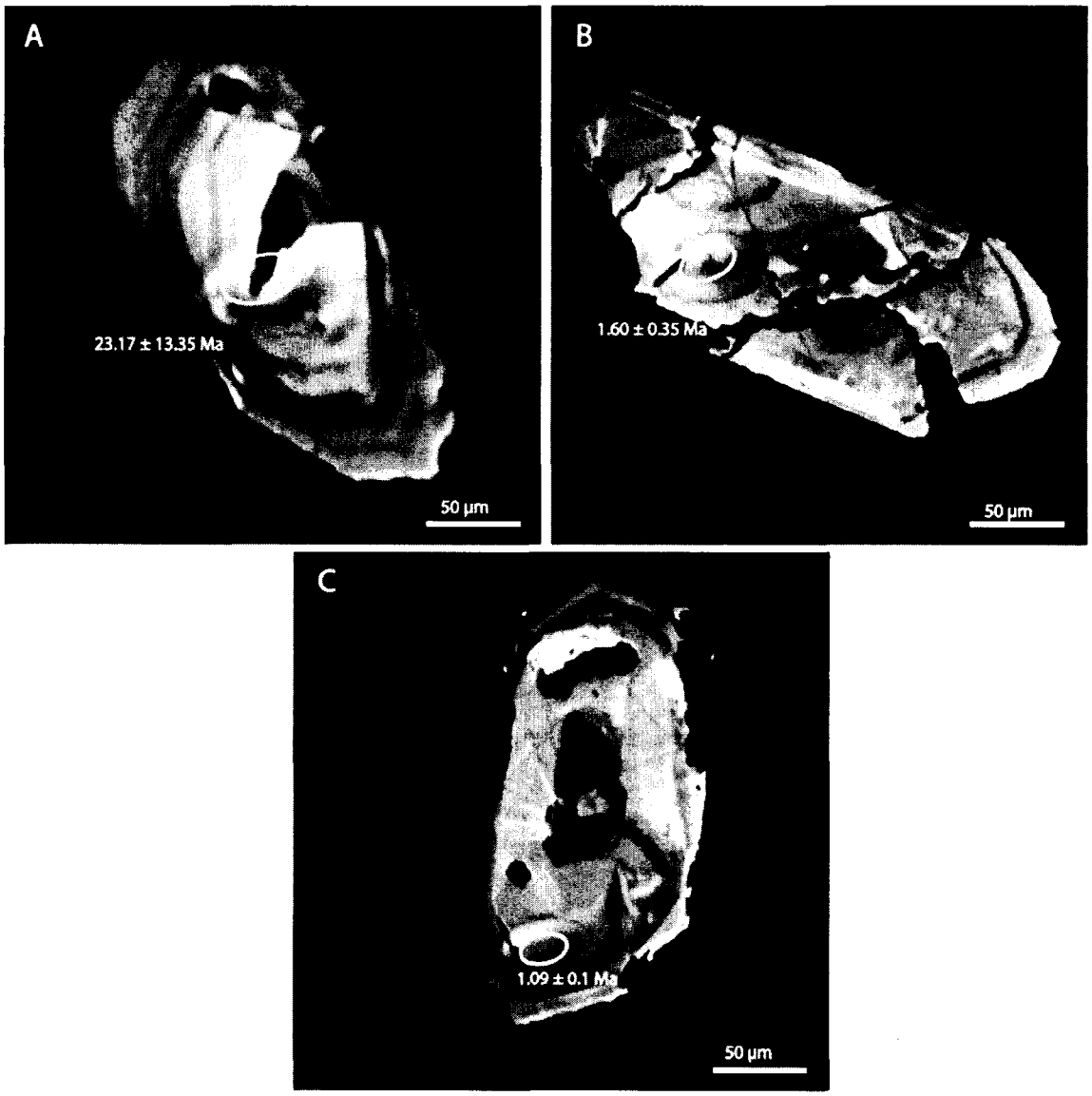

Figure 8.04. Cathodoluminescence images of RC07 zircons showing ages obtained by ion microprobe. Ellipses represent the locations of individual analyses. Zoning on these euhedral to subhedral, fractured zircons appears to be generally restricted to the rims as shown by light and dark bands. Xenocrystic, zoned zircon with core age of ~ 23 Ma (A). Fractured zircon with euhedral crystal form, zoned rim (B). Subhedral zircon with zoned rim (C).

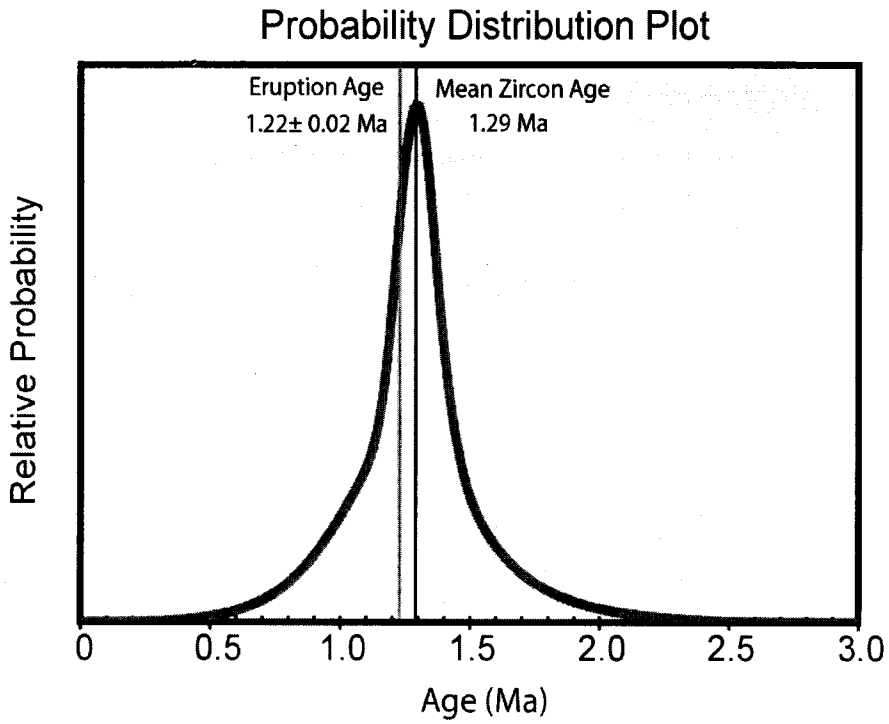

Figure 8.05. Probability distribution plot of Redondo Creek RC07 zircon population. Eruption age indicated with red bar on the left was reported by Phillips (2004). Mean zircon age of 1.29 Ma is indicated by the blue bar on the right.

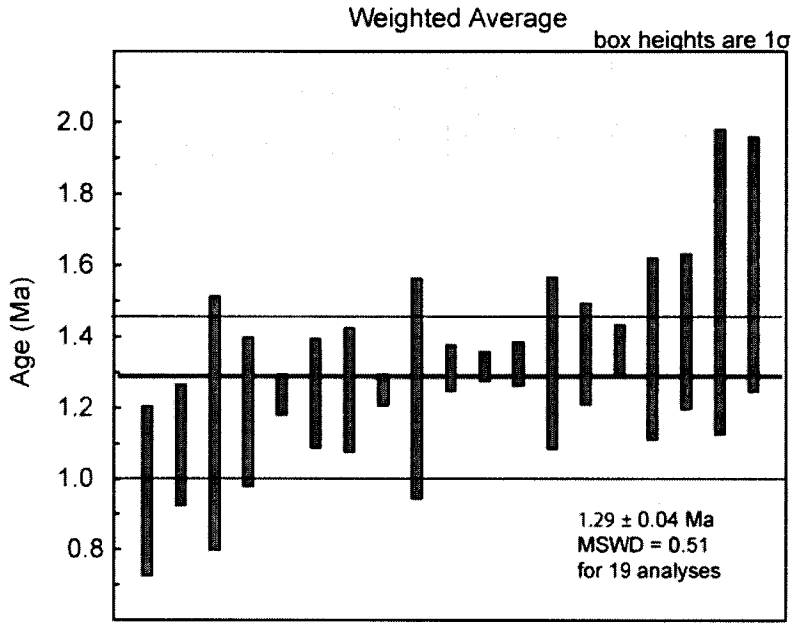

Figure 8.06. Plot showing the weighted average of 23 $^{238}U/^{206}Pb$ zircon ages. The green line is the weighted mean of 1.29 ± 0.04 Ma. The maximum age possible is 1.44 ± 0.28 Ma and the minimum age is 1.10 ± 0.22 Ma.

Table 8.01. Summary of zircon crystallization ages of Deer Canyon and Redondo Creek rhyolites[a]

Sample	Mean Age (Ma)	Analyses (n)	Grains	MSWD[b]	Eruption age (Ma)[c]	Mean Pre-eruption age (Ma)[d]	Limits on age range (Ma)[e] Min (n, MSWD)	Max (n, MSWD)
DC03	5.249 ± 0.235 (n=27)	27	18	1.5 (1.7)	1.256 ± 0.015	5.171 ± 0.091 (n=23)	4.904 ± 0.140 (n=4, 0.19)	5.447 ± 0.160 (n=4, 0.87)
RC07	1.292 ± 0.145 (n=19)	19	19	0.2 (1.7)	1.224 ± 0.017	1.288 ± 0.040 (n=19)	1.098 ± 0.220 (n=4, 0.17)	1.443 ± 0.280 (n=4, 0.13)

[a] All uncertainties are reported as 1σ. [b] Mean Square of Weighted Deviates (MSWD). Value in parentheses is the highest value expected at the 95% confidence interval for normal scatter within a single age population (Wendt and Carl, 1985).
[c] Ar/Ar eruptions ages from Phillips (2004).
[d] Mean pre-eruption ages were determined by the sequential omission of analyses with the highest weighted residuals in Deer Canyon rhyolite.
[e] Minimum and maximum ages were determined by pooling 4 of the youngest and oldest ages respectively.

CHAPTER 9

INTERPRETATIONS OF PETROGRAPHY, PHENOCRYST CHEMISTRY AND ZIRCON $^{238}U/^{206}Pb$ AGES

Interpretations from Petrography

Observations on the variable textures of Deer Canyon, Redondo Creek, and Del Medio rhyolites show that these units are petrographically heterogeneous. Deer Canyon has two distinct textural types, sparsely porphyritic and porphyritic, Redondo Creek is porphyritic and Del Medio is sparsely porphyritic to aphyric (Figure 5.01). The petrographic differences in these units are the result of distinctive crystal growth and magma differentiation histories.

Aphyric Rhyolites

Aphyric rhyolites could be formed from relatively hot magma generated and erupted rapidly, which is in contrast to porphyritic magmas undergoing slow cooling. The rhyolite units in this study can be arranged in order from most aphyric (possibly hottest) to most porphyritic (possibly coolest) based on percent phenocrysts. Del Medio has 3%, type A Deer Canyon has 4%, Redondo Creek has 16%, and type B Deer Canyon has 22% phenocrysts. Redondo Creek ilmenite/magnetite pairs record a temperature of 810 ± 6°C (Phillips, 2004), whereas the temperatures of Deer Canyon and Del Medio rhyolites have not been constrained. The data above allow that aphyric textures of Deer Canyon and Del

Medio rhyolites could have formed by the rapid eruption of relatively hot magmas, which inhibited phenocryst crystallization.

An alternative explanation is that the aphyric to sparsely porphyritic textures of Deer Canyon and Del Medio rhyolites were formed as a result of the removal of liquid from a partially crystalline mush. This model involves extraction of interstitial liquid from silicic crystal mushes of granodiorite composition on time scales ranging from 10^4 to 10^5 years (Bachman and Bergantz, 2004). An important point is that when these crystal mushes have reached approximately 40 to 45% crystallinity the interstitial liquid is of rhyolitic composition (Cashman and Blundy, 2000; Bachmann et al., 2002; Schmitt et al., 2003). In this model the crystals are effectively left behind and crystal poor rhyolite produced from the interstitial melt does not have to be a high temperature rhyolite.

The time required to extract enough melt to produce the small volumes of rhyolite represented by the Deer Canyon and Del Medio rhyolite eruptions has to be shorter than the residence time of mushes in the crust. One model, based on Rb/Sr isochrons from Glass Mountain lavas, Long Valley, California, is that silicic magmas may reside in the crust for up to 700 ka (Haliday et al., 1989). Such prolonged residence has been rejected in more recent studies because of two major problems; the delicate heat balance required to keep a system liquid in the crust for such long periods of time, (Sparks et al., 1990), and long residence time results in contamination from wall rock, thus producing invalid Rb/Sr ages (Kensel et al., 1999). Current models suggest that phenocrysts are retained in thermally changing crystal mushes, which are cooled and reheated over long intervals (Hildreth and Wilson, 2007). Hindered settling, micro-settling, and compaction are three processes that when working together, could separate enough melt from interstitial spaces

in crystal mushes to produce multiple eruptions of small volume aphyric rhyolite, or to produce crystal poor rhyolite in large-scale caldera forming eruptions (Figure 9.01) (Bachman and Bergantz, 2002; Hildreth and Wilson, 2007). In shallow, water-rich systems, gas driven filter pressing could accelerate the production of crystal poor rhyolitic melt. Gas driven filter pressing may occur in silicic mushes where water-rich interstitial melts (average 4-6 wt.% H_2O, and range up to 8 wt. % H_2O) are stored in the upper crust (Bachmann and Bergantz, 2004). When these melts reach volatile saturation a low density, low viscosity fluid phase is exsolved (Wallace et al., 1995; Wallace et al., 1999). Overpressure following exsolution of the gas phase drives the interstitial melt out of the matrix, effectively separating melt from crystal mush (Sisson and Bacon, 1999).

The crystal mush model (Figure 9.01) explains crystal poor rhyolites as having formed by leaving the crystals behind. Such a model could explain production of the aphyric to sparsely porphyritic rocks of type A Deer Canyon and Del Medio rhyolites. Immediately following such a major caldera forming event as the eruption of the Upper Bandelier Tuff, one might logically expect a residual crystal mush to exist in the magma system beneath the caldera, setting the stage for this model. This is because large caldera forming eruptions evacuate only a fraction of the magma generated in the crust (Bachmann and Bergantz, 2004).

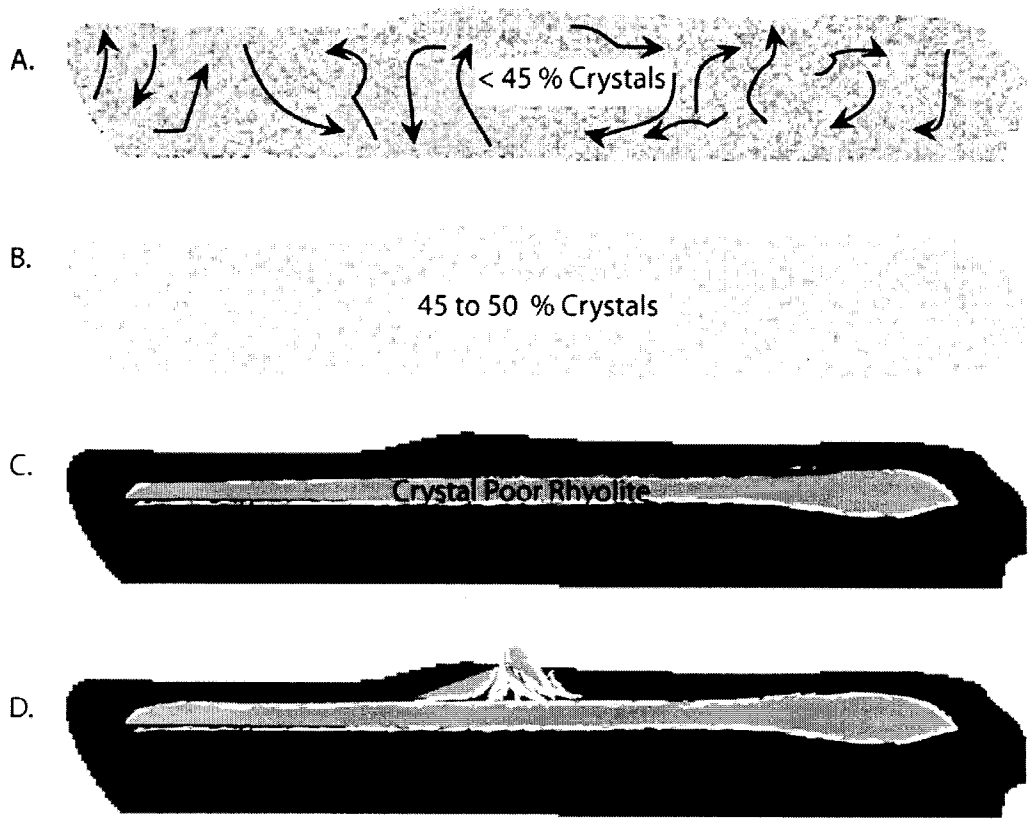

Figure 9.01. Model for the formation of aphric to sparsely porphyritic rhyolites. Modified from Bachman and Bergantz (2004). (A) Dacite magma is cooling. Crystals remain in suspension. Phenocrysts percentages are less than 45%. (B) Interstitial melt is rhyolitic in composition when phenocryst percentages reach 45 to 50 %. A rigid framework hinders convection and melt is extracted from the crystal mush. (C) A rhyolite horizon develops above the crystal mush and below a cool crystallizing roof. (D) Aphyric rhyolites erupt on the surface.

Resorption Textures

All three units contain phenocryst assemblages and textures indicating that during magma genesis relatively low temperature silicic magma, possibly undergoing fractional crystallization, could have been reheated. Phenocryst assemblages and textures also suggest that crystals could have been transferred to higher temperature magma. Textural evidence for thermal excursions or magma mingling is seen in the form of embayed and resorbed quartz and resorbed plagioclase phenocrysts found in Deer Canyon rhyolite, resorbed plagioclase with antirapakivi texture found in Redondo Creek rhyolite and patchy zoned sanidine found in Del Medio rhyolite. EMPA analyses of plagioclase in Deer Canyon and Redondo Creek rhyolites document andesine with resorption surfaces, which suggests that it could have crystallized in a dacitic magma before becoming unstable and partially resorbed by mingling with hotter magma of a more mafic composition. In addition, textural evidence in the form of resorbed quartz, and sanidine overgrowths support the idea that these crystals were transferred between magmas where they underwent alternating dissolution and regrowth during their crystallization histories. Andesites and dacites from the Abu volcano group, southwestern Japan, show textural evidence for magma mingling (Koyaguchi, 1986), which is similar to the resorption seen in quartz and plagioclase in Deer Canyon and Redondo Creek rhyolites. The textural results of mingling partially crystallized dacite and basalt magmas are resorbed quartz, sodic plagioclase and basaltic inclusions in the dacite. During mingling higher temperature basalt was quenched to produce inclusions, while phenocrysts in the lower temperature dacite underwent dissolution to produce resorption. Chemical evidence in the form of increasing FeO, and MgO with increasing SiO_2 supports the textural evidence for

mixing in the Abu volcano group (Koyaguchi, 1986). Although Deer Canyon, Redondo Creek and Del Medio rhyolites are much more silicic than the Abu group dacites and andesites, and they do not contain any mafic inclusions, the dissolution textures and zoning seen in individual phenocrysts is suggestive of similar magma mingling processes.

Brown Glass Inclusions in Redondo Creek Plagioclase

Redondo Creek rhyolites commonly have highly resorbed plagioclase and in a few cases these phenocrysts house multiple brown glass inclusions (Figure 5.06). Mafic composition glass is typically brown, whereas silicic glass is usually clear. Unfortunately, no chemical data was gathered on the brown glass during EMPA analysis. These textures suggest that resorption of plagioclase in Redondo Creek rhyolite may have been precipitated by the introduction of mafic magma into the rhyolite magma.

Antirapakivi Texture

Anorthoclase rimmed plagioclase found in Deer Canyon, and sanidine rimmed plagioclase found in Redondo Creek rhyolites (Figure 5.05), are examples of antirapakivi textures. Antirapakivi feldspar develops when pressure, temperature or compositional changes have occurred in the magma chamber (Hibbard, 1981, Nekvasil 1991). One mechanism that can produce this texture is when plagioclase growing in a more mafic magma, such as andesite or dacite, is transferred to a rhyolite magma and alkali feldspar overgrowths form. Sharp contacts between plagioclase and alkali feldspars suggest that the event that precipitates the transition to potassium rich feldspar has to be sudden in order for the outer zone of these crystals to form. This could result when ascension of phenocryst bearing mafic magma to a rhyolitic magma chamber causes exchange of

crystals, or alternatively as a result of the sudden loss of volatiles (eruption) from a sub-volcanic magma chamber (Hibbard, 1981).

Interpretations from Phenocryst Chemistry

The zonation in phenocrysts are interpreted as reflecting open system magma genesis. Evidence for magma mingling and mixing recorded in feldspar phenocrysts is exhibited in the form of partial (e.g. DC03-1, Figure 5.02, and 6.03) to advanced (e.g. RC12-14) dissolution and resorption, distinct zones of dramatically varying composition (e.g., RC12-4, Figure 6.05), and overgrowth textures on previously resorbed crystals (e.g., RC07-12, Figure 6.04A).

Feldspars in all three rhyolite units exhibit characteristic compositional zonation which provides a record of crystallization history. Numerous studies have used major element zoning patterns exhibited by plagioclase to constrain magma chamber dynamics (e.g., Anderson, 1983; Nixon and Pearce, 1987; Pearce et al., 1987; Pearce and Kolisnik, 1990; Singer et al., 1995; Tepley et al., 1999; Ginibre et al., 2002). The interpretation that large fluctuations in An content reflect major thermal and compositional changes in magma chambers, whereas small fluctuations, such as oscillatory zoning, may be the result of convection is based on experimental studies of crystallization (Lofgren, 1974), resorption (Tsuychiyama, 1985) and numerical modeling (Allègre et al., 1981; Lasaga, 1982; Loomis 1982; L'Heureux and Fowler, 1994).

Feldspars in Deer Canyon, Redondo Creek, and Del Medio rhyolites are normally, reverse and complexly zoned. Plagioclase with normal zonation reveals growth patterns that become more Na rich from core to rim. Such normal zonation occurs during

fractional crystallization accompanied by progressive temperature drop. Reverse zonation refers to the opposite situation in which core to rim growth patterns exhibit increasing Ca. This could occur following an abrupt change in magma chamber conditions, such as a compositional change to more mafic magma and rapid temperature rise (Hibbard, 1991; Troll and Schminke, 2001; Ginibre et al., 2002, 2004). Complex zonation refers to growth patterns where chemistry oscillates between sodic and calcic compositions.

Two types of complex zonation and their respective petrogenetic origins have been proposed (Pearce and Kolinsky, 1990). Type I zoning is repetitive and occurs in minute regions, 1-10 μm wide, with ΔAn of 1-10%. Zonation in this case is thought to be controlled by minor temperature and pressure changes due to convection, or localized effects during growth (Hasse et al., 1980; Pearce and Kolinsky 1990; Pearce, 1993; Singer et al., 1995; Tepley et al., 1999). Type II zonation occurs over larger regions, up to 100 μm wide, with large ΔAn of 10-25%. This type of phenocryst zonation is thought to reflect changes, such as magma mixing or mafic recharge during crystallization in open system conditions (Tepley et al., 1999).

An andesine phenocryst, DC03-2 exhibits ΔAn of 4-9% within 10 μm intervals (Figure 9.02, Appendix B), suggesting that minor changes in temperature and or pressure were occurring in the magma chamber. An andesine phenocryst DC03-1, exhibits step like An_{40} to An_{34} zoning within ~100 μm and ΔAn of up to 18% (Figure 6.03, Appendix B), which requires open system conditions in which mixing or recharge was occurring. Phenocrysts analyzed in Deer Canyon and Redondo Creek show zoning patterns that suggest mixing between distinct magmas was occurring, while zonation in Del Medio

feldspars could have been a result of localized convection and minor changes in temperature and pressure.

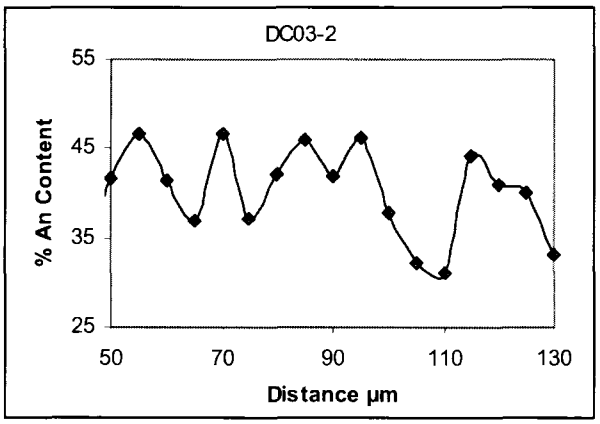

Figure 9.02. Repetitive fine scale zonation seen in andesine from Deer Canyon rhyolite.

Deer Canyon Feldspar Zoning

Deer Canyon alkali feldspars contain compositions from sanidine with Or_{60}, through the entire anorthoclase range to Or_{10} and plagioclase with compositions from andesine with An_{46} to oligoclase with An_{24} (Appendix B). Zonation is complex and characterized by large ΔAn up to 18% in plagioclase and ΔOr up to 30% in anorthoclase to relatively small compositional changes (Figure 9.03, Appendix B). Subtypes of these models will be used to describe the oscillatory zoning and the petrographic character of Del Medio rhyolites in more detail (Figures 9.06 and 9.07).

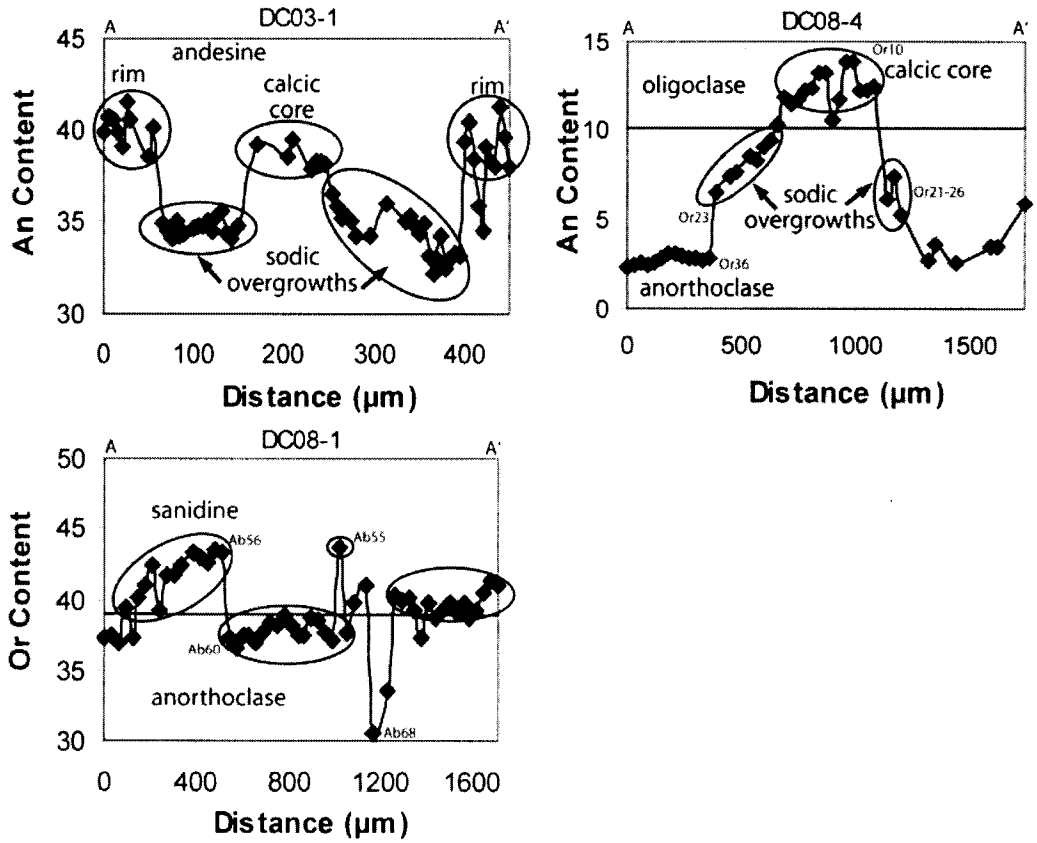

Figure 9.03. Complex zoning exhibited by Deer Canyon feldspars.

Redondo Creek Feldspar Zoning

Redondo Creek alkali feldspars are mostly sanidine with compositions ranging widely from Or_{38} to O_{57} and plagioclase feldspars ranging from oligoclase with An_{19} to andesine with An_{39} (Figure 6.02, Appendix B). Changing magmatic conditions are suggested by step like An_{22} to An_{38} zonation over ~80 μm intervals, and by normal zonation within the cores followed first by resorption textures and then by sanidine overgrowths along the rims (e.g., phenocryst RC12-2, Figure 6.04). Antirapakivi textures seen in Redondo Creek feldspars could be caused by the overgrowth of sanidine on plagioclase following

minor resorption which was due to an increasing temperature excursion (Figure 6.05, Figure 9.04).

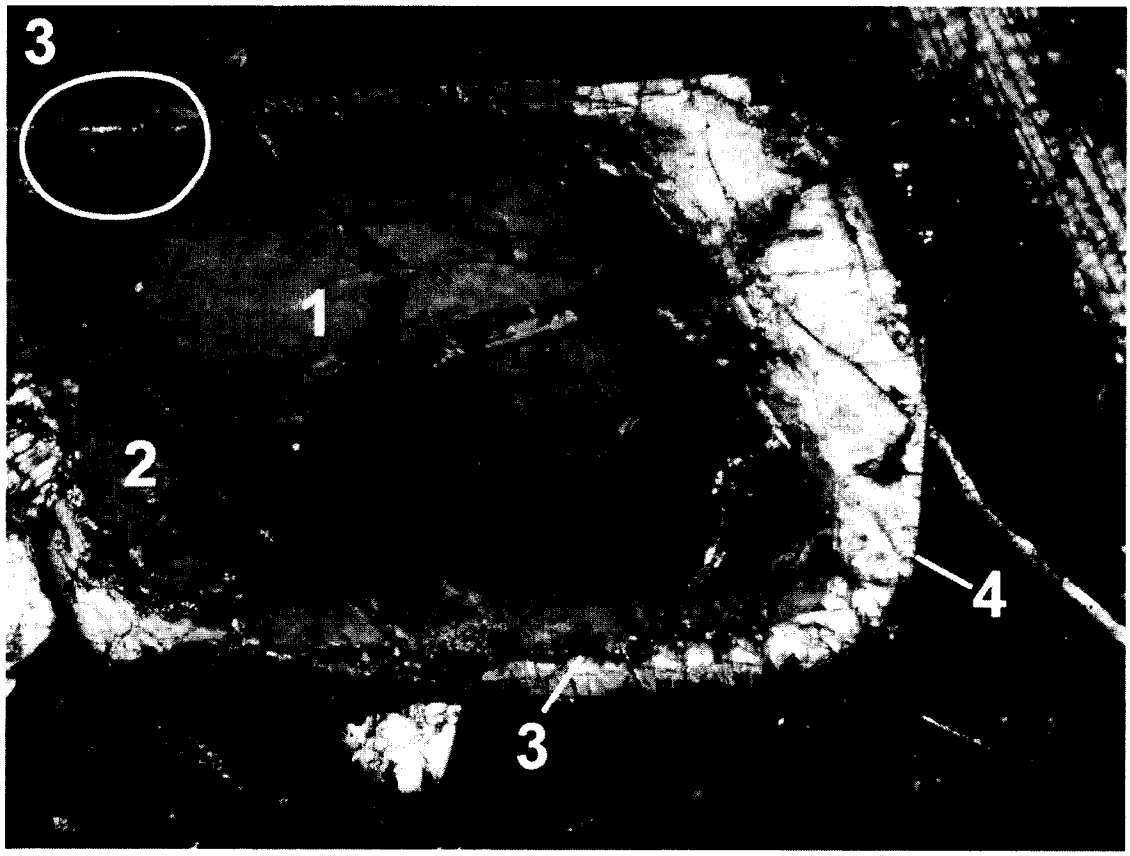

Figure 9.04. Phenocryst RC12-4 exhibiting (1) Andesine core. (2) Oligoclase overgrowth. (3) Irregular resorption surface. Circled region shows truncation of oligoclase overgrowth. (4) Sanidine overgowth. Cross polarized light. Width of image is 1.1mm.

Del Medio Feldspar Zoning

Del Medio compositions include alkali feldspars ranging from anorthoclase with Or_{24} to sanidine with Or_{47} (Figure 6.02, Appendix B). Phenocrysts exhibit patchy zonation with minor fluctuations in composition of ~ΔOr_4 to ~ΔOr_7. For example, sample DM2-10-2 has compositions ranging from Or_{20} and Or_{27} (Figure 9.05). Zonation in Del Medio

feldspars could be related to minor fluctuation in temperature and pressure during crystallization (Hibbard, 1981, Ginibre et al., 2004).

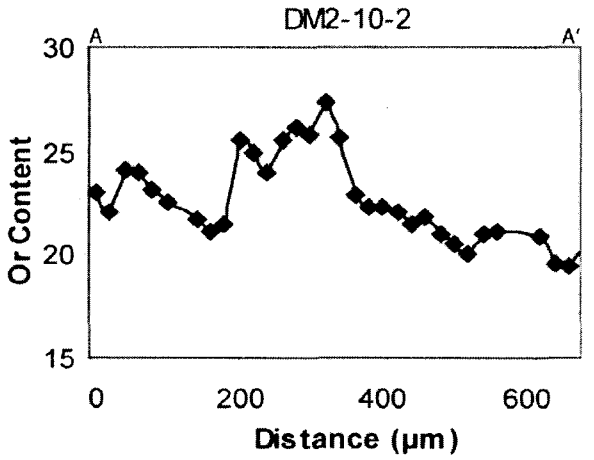

Figure 9.05. Patchy zonation in Del Medio alkali feldspar showing minor fluctuations in mineral composition.

Petrogenetic Models for Deer Canyon Rhyolite Feldspars

Zoning and resorption in Deer Canyon anorthoclase, andesine, and oligoclase could have been produced when crystals were transferred between different composition magmas. This could have been accomplished by the injection of more mafic magma into silicic magma combined with crystal settling. Feldspars in the Gran Canaria ignimbrite 'A', Canary Islands, are similar in zoning to Deer Canyon feldspars (Troll and Schminke, 2002). Oligoclase cores are overgrown by anorthoclase which is overgrown by oligoclase producing an oscillatory pattern hundreds of μm wide. A similar model to that proposed here was used in which crystals were moved within the magma chamber and across compositional boundaries producing complex zoning with large compositional changes in

phenocrysts. Resorption textures in anorthoclase and oligoclase phenocrysts were attributed to the exchange of crystals from one magma to another (Troll and Schmincke, 2002). The chemistry and textures of biotite, plagioclase, hornblende and quartz phenocrysts found in Chaos Crags, Lassen Volcanic Center, California, suggests that phenocrysts were crystallized in a silicic magma, transferred to a mafic magma, partially resorbed, subsequently overgrown, then recycled back into the silicic magma (Tepley et al., 1999).

The following complex zoning models for plagioclase and alkali feldspar attempt to explain the texture and composition of the Deer Canyon feldspars. These models are similar to those proposed by Troll and Schmincke (2002). In addition the model to describe type A Deer Canyon rhyolite requires a previous step in which the 4.9-5.4 Ma xenocrystic zircons were incorporated into the rhyolitic melts. The melt was produced when more mafic magma rejuvenated an old 4.5 to 5.2 Ma plutonic body from previous magmatism in the Jemez volcanic field.

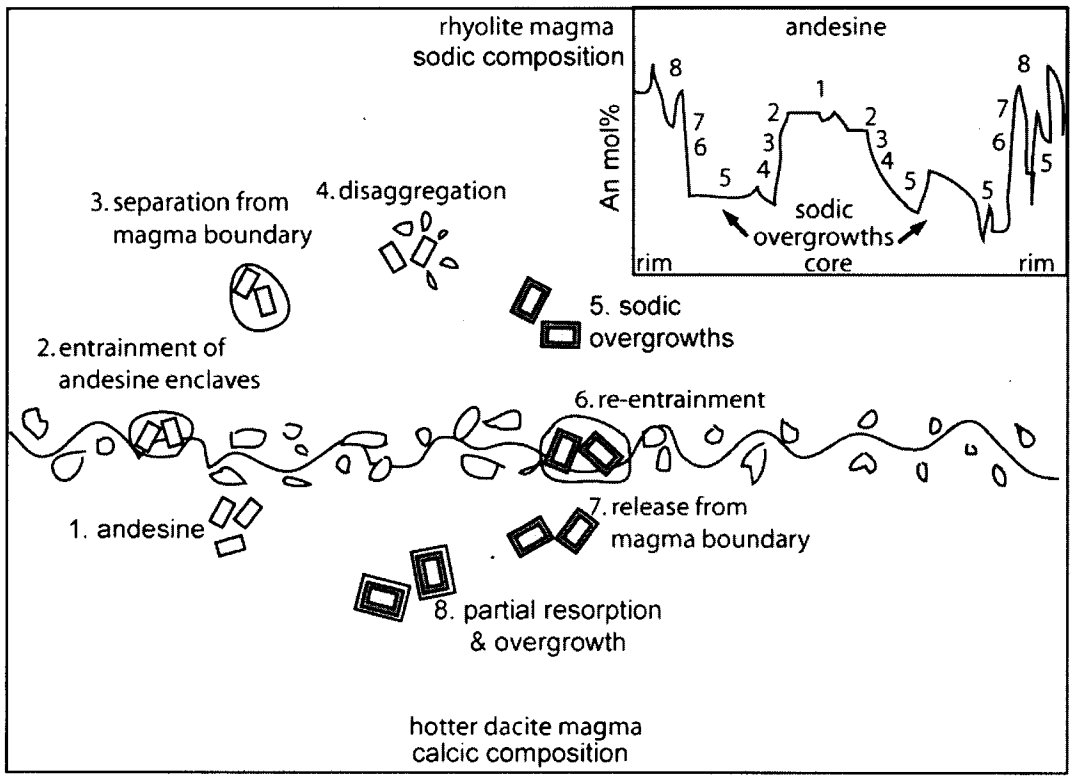

Figure 9.06. Model for the crystallization history of plagioclase in sparsely porphyritic type A Deer Canyon rhyolite, using mineral chemistry from line analysis of sample DC03-1.

Model to Produce Type A Deer Canyon Plagioclase

The steps in this model (Figure 9.06) are as follows: (1) Andesine phenocrysts grow in a less evolved dacite magma. (2) Viscous entrainment of enclaves containing andesine phenocryst occurs along the compositional boundary. (3) Batches separate into more evolved rhyolite melt by either volatile exsolution (Eichelberg, 1980) or by convection from within the rhyolite. (4) Enclaves are disaggregated (due to shearing or vesiculation). (5) Sodic overgrowths form on more calcic plagioclase cores. (6) Phenocryst bearing enclaves are isolated due to entrainment along the compositional boundary. (7) Phenocrysts are released from the compositional boundary into the dacite magma where

more sodic overgrowths are partially resorbed. (8) Renewed more calcic andesine overgrowths form along the phenocryst rims.

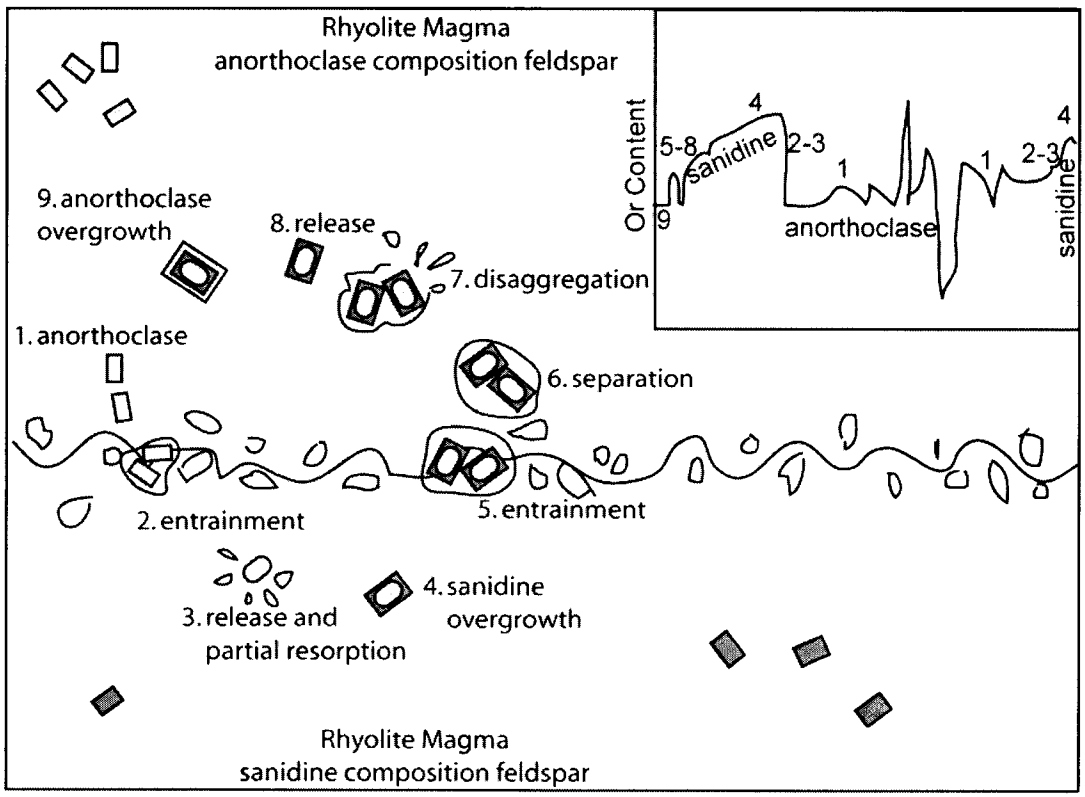

Figure 9.07. Complex zoning model to explain compositional changes in alkali feldspar using mineral chemistry from type B porphyritic Deer Canyon, sample DC08-1.

Model to Produce Type B Deer Canyon Plagioclase

The steps in this model (Figure 9.06) are as follows: (1) Anorthoclase grows in a rhyolite magma. (2) An influx of relatively Or rich rhyolitic magma produces a compositional boundary where enclaves containing feldspars become entrained. (3) Phenocrysts are released from the compositional boundary into the more Or rich magma. (4) Sanidine

overgrowths form on anorthoclase cores. (5) Phenocrysts become entrained at the compositional boundary. (6) Separation of phenocrysts bearing enclaves from boundary. (7) Phenocryst bearing enclaves are disaggregated. (8) Phenocrysts are released into anorthoclase composition magma. (9) Renewed anorthoclase overgrowths form.

The above modes of crystal transport and exchange are possible models to explain compositional zoning found in Deer Canyon. These models require the contemporaneous residence and mingling of several magmas in a single reservoir.

Petrogenetic Models for Redondo Creek Rhyolite Feldspars

Reverse Zoning

Reverse zoning cannot be explained by fractional crystallization. However, thermal and chemical disequilibrium in a system produced by the mingling of magmas of contrasting composition may promote textures that would not be produced in a single homogenous magma crystallizing in response to decreasing temperature. Reverse zoning seen in Redondo Creek rhyolite could be due to mingling with a more mafic magma. Reverse zoning in plagioclase has been attributed to changes in pressure, temperature, or melt composition as a result of interactions with less evolved melt (Bachman et al., 2002).

Normal Zonation and Antirapakivi Texture

Most Redondo Creek plagioclase exhibits normal zonation within the cores followed by abrupt overgrowths of sanidine producing antirapakivi texture. The sudden compositional change from plagioclase crystallization to sanidine requires a

compositional change in the magma where the crystals were forming, which suggests that magmas of different compositions were in contact during the crystallization history of Redondo Creek feldspars. Two similar models describe the mantling relationships of plagioclase, dendritic plagioclase, and K-feldspar to each other (Hibbard, 1981). The first model is for phenocrysts showing characteristics similar to Redondo Creek feldspars. Plagioclase is overgrown by K-feldspar (e.g., RC12-4, RC07-12, Figures 6.04 and 6.05) producing antirapakivi texture. The second model is for plagioclase phenocrysts overgrown by a dendritic plagioclase zone which becomes more sodic, overgrown by a K-feldspar rim (e.g., RC12-2, Figure 6.04). Such disequilibrium features may be produced by magma mixing (Hibbard, 1981). Decompression is an alternative model in which pressure changes result in rapakivi textures (Nekvasil, 1991). While decompression may produce rapakivi texture, it does not explain antirapakivi or the resorption textures in Redondo Creek rhyolite. The processes which form rapakivi textures must be very different from those that produce antirapakivi texture such as seen in Redondo Creek feldspars (Nekvasil, 1991).

Redondo Creek feldspars have a general tendency toward ovoidal shapes (Figures 6.04 A and 6.04 B). Since temperatures of differing composition magmas can vary by several hundred degrees, plagioclase that has previously crystallized in a more felsic magma may become partially resorbed and rounded when it is entrained in more mafic magma. This results in ovoid shaped phenocrysts and dissolution textures. A plausible model for the formation of Redondo Creek feldspars can be illustrated using the chemistry of phenocryst RC12-4. Phenocryst RC12-4 began its growth in a relatively hot dacite magma forming an andesine core (Figure 6.05, Appendix B). Subsequent cooling

and fractional crystallization produced normal zonation. A sudden transition due to magma mingling and phenocryst transfer to a rhyolitic composition magma produced oligoclase overgrowths. The abrupt compositional transition from andesine to oligoclase is an indication that magmas of contrasting compositions were mingled rapidly to affect drastic chemical changes. This was followed by resorption (Figure 9.04) along the oligoclase boundary, suggesting that the phenocryst was transferred back to a hotter magma. Finally sanidine formed when this magma mingled with a cooler more silicic rhyolite magma. In all, three separate magmas may have come into contact and mingled with each other to produce these complexly zoned feldspars.

Petrogenetic Model for Del Medio Rhyolite Feldspars

Del Medio feldspars consist of resorbed, patchy zoned sanidine and anorthoclase rimmed by sanidine (Figure 6.06A and B, Appendix B). Mechanisms described for the transfer of crystals between contrasting magma, including phenocryst exchange (Troll and Schmincke, 2002), replenishment (Tepley et al., 1999), and the models for Deer Canyon and Redondo Creek feldspars previously described do not explain the patchy zonation and resorption in Del Medio feldspars (Figure 6.06B). Zonation in Del Medio feldspars may have been produced by localized thermal and pressure perturbations. Recharge involving the injection of new more mafic magma as a source of heat beneath the cooler more felsic magma could provide the driving force for convection and subsequent local mixing in the overlying felsic magma and the resultant resorption and patchy zonation seen in Del Medio feldspar. An alternative model for resorption and patchy zoning in Del Medio alkali feldspars is that after crystals grew they were

transferred to a hotter magma and started to become resorbed. The resorbed areas were then filled in by newly crystallizing feldspar. A similar model for the Laacher See magma chamber "R-type" resorbed patchy zoned sanidines, which are similar to Del Medio sanidines, involves the bouyant rise of phenocrysts to produce patchy zonation (Ginibre et al., 2004). Crystals in a boundary layer rise until they reach equal density, at which time they spread out laterally into the interior of the magma body. Following lateral spreading crystals begin to sink into the hotter magma directly below.

Summary of Mineral Chemistry and Petrography

Deer Canyon and Redondo Creek rhyolites may represent successive eruptions which progressively tapped deeper levels of a compositionally zoned residual Bandelier Tuff magma (Phillips, 2004). However, the character of zonation in feldspars suggests that there may have been a more complex magmatic history. Compositional zonation is often abrupt and from tens to several hundreds of microns in width. These changes could not have been produced by convection within a single composition magma, convection in a zoned rhyolitic magma chamber, nor by minor pressure and temperature changes caused by convection which the simple magma chamber model above implies. In addition, both sanidine and plagioclase phenocrysts in each of the three units are partially to extremely resorbed, indicating that crystals were subject to large deviations in composition and/or temperature during their crystallization histories. Deer Canyon and Redondo Creek plagioclase often exhibit patterns of resorption surfaces associated with abrupt increases in An content, followed by a more continuous decrease in An at scales of 100 μm, which could be interpreted as a characteristic of magma mixing. Similar resorption

characteristics and minor and trace element zoning in dacite plagioclase at Parinacota Volcano, northern Chile, is indicative of magma mixing and recharge (Ginibre et al., 2002).

The distinct chemical zonation in feldspar and phenocryst assemblages of Deer Canyon, Redondo Creek and Del Medio rhyolites suggest that they are unrelated to each other and that they are not comagmatic. In addition, biotites exist only in Redondo Creek rhyolite, and clinopyroxenes are chemically distinct between Redondo Creek and Del Medio rhyolites (Figures 5.01B, 5.08 and 6.09, Appendix D).

$^{238}U/^{206}Pb$ Zircon Ages and Time Scales of Silicic Magmatism

Understanding the manner, timing and rate of zircon growth is important for making interpretations on the formation of large calderas and on the evolution of silicic magmas. The range of zircon ages for Deer Canyon and Redondo Creek rhyolites is an indication of time periods where compositional and thermal conditions were favorable to zircon growth, and thus provide a quantitative time scale for reconstructing the pre-eruptive history of these silicic magmas. In addition, the U/Pb ages and growth history seen in CL images of individual zircons from Deer Canyon and Redondo Creek rhyolites can be used to constrain the relationship between these units, the preceding Upper Bandelier Tuff, and the subsequently erupted Del Medio rhyolite. Similarly the lack of zircons in Del Medio rhyolite suggest that zircons were melted prior to eruption or that they never existed in the magma chamber.

Deer Canyon Zircons

The range of ages for Deer Canyon zircons is represented by the minimum and maximum weighted mean ages, 4.90 ± 0.14 and 5.45 ± 0.16 Ma respectively (Table 8.01), which indicates that Deer Canyon zircon had a crystallization interval between 240 and 840 ka. In agreement with these intervals, core-rim pairs record age differences between 100 and 460 ka. In addition, MSWD values for Deer Canyon zircons exceeds that expected for a single population (Chapter 8). These combined data indicate that crystallization of Deer Canyon zircon population was protracted, between 100 to 840 ka.

The timing of zircon crystallization is expected to accompany crystallization of the major mineral phases in rhyolites (Simon and Reid, 2005). The weighted mean crystallization age of Deer Canyon zircons, 5.17 Ma (Table 8.01), is significantly older (3.91 Ma) than the sanidine eruption age of 1.26 Ma (Phillips, 2004), and predates the formation of the Toledo (1.61 Ma) and Valles (1.26 Ma) calderas and the eruption of the upper Bandelier Tuff by approximately 3.56 and 3.91 Ma respectively. These ages thus imply that Deer Canyon zircons could not have crystallized at the same time as the major mineral phases (Table 5.01). These zircon ages also imply that Deer Canyon rhyolite is not the product of residual Bandelier Tuff magma. Zircon ages typically predate eruptions by tens of thousands (Reid and Coath, 2000) up to 200 ka (Schmitt et al., 2002; Miller and Wooden, 2004; Simon and Reid, 2005; Bindmen et al., 2006). Therefore, the most straightforward interpretation is that they represent xenocrysts incorporated during the melting event that produced the Deer Canyon rhyolite magma.

The growth history is recorded in CL images which show euhedral zircons with concentric growth bands surrounding each core. Cores are euhedral, but some are

truncated (Figure 8.01), which indicates that changes in the thermal conditions or magma compositions of the magma chamber occurred during their crystallization history producing resorption. Zircons also have minor resorption textures along the crystal edges (e.g. truncation of growth zones), an indication that these crystals were beginning to undergo dissolution immediately prior to their eruption, but that they did not have time to be strongly resorbed or to produce new zircon growth during subsequent cooling and crystallization (Figure 8.01).

These observations suggest that the Deer Canyon magma must have been rapidly generated and erupted. Zircons could have been recycled from a solidified, precaldera, plutonic intrusion (or intrusions) with ages of ~4.9 to 5.4 Ma which was remelted. The melt event remobilized already crystallized zircons from the pluton which were incorporated into the Deer Canyon magma. This magma was then erupted over a short timescale, which is in contrast to large, long lived magma chamber models. A similar interpretation has been suggested for a biotite bearing rhyolite of the Mono Craters, associated with Long Valley caldera in eastern-central California. The eruption age of Mono Craters rhyolite is reported to have a maximum age of 7 to 20 ka (Reid, 2003). Zircons in this rhyolite have ages of ~1.3 to 1.4 Ma. These anomalously old ages are evidence for the remelting of solidified intrusions, or plutons, which released xenocrystic zircons into the young magmas that erupted in the Mono Craters (Reid, personal communication, 2007).

Redondo Creek Zircons

In contrast to Deer Canyon, Redondo Creek zircon ages indicate that within uncertainty they formed during the interval between the lower Bandelier Tuff, 1.61 Ma, to the upper Bandelier Tuff, 1.26 Ma, to just prior to the eruption of the Redondo Creek rhyolite at 1.22 Ma (Phillips, 2004). These zircons could have formed during crystallization of the magma in which they were erupted. Zircon crystallization immediately prior to eruption is supported by the ~67 ka pre-eruptive residence time indicated by the difference between the eruption age, 1.22 Ma, and the weighted mean zircon crystallization age 1.29 Ma (Table 8.01). This is typical of zircons in most silicic rhyolites, such as zircons from Glass Mountain and Bishop Tuff, Long Valley caldera rhyolites, (Simon and Reid, 2005), zircons from Devils Kitchen rhyolite, Coso Volcanic field (Miller and Wooden, 2004), and zircons from Timber Mountain/Oasis Valley Caldera complex (Bindeman et al., 2006). Zircons from the Bishop Tuff have ~ 90 ka residence times (Simon and Reid, 2005), and from the Devils Kitchen rhyolite have ~50 ka residence times (Miller and Wooden, 2004). There is less scatter in the ages of Redondo Creek compared to those of Deer Canyon zircons, which reflects a greater proportion of near eruption aged zircon crystallization in the case of Redondo Creek. Redondo Creek zircons are subhedral, significantly more resorbed and have less overgrowth bands than Deer Canyon zircons. Resorption along the edges of crystals (Figure 8.04) is an indication that just prior to their eruption they were undergoing dissolution. This could be due to increased temperature in the melt. This late stage thermal excursion was apparently much larger in magnitude compared to the Deer Canyon zircons. In the Devils Kitchen rhyolite, Coso Volcanic field, zircons record

temperature fluctuations during crustal extension, where pulses of rhyolitic magma were accompanied by pulses of basaltic magma producing alternating crystallization and remelting/heating events during piecemeal assembly of magma bodies (Miller and Wooden, 2004). Resorption and oscillatory zoning textures seen in the Devils Kitchen rhyolite zircons are similar to those seen in Deer Canyon rhyolite zircons. Finally, distinctive age and textural differences between Deer Canyon and Redondo Creek zircons rules out any possibility that these rhyolites are comagmatic.

CHAPTER 10

MODELS FOR THE EVOLUTION OF DEER CANYON, REDONDO CREEK AND DEL MEDIO MAGMA SYSTEM

Major and trace element analyses for the Deer Canyon, Redondo Creek and Del Medio rhyolites are important for identifying changes in magma genesis after the eruption of the Upper Bandelier Tuff and caldera collapse. In addition to data gathered during this study, published analyses of Upper Bandelier Tuff from Balsley (1986), and of Deer Canyon, Redondo Creek and Del Medio rhyolites from Spell (1993) and from Phillips (2004) are used in order to form a more complete comparison of these four rhyolites. The complete data set is shown on the LeBas (1986) classification diagram in Figure 10.01.

The majority of Upper Bandelier Tuff analyses are high silica rhyolites with >75 wt. % SiO_2. Also included are analyses of rare pumices with low silica (72-73 wt. % SiO_2) and dacite (68-69 wt. % SiO_2) compositions (Balsley, 1986). Previous data from Deer Canyon, Redondo Creek and Del Medio rhyolites compare well with analyses collected during this study. The data show two distinct trends, one with high silica Upper Bandelier Tuff, 33% of the Deer Canyon rhyolites and Redondo Creek rhyolites and the other with 66 % of the Deer Canyon rhyolites and Del Medio rhyolites (Figure 10.01).

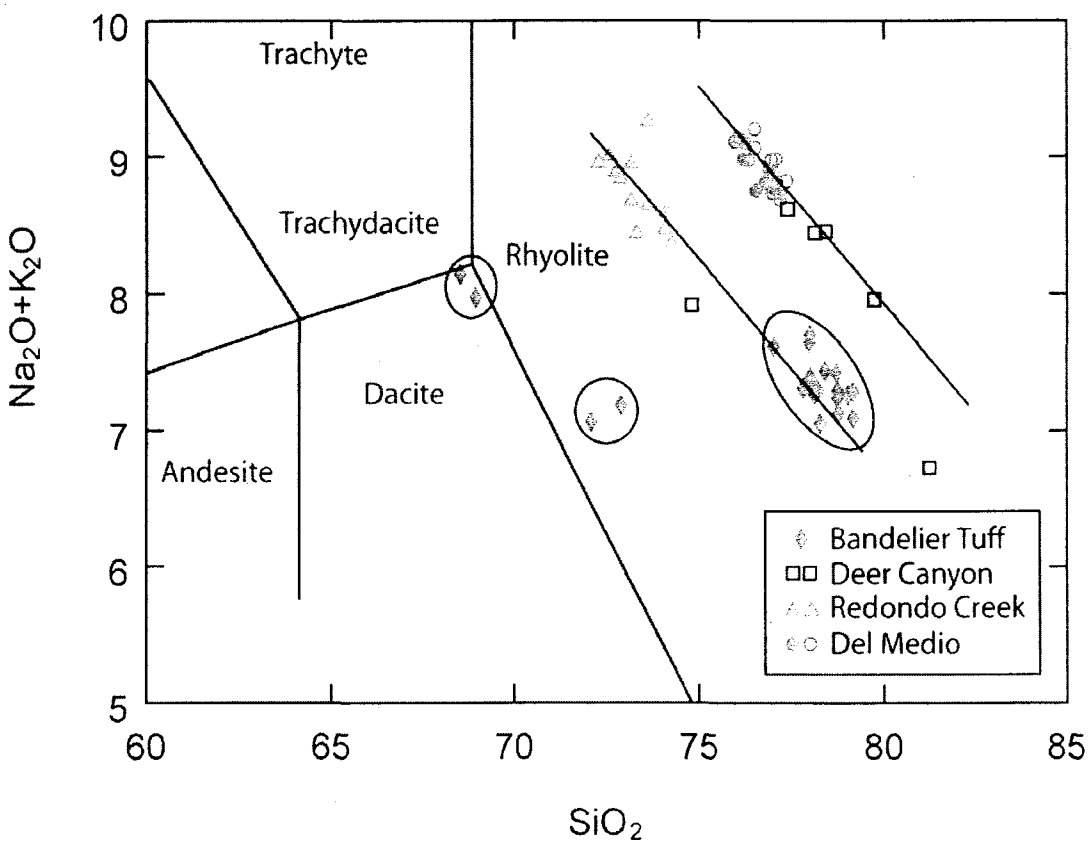

Figure 10.01. Le Bas (1986) classification of analyses gathered during this study and analyses from previous studies (see text). Open symbols refer to analyses from previous studies. Three separate Upper Bandelier Tuff components, dacite, low silica rhyolite and high silica rhyolite, are circled for reference.

Fractional Crystallization

In order to constrain the relationships of the Upper Bandelier Tuff and the post collapse rhyolites, models for fractional crystallization of older, less evolved parental magmas to produce younger, more evolved daughter magmas were considered. Models for fractionation of residual high silica Upper Bandelier Tuff magma to produce Deer Canyon and Redondo Creek rhyolites, fractionation of residual low silica and dacite Upper Bandelier Tuff magma to produce Redondo Creek rhyolite, fractionation of Deer

Canyon magma to produce Redondo Creek and Del Medio rhyolites, and fractionation of Redondo Creek magma to produce Del Medio rhyolite were considered. Representative major element plots of SiO_2 versus FeO, MgO, P_2O_5 and TiO_2 (Figure 10.02) show that Deer Canyon rhyolite is chemically heterogeneous. Thus, its highly variable compositions could not have reasonably been produced by fractionation from a single parental magma represented by residual high silica Upper Bandelier Tuff magma. Similarly, simple fractional crystallization models could not produce Redondo Creek or Del Medio rhyolites from heterogeneous Deer Canyon parental magma (Figure 10.02). Major element plots show that Redondo Creek rhyolite is significantly less evolved than the high silica Bandelier Tuff. This excludes the possibility that residual high silica Bandelier Tuff magma could be parental to Redondo Creek rhyolite by fractional crystallization. Redondo Creek rhyolite has similar SiO_2 to low silica Bandelier Tuff compositions, but it is significantly lower in MgO and FeO and higher in P_2O_5, which excludes the possibility that the low silica Upper Bandelier Tuff could have produced Redondo Creek rhyolite by fractionation. The possibility the Redondo Creek is simply residual Upper Bandelier Tuff low silica rhyolite is also excluded based on chemistry. Finally, models for the fractionation of the Bandelier Tuff dacite failed to produce Redondo Creek rhyolite compositions.

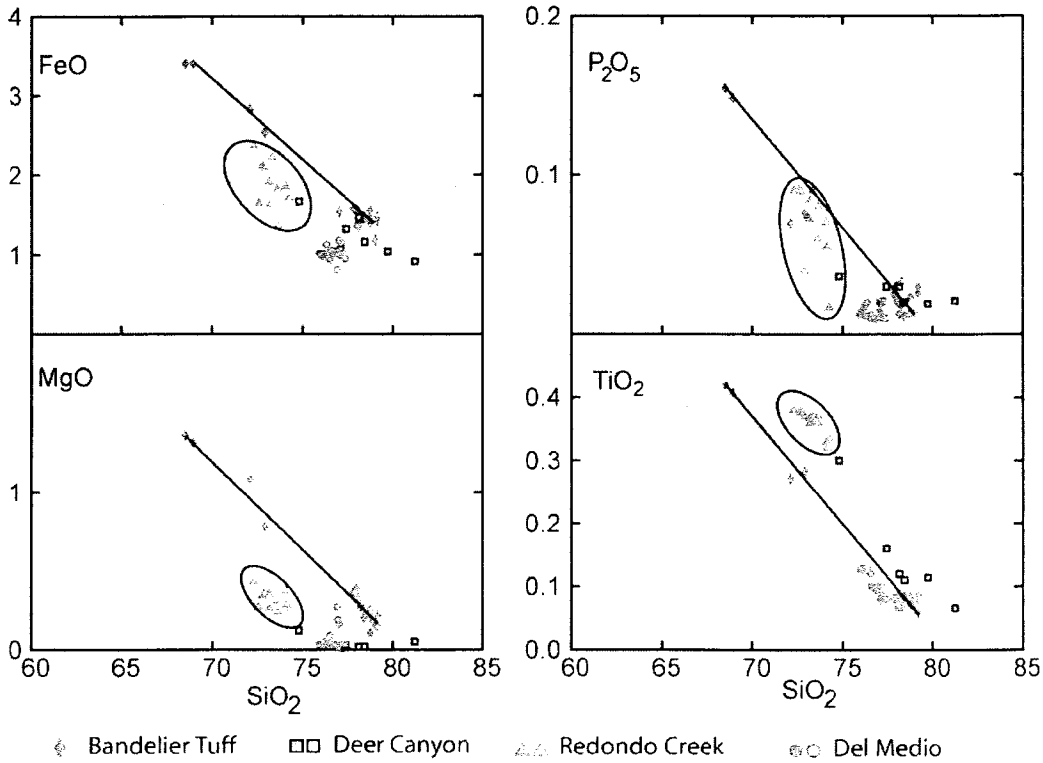

Figure 10.02. Major element plots of SiO_2 versus FeO, MgO, P_2O_5, and TiO_2. Lines show the mixing trends for the Bandelier Tuff dacite, low silica rhyolite and high silica rhyolite. Redondo Creek rhyolite is circled in order to emphasize its major element chemistry with respect to other rhyolites.

Figure 10.03 shows possible fractional crystallization trends for representative trace elements. These trace elements were picked because of their compatibility or incompatibility in rhyolite magma. Nb, Th, and Rb are incompatible, whereas Ba and Zr are compatible. For example, Ba/Nb will decrease while Th/Nb remains constant during fractional crystallization. This is because the bulk distribution coefficient for Ba is high (>>1) making this compatible in rhyolite magma, whereas the bulk distribution coefficients for Nb and Th are similar and low (<<1). It should be noted that some of the Deer Canyon samples and the high silica BandelierTuff rhyolite form a linear trend on

trace element plots of Nb versus Th, Zr, and Rb/Nb. However most Deer Canyon samples are less evolved than the high silica Upper Bandelier Tuff rhyolite (Figure 10.03). Thus, fractional crystallization models in which parental high silica Bandelier Tuff magma produces Deer Canyon compositions are unreasonable.

Figure 10.03 suggests that it may be possible to fractionate Redondo Creek rhyolite to produce Del Medio rhyolite. One problem with this model is that Redondo Creek is porphyritic and Del Medio is almost aphyric. For a simple fractionation model, Del Medio rhyolite might be expected to be more porphyritic than Redondo Creek rhyolite. Aphyric rhyolite can also be produced by adding H_2O to the magma (which suppresses crystallization), increasing the magma temperature, or erupting only interstitial melts from a more primitive parental crystal mush (Redondo Creek?). The crystal mush model for crystal poor rhyolites may apply for the production of Del Medio rhyolite from Redondo Creek magma (Bachman and Bergantz, 2004) (Chapter 9, Figure 9.01).

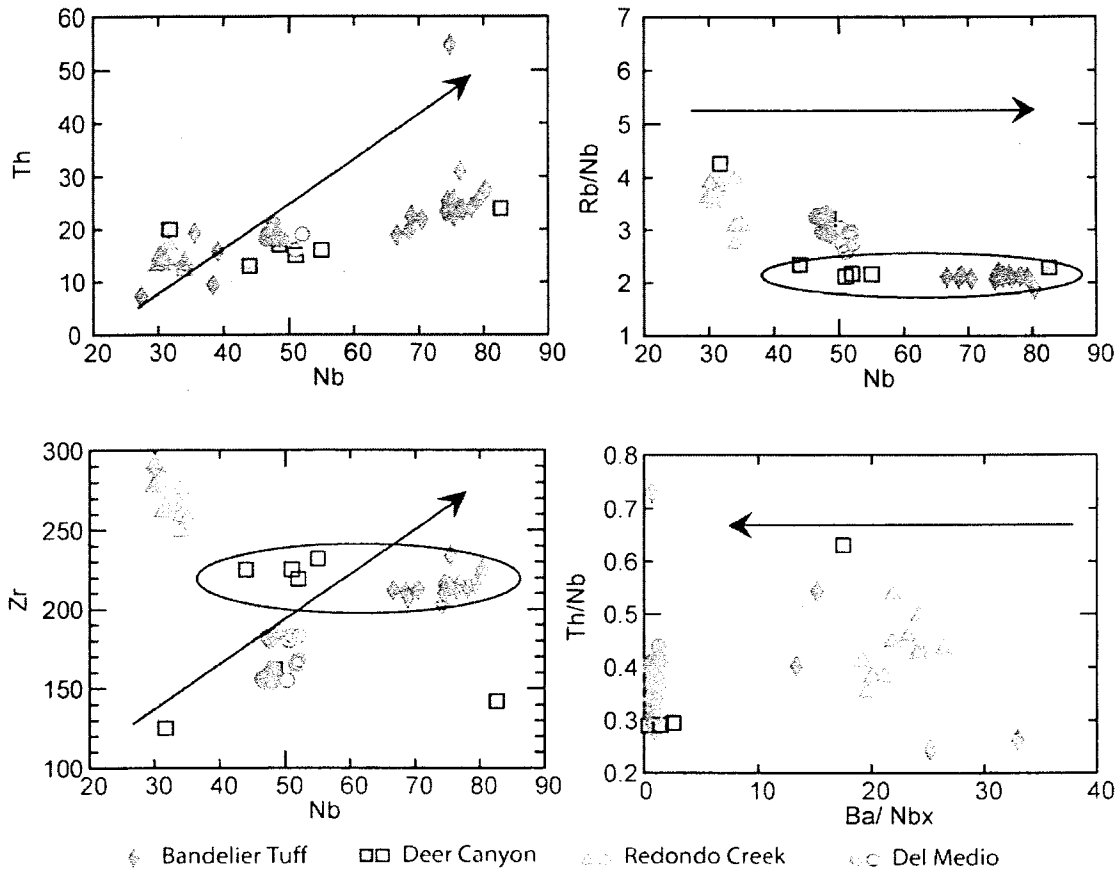

Figure 10.03. Trace element plots showing generalized fractional crystallization trends (see text) expected for typical phenocryst assemblages. All elements are by XRF analyses.

Fractional crystallization calculations were completed using data from representative samples RC07 and DM1-01, modal abundances (Table 5.03) and EMPA mineral compositions from RC07 and major element whole rock data. The results suggest that DM1-01 could be produced from ~60% fractionation of RC07 composition parental magma, but only if quartz is added to the mineral assemblage (Table 10.01). However, using phenocryst abundances from major element modeling the calculated trace element abundances did not equal the measured abundances for DM1-01 (Table 10.01). In order to more closely model the trace element chemistry, modifications were made to the major

element model. Biotite was reduced by 5%, quartz was increased by 5% and trace amounts of zircon, allanite and apatite were added to the mineral assemblage (Table 10.02). With these modifications, the major element model matches the observational results less well, but the trace element model results are more similar to those measured for DM1-01. However, for many elements significant discrepancies remain: Sc is 1.01 ppm too low, Rb is 26.06 ppm too high, and Hf, Ta, Th, and U are 2.05, 2.08, 9.19, and 3.71 ppm too high respectively. Thus while this model approximates fractional crystallization of Redondo Creek rhyolite to produce Del Medio rhyolite, trace elements cannot be modeled using the same mineral assemblage as major elements, and modification of the major element model to better fit trace elements can only approximate Del Medio major element composition leaving significant discrepancies.

In summary, fractional crystallization models of less evolved previously erupted compositions fail to acceptably produce any of the postcollaspse rhyolites. Deer Canyon rhyolite is extremely heterogeneous, thus no single model can account for its production by fractional crystallization. Residual Upper Bandelier Tuff compositions fail to provide suitable parental compositions for production of any of the post collapse rhyolites. Finally, Redondo Creek rhyolite magma appears to be the most viable candidate for fractional crystallization models to produce Del Medio rhyolite, however major and trace element models cannot be reconciled.

Table 10.01. Model for fractional crystallization of Redondo Creek magma to produce Del Medio rhyolite. RC07 is the parent magma and DM1-01 is the daughter magma.

Mineral Phases					
	Quartz	Sanidine	Plagioclase	Clinopyroxene	Biotite
% solid	25.7	43.6	19.5	1.5	9.7
Coef	0.155	0.263	0.118	0.009	0.058

Major Elements

	SiO_2	TiO_2	Al_2O_3	FeO	MnO	MgO	CaO	Na_2O	K_2O	P_2O_5
Daughter Parent RC07	77.0	0.09	12.53	1.00	0.05	0.03	0.38	3.95	4.94	0.0
Obs	73.2	0.38	14.27	1.91	0.06	0.36	1.11	3.59	5.07	0.1
Calc	73.2	0.36	13.92	1.62	0.06	0.86	0.95	3.92	5.12	0.0
Diff wt.	-0.02	0.02	0.18	0.29	0.00	-0.50	0.16	-0.33	-0.05	0.1

Sum of the square of the residuals = 0.506.

Trace Elements

	D	Obs (P) RC09	Calc (P) RC09	Diff	DM1-01 (D)	F=0.397
Sc	3.57	4.41	20.2	-15.78	1.88	
Rb	0.66	113	114	-0.98	155.6	
Sr	4.47	137.6	132.6	4.94	4.17	
Y	0.26	31.6	21.6	10	42.9	
Nb	0.95	34.2	48.6	-14.37	51.1	
Cs	0.24	3.48	2.5	0.97	5.07	
Ba	5.2	783.5	1420.6	-637.14	29.2	
La	0.62	63	34.1	29	48.2	
Ce	0.45	112.6	56.3	56.2	93.8	
Sm	0.32	7.58	3.87	3.71	7.29	
Eu	2.89	1.08	1.19	-0.11	0.21	
Tb	0.19	1.02	0.59	0.42	1.25	
Yb	0.17	3.26	2.07	1.19	4.45	
Lu	0.17	0.51	0.32	0.2	0.68	
Hf	0.1	7.84	2.87	4.97	6.61	
Ta	0.16	2.6	1.69	0.91	3.67	
Th	0.06	14.1	8.22	5.88	17.9	
U	0.06	3.37	2.06	1.67	4.9	
Pb	0.67	21.9	20.6	1.28	28	

Table 10.02. Trace element model for fractional crystallization of Redondo Creek rhyolite to produce Del Medio rhyolite.

	Mineral Phases							
	Qtz	San	Plag	Bi	Zir	Alla	Ap	Cpx
Wt %	30.4	43.6	19.5	5.0	0.025	0.022	1.3	1.5

	Trace Elements				
	Parent RC07	Bulk Dist Coeff.	Daughter DM1-01	60% FC	Actual values – model values
Sc	4.2	2.82	1.8	0.79	-1.01
Rb	107.6	0.47	149.1	175.18	26.08
Sr	131	4.43	4.86	5.65	0.79
Y	30.1	0.70	41.1	39.51	-1.59
Zr	275	1.72	152	141.89	-10.11
Nb	32.59	0.54	48.98	49.87	0.89
Cs	3.31	0.13	4.86	7.35	2.49
Ba	746	4.98	28	19.52	-8.48
La	60	1.30	46.2	45.42	-0.78
Ce	107.17	1.27	89.89	83.32	-6.57
Sm	7.22	1.25	6.99	5.73	-1.26
Eu	1.03	3.26	0.2	0.13	-0.07
Tb	0.97	0.47	1.2	1.57	0.37
Yb	3.1	0.63	4.26	4.34	0.08
Lu	0.49	0.65	0.65	0.68	0.03
Hf	7.46	0.87	6.33	8.38	2.05
Ta	2.48	0.11	3.52	5.60	2.08
Th	13.43	0.27	17.13	26.32	9.19
U	3.55	0.06	4.7	8.41	3.71
Pb	20.83	0.57	26.88	30.93	4.05

Note: Qtz = quartz, San = sanidine, Plag = plagioclase, Bi = biotite, Alla = allanite, Cpx = clinopyroxene.

Magma Mixing

Considerable evidence from both petrographic observations and mineral chemistry (Chapter 9) suggests magma mixing could be an important process forming Deer Canyon, Del Medio and Redondo Creek rhyolites. In order to investigate magma mixing several models were considered. Mixing models of residual Upper Bandelier Tuff compositions to produce Deer Canyon and Redondo Creek rhyolites, Upper Bandelier Tuff compositions and Deer Canyon rhyolite to produce Redondo Creek and Del Medio rhyolites, and high silica Bandelier Tuff and Redondo Creek rhyolites to produce Del Medio rhyolite were considered. Figure 10.02 shows mixing trend for the dacite Upper Bandier Tuff and the high silica rhyolite Upper Bandelier Tuff.

The high and variable SiO_2 content and the heterogeneous major and trace element chemistry of Deer Canyon rhyolite does not allow its production by mixing any of the Upper Bandelier Tuff compositions, because Deer Canyon compositions do not fall on mixing arrays (Figure 10.02). Similarly the heterogeneity of Deer Canyon rhyolites makes it unsuitable as a mixing end member for the production of Redondo Creek or Del Medio rhyolites (Figures 10.02, 10.03, and 10.04). Redondo Creek rhyolite could not have been produced by mixing the high silica Bandelier Tuff and Deer Canyon rhyolite, since it is less evolved (lower in SiO_2) than either of these rhyolites. Trace element plots in Figure 10.04 show that Redondo Creek compositions lie on a trend between the high silica and dacite end members of the Upper Bandelier Tuff, which suggest that Redondo Creek rhyolite could be produced by mixing these two residual magmas. However this relationship is not seen on other trace element plots (Figure 10.03 and 10.05) or on major element plots (Figure 10.02). Mixing calculations for Upper Bandelier Tuff dacite

magma, BT22-70, with Upper Bandelier Tuff high silica rhyolite magma, BT20-70 to produce representative Redondo Creek RC02 rhyolite was modeled. The results show that major elements and trace elements do not match. Thus this model is unreasonable (Table 10.03). This does not rule out the possibility that Redondo Creek magma could be the product of mixing between upper Bandelier Tuff high silca rhyolite or low silica rhyolite and an unknown more mafic andesite or dacite magma. The range of Redondo Creek zircon ages allows this interpretation since they span the eruption age of the Upper Bandelier Tuff (Chapter 8). There is also considerable petrographic evidence of magma mixing in Redondo Creek rhyolite (Chapter 5).

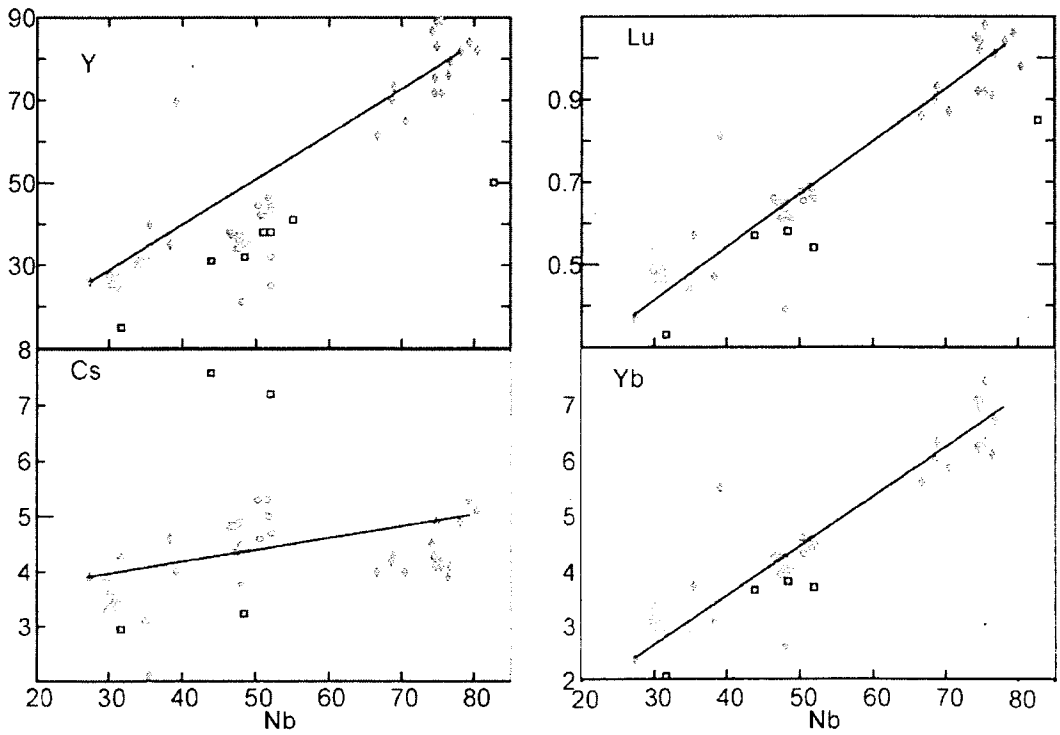

Figure 10.04. Trace element plots to show mixing models to produce Redondo Creek rhyolite from Upper Bandelier Tuff high silica rhyolite and dacite end member magmas. All elements by XRF.

Table 10.03. Mixing model for the production of Redondo Creek rhyolite from end members Bandelier Tuff dacite and high silica rhyolite. The hybrid magma is RC02.

Major Elements

	BT22-70	BT20-70		Obs	Calc	Diff wt.
SiO_2	68.51	78.77		74.25	75.92	-0.67
TiO_2	0.42	0.08		0.33	0.17	0.16
Al_2O_3	14.96	11.85		14.23	12.68	0.78
FeO	3.4	1.47		1.71	1.99	-0.28
MgO	0.07	0.05	Hybrid RC-02	0.05	0.06	-0.01
BaO	1.36	0.26		0.26	0.55	-0.29
CaO	2.98	0.36		0.8	1.07	-0.27
Na_2O	4.85	2.67		2.86	3.25	-0.39
K_2O	3.29	4.46		5.5	4.14	1.36
P_2O_5	0.15	0.02		0.02	0.06	-0.04

Note: 26.9% BT22-70 and 73.1% BT20-70. Sum of squares of residuals = 3.309.

Trace Elements

	Obs	Calc	Residual	BT22-70	BT20-70
Sc	3.8	2.5	1.3	5.8	1.3
Rb	124	162.9	-38.9	173.5	159.3
Cs	4.5	4.3	0.2	4	4.4
Ba	734.4	310.5	423.9	935.7	80.7
La	54.5	62.6	-8.2	37.5	72
Ce	98	111.1	-13	70.4	126.2
Sm	5.9	10.5	-4.5	5.2	12.4
Eu	0.9	0.5	0.4	0.9	0.4
Tb	0.8	1.8	-1	0.7	2.3
Yb	3	5.4	-2.4	2.4	6.5
Lu	0.5	0.8	-0.3	0.4	1
Hf	7.5	8	-0.5	6.4	8.6
Ta	2.8	4	-1.2	2	4.8
Th	15.2	15.8	-0.6	7.8	18.8
U	3.9	4.6	-0.7	2.2	5.5

Trace element plots show Del Medio rhyolite located consistently between Redondo Creek and high silica Upper Bandelier Tuff rhyolite (Figure 10.04), which suggests that it could have been the product of mixing these two end members. However, Del Medio falls off the mixing trend between Redondo Creek and high silica Upper Bandelier Tuff rhyolite in the major element plots (Figures 10.02 and 10.04). A mixing model between Redondo Creek RC12 magma and high silica Upper Bandelier Tuff BT20-20 magma to produce representative Del Medio DM3-01 rhyolite show that major and trace elements do not match, making this model unviable (Table 10.04).

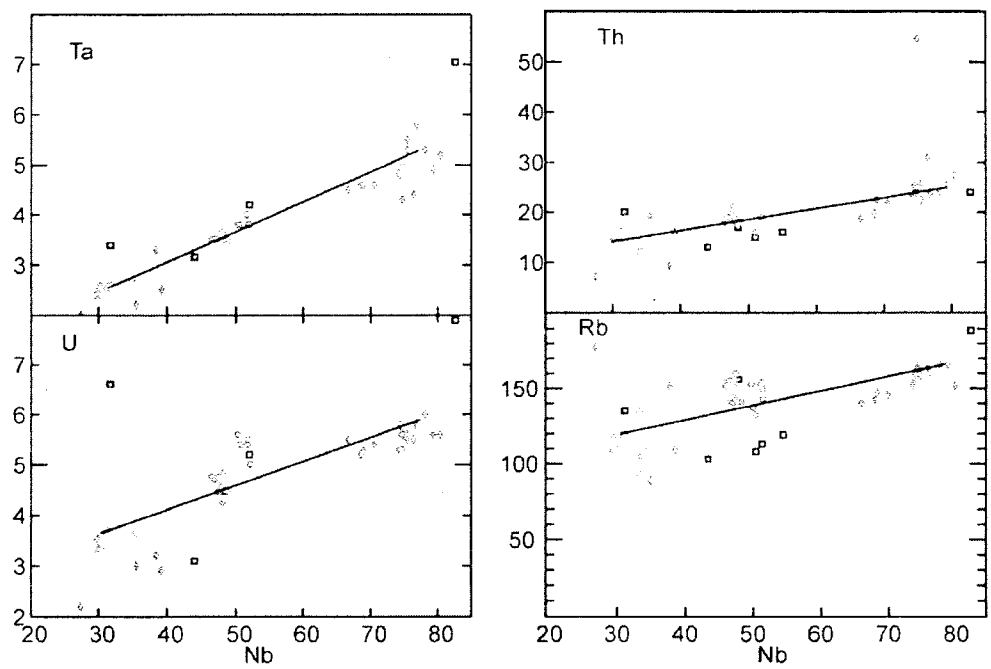

Figure 10.05. Trace element plots to model mixing between Redondo Creek rhyolite and high silica Upper Bandelier Tuff end members to produce Del Medio rhyolite. All analyses are from XRF.

In summary, models fail to reproduce any of the postcollapse rhyolites by mixing using end member compositions including those represented by residual Upper Bandelier Tuff. This suggests that Deer Canyon, Redondo Creek and Del Medio rhyolites may represent separate magmas batches which are unrelated to each other and to the Upper Bandelier Tuff.

Table 10.04. Mixing model for the production of Del Medio rhyolite from end members high silica Upper BandelierTuff rhyolite and Redondo Creek rhyolite. The hybrid magma is DM3-01.

Major Elements

	RC-12	BT20-20		Obs	Calc	Diff wt.
SiO_2	72.58	79.03		76.26	76.05	0.08
TiO_2	0.38	0.07		0.13	0.22	-0.09
Al_2O_3	14.75	11.92		13.01	13.24	-0.12
FeO	1.64	1.18		1	1.4	-0.4
MnO	0.04	0.04	Hybrid	0.06	0.04	-0.02
MgO	0.27	0.15	DM3-01	0.04	0.21	-0.17
CaO	1.25	0.33		0.39	0.76	-0.37
Na_2O	3.71	2.77		4.16	3.21	0.95
K_2O	5.29	4.49		4.94	4.87	0.07
P_2O_5	0.09	0.01		0.01	0.05	-0.04

Note: 46% RC12 and 53.3% BT20-20. Sum of squares of residuals = 1.258.

Trace Elements

	Obs	Calc	Residual	RC12	BT20-20
Sc	2.3	2.9	-0.6	4.6	1.4
Rb	141.8	144.8	-3	109.8	175.4
Sr	5.1	78.7	-73.6	168.6	0
Yb	40.4	14.4	26.1	30.8	0
Nb	51.8	15.2	36.6	32.6	0
Cs	4.6	4.6	0	4	5
Ba	31.8	440.3	-408.5	832.5	96.4
La	48.4	65.4	-17	58.8	71.1
Ce	95	115.3	-20.3	106.8	122.6
Sm	7.3	10.8	-3.4	7.3	13.8
Eu	0.3	0.7	-0.5	1.2	0.4
Tb	1.2	1.8	-0.6	1	2.6
Yb	4.2	5.3	-1.1	3.2	7.2
Lu	0.6	0.8	-0.2	0.5	1.1
Hf	7	8.5	-1.4	7.7	9.1
Ta	3.6	3.9	-0.3	2.4	5.1
Th	17.9	16.4	1.5	12.8	19.5
U	4.7	4.7	0	3.4	5.7
Pb	27.6	10.3	17.3	22.1	0

New Genetically Unrelated Magma Batches

Deer Canyon Rhyolite

Deer Canyon rhyolite zircon ages combined with major and trace element chemistry suggest that it is not genetically related to the Upper Bandelier Tuff, Redondo Creek or Del Medio rhyolites by fractional crystallization or magma mixing. An alternative model is that it may represent an independent magma batch. Heterogeneous, disequilibrium phenocryst compositions and textures, zoning, and major and trace element chemistry imply that type A and type B Deer Canyon rhyolite were generated separately, mingled and erupted quickly such that sufficient time was not available for homogenization. A similar process has been inferred for mingled rhyolites in the Inyo Craters at Long Valley, California. In Obsidian Dome compositionally and mineralogically distinct low SiO_2, high Ba, porphyritic rhyolite and high SiO_2, low Ba sparsely porphyritic rhyolite magmas were emplaced simultaneously forming a zoned dome complex, and are interpreted as representing mingling and mixing of two distinct magmas during eruption (Vogel et al., 1989).

Redondo Creek Rhyolite

Redondo Creek rhyolite is less evolved, having lower SiO_2 and Nb and higher TiO_2, Al_2O_3 and FeO, than the other rhyolites. Fractional crystallization models thus cannot reproduce Redondo Creek compositions from high or low silica Upper Bandelier Tuff rhyolites or from Deer Canyon rhyolites. Mixing models rule out the possibility that is was a mixture of residual high silica Upper Bandelier Tuff and Upper Bandelier Tuff dacite magmas. Trace element chemistry suggests that Redondo Creek rhyolite could be related to the high silica Upper Bandelier Tuff by mixing this rhyolite with a more mafic

andesite or dacite magma. However the mafic end member is hypothetical, as no erupted products with appropriate chemistry have been sampled. An alternative model for the derivation of Redondo Creek rhyolites is production by mingling of new, independent magma batches. Such a model may also explain Redondo Creek feldspars, including the andesine cores overgrown by oligoclase which are overgrown by sanidine discussed in previous chapters (Chapters 5, 6, and 9).

Intrusion of hotter magma may have thermally rejuvinated a residual mush from the Upper Bandelier Tuff magma system. Rhyolitic melt was extracted from the residual mush, and andesine phenocrysts were transferred from the mush into the rhyolite melt where they were overgrown by oligoclase. Resorption of the oligoclase overgrowths and the following sanidine overgrowths formed when the Redondo Creek rhyolite interacted with a hotter K-rich melt.

Del Medio Rhyolite

Previously discussed fractional crystallization models indicate that production of Del Medio rhyolite from parental Upper Bandelier Tuff components or Deer Canyon rhyolite magmas is unlikely. Parental Redondo Creek rhyolite magma can produce Del Medio major element compositions by fractional crystallization only if a non-modal phenocryst assemblage is fractionated, and the model fails to reproduce the trace element data (Tables 10.01 and 10.02). In addition, mixing models between Redondo Creek and the high or low silica Upper Bandelier Tuff end member magma suggest that Del Medio rhyolite could not have been produced by this process (Table 10.04) . $^{143}Nd/^{144}Nd$ ratios in Del Medio rhyolite are too high to have been derived from the open system evolution of the Bandelier magma chamber or from progressively deeper layers in the Bandelier

magma chamber (Spell et al., 1993). Del Medio rhyolite exhibits distinctive textural, petrographic and chemical characteristics, which suggest that it may have been derived from a new magma batch genetically unrelated to the older rhyolites.

General Models for Large Scale Silicic Magmatism

Three models for silicic magmatism can be tested with the Deer Canyon, Redondo Creek and Del Medio rhyolites. The first model describes the evolution of a single long lived (~1 Ma) sub-caldera magma system in the mid to upper crust that is thermally sustained by mafic recharge. Periodic eruptions result in both large scale explosive and related small scale effusive eruptions (Smith, 1979; Hildreth, 1981; Davies et al., 1989; Halliday, 1990; Reid et al., 1997; Davies and Halliday, 1998). The second model suggests that independent batches of silicic magmas rapidly form and erupt in less than 100 ka. Melting results from the injection of basalt into country rock (Huppert and Sparks, 1988; Sparks et al., 1990; Mahood, 1990; Reid and Coath, 2000; Bindeman and Valley, 2001; Bachman et al., 2002, Bindeman et al., 2006). In the third model, silicic magmas are produced from crystal mushes, which can reside in the crust for > 10^5 years, sufficiently long to produce >500 km^3 of crystal poor rhyolites which are extracted in 10^4 to 10^5 years (Schmitt et al., 2002; Bachman and Bergantz, 2004; Hildreth and Wilson, 2007).

The geochemical, petrographic, mineral chemistry and zircon data from this study favors a combination of the second and third models in which independent magmas are generated and erupted over short time scales. However, these magmas generally originate from the same crystal mush dominated magma system. Most of the data suggest that Deer

Canyon, Redondo Creek and Del Medio rhyolite are not comagmatic and are not derived directly from residual Upper Bandelier Tuff magma (as opposed to remelting residual Upper Bandelier mush). Evidence for magma mingling and fractional crystallization trends seen within individual rhyolites, the two types of Deer Canyon rhyolites, the plagioclase zoning and antirapakivi textures in Redondo Creek rhyolites, and the phenocryst zonation in Del Medio rhyolites can be explained by a model in which recharge from more mafic magma provides the heat necessary to release interstitial rhyolitc melts from a crystal mush zone. These heat-providing magmas in some cases interact with the rhyolitic melts that are produced following a large-scale caldera forming eruption. It is probable that at crystallinities of > 40% batholith sized crystal mushes store vast amounts of high silica interstitial melt. Extraction facilitated by hindered settling, compaction, micro-settling and by gas driven filter pressing, can produce both large-scale and small scale eruptions of crystal poor rhyolites (Bachman and Bergantz, 2004).

The two types of Deer Canyon rhyolite might be produced by two separate magma batches that mingled during their ascent to higher levels above a crystal mush zone (Figure 10.06). The aphyric texture of type A magma may indicate that it was hotter that the porphyritic type B magma. Mingling could have caused resorption in plagioclase, formation of embayments in quartz and the patchy zonation in sanidines. The production of type A Deer Canyon magma, at least initially, was unrelated to the crystal mush system. Anomalously old zircon ages that predate eruption by ~3.4 Ma suggest derivation from a pre-caldera pluton which was remelted immediately prior to eruption. The 4.9 to 5.4 Ma zircons are xenocrystic and were inherited from this plutonic source rock. Type A Deer Canyon magma rose rapidly into the overlying crystal mush system where type B

Deer canyon magma was being generated by crystal liquid separation (hindered settling, compaction, and micro-settling) (Figure 10.06). These two magmas were erupted simultaneously and may not have interacted substantially.

Redondo Creek rhyolite may have been produced when an intrusion of hotter mafic magma thermally rejuvinated the Bandelier crystal mush system. Rhyolitic melt was extracted from the residual mush, and andesine phenocrysts were transferred into the rhyolite melt by viscous entrainment of phenocryst bearing enclaves along the compositional boundary between the intruding mafic magma and rhyolite melt. Andesine was subsequently overgrown by oligoclase. Prior to eruption the rhyolite magma batch interacted with another hotter K-rich melt producing resorption of the oligoclase overgrowths. This was followed by sanidine overgrowths which produced antirapakivi texture (Figure 9.04).

Del Medio rhyolite can be explained by a simple model in which a batch of crystal poor melt was extracted from the mush zone. The batch rose to an appropriate bouyancy level where it was isolated from the deeper mafic recharge zone and it became zoned in crystallinity (Figure 10.06). The upper aphyric magma was erupted first as DM1 and DM2. This was followed by the eruption of DM3 from deeper, slightly more porphyritic levels of the magma chamber. The Bishop Tuff shows trends towards higher phenocryst content with depth which is similar to Del Medio rhyolites (Hildreth and Wilson, 2007). Zonation is common, although usually seen in larger (ignimbrite) eruptions.

Many rhyolites have textures and mineral chemistry similar to what has been found in this study and have been shown to have been produced by similar processes. For example, similar petrographic textures and reverse zoning in feldspars in the Fish Canyon

Tuff, Colorado were formed in a dynamic environment where crystals with a variety of growth histories were combined just prior to their eruption from a >5000km^3 partially solidified crystal mush. The mush was rejuvinated by underplating of mafic magma at the base of the crystal mush zone (Bachmann et al., 2002). Numerous batches of crystal poor melt was extracted from a granitoid mush body to form the magma that erupted to produce the Bishop Tuff (Hildreth and Wilson, 2007).

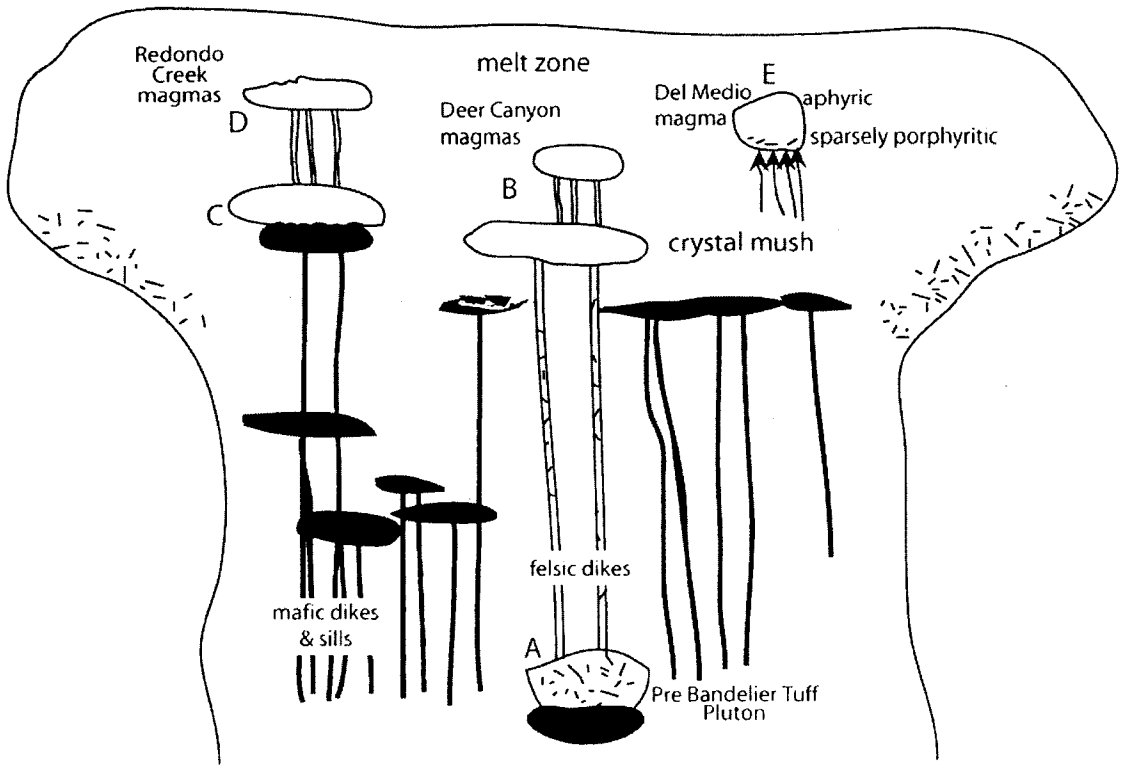

Figure 10.06. General model for Valles post collapse rhyolites, showing residual Bandelier crystal mush system. A. Type A Deer Canyon rhyolite is produced when a mafic intrusion remelts a ~4 to ~5 Ma Pre-Bandelier Tuff pluton. B. Type B Deer Canyon rhyolite is formed from interstitial melt in the crystal mush and mixes with type A Deer Canyon rhyolite immediately prior to eruption. C. Redondo Creek rhyolite is formed from interstitial melts in the crystal mush. Plagioclase phenocrysts of andesine compostion are transferred to the rhyolite magma at the boundary between it and a mafic sill. D. Redondo Creek magma mixes with a different composition rhyolite magma producing antirapakivi overgrowths. E. Del Medio Magma is produced from the interstitial melts of the Bandelier Tuff magma system. The Del Medio magma body is aphyric near the top and sparsely porphyritic at the bottom.

CHAPTER 11

CONCLUSIONS

The eruptive history of the Valles caldera and postcollapse rhyolites is complicated and requires a separate mechanism for production of each rhyolite magma.

1. Two magma types formed and erupted simultaneously to produce Deer Canyon rhyolite. Type A sparsely pophyritic rhyolite originated from melting of a pre-caldera pluton which contained 4.9 to 5.4 Ma zircons. Type B porphyritic rhyolite formed the crystal mush zone of the residual Bandelier magma system. These two rhyolites were rapidly and simultaneously erupted and may not have interacted significantly.
2. Redondo Creek rhyolite was formed by rejuvination of residual Bandelier Tuff mush by mafic intrusion. Rhyolite magma was extracted from the mush and phenocryst bearing enclaves were transferred to the rhyolitic melt. Oligoclase overgrowths formed on the transferred andesine phenocrysts. A hotter K-rich rhyolite magma interacted with this rhyolite magma and produced resorption at the oligoclase surface followed by sanidine overgrowths prior to eruption.
3. Del Medio rhyolites were produced from the rejuvenation of the Bandelier crystal mush. This occurred as a result of hindered settling, micro-settling, and compaction and may have been facilitated by gas driven filter pressing.

Each rhyolite originated as a separate magma batch unrelated to the others, and to the preceding Upper Bandelier Tuff dacite, low silica rhyolite and high silica rhyolite components.

A model for post collapse silicic magmatism that fits the Valles caldera is one in which residual Bandelier crystal mush is thermally sustained by intermittent mafic recharge. Silicic magmas are generated by extraction from interstitial melts in the crystal mush system. Recurrent mingling, mixing and magma generation result in punctuated phenocryst growth including episodes of crystallization and resorption due to varied compositional inputs. Processes controlling such crustal magma systems include mafic recharge, incremental or piecemeal assembly of magma bodies above a crystal mush zone, and periodic eruptions which may or may not be related to each other.

APPENDIX A

SAMPLE LOCATIONS

&

ANALYTICAL METHODS PERFORMED

Appendix A. Sample locations and analytical methods performed.

Analyses	Latitude UTM	Longitude UTM	Thin Section petrography	Point Count	XRF	ICPMS	U/PB	EMPA
DC01	N3974708	E365520	x	x	x	x		
DC02	N3974708	E365520						
DC03	N3973107	E365090	x	x	x	x	x	x
DC04	N3971321	E354151						
DC05	N3970853	E356022						
DC06	N3970961	E355105						
DC07	N3973966	E359776						
DC08	N3974190	E359551	x	x	x	x		
DC09	N3972681	E365247	x	x				
DC10	N3972616	E364411						
DC11	N3972020	E364090						
DC12	N3970853	E356022	x	x	x	x		
RC01	N3978067	E356724						
RC02	N3977899	E356629	x	x	x	x		
RC03	N3978769	E356112	x	x	x	x		
RC04	N3978801	E356203						
RC05	N3974034	E358659						
RC06	N3974034	E358659						
RC07	N3973950	E358483	x	x	x	x	x	x
RC08	N3973906	E358178						
RC09	N3974189	E358426	x	x	x	x		
RC10	N3972507	E352353	x	x	x	x		
RC11	N3980003	E352791						
RC12	N3979718	E353698	x	x	x	x	x	x
RC13	N3979625	E352314						
RC14	N3979624	E352315						
RC15	N3978822	E351833						
RC16	N3974457	E352347						
RC17	N3975181	E302645						
RC18	N3973225	E353234	x	x	x	x		
RC19	N3973225	E350340						
RC20	N3973078	E351007						
RC21	N3971653	E352542						
RC22	N3973191	E357482						

Appendix A. Sample locations and analytical methods performed (continued).

Analyses	Latitude UTM	Longitude UTM	Thin Section petrography	Point Count	XRF	ICPMS	U/PB	EMPA
DM1-01	N3975314	E366134	x	x	x	x		
DM1-02	N3975450	E366499						
DM1-03	N3975419	E367499						
DM1-04	N3975286	E367896	x	x	x	x		
DM1-05	N3973620	E367009						
DM1-06	N3973942	E366105						
DM2-01	N3971039	E369725						
DM2-02	N3971703	E368804	x	x	x	x		x
DM2-03	N3972311	E369214						
DM2-04	N3976946	E371255						
DM2-05	N3974359	E368509						
DM2-06	N3975924	E370056						
DM2-07	N3977273	E370160	x	x	x	x		
DM2-08	N3976211	E367924						
DM2-09	N3976736	E368488	x	x	x	x		
DM2-10	N3978433	E368980	x	x	x	x		x
DM2-11	N3971046	E369410	x	x	x	x		
DM3-01	N3975174	E369706	x	x	x	x		
DM3-02	N3974776	E369880						
DM3-03	N3973395	E370450	x	x	x	x		
DM3-05	N3974470	E368669	x	x	x	x		
DM3-06	N3973968	E368840						
DM3-07	N3973920	E370596						

APPENDIX B

ELECTRON MICROPROBE ANALYSES

OF

FELDSPAR

Appendix B. Electron Microprobe Analyses of Feldspar.

	Point Analyses												
Sample	SiO_2	TiO_2	Al_2O_3	FeO	MgO	CaO	Na_2O	K_2O	MnO	Total	An	Ab	Or
DC03	57.31	0.01	25.37	0.32	0.02	8.21	6.18	0.75	0.00	98.17	40.48	55.13	4.39
DC03	58.36	0.01	25.07	0.36	0.02	7.61	6.52	0.87	0.00	98.82	37.24	57.69	5.06
DC03	59.13	0.00	24.68	0.33	0.01	6.32	6.95	0.89	0.00	98.31	31.70	63.00	5.29
DC03	57.09	0.00	26.52	0.36	0.01	8.09	5.71	0.71	0.02	98.51	42.01	53.61	4.38
DC03	56.50	0.00	25.97	0.42	0.02	8.12	5.66	0.61	0.01	97.31	42.53	53.68	3.78
DC03	57.41	0.01	25.84	0.40	0.01	7.76	5.94	0.67	0.00	98.04	40.19	55.69	4.13
DC03	56.63	0.02	26.62	0.35	0.01	8.76	5.52	0.56	0.01	98.47	45.10	51.44	3.46
DC03	69.98	0.07	16.34	0.36	0.00	0.94	3.50	7.10	0.00	98.29	5.95	40.28	53.77
DC03	57.92	0.01	26.20	0.38	0.02	8.00	6.43	0.65	0.02	99.65	39.18	57.02	3.80
DC03	56.28	0.02	26.73	0.40	0.01	9.04	5.86	0.60	0.02	98.96	44.40	52.08	3.53
DC03	58.02	0.00	26.05	0.31	0.02	7.30	6.08	0.93	0.00	98.71	37.62	56.69	5.69
DC03	57.18	0.00	26.50	0.37	0.02	8.32	6.04	0.68	0.00	99.11	41.46	54.49	4.05
DC03	56.70	0.01	26.06	0.37	0.01	8.14	6.14	0.80	0.00	98.24	40.32	54.99	4.69
DC03	58.13	0.00	25.41	0.34	0.02	7.23	6.52	0.94	0.00	98.59	35.88	58.55	5.58
DC03	65.09	0.02	19.90	0.15	0.00	0.49	4.50	9.20	0.03	99.37	2.49	41.58	55.93
DC03	66.56	0.01	20.73	0.13	0.00	0.50	3.60	8.84	0.00	100.37	2.82	37.15	60.02
DC03	63.06	0.03	21.86	0.15	0.00	0.45	4.45	8.57	0.01	98.58	2.42	43.07	54.51
DC03	64.66	0.05	19.80	0.15	0.00	0.48	4.63	9.19	0.00	98.95	2.42	42.30	55.28
DC03	54.75	0.05	34.23	0.19	0.00	0.40	3.26	7.18	0.02	100.06	2.68	39.70	57.62
DC03	64.35	0.03	20.41	0.19	0.00	0.49	4.32	8.75	0.02	98.55	2.60	41.72	55.68
DC03	65.55	0.00	19.31	0.18	0.00	0.21	4.30	9.04	0.00	98.59	1.10	41.51	57.39
RC07	64.45	0.03	20.08	0.15	0.00	0.44	4.10	8.99	0.02	98.24	2.37	39.95	57.68
RC07	63.93	0.02	19.94	0.16	0.00	0.43	4.30	9.21	0.01	97.99	2.23	40.61	57.17
RC07	63.68	0.02	19.38	0.18	0.00	0.44	4.56	9.25	0.01	97.52	2.24	41.88	55.88
RC07	64.15	0.03	19.31	0.16	0.00	0.41	4.67	9.55	0.00	98.27	2.01	41.77	56.23
RC07	67.22	0.03	20.38	0.13	0.00	0.46	4.43	9.29	0.02	101.99	2.37	41.02	56.61
RC07	65.25	0.05	19.97	0.12	0.00	0.51	4.30	9.16	0.00	99.35	2.64	40.54	56.83
RC07	63.03	0.03	20.17	0.17	0.00	0.53	4.92	9.21	0.02	98.09	2.62	43.64	53.74

Appendix B. Electron Microprobe Analyses of Feldspar (continued).

	Point Analyses												
Sample	SiO_2	TiO_2	Al_2O_3	FeO	MgO	CaO	Na_2O	K_2O	MnO	Total	An	Ab	Or
RC07	65.08	0.05	19.90	0.14	0.00	0.48	4.54	9.13	0.00	99.32	2.45	42.00	55.55
RC07	63.53	0.03	21.42	0.13	0.00	0.41	3.80	8.79	0.00	98.11	2.29	38.73	58.99
RC07	65.08	0.02	19.99	0.15	0.00	0.48	4.09	9.15	0.00	98.96	2.58	39.41	58.01
RC07	64.25	0.02	19.59	0.14	0.00	0.47	4.48	9.39	0.00	98.33	2.37	41.01	56.62
RC07	57.02	0.00	28.89	3.27	0.02	0.41	3.78	7.42	0.04	100.85	2.56	42.50	54.94
RC07	65.30	0.00	19.80	0.13	0.00	0.38	4.35	9.02	0.01	98.98	1.98	41.47	56.55
RC07	65.09	0.02	19.90	0.15	0.00	0.49	4.50	9.20	0.03	99.37	2.49	41.58	55.93
RC07	66.56	0.01	20.73	0.13	0.00	0.50	3.60	8.84	0.00	100.37	2.82	37.15	60.02
RC07	63.06	0.03	21.86	0.15	0.00	0.45	4.45	8.57	0.01	98.58	2.42	43.07	54.51
RC07	64.66	0.05	19.80	0.15	0.00	0.48	4.63	9.19	0.00	98.95	2.42	42.30	55.28
RC07	54.75	0.05	34.23	0.19	0.00	0.40	3.26	7.18	0.02	100.06	2.68	39.70	57.62
RC07	64.35	0.03	20.41	0.19	0.00	0.49	4.32	8.75	0.02	98.55	2.60	41.72	55.68
RC07	65.55	0.00	19.31	0.18	0.00	0.21	4.30	9.04	0.00	98.59	1.10	41.51	57.39
RC12	63.06	0.00	22.94	0.19	0.00	3.76	8.36	1.59	0.00	99.92	18.09	72.78	9.13
RC12	64.08	0.01	19.32	0.15	0.00	0.48	4.93	9.30	0.00	98.27	2.34	43.57	54.09
RC12	64.07	0.02	19.26	0.13	0.00	0.53	5.17	8.88	0.00	98.06	2.61	45.71	51.68
RC12	64.15	0.00	19.28	0.14	0.00	0.37	4.60	9.52	0.00	98.05	1.85	41.58	56.57
RC12	56.53	0.06	27.34	0.20	0.00	9.01	6.20	0.46	0.00	99.81	43.35	54.02	2.62
RC12	58.37	0.00	25.75	0.24	0.00	7.48	6.94	0.63	0.00	99.42	35.99	60.43	3.58
RC12	57.20	0.06	26.65	0.30	0.00	8.31	6.44	0.51	0.01	99.50	40.40	56.63	2.97
RC12	64.47	0.03	19.12	0.16	0.00	0.36	4.50	9.65	0.00	98.30	1.78	40.72	57.50
RC12	64.21	0.01	19.04	0.17	0.00	0.33	4.75	9.43	0.00	97.93	1.62	42.67	55.72
RC12	63.17	0.02	23.61	0.21	0.00	3.82	8.21	1.64	0.00	100.68	18.52	72.03	9.45
RC12	63.90	0.03	19.76	0.16	0.00	0.51	4.62	9.02	0.00	98.02	2.62	42.60	54.78
RC12	62.63	0.00	22.73	0.22	0.00	3.81	8.39	1.44	0.00	99.23	18.40	73.33	8.27
RC12	63.62	0.03	19.14	0.16	0.00	0.45	4.91	8.81	0.00	97.13	2.27	44.83	52.90
RC12	63.51	0.04	20.25	0.15	0.00	0.62	5.20	8.33	0.01	98.11	3.11	47.17	49.72
RC12	62.46	0.01	22.44	0.21	0.00	3.86	8.30	1.49	0.02	98.80	18.70	72.71	8.59

Appendix B. Electron Microprobe Analyses of Feldspar (continued).

	Point Analyses												
Sample	SiO_2	TiO_2	Al_2O_3	FeO	MgO	CaO	Na_2O	K_2O	MnO	Total	An	Ab	Or
RC12	64.07	0.03	19.52	0.17	0.00	0.55	4.83	8.67	0.01	97.85	2.82	44.56	52.63
RC12	64.43	0.02	19.21	0.14	0.00	0.41	4.67	9.46	0.00	98.34	2.03	42.01	55.96
RC12	63.99	0.02	19.35	0.14	0.00	0.45	4.61	9.23	0.00	97.78	2.28	42.19	55.53
RC12	64.68	0.01	19.78	0.15	0.00	0.41	4.52	9.37	0.00	98.91	2.10	41.39	56.51
RC12	64.02	0.03	19.20	0.16	0.00	0.41	4.67	9.28	0.01	97.78	2.07	42.45	55.48
DM2-02	66.02	0.00	20.01	0.10	0.00	0.34	5.55	8.05	0.00	100.05	1.69	50.28	48.03
DM2-02	65.10	0.00	19.65	0.12	0.00	0.34	5.65	7.93	0.00	98.79	1.69	51.11	47.20
DM2-02	67.76	0.00	20.10	0.09	0.00	0.44	5.59	7.42	0.00	101.40	2.26	52.16	45.58
DM2-02	65.64	0.00	21.02	0.15	0.00	0.81	7.21	5.02	0.03	99.90	4.10	65.75	30.14
DM2-02	65.00	0.00	19.24	0.11	0.00	0.32	5.62	7.99	0.00	98.30	1.61	50.84	47.55
DM2-02	65.70	0.00	19.35	0.11	0.00	0.44	6.12	7.35	0.00	99.07	2.16	54.67	43.17
DM2-02	65.92	0.01	20.05	0.12	0.00	0.38	5.76	7.69	0.01	99.95	1.92	52.22	45.87
DM2-02	65.67	0.01	19.45	0.10	0.00	0.41	6.14	7.40	0.00	99.17	2.01	54.66	43.33
DM2-02	65.37	0.00	18.98	0.13	0.00	0.42	6.30	7.37	0.01	98.57	2.02	55.37	42.60
DM2-10	65.55	0.01	20.72	0.18	0.00	1.42	7.71	3.81	0.01	99.42	7.13	70.07	22.80
DM2-10	65.97	0.00	19.50	0.19	0.00	0.39	6.12	7.91	0.00	100.08	1.86	53.02	45.12
DM2-10	65.65	0.00	20.48	0.20	0.00	1.38	7.91	4.24	0.00	99.86	6.64	69.01	24.34
DM2-10	65.12	0.00	21.03	0.17	0.00	1.27	7.71	4.09	0.00	99.40	6.30	69.46	24.24
DM2-10	64.81	0.01	20.46	0.17	0.00	1.37	7.91	4.09	0.00	98.84	6.67	69.65	23.68
DM2-10	65.63	0.00	19.51	0.18	0.00	0.45	6.09	7.73	0.00	99.60	2.17	53.31	44.53
DM2-10	65.35	0.00	20.16	0.19	0.00	1.02	7.68	4.83	0.00	99.23	4.94	67.24	27.83
DM2-10	63.74	0.00	20.66	0.20	0.00	1.43	7.83	3.91	0.00	97.77	7.06	69.95	22.99
DM2-10	64.42	0.00	19.39	0.17	0.00	0.38	5.67	7.99	0.00	98.04	1.89	50.92	47.19
DM2-10	66.41	0.01	21.59	0.16	0.00	1.35	7.23	3.81	0.00	100.56	7.10	68.97	23.93
DM2-10	65.55	0.00	19.67	0.19	0.00	0.66	6.88	6.05	0.00	99.00	3.23	61.33	35.44
DM2-10	66.36	0.00	21.33	0.15	0.00	0.82	6.93	5.59	0.00	101.17	4.10	62.65	33.26
DM2-10	65.12	0.02	19.37	0.18	0.00	0.40	6.11	7.84	0.00	99.04	1.94	53.17	44.89

Appendix B. Electron Microprobe Analyses of Feldspar.

	Line Analyses															
Sample	Dist. μ	SiO_2	TiO_2	Al_2O_3	FeO	MgO	BaO	CaO	Na_2O	K_2O	MnO	SrO	Total	An	Ab	Or
DC03-1	0	57.30	0.00	25.95	0.36	0.01	n.a.	8.11	6.32	0.67	0.00	-	98.73	39.85	56.23	3.91
	20	57.25	0.02	25.86	0.36	0.01	n.a.	8.30	6.25	0.69	0.00	-	98.73	40.64	55.37	3.99
	40	56.85	0.00	25.97	0.32	0.01	n.a.	8.23	6.22	0.72	0.02	-	98.32	40.48	55.32	4.20
	60	57.09	0.02	26.07	0.33	0.01	n.a.	8.09	6.28	0.72	0.01	-	98.64	39.84	55.92	4.24
	80	57.32	0.00	25.84	0.32	0.01	n.a.	8.04	6.43	0.79	0.00	-	98.76	39.02	56.41	4.57
	100	56.56	0.01	26.13	0.38	0.00	n.a.	8.43	6.12	0.71	0.02	-	98.35	41.45	54.42	4.13
	120	56.59	0.00	25.77	0.32	0.03	n.a.	8.15	6.12	0.75	0.00	-	97.73	40.51	55.08	4.41
	200	57.41	0.00	25.45	0.36	0.01	n.a.	7.83	6.35	0.87	0.00	-	98.29	38.46	56.44	5.10
	220	57.41	0.01	26.01	0.33	0.02	n.a.	8.22	6.27	0.76	0.00	-	99.03	40.18	55.40	4.42
	260	58.41	0.00	24.86	0.27	0.02	n.a.	7.03	6.66	0.94	0.00	-	98.19	34.82	59.63	5.55
	280	58.52	0.01	24.76	0.32	0.02	n.a.	6.96	6.72	0.95	0.00	-	98.26	34.40	60.04	5.56
	300	58.56	0.02	25.07	0.30	0.01	n.a.	6.90	6.70	1.02	0.00	-	98.57	34.10	59.90	6.00
	320	58.15	0.00	24.93	0.31	0.00	n.a.	7.11	6.66	0.97	0.00	-	98.15	34.99	59.30	5.71
	340	58.43	0.03	24.58	0.30	0.02	n.a.	6.97	6.76	1.01	0.02	-	98.14	34.16	59.95	5.90
	360	58.53	0.01	24.58	0.33	0.01	n.a.	6.99	6.71	1.02	0.01	-	98.18	34.35	59.71	5.95
	400	58.37	0.03	24.86	0.32	0.01	n.a.	6.96	6.54	1.09	0.02	-	98.19	34.64	58.91	6.45
	420	58.33	0.02	24.74	0.31	0.03	n.a.	7.05	6.62	1.03	0.01	-	98.11	34.80	59.17	6.03
	440	58.16	0.00	24.70	0.30	0.02	n.a.	6.97	6.52	1.08	0.00	-	97.76	34.74	58.85	6.40
	460	58.68	0.01	25.17	0.33	0.00	n.a.	7.18	6.67	1.05	0.00	-	99.10	35.02	58.90	6.07
	480	58.09	0.01	24.71	0.31	0.01	n.a.	6.92	6.63	0.96	0.00	-	97.65	34.51	59.83	5.67
	500	58.33	0.01	24.87	0.31	0.00	n.a.	7.18	6.67	0.96	0.01	-	98.33	35.21	59.21	5.58
	520	58.08	0.01	24.81	0.33	0.02	n.a.	7.21	6.61	0.93	0.00	-	97.99	35.56	58.99	5.45
	540	58.75	0.01	25.12	0.29	0.02	n.a.	6.85	6.53	1.09	0.00	-	98.68	34.32	59.19	6.49
	560	58.40	0.00	24.84	0.31	0.03	n.a.	6.83	6.64	1.02	0.01	-	98.09	34.04	59.91	6.05
	600	57.97	0.02	24.86	0.30	0.02	n.a.	7.00	6.64	0.95	0.02	-	97.79	34.75	59.66	5.59
	680	56.70	0.05	27.49	0.34	0.02	n.a.	7.09	5.48	0.89	0.02	-	98.10	39.22	54.92	5.86
	820	57.97	0.00	25.09	0.32	0.02	n.a.	7.39	5.98	0.80	0.00	-	97.58	38.55	56.46	4.99
	840	57.69	0.00	25.35	0.33	0.01	n.a.	7.73	6.03	0.78	0.01	-	97.95	39.50	55.74	4.76
	920	57.88	0.04	25.50	0.35	0.01	n.a.	7.77	6.50	0.82	0.01	-	98.87	37.90	57.36	4.74
	940	57.61	0.01	25.76	0.36	0.02	n.a.	7.77	6.44	0.79	0.01	-	98.77	38.18	57.21	4.61

Appendix B. Electron Microprobe Analyses of Feldspar (continued).

		Line Analyses														
Sample	Dist. μ	SiO_2	TiO_2	Al_2O_3	FeO	MgO	BaO	CaO	Na_2O	K_2O	MnO	SrO	Total	An	Ab	Or
DC03-1	960	57.41	0.01	25.50	0.35	0.01	n.a.	7.79	6.43	0.78	0.01	-	98.29	38.26	57.15	4.58
	980	57.08	0.01	25.47	0.33	0.02	n.a.	7.69	6.38	0.83	0.00	-	97.82	38.04	57.07	4.89
	1020	58.08	0.01	25.33	0.35	0.01	n.a.	7.31	6.46	0.89	0.01	-	98.45	36.43	58.30	5.27
	1040	57.85	0.02	24.97	0.35	0.01	n.a.	7.17	6.50	0.90	0.00	-	97.76	35.84	58.80	5.35
	1060	57.91	0.01	24.84	0.32	0.02	n.a.	7.12	6.66	0.90	0.01	-	97.78	35.18	59.55	5.27
	1080	58.13	0.01	24.72	0.35	0.01	n.a.	7.12	6.62	0.92	0.03	-	97.92	35.27	59.29	5.44
	1100	58.45	0.02	25.39	0.34	0.02	n.a.	7.18	6.79	0.90	0.00	-	99.08	34.95	59.83	5.21
	1120	58.58	0.00	25.04	0.33	0.03	n.a.	7.07	6.93	0.91	0.00	-	98.91	34.17	60.57	5.26
	1180	58.88	0.00	24.76	0.34	0.02	n.a.	6.95	6.72	1.00	0.00	-	98.65	34.23	59.92	5.85
	1260	58.37	0.04	25.33	0.32	0.02	n.a.	7.30	6.58	0.96	0.00	-	98.92	35.89	58.50	5.61
	1340	58.37	0.00	25.17	0.31	0.00	n.a.	7.01	6.53	0.99	0.01	-	98.40	35.05	59.05	5.90
	1360	57.99	0.00	24.63	0.28	0.03	n.a.	7.03	6.48	0.96	0.02	-	97.42	35.29	58.95	5.75
	1380	58.32	0.01	24.76	0.31	0.03	n.a.	6.90	6.51	0.98	0.00	-	97.81	34.78	59.37	5.86
	1400	58.43	0.01	24.78	0.29	0.01	n.a.	6.86	6.63	0.95	0.01	-	97.96	34.29	60.02	5.68
	1420	58.43	0.01	25.28	0.29	0.02	n.a.	7.07	6.67	0.99	0.01	-	98.78	34.80	59.40	5.80
	1440	58.90	0.00	24.61	0.32	0.00	n.a.	6.69	6.77	1.07	0.00	-	98.37	33.07	60.63	6.30
	1460	59.16	0.01	24.47	0.31	0.01	n.a.	6.53	6.87	1.09	0.02	-	98.47	32.23	61.35	6.42
	1480	59.01	0.00	24.52	0.31	0.01	n.a.	6.75	6.89	1.05	0.00	-	98.58	32.97	60.91	6.12
	1500	59.00	0.00	25.20	0.31	0.02	n.a.	6.85	6.65	0.97	0.00	-	98.99	34.18	60.08	5.73
	1520	59.30	0.03	24.76	0.34	0.00	n.a.	6.53	6.85	1.02	0.01	-	98.83	32.40	61.56	6.03
	1540	59.04	0.01	24.68	0.29	0.03	n.a.	6.66	6.79	1.05	0.00	-	98.55	33.00	60.82	6.18
	1560	59.15	0.00	24.65	0.30	0.01	n.a.	6.65	6.70	1.04	0.01	-	98.49	33.25	60.58	6.16
	1580	59.23	0.00	25.17	0.31	0.00	n.a.	6.80	6.90	1.04	0.00	-	99.46	33.12	60.84	6.04
	1600	57.65	0.02	25.85	0.34	0.01	n.a.	8.04	6.35	0.78	0.00	-	99.05	39.29	56.17	4.54
	1620	57.14	0.00	26.02	0.35	0.02	n.a.	8.32	6.30	0.71	0.00	-	98.85	40.44	55.43	4.13
	1640	58.02	0.01	26.10	0.40	0.02	n.a.	8.02	6.59	0.76	0.01	-	99.94	38.45	57.19	4.36
	1660	57.00	0.00	25.98	0.34	0.02	n.a.	7.69	7.10	0.81	0.00	-	98.93	35.78	59.74	4.47
	1680	58.80	0.01	26.12	0.34	0.03	n.a.	7.65	7.50	0.82	0.00	-	101.29	34.44	61.15	4.40
	1700	59.00	0.01	26.47	0.38	0.01	n.a.	7.91	6.30	0.80	0.04	-	100.92	39.05	56.27	4.68
	1720	58.12	0.01	25.52	0.36	0.01	n.a.	7.67	6.30	0.85	0.01	-	98.85	38.18	56.76	5.06
	1740	58.03	0.00	25.97	0.36	0.02	n.a.	7.67	6.40	0.82	0.00	-	99.27	37.94	57.27	4.80

Appendix B. Electron Microprobe Analyses of Feldspar (continued).

		Line Analyses														
Sample	Dist. μ	SiO_2	TiO_2	Al_2O_3	FeO	MgO	BaO	CaO	Na_2O	K_2O	MnO	SrO	Total	An	Ab	Or
DC03-1	1760	56.73	0.03	26.03	0.38	0.02	n.a.	8.36	6.14	0.70	0.03	-	98.42	41.16	54.74	4.10
	1780	56.84	0.00	25.75	0.40	0.02	n.a.	8.03	6.28	0.72	0.02	-	98.06	39.63	56.12	4.24
	1800	57.34	0.02	25.53	0.41	0.03	n.a.	7.70	6.47	0.75	0.00	-	98.26	37.92	57.68	4.41
DC03-2	0	57.94	0.00	25.68	0.28	0.01	n.a.	7.43	6.53	0.72	0.00	-	98.60	36.95	58.79	4.26
	5	56.66	0.00	26.26	0.31	0.01	n.a.	8.39	6.28	0.53	0.00	-	98.43	41.17	55.74	3.09
	10	57.47	0.00	26.18	0.34	0.01	n.a.	8.08	6.36	0.59	0.01	-	99.03	39.80	56.74	3.47
	15	56.41	0.00	26.73	0.40	0.01	n.a.	8.90	5.87	0.52	0.02	-	98.86	44.20	52.74	3.06
	20	55.95	0.02	26.72	0.38	0.01	n.a.	9.13	5.82	0.50	0.01	-	98.53	45.07	51.97	2.96
	25	58.94	0.00	25.30	0.39	0.02	n.a.	7.02	6.65	0.91	0.02	-	99.25	34.85	59.78	5.37
	30	56.47	0.03	26.34	0.39	0.03	n.a.	8.98	6.16	0.46	0.02	-	98.87	43.44	53.92	2.64
	35	57.76	0.01	27.35	0.37	0.02	n.a.	8.98	3.26	0.48	0.00	-	98.21	58.13	38.21	3.66
	40	55.99	0.02	27.00	0.38	0.01	n.a.	9.07	5.87	0.47	0.01	-	98.81	44.78	52.45	2.77
	45	58.17	0.01	25.63	0.33	0.02	n.a.	7.33	6.76	0.85	0.00	-	99.09	35.65	59.44	4.91
	50	56.59	0.00	26.22	0.36	0.01	n.a.	8.57	6.19	0.63	0.02	-	98.58	41.79	54.58	3.63
	55	56.01	0.01	26.65	0.39	0.01	n.a.	9.24	5.48	0.51	0.00	-	98.29	46.75	50.20	3.06
	60	57.24	0.01	26.44	0.32	0.00	n.a.	8.42	6.19	0.58	0.00	-	99.20	41.43	55.17	3.40
	65	58.06	0.02	25.09	0.35	0.00	n.a.	7.46	6.47	0.82	0.00	-	98.27	37.01	58.16	4.83
	70	55.76	0.01	26.87	0.37	0.01	n.a.	9.24	5.51	0.49	0.00	-	98.26	46.68	50.35	2.97
	75	58.80	0.00	25.93	0.37	0.02	n.a.	7.64	6.63	0.80	0.00	-	100.21	37.09	58.27	4.65
	80	56.55	0.03	26.37	0.38	0.02	n.a.	8.68	6.19	0.57	0.00	-	98.79	42.22	54.47	3.31
	85	54.41	0.00	30.02	0.35	0.02	n.a.	8.42	5.16	0.46	0.00	-	98.84	45.99	51.03	2.99
	90	51.00	0.00	32.84	0.39	0.03	n.a.	7.95	5.82	0.45	0.00	-	98.49	41.81	55.38	2.81
	95	57.81	0.00	27.83	0.37	0.03	n.a.	9.33	5.72	0.47	0.00	-	101.57	46.11	51.15	2.74
	100	49.96	0.04	37.85	0.38	0.04	n.a.	5.70	4.78	0.58	0.03	-	99.35	37.90	57.55	4.56
	105	59.68	0.03	25.14	0.33	0.00	n.a.	6.59	7.01	0.97	0.01	-	99.75	32.26	62.07	5.67
	110	60.26	0.00	25.40	0.34	0.02	n.a.	6.30	7.16	0.85	0.00	-	100.34	31.07	63.92	5.01
	115	56.47	0.02	26.87	0.36	0.01	n.a.	8.97	5.96	0.48	0.00	-	99.13	44.11	53.07	2.83
	120	56.57	0.03	26.50	0.40	0.02	n.a.	8.51	6.42	0.52	0.01	-	98.96	41.02	56.01	2.97
	125	57.45	0.00	26.10	0.33	0.02	n.a.	8.14	6.32	0.62	0.02	-	98.99	40.09	56.27	3.64
	130	59.90	0.03	25.67	0.28	0.00	n.a.	6.78	6.97	0.96	0.00	-	100.58	33.01	61.44	5.54

Appendix B. Electron Microprobe Analyses of Feldspar (continued).

		Line Analyses														
Sample	Dist. μ	SiO_2	TiO_2	Al_2O_3	FeO	MgO	BaO	CaO	Na_2O	K_2O	MnO	SrO	Total	An	Ab	Or
DC03-2	135	59.02	0.01	28.37	0.36	0.01	n.a.	9.18	6.06	0.48	0.00	-	103.47	44.31	52.96	2.73
	140	60.55	0.02	23.13	0.24	0.01	n.a.	5.11	7.36	0.92	0.00	-	97.34	26.18	68.23	5.59
	145	57.81	0.00	26.03	0.31	0.03	n.a.	7.97	6.09	0.64	0.02	-	98.90	40.34	55.79	3.87
	150	56.88	0.02	26.49	0.29	0.02	n.a.	8.27	6.41	0.61	0.01	-	98.98	40.16	56.31	3.53
	155	62.92	0.00	24.24	0.36	0.02	n.a.	4.89	7.74	1.23	0.00	-	101.40	24.00	68.82	7.18
	160	66.70	0.07	21.51	0.34	0.03	n.a.	2.96	7.07	2.26	0.00	-	100.96	16.07	69.37	14.56
	165	57.20	0.00	25.93	0.32	0.03	n.a.	8.14	6.19	0.70	0.01	-	98.52	40.33	55.53	4.14
	170	59.35	0.00	25.05	0.30	0.02	n.a.	6.69	7.09	0.80	0.01	-	99.34	32.69	62.67	4.65
	175	64.93	0.09	23.66	0.25	0.07	n.a.	0.77	2.61	7.15	0.00	-	99.54	5.53	33.67	60.80
	180	57.05	0.01	26.24	0.24	0.01	n.a.	7.58	6.57	0.67	0.02	-	98.38	37.41	58.66	3.93
	185	63.78	0.04	19.99	0.27	0.00	n.a.	1.23	4.91	8.09	0.00	-	98.29	6.21	44.99	48.80
	190	55.27	0.00	28.15	0.35	0.02	n.a.	8.64	5.69	0.47	0.00	-	98.60	44.28	52.83	2.89
	195	56.24	0.02	27.00	0.37	0.02	n.a.	9.27	5.78	0.54	0.00	-	99.23	45.52	51.33	3.16
	200	57.51	0.00	26.65	0.37	0.02	n.a.	8.64	6.15	0.53	0.00	-	99.86	42.35	54.54	3.11
	205	57.82	0.02	25.36	0.35	0.02	n.a.	7.42	6.54	0.66	0.02	-	98.19	37.01	59.04	3.95
	210	60.15	0.00	26.20	0.31	0.02		6.50	6.50	0.87	0.00	-	100.55	33.69	60.94	5.37
DC08-1	rim	67.69	0.01	20.01	0.19	0.00	0.10	0.38	5.01	5.95	0.00	0.51	99.85	2.31	54.86	42.83
	core	65.53	0.00	19.27	0.15	0.00	0.03	0.40	5.68	6.39	0.01	0.53	97.99	2.18	56.22	41.60
	0	65.48	0.00	19.07	0.20	0.00	0.07	0.39	6.55	6.10	0.00	0.50	98.34	1.99	60.75	37.26
	30	65.22	0.00	18.81	0.18	0.00	0.05	0.35	6.39	5.99	0.00	0.49	97.48	1.85	60.70	37.45
	60	65.69	0.01	18.96	0.18	0.00	0.07	0.34	6.82	6.24	0.00	0.48	98.81	1.71	61.34	36.95
	90	65.53	0.00	19.18	0.19	0.00	0.06	0.35	6.59	6.71	0.00	0.50	99.11	1.70	58.87	39.42
	120	65.38	0.02	19.37	0.18	0.00	0.09	0.49	6.84	6.41	0.00	0.49	99.27	2.37	60.40	37.23
	150	65.36	0.01	19.25	0.16	0.00	0.08	0.38	6.58	6.90	0.03	0.52	99.26	1.83	58.06	40.10
	180	65.49	0.00	19.10	0.19	0.00	0.04	0.36	6.41	6.95	0.00	0.51	99.06	1.79	57.31	40.90
	210	65.45	0.00	19.07	0.22	0.00	0.12	0.28	6.26	7.18	0.00	0.50	99.08	1.37	56.21	42.42
	240	65.60	0.01	19.18	0.17	0.00	0.09	0.40	6.61	6.68	0.00	0.50	99.24	1.96	58.88	39.16
	270	65.60	0.00	19.17	0.16	0.00	0.07	0.34	6.30	7.03	0.03	0.49	99.19	1.67	56.72	41.61
	300	65.82	0.02	19.05	0.18	0.00	0.04	0.29	6.32	7.03	0.01	0.50	99.24	1.42	56.93	41.65
	330	65.70	0.00	19.03	0.19	0.00	0.04	0.26	6.31	7.20	0.02	0.51	99.26	1.29	56.38	42.32

Appendix B. Electron Microprobe Analyses of Feldspar (continued).

		Line Analyses														
Sample	Dist. μ	SiO_2	TiO_2	Al_2O_3	FeO	MgO	BaO	CaO	Na_2O	K_2O	MnO	SrO	Total	An	Ab	Or
DC08-1	390	65.90	0.02	18.84	0.21	0.00	0.06	0.25	6.11	7.26	0.00	0.50	99.14	1.25	55.39	43.36
	420	65.42	0.00	18.74	0.19	0.00	0.07	0.25	6.26	7.30	0.00	0.51	98.74	1.21	55.90	42.88
	450	65.41	0.02	18.84	0.19	0.00	0.01	0.24	6.29	7.22	0.00	0.51	98.72	1.18	56.30	42.52
	480	65.11	0.02	18.80	0.18	0.00	0.01	0.22	6.19	7.36	0.01	0.51	98.40	1.08	55.52	43.41
	510	65.41	0.00	18.79	0.23	0.00	0.04	0.22	6.20	7.34	0.00	0.51	98.74	1.10	55.61	43.29
	540	65.73	0.00	19.22	0.18	0.00	0.01	0.45	6.78	6.32	0.00	0.48	99.17	2.21	60.61	37.18
	570	65.70	0.00	19.29	0.16	0.00	0.06	0.46	6.90	6.28	0.00	0.51	99.36	2.25	61.15	36.60
	600	65.68	0.02	19.27	0.17	0.00	0.09	0.39	6.77	6.36	0.00	0.52	99.26	1.94	60.59	37.47
	630	64.70	0.00	18.95	0.19	0.00	0.07	0.47	6.62	6.27	0.00	0.49	97.76	2.37	60.17	37.46
	660	65.27	0.02	19.18	0.14	0.00	0.09	0.46	6.86	6.33	0.01	0.51	98.88	2.24	60.85	36.91
	690	65.35	0.00	19.27	0.18	0.00	0.06	0.47	6.76	6.40	0.01	0.50	98.99	2.30	60.17	37.53
	720	65.51	0.01	19.26	0.15	0.00	0.08	0.44	6.66	6.50	0.04	0.51	99.15	2.16	59.56	38.29
	750	65.64	0.00	19.39	0.18	0.00	0.10	0.47	6.70	6.50	0.01	0.50	99.47	2.29	59.64	38.06
	780	65.68	0.00	19.44	0.27	0.00	0.08	0.38	6.62	6.59	0.01	0.50	99.56	1.87	59.29	38.84
	810	65.72	0.00	19.19	0.17	0.00	0.05	0.38	6.66	6.42	0.02	0.52	99.12	1.89	60.04	38.07
	840	65.41	0.00	19.19	0.20	0.00	0.08	0.40	6.70	6.30	0.00	0.49	98.77	1.97	60.55	37.48
	870	65.17	0.02	19.04	0.20	0.00	0.06	0.41	6.68	6.26	0.01	0.50	98.35	2.07	60.55	37.39
	900	65.25	0.00	18.77	0.18	0.00	0.09	0.40	6.66	6.60	0.00	0.49	98.45	1.97	59.32	38.71
	930	65.33	0.00	18.72	0.18	0.00	0.04	0.40	6.59	6.49	0.00	0.52	98.25	2.00	59.46	38.54
	960	65.36	0.02	18.74	0.16	0.00	0.07	0.42	6.74	6.37	0.00	0.49	98.38	2.09	60.37	37.54
	990	65.61	0.00	18.96	0.22	0.00	0.05	0.43	6.84	6.34	0.01	0.49	98.93	2.09	60.80	37.11
	1020	65.54	0.00	18.91	0.20	0.00	0.05	0.27	6.19	7.48	0.00	0.51	99.14	1.31	54.99	43.70
	1050	65.68	0.01	19.24	0.18	0.00	0.06	0.44	6.75	6.41	0.00	0.50	99.27	2.18	60.19	37.63
	1080	65.95	0.00	19.26	0.18	0.00	0.07	0.42	6.58	6.80	0.00	0.51	99.77	2.06	58.29	39.65
	1140	66.01	0.01	19.21	0.17	0.00	0.05	0.34	6.24	6.79	0.02	0.53	99.37	1.74	57.26	41.01
	1170	66.04	0.00	19.17	0.20	0.00	0.06	0.36	7.50	5.14	0.00	0.51	98.97	1.79	67.70	30.52
	1230	65.53	0.01	19.25	0.19	0.00	0.02	0.41	7.11	5.62	0.00	0.51	98.64	2.04	64.44	33.52
	1260	65.23	0.01	19.10	0.19	0.00	0.06	0.40	6.51	6.88	0.02	0.51	98.93	1.98	57.82	40.20
	1290	65.30	0.00	19.16	0.16	0.00	0.09	0.41	6.55	6.82	0.00	0.51	99.01	2.02	58.14	39.84
	1320	65.35	0.00	19.16	0.16	0.00	0.07	0.38	6.53	6.86	0.00	0.51	99.00	1.88	58.02	40.10
	1350	65.25	0.03	19.11	0.16	0.00	0.11	0.40	6.61	6.67	0.00	0.51	98.86	1.98	58.89	39.12

Appendix B. Electron Microprobe Analyses of Feldspar (continued).

	Line Analyses															
Sample	Dist. μ	SiO_2	TiO_2	Al_2O_3	FeO	MgO	BaO	CaO	Na_2O	K_2O	MnO	SrO	Total	An	Ab	Or
DC08-1	1380	65.42	0.00	19.17	0.19	0.00	0.12	0.42	6.75	6.29	0.00	0.51	98.88	2.09	60.72	37.20
	1410	65.31	0.00	19.08	0.17	0.00	0.10	0.38	6.51	6.74	0.00	0.51	98.79	1.89	58.38	39.73
	1440	65.65	0.02	19.23	0.12	0.00	0.09	0.44	6.64	6.61	0.00	0.49	99.30	2.16	59.10	38.74
	1470	65.91	0.00	19.06	0.16	0.00	0.10	0.39	6.60	6.66	0.00	0.52	99.39	1.91	58.93	39.16
	1500	65.32	0.00	19.08	0.17	0.00	0.11	0.34	6.62	6.81	0.00	0.51	98.96	1.67	58.67	39.66
	1530	65.17	0.00	19.06	0.19	0.00	0.10	0.38	6.61	6.62	0.00	0.50	98.63	1.89	59.14	38.97
	1560	65.03	0.00	19.12	0.19	0.00	0.04	0.40	6.50	6.72	0.01	0.50	98.51	1.96	58.38	39.66
	1590	65.36	0.02	19.21	0.16	0.00	0.05	0.41	6.75	6.71	0.01	0.51	99.18	2.00	59.27	38.73
	1620	65.81	0.00	19.37	0.19	0.00	0.04	0.42	6.54	6.61	0.01	0.52	99.51	2.08	58.78	39.13
	1650	65.31	0.01	18.99	0.15	0.00	0.03	0.36	6.44	6.82	0.00	0.52	98.63	1.76	57.87	40.36
	1680	65.29	0.00	18.91	0.18	0.00	0.03	0.34	6.33	6.98	0.00	0.51	98.58	1.69	56.97	41.34
	1710	65.24	0.01	18.98	0.18	0.00	0.07	0.33	6.38	6.90	0.00	0.50	98.58	1.63	57.45	40.91
DC08-4	rim	64.98	0.00	19.10	0.20	0.00	0.01	0.48	5.97	5.96	0.00	0.51	97.21	2.63	58.77	38.59
	0	65.16	0.04	19.02	0.18	0.00	0.06	0.46	6.78	6.30	0.00	0.50	98.48	2.25	60.64	37.11
	30	64.91	0.03	19.07	0.14	0.00	0.04	0.48	6.71	6.23	0.00	0.50	98.11	2.37	60.62	37.01
	60	64.83	0.00	19.06	0.16	0.00	0.06	0.50	6.73	6.21	0.00	0.51	98.06	2.49	60.68	36.83
	90	64.98	0.00	19.09	0.19	0.00	0.08	0.49	6.79	6.21	0.00	0.51	98.34	2.43	60.90	36.67
	120	65.03	0.01	19.06	0.20	0.00	0.10	0.51	6.67	6.08	0.01	0.50	98.17	2.55	60.93	36.52
	150	64.40	0.01	19.06	0.22	0.00	0.15	0.56	6.91	5.84	0.01	0.50	97.66	2.79	62.48	34.74
	180	66.01	0.01	19.35	0.20	0.00	0.12	0.60	6.62	5.54	0.00	0.50	98.95	3.11	62.49	34.40
	210	65.12	0.02	19.12	0.21	0.00	0.07	0.61	6.93	5.45	0.01	0.51	98.03	3.10	63.85	33.05
	240	65.04	0.02	19.22	0.17	0.00	0.14	0.58	6.92	5.53	0.00	0.50	98.12	2.95	63.61	33.44
	270	65.15	0.02	19.16	0.20	0.00	0.09	0.56	6.82	5.67	0.00	0.49	98.16	2.83	62.81	34.36
	300	65.70	0.00	19.46	0.18	0.00	0.11	0.55	6.72	5.77	0.00	0.52	99.01	2.81	62.11	35.08
	330	65.20	0.02	19.22	0.21	0.00	0.09	0.52	6.73	5.97	0.00	0.50	98.45	2.62	61.48	35.90
	360	64.88	0.02	18.87	0.21	0.00	0.16	0.57	6.80	5.99	0.00	0.50	98.00	2.86	61.50	35.64
	390	64.48	0.04	19.60	0.18	0.00	0.04	1.31	7.90	3.94	0.00	0.47	97.94	6.44	70.45	23.12
	450	65.87	0.02	20.21	0.20	0.00	0.16	1.46	7.83	3.65	0.00	0.47	99.86	7.32	70.90	21.78
	480	66.05	0.03	21.22	0.16	0.00	0.17	1.44	7.25	3.50	0.00	0.49	100.32	7.68	70.06	22.26
	540	63.67	0.04	20.34	0.18	0.00	0.18	1.70	7.97	3.12	0.00	0.46	97.66	8.56	72.70	18.74

Appendix B. Electron Microprobe Analyses of Feldspar (continued).

	Line Analyses															
Sample	Dist. μ	SiO_2	TiO_2	Al_2O_3	FeO	MgO	BaO	CaO	Na_2O	K_2O	MnO	SrO	Total	An	Ab	Or
	570	63.97	0.00	20.23	0.19	0.00	0.15	1.60	7.79	3.20	0.00	0.46	97.61	8.22	72.24	19.54
DC08-4	600	63.97	0.01	20.87	0.17	0.00	0.23	1.84	8.29	3.01	0.00	0.47	98.84	9.01	73.45	17.53
	630	63.68	0.02	20.91	0.17	0.00	0.23	1.92	8.30	2.84	0.00	0.46	98.52	9.43	73.94	16.63
	660	63.13	0.02	20.76	0.21	0.00	0.26	2.08	8.29	2.64	0.02	0.46	97.87	10.26	74.22	15.52
	690	62.70	0.07	21.14	0.21	0.00	0.34	2.40	8.38	2.23	0.00	0.44	97.90	11.85	75.00	13.15
	720	63.45	0.03	21.13	0.19	0.00	0.28	2.29	8.30	2.36	0.03	0.46	98.54	11.39	74.64	13.96
	750	63.35	0.05	21.09	0.21	0.00	0.42	2.33	8.25	2.28	0.01	0.45	98.44	11.67	74.76	13.57
	780	63.07	0.02	21.14	0.19	0.00	0.33	2.43	8.32	2.14	0.00	0.44	98.09	12.14	75.16	12.70
	810	61.82	0.04	21.18	0.20	0.00	0.32	2.53	8.51	2.14	0.00	0.44	97.17	12.37	75.20	12.43
	840	62.59	0.00	21.33	0.16	0.00	0.27	2.65	8.35	1.91	0.00	0.43	97.68	13.22	75.44	11.34
	870	62.63	0.03	21.24	0.20	0.00	0.34	2.65	8.37	1.91	0.00	0.44	97.80	13.21	75.46	11.33
	900	62.72	0.05	20.83	0.17	0.00	0.58	2.09	7.87	2.89	0.00	0.45	97.65	10.57	72.01	17.43
	930	62.92	0.01	20.98	0.17	0.00	0.37	2.36	8.40	2.18	0.00	0.44	97.82	11.71	75.42	12.87
	960	62.60	0.05	21.50	0.19	0.00	0.24	2.80	8.47	1.70	0.02	0.43	97.99	13.88	76.08	10.04
	990	62.56	0.05	21.46	0.14	0.00	0.33	2.82	8.50	1.73	0.02	0.45	98.06	13.92	75.92	10.16
	1020	62.59	0.06	21.09	0.20	0.01	0.40	2.46	8.38	2.08	0.00	0.45	97.70	12.22	75.45	12.34
	1050	62.86	0.06	21.10	0.18	0.00	0.33	2.46	8.45	2.05	0.00	0.44	97.94	12.19	75.72	11.16
	1080	62.67	0.05	20.82	0.17	0.00	0.30	2.46	8.10	2.20	0.00	0.45	97.20	12.48	74.26	10.92
	1140	64.69	0.04	20.22	0.20	0.00	0.40	1.23	7.93	3.95	0.00	0.48	99.15	6.08	70.76	23.16
	1170	64.04	0.01	20.31	0.16	0.00	0.32	1.50	7.97	3.62	0.01	0.48	98.40	7.40	71.31	21.28
	1200	64.17	0.02	19.88	0.17	0.00	0.31	1.05	7.59	4.48	0.00	0.47	98.13	5.21	68.27	26.51
	1320	64.77	0.01	18.89	0.16	0.00	0.13	0.53	6.72	6.12	0.01	0.51	97.85	2.65	60.89	36.46
	1350	64.69	0.00	19.26	0.16	0.00	0.08	0.72	7.16	5.36	0.00	0.48	97.91	3.58	64.62	31.80
	1440	64.87	0.00	18.96	0.17	0.00	0.07	0.50	6.84	5.96	0.00	0.49	97.85	2.48	61.95	35.56
	1590	65.02	0.00	19.59	0.18	0.00	0.18	0.67	6.83	5.71	0.00	0.49	98.68	3.37	62.33	34.30
	1620	65.75	0.02	20.06	0.20	0.00	0.18	0.66	6.35	5.71	0.00	0.50	99.43	3.46	60.65	35.89
	1740	63.37	0.02	19.71	0.13	0.00	0.19	1.18	7.82	4.20	0.02	0.47	97.09	5.79	69.59	24.62
DC08-6	1650	65.72	0.00	19.63	0.18	0.00	0.00	0.29	6.32	7.30	0.00	0.52	99.97	1.43	55.99	42.58
	1680	65.59	0.00	19.02	0.15	0.00	0.00	0.24	6.58	7.35	0.01	0.53	99.47	1.17	56.97	41.86

Appendix B. Electron Microprobe Analyses of Feldspar (continued).

		Line Analyses														
Sample	Dist. μ	SiO_2	TiO_2	Al_2O_3	FeO	MgO	BaO	CaO	Na_2O	K_2O	MnO	SrO	Total	An	Ab	Or
RC07-12	core	61.27	0.03	22.71	0.25	0.00	0.13	4.26	7.96	1.32	0.01	0.46	98.40	21.06	71.19	7.75
	rim	62.76	0.05	19.47	0.15	0.00	1.38	0.55	4.67	8.69	0.00	0.53	98.26	2.85	43.67	53.48
	0	62.92	0.01	19.19	0.23	0.00	1.32	0.52	4.94	8.84	0.01	0.53	98.50	2.60	44.72	52.69
	20	63.08	0.03	19.28	0.16	0.00	1.38	0.48	4.89	8.67	0.00	0.54	98.51	2.46	45.02	52.51
	60	63.10	0.00	19.18	0.16	0.00	1.06	0.60	5.13	8.22	0.00	0.52	97.97	3.07	47.20	49.73
	80	61.16	0.03	22.23	0.23	0.01	0.17	4.11	8.39	1.41	0.01	0.42	98.17	19.58	72.40	8.03
	120	61.10	0.02	22.76	0.23	0.00	0.13	4.41	8.48	1.22	0.02	0.43	98.82	20.79	72.33	6.87
	140	60.95	0.00	22.48	0.22	0.00	0.09	4.16	8.45	1.30	0.00	0.43	98.08	19.81	72.81	7.38
	200	62.61	0.00	19.33	0.14	0.00	1.25	0.51	5.02	8.53	0.03	0.53	97.94	2.59	46.02	51.39
RC07-15	core	60.19	0.04	22.79	0.21	0.00	0.28	4.54	8.36	1.26	0.01	0.46	98.13	21.46	71.45	7.08
	rim	64.19	0.03	19.31	0.16	0.00	0.80	0.44	4.96	9.01	0.01	0.52	99.42	2.19	44.53	53.27
	120	60.58	0.01	23.02	0.24	0.00	0.22	4.39	8.32	1.35	0.00	0.46	98.60	20.86	71.51	7.63
	140	60.81	0.00	23.03	0.26	0.02	0.25	4.40	7.99	1.30	0.00	0.46	98.51	21.57	70.86	7.57
	180	60.71	0.01	23.29	0.24	0.01	0.09	4.95	7.86	1.11	0.00	0.44	98.71	24.17	69.40	6.43
	200	60.41	0.03	23.29	0.27	0.02	0.08	5.08	7.88	1.04	0.01	0.43	98.53	24.69	69.29	6.02
	240	60.52	0.02	23.49	0.26	0.01	0.12	4.81	7.97	1.05	0.02	0.42	98.70	23.49	70.42	6.10
	260	61.19	0.00	22.91	0.23	0.00	0.16	4.92	8.52	1.23	0.00	0.43	99.59	22.56	70.71	6.73
RC07-15	320	61.19	0.03	23.48	0.25	0.01	0.08	5.07	8.46	1.09	0.00	0.43	100.08	23.37	70.64	5.99
	340	61.18	0.00	23.63	0.24	0.01	0.12	4.97	8.25	1.13	0.00	0.44	99.98	23.37	70.27	6.35
	360	64.33	0.05	19.40	0.17	0.00	0.92	0.47	5.53	8.16	0.00	0.56	99.58	2.33	49.57	48.10
	380	64.00	0.02	19.27	0.22	0.00	0.85	0.53	5.07	8.90	0.00	0.55	99.40	2.63	45.18	52.19
RC12-2	core	61.62	0.01	23.45	0.26	0.01	0.14	4.91	8.46	1.17	0.00	0.45	100.48	22.70	70.86	6.44
Line A	rim	64.14	0.00	19.51	0.20	0.00	0.79	0.45	5.04	9.21	0.01	0.53	99.89	2.20	44.40	53.40
	20	64.63	0.06	19.49	0.15	0.00	0.79	0.41	5.24	8.95	0.00	0.55	100.26	1.99	46.16	51.85
	60	64.65	0.03	19.31	0.17	0.00	0.90	0.48	5.17	8.92	0.00	0.53	100.16	2.36	45.74	51.90
	100	62.31	0.01	23.33	0.23	0.00	0.14	4.54	8.60	1.27	0.00	0.46	100.87	21.00	72.01	6.99
	140	61.06	0.02	24.02	0.27	0.00	0.05	5.60	8.31	0.95	0.00	0.45	100.72	25.71	69.10	5.19
	160	59.49	0.04	24.91	0.27	0.01	0.06	6.50	7.88	0.78	0.00	0.43	100.37	29.99	65.74	4.27
	180	58.72	0.03	25.24	0.22	0.01	0.06	7.10	7.38	0.67	0.00	0.42	99.86	33.39	62.83	3.77

Appendix B. Electron Microprobe Analyses of Feldspar (continued).

		Line Analyses														
Sample	Dist. μ	SiO_2	TiO_2	Al_2O_3	FeO	MgO	BaO	CaO	Na_2O	K_2O	MnO	SrO	Total	An	Ab	Or
	220	60.93	0.04	23.14	0.24	0.00	0.08	5.00	8.22	1.12	0.01	0.44	99.22	23.59	70.15	6.27
	240	60.73	0.00	23.31	0.29	0.00	0.10	5.29	8.09	1.05	0.01	0.44	99.30	24.98	69.13	5.89
	260	60.63	0.02	23.27	0.32	0.00	0.10	5.18	8.02	1.05	0.00	0.43	99.01	24.73	69.31	5.97
	300	59.25	0.04	24.58	0.23	0.00	0.05	6.52	7.81	0.77	0.00	0.42	99.67	30.22	65.53	4.25
	320	59.87	0.04	24.55	0.24	0.00	0.10	6.26	7.92	0.79	0.01	0.45	100.23	29.07	66.56	4.37
	340	61.41	0.00	23.56	0.22	0.01	0.09	5.01	8.45	1.09	0.01	0.45	100.29	23.18	70.83	6.00
	380	61.58	0.00	23.53	0.24	0.01	0.12	4.96	8.39	1.13	0.02	0.45	100.42	23.11	70.66	6.24
	420	61.42	0.02	23.67	0.27	0.01	0.07	5.02	8.53	1.14	0.01	0.44	100.59	23.02	70.77	6.21
	440	62.05	0.00	23.14	0.25	0.01	0.14	4.48	8.53	1.32	0.01	0.45	100.39	20.86	71.83	7.31
	480	59.09	0.00	25.68	0.27	0.00	0.05	7.12	7.44	0.68	0.00	0.43	100.76	33.28	62.94	3.78
	500	60.60	0.04	24.33	0.25	0.02	0.12	5.75	8.06	0.89	0.00	0.46	100.51	26.88	68.15	4.97
	520	59.84	0.07	24.97	0.26	0.02	0.08	6.55	7.71	0.74	0.01	0.43	100.68	30.62	65.25	4.13
	540	60.61	0.03	24.25	0.30	0.02	0.09	5.87	8.14	0.86	0.00	0.44	100.61	27.15	68.13	4.72
	560	59.81	0.02	24.67	0.25	0.00	0.13	6.39	7.86	0.75	0.01	0.43	100.31	29.70	66.13	4.17
	580	59.97	0.00	24.49	0.28	0.01	0.07	6.09	7.93	0.81	0.00	0.43	100.08	28.48	67.04	4.48
	600	59.65	0.05	24.53	0.26	0.01	0.03	6.38	7.99	0.81	0.00	0.42	100.12	29.28	66.31	4.40
	620	59.98	0.04	24.52	0.26	0.01	0.06	6.22	7.86	0.79	0.00	0.43	100.17	29.08	66.51	4.42
	640	60.87	0.02	24.00	0.27	0.01	0.12	5.59	8.29	0.94	0.00	0.44	100.54	25.75	69.11	5.14
	660	62.15	0.00	22.97	0.25	0.01	0.19	4.50	8.71	1.30	0.00	0.45	100.53	20.61	72.29	7.10
	700	64.51	0.02	19.57	0.16	0.00	0.78	0.68	5.19	8.70	0.01	0.53	100.13	3.32	45.97	50.70
	760	64.32	0.01	19.58	0.18	0.00	0.94	0.58	5.16	8.84	0.00	0.55	100.15	2.85	45.66	51.49
RC12-2	20	63.91	0.04	19.57	0.13	0.00	0.87	0.51	4.91	8.93	0.01	0.51	99.40	2.57	44.35	53.09
Line B	40	63.82	0.02	19.57	0.18	0.00	1.04	0.49	4.91	9.17	0.01	0.54	99.74	2.40	43.80	53.80
	60	63.88	0.02	19.35	0.18	0.00	0.90	0.45	5.05	9.27	0.00	0.52	99.63	2.18	44.32	53.50
	120	63.65	0.00	21.80	0.23	0.00	0.16	3.04	8.80	2.07	0.00	0.47	100.23	14.20	74.32	11.49
	180	63.16	0.00	22.41	0.26	0.00	0.14	3.74	8.83	1.58	0.02	0.44	100.59	17.31	74.00	8.69
	220	62.99	0.00	22.45	0.25	0.00	0.07	3.90	8.86	1.53	0.00	0.45	100.50	17.93	73.70	8.37
	260	64.43	0.00	22.75	0.26	0.01	0.10	3.65	9.31	0.77	0.00	0.46	101.73	17.04	78.67	4.29
	300	62.51	0.00	22.84	0.29	0.01	0.18	4.14	8.70	1.38	0.01	0.44	100.50	19.23	73.13	7.64
	320	62.26	0.03	23.39	0.30	0.01	0.13	4.58	8.61	1.23	0.00	0.44	100.98	21.17	72.08	6.75

Appendix B. Electron Microprobe Analyses of Feldspar (continued).

		Line Analyses														
Sample	Dist. μ	SiO_2	TiO_2	Al_2O_3	FeO	MgO	BaO	CaO	Na_2O	K_2O	MnO	SrO	Total	An	Ab	Or
	340	62.10	0.03	23.22	0.25	0.00	0.10	4.50	8.67	1.19	0.00	0.45	100.51	20.83	72.60	6.56
	400	60.24	0.02	24.10	0.31	0.02	0.10	5.65	8.09	0.94	0.00	0.44	99.91	26.40	68.37	5.23
	420	59.79	0.05	24.76	0.27	0.00	0.11	6.19	7.86	0.83	0.01	0.44	100.32	28.92	66.46	4.63
	440	60.75	0.04	24.40	0.27	0.01	0.09	5.78	8.08	0.86	0.01	0.44	100.73	26.99	68.21	4.80
	460	60.33	0.00	24.30	0.31	0.00	0.05	5.83	8.06	0.88	0.00	0.44	100.20	27.16	67.97	4.88
	480	60.37	0.03	24.36	0.32	0.02	0.14	5.87	8.14	0.91	0.00	0.43	100.60	27.08	67.95	4.97
	540	61.59	0.02	24.24	0.29	0.01	0.12	5.52	8.24	0.99	0.00	0.45	101.47	25.56	69.00	5.44
	560	61.02	0.02	24.11	0.28	0.00	0.10	5.52	8.31	0.98	0.00	0.44	100.78	25.43	69.21	5.36
	580	60.98	0.00	24.03	0.28	0.02	0.12	5.48	8.26	0.95	0.02	0.44	100.56	25.43	69.34	5.24
	600	60.49	0.02	24.19	0.28	0.00	0.11	5.79	8.25	0.89	0.01	0.44	100.47	26.59	68.52	4.88
	620	60.29	0.04	24.57	0.30	0.00	0.10	6.06	8.03	0.83	0.01	0.44	100.67	28.09	67.34	4.57
	660	60.36	0.01	24.26	0.29	0.02	0.10	5.70	8.20	0.92	0.02	0.44	100.32	26.35	68.57	5.08
	680	60.33	0.04	24.33	0.28	0.00	0.20	5.86	8.16	0.90	0.00	0.44	100.54	27.02	68.05	4.93
	700	60.69	0.03	24.26	0.31	0.00	0.10	5.64	8.21	0.84	0.00	0.45	100.52	26.23	69.11	4.65
	780	60.73	0.02	24.15	0.23	0.01	0.07	5.71	8.18	0.82	0.00	0.44	100.35	26.56	68.88	4.56
	800	61.16	0.03	23.85	0.28	0.00	0.09	5.37	8.31	0.96	0.00	0.44	100.50	24.91	69.76	5.32
	820	60.77	0.03	23.98	0.26	0.02	0.14	5.54	8.22	0.87	0.00	0.44	100.27	25.80	69.38	4.81
	840	60.73	0.03	23.98	0.29	0.01	0.12	5.58	7.45	0.91	0.02	0.44	99.55	27.67	66.93	5.40
	860	61.21	0.00	23.67	0.23	0.01	0.20	5.21	7.56	0.97	0.00	0.43	99.49	25.99	68.24	5.77
	880	62.24	0.03	22.98	0.24	0.00	0.16	4.33	7.90	1.21	0.01	0.44	99.52	21.58	71.22	7.20
	920	61.77	0.01	22.90	0.29	0.01	0.12	4.41	7.79	1.26	0.00	0.46	99.03	22.06	70.46	7.47
	960	64.19	0.02	19.27	0.19	0.00	0.76	0.41	4.43	9.59	0.00	0.52	99.37	2.06	40.40	57.54
	980	64.26	0.02	19.22	0.19	0.00	0.76	0.38	4.52	9.64	0.01	0.53	99.52	1.88	40.83	57.29
RC12-4	5	62.26	0.00	22.49	0.29	0.00	0.13	3.71	8.84	1.67	0.00	0.42	99.82	17.12	73.72	9.16
	10	62.55	0.00	22.66	0.27	0.01	0.15	3.95	7.57	1.54	0.00	0.43	99.12	20.25	70.33	9.42
	15	62.88	0.03	22.49	0.26	0.00	0.11	3.70	8.03	1.66	0.01	0.42	99.57	18.30	71.94	9.75
	20	62.62	0.02	22.73	0.28	0.00	0.12	4.03	8.91	1.52	0.02	0.42	100.67	18.34	73.42	8.24
	35	61.61	0.04	22.57	0.36	0.02	0.11	3.83	8.21	1.46	0.00	0.42	98.62	18.75	72.74	8.51
	55	62.54	0.00	23.75	0.27	0.00	0.08	4.61	8.39	1.22	0.01	0.41	101.28	21.68	71.46	6.85
	60	62.66	0.01	24.16	0.23	0.00	0.08	4.88	8.35	1.13	0.00	0.44	101.93	22.87	70.83	6.30
	80	60.88	0.05	23.76	0.25	0.00	0.11	5.12	8.33	1.08	0.00	0.40	99.97	23.82	70.17	6.01

Appendix B. Electron Microprobe Analyses of Feldspar (continued).

	Line Analyses															
Sample	Dist. μ	SiO_2	TiO_2	Al_2O_3	FeO	MgO	BaO	CaO	Na_2O	K_2O	MnO	SrO	Total	An	Ab	Or
RC12-4	190	56.37	0.02	25.24	0.23	0.00	0.09	7.55	6.79	0.58	0.01	0.37	97.24	36.79	59.86	3.35
	195	56.61	0.00	25.68	0.22	0.01	0.03	7.75	6.90	0.56	0.00	0.40	98.15	37.08	59.74	3.18
	200	56.83	0.00	26.26	0.25	0.01	0.04	8.22	6.94	0.55	0.01	0.39	99.51	38.35	58.58	3.07
	205	56.98	0.01	26.55	0.24	0.00	0.05	8.29	6.99	0.50	0.00	0.40	100.01	38.46	58.76	2.78
	210	56.82	0.00	26.48	0.25	0.01	0.04	8.35	6.86	0.55	0.02	0.40	99.77	38.98	57.98	3.04
	215	56.60	0.02	26.37	0.23	0.01	0.06	8.32	7.02	0.55	0.00	0.39	99.56	38.36	58.60	3.04
	220	57.40	0.02	26.55	0.26	0.00	0.09	8.35	6.99	0.53	0.01	0.39	100.58	38.62	58.47	2.91
	225	57.35	0.02	26.37	0.21	0.00	0.07	8.26	6.91	0.56	0.00	0.40	100.15	38.53	58.36	3.10
	230	57.54	0.01	26.71	0.24	0.00	0.10	8.36	6.89	0.58	0.00	0.39	100.81	38.88	57.91	3.21
	245	57.11	0.01	26.31	0.24	0.00	0.04	8.33	7.02	0.61	0.00	0.39	100.07	38.28	58.37	3.35
	250	56.90	0.01	26.18	0.24	0.01	0.05	8.09	7.07	0.59	0.00	0.38	99.52	37.47	59.28	3.24
	255	57.43	0.00	26.35	0.24	0.00	0.06	8.28	7.01	0.58	0.01	0.40	100.35	38.24	58.59	3.17
	260	57.46	0.01	26.20	0.22	0.02	0.05	8.13	7.01	0.58	0.02	0.39	100.09	37.80	58.98	3.22
	265	57.58	0.00	26.31	0.25	0.01	0.04	8.26	7.09	0.59	0.00	0.39	100.52	37.91	58.88	3.21
	270	57.54	0.01	26.33	0.23	0.01	0.04	8.20	7.04	0.57	0.02	0.40	100.39	37.93	58.91	3.16
	275	57.74	0.01	26.35	0.24	0.01	0.03	8.13	7.09	0.60	0.00	0.39	100.57	37.49	59.21	3.29
	280	57.50	0.02	26.19	0.24	0.01	0.08	8.04	7.13	0.67	0.02	0.38	100.26	36.97	59.39	3.64
	285	57.85	0.05	26.23	0.23	0.01	0.05	7.95	7.14	0.64	0.03	0.40	100.58	36.74	59.75	3.51
	290	57.73	0.04	26.17	0.22	0.02	0.09	8.11	7.10	0.61	0.01	0.40	100.50	37.40	59.23	3.37
	295	57.70	0.00	26.09	0.23	0.01	0.05	8.03	7.13	0.61	0.01	0.38	100.22	37.07	59.56	3.37
	320	57.46	0.00	26.04	0.23	0.01	0.04	7.95	7.19	0.65	0.01	0.39	99.97	36.55	59.88	3.57
	325	58.09	0.01	26.02	0.24	0.00	0.01	7.84	7.04	0.61	0.03	0.40	100.27	36.79	59.82	3.40
	385	61.37	0.00	23.46	0.23	0.00	0.06	4.76	8.39	1.12	0.00	0.42	99.80	22.35	71.35	6.29
	390	61.28	0.00	23.51	0.19	0.00	0.08	4.95	8.45	1.09	0.01	0.41	99.97	22.97	71.00	6.03
	395	61.73	0.01	23.54	0.22	0.02	0.09	4.93	8.52	1.16	0.01	0.43	100.66	22.71	70.93	6.36
	400	61.25	0.00	23.59	0.21	0.00	0.09	4.93	8.42	1.12	0.00	0.43	100.05	22.92	70.89	6.18
	410	59.84	0.00	24.62	0.23	0.00	0.06	6.26	7.66	0.88	0.00	0.40	99.97	29.58	65.50	4.92
	415	57.89	0.00	25.74	0.23	0.00	0.03	7.59	7.21	0.67	0.00	0.40	99.76	35.41	60.88	3.71
	420	57.74	0.00	26.10	0.19	0.02	0.07	7.89	7.10	0.62	0.01	0.40	100.12	36.73	59.86	3.41
	425	57.88	0.00	26.15	0.20	0.01	0.04	7.95	7.10	0.59	0.02	0.41	100.34	36.98	59.76	3.27
	430	57.64	0.00	26.10	0.20	0.01	0.04	7.91	7.16	0.61	0.00	0.40	100.06	36.63	60.01	3.36

Appendix B. Electron Microprobe Analyses of Feldspar (continued).

	Line Analyses															
Sample	Dist. μ	SiO_2	TiO_2	Al_2O_3	FeO	MgO	BaO	CaO	Na_2O	K_2O	MnO	SrO	Total	An	Ab	Or
RC12-4	435	57.86	0.03	26.14	0.19	0.01	0.04	7.89	7.20	0.61	0.02	0.39	100.38	36.46	60.21	3.33
	440	57.91	0.00	26.18	0.21	0.00	0.04	7.92	7.19	0.62	0.00	0.41	100.47	36.56	60.04	3.39
	445	58.17	0.01	26.35	0.21	0.01	0.04	7.93	7.36	0.59	0.01	0.40	101.06	36.11	60.70	3.19
	450	57.96	0.05	26.33	0.20	0.00	0.06	8.03	7.30	0.62	0.00	0.38	100.92	36.51	60.11	3.37
	455	58.00	0.01	26.06	0.20	0.01	0.06	7.84	7.30	0.63	0.01	0.40	100.51	35.96	60.60	3.43
	460	58.17	0.00	26.00	0.23	0.00	0.04	7.70	7.24	0.62	0.00	0.40	100.39	35.77	60.83	3.41
	465	58.08	0.02	25.94	0.22	0.02	0.07	7.75	7.20	0.63	0.01	0.39	100.30	36.01	60.52	3.46
	470	58.33	0.01	26.16	0.22	0.01	0.06	7.70	7.25	0.63	0.01	0.39	100.77	35.70	60.81	3.48
	475	58.26	0.00	26.01	0.21	0.00	0.06	7.88	7.27	0.64	0.00	0.41	100.73	36.16	60.34	3.50
	480	58.46	0.00	26.06	0.22	0.01	0.07	7.99	7.19	0.65	0.02	0.41	101.08	36.68	59.76	3.56
	485	57.98	0.02	26.06	0.25	0.01	0.05	7.70	7.26	0.62	0.01	0.39	100.34	35.72	60.89	3.40
	490	57.61	0.00	25.92	0.20	0.01	0.06	7.74	7.31	0.61	0.02	0.40	99.86	35.67	60.96	3.37
	495	57.68	0.00	25.75	0.21	0.00	0.07	7.66	7.21	0.59	0.02	0.40	99.58	35.78	60.96	3.26
	500	57.56	0.01	25.90	0.22	0.02	0.05	7.82	7.08	0.57	0.00	0.38	99.61	36.70	60.14	3.16
	505	57.67	0.00	25.87	0.21	0.01	0.06	7.73	7.09	0.56	0.02	0.40	99.61	36.43	60.45	3.13
	510	57.90	0.00	25.91	0.19	0.02	0.02	7.72	7.22	0.62	0.02	0.40	100.01	35.90	60.68	3.43
	515	57.74	0.00	26.00	0.25	0.00	0.06	7.87	7.22	0.61	0.02	0.40	100.16	36.34	60.30	3.36
	520	57.57	0.00	25.82	0.24	0.01	0.03	7.76	7.22	0.63	0.01	0.40	99.68	35.97	60.56	3.47
	525	57.39	0.01	25.77	0.23	0.01	0.01	7.76	7.18	0.64	0.00	0.38	99.38	36.09	60.40	3.52
	530	57.45	0.00	25.74	0.25	0.00	0.06	7.85	7.22	0.62	0.01	0.41	99.61	36.23	60.35	3.42
	535	57.53	0.01	25.56	0.26	0.01	0.09	7.65	7.12	0.64	0.00	0.39	99.26	35.92	60.50	3.58
	540	57.55	0.02	25.76	0.23	0.02	0.05	7.60	7.15	0.64	0.00	0.40	99.41	35.69	60.71	3.60
	545	57.64	0.00	25.73	0.26	0.02	0.04	7.57	7.25	0.64	0.00	0.40	99.55	35.30	61.16	3.54
	550	57.52	0.01	25.66	0.23	0.01	0.07	7.53	7.27	0.64	0.00	0.40	99.33	35.11	61.33	3.56
	555	57.96	0.01	25.80	0.27	0.02	0.06	7.41	7.17	0.63	0.00	0.39	99.73	35.07	61.39	3.54
	560	58.24	0.01	25.77	0.27	0.02	0.06	7.44	7.23	0.64	0.00	0.40	100.09	34.95	61.47	3.58
	565	58.10	0.00	25.84	0.28	0.01	0.02	7.37	7.24	0.63	0.03	0.40	99.91	34.70	61.75	3.56
	570	58.10	0.01	25.64	0.38	0.01	0.11	7.23	7.12	0.65	0.01	0.41	99.68	34.59	61.69	3.73
	575	58.29	0.00	25.89	0.28	0.02	0.08	7.76	7.20	0.60	0.00	0.43	100.54	36.11	60.58	3.31
	580	58.05	0.00	25.76	0.26	0.00	0.07	7.63	7.33	0.56	0.00	0.39	100.04	35.36	61.55	3.09
	585	57.66	0.02	25.62	0.26	0.01	0.07	7.72	7.29	0.61	0.02	0.39	99.67	35.67	60.95	3.37

Appendix B. Electron Microprobe Analyses of Feldspar (continued).

		Line Analyses														
Sample	Dist. μ	SiO_2	TiO_2	Al_2O_3	FeO	MgO	BaO	CaO	Na_2O	K_2O	MnO	SrO	Total	An	Ab	Or
RC12-4	595	58.03	0.00	25.55	0.26	0.01	0.04	7.73	7.31	0.53	0.01	0.40	99.86	35.81	61.28	2.90
	600	57.83	0.03	25.91	0.26	0.01	0.08	7.84	7.27	0.58	0.01	0.39	100.21	36.15	60.65	3.20
	605	57.90	0.00	25.76	0.26	0.02	0.07	7.73	7.26	0.62	0.00	0.42	100.03	35.79	60.80	3.41
	610	58.54	0.00	25.40	0.26	0.00	0.06	7.31	7.56	0.64	0.00	0.39	100.16	33.60	62.88	3.51
	615	58.66	0.00	25.07	0.25	0.01	0.03	6.93	7.57	0.71	0.03	0.40	99.66	32.26	63.80	3.94
	620	58.54	0.00	25.04	0.26	0.00	0.11	7.07	7.71	0.76	0.01	0.40	99.91	32.24	63.61	4.15
	625	58.58	0.01	25.06	0.27	0.00	0.10	6.86	7.67	0.75	0.00	0.40	99.69	31.71	64.19	4.10
	630	59.00	0.00	24.85	0.25	0.01	0.07	6.67	7.77	0.81	0.00	0.40	99.81	30.73	64.81	4.46
	635	58.77	0.00	24.65	0.28	0.01	0.07	6.46	7.98	0.82	0.00	0.39	99.42	29.55	66.01	4.44
	640	59.18	0.01	24.49	0.26	0.00	0.04	6.27	7.67	0.86	0.00	0.42	99.18	29.62	65.55	4.83
	645	59.57	0.00	24.33	0.27	0.01	0.05	6.25	7.74	0.83	0.00	0.40	99.44	29.41	65.93	4.66
	650	59.52	0.00	24.37	0.24	0.00	0.09	6.35	7.86	0.82	0.00	0.41	99.67	29.49	66.01	4.50
	655	59.83	0.00	24.41	0.29	0.01	0.05	6.22	7.82	0.82	0.00	0.41	99.85	29.13	66.28	4.59
	660	59.89	0.00	24.57	0.25	0.00	0.10	6.19	7.84	0.83	0.02	0.41	100.10	28.96	66.41	4.62
	665	60.53	0.00	22.99	0.25	0.01	0.09	4.79	7.50	1.21	0.02	0.42	97.80	24.16	68.55	7.29
	670	60.54	0.00	23.17	0.23	0.02	0.12	5.09	7.21	1.10	0.02	0.41	97.88	26.17	67.12	6.71
	675	60.89	0.00	22.81	0.28	0.01	0.10	4.76	7.35	1.17	0.02	0.41	97.78	24.46	68.37	7.17
	685	63.97	0.01	23.65	0.26	0.01	0.07	4.23	8.65	1.44	0.01	0.43	102.73	19.59	72.48	7.93
	705	63.20	0.00	23.09	0.28	0.02	0.12	4.02	8.55	1.47	0.00	0.42	101.16	18.92	72.86	8.22
	710	63.45	0.00	23.10	0.22	0.01	0.11	4.12	8.60	1.46	0.00	0.43	101.49	19.21	72.67	8.12
	715	62.08	0.00	22.75	0.23	0.01	0.11	4.11	8.15	1.47	0.00	0.44	99.35	19.94	71.55	8.51
	720	64.22	0.00	23.59	0.25	0.01	0.09	4.18	8.53	1.51	0.00	0.43	102.81	19.53	72.09	8.38
	725	64.03	0.01	23.16	0.26	0.03	0.11	3.76	8.07	1.56	0.00	0.44	101.43	18.59	72.25	9.16
	730	61.53	0.00	21.98	0.23	0.00	0.15	3.75	8.38	1.53	0.00	0.42	97.96	18.08	73.13	8.79
	735	62.42	0.01	22.51	0.24	0.01	0.15	3.94	8.77	1.38	0.00	0.41	99.85	18.37	73.96	7.66
	740	62.67	0.01	22.42	0.26	0.00	0.14	3.82	8.72	1.45	0.00	0.43	99.93	17.91	73.99	8.10
	745	62.98	0.03	22.86	0.25	0.00	0.15	4.06	8.68	1.45	0.02	0.43	100.90	18.90	73.06	8.04
	765	62.57	0.01	22.07	0.27	0.01	0.11	3.47	8.68	1.58	0.00	0.44	99.21	16.48	74.57	8.95
	770	62.35	0.00	22.28	0.22	0.00	0.08	3.64	8.61	1.69	0.01	0.44	99.33	17.15	73.36	9.49
	780	62.42	0.00	22.20	0.29	0.01	0.12	3.65	8.54	1.63	0.00	0.42	99.29	17.33	73.43	9.24
	795	63.62	0.02	19.38	0.18	0.00	0.82	0.58	6.06	7.39	0.00	0.49	98.53	2.86	53.89	43.25
	800	63.81	0.02	19.31	0.18	0.00	0.89	0.47	5.99	7.43	0.00	0.48	98.58	2.34	53.75	43.91

Appendix B. Electron Microprobe Analyses of Feldspar (continued).

	Line Analyses															
Sample	Dist. μ	SiO_2	TiO_2	Al_2O_3	FeO	MgO	BaO	CaO	Na_2O	K_2O	MnO	SrO	Total	An	Ab	Or
	810	64.33	0.02	19.22	0.17	0.00	0.79	0.46	5.30	8.73	0.00	0.49	99.51	2.25	46.89	50.87
	815	64.26	0.00	19.28	0.19	0.00	0.83	0.45	5.11	8.91	0.01	0.48	99.52	2.21	45.53	52.26
RC12-14	185	61.55	0.00	22.79	0.25	0.00	0.05	4.37	7.77	1.32	0.00	0.44	98.53	21.88	70.29	7.84
	195	61.56	0.02	22.93	0.22	0.01	0.10	4.30	8.00	1.37	0.03	0.42	98.95	21.06	70.96	7.98
	200	62.09	0.00	22.96	0.26	0.00	0.10	4.27	8.58	1.34	0.00	0.43	100.02	19.97	72.58	7.45
	250	61.61	0.03	23.00	0.25	0.00	0.06	4.37	8.40	1.37	0.00	0.43	99.49	20.60	71.72	7.68
	255	61.29	0.02	22.72	0.26	0.01	0.07	4.38	8.42	1.38	0.01	0.41	98.95	20.61	71.68	7.71
	260	62.11	0.01	22.79	0.26	0.00	0.10	3.58	8.72	1.44	0.00	0.40	99.40	16.97	74.87	8.16
	270	61.32	0.00	23.09	0.23	0.00	0.13	3.70	8.63	1.29	0.01	0.41	98.82	17.75	74.86	7.38
	490	61.46	0.03	23.05	0.20	0.00	0.06	4.73	8.44	1.21	0.00	0.43	99.62	22.06	71.24	6.70
	495	61.34	0.00	22.82	0.23	0.00	0.06	4.74	8.43	1.13	0.01	0.41	99.15	22.20	71.48	6.32
	510	60.91	0.02	22.49	0.26	0.00	0.09	4.55	8.35	0.93	0.02	0.42	98.04	21.90	72.76	5.34
	530	61.67	0.02	22.49	0.25	0.00	0.14	4.14	8.60	1.45	0.00	0.42	99.18	19.32	72.64	8.04
	535	60.95	0.07	22.15	0.40	0.02	0.10	4.11	8.26	1.40	0.00	0.43	97.88	19.82	72.15	8.03
	555	61.22	0.00	22.66	0.26	0.00	0.12	4.12	8.22	1.46	0.02	0.41	98.49	19.88	71.76	8.36
	560	63.90	0.01	20.76	0.40	0.00	0.12	2.66	7.81	3.69	0.00	0.46	99.80	12.54	66.70	20.75
	575	61.46	0.00	22.98	0.26	0.00	0.11	4.49	8.32	1.18	0.00	0.44	99.25	21.43	71.86	6.71
	585	61.12	0.00	22.61	0.27	0.00	0.13	4.51	8.63	1.25	0.00	0.43	98.97	20.88	72.22	6.90
	590	61.89	0.01	22.51	0.23	0.01	0.13	4.32	8.72	1.31	0.00	0.44	99.57	19.94	72.86	7.20
	595	62.27	0.04	23.15	0.27	0.01	0.12	4.40	8.77	1.21	0.00	0.43	100.67	20.29	73.09	6.62
	600	62.53	0.02	22.87	0.26	0.00	0.15	4.19	8.91	1.32	0.00	0.44	100.67	19.15	73.67	7.18
	605	62.53	0.00	22.95	0.24	0.00	0.13	4.26	8.76	1.30	0.03	0.44	100.63	19.66	73.19	7.15
	610	62.33	0.00	22.84	0.25	0.01	0.14	4.15	8.96	1.21	0.00	0.43	100.30	19.01	74.39	6.60
	615	71.78	0.18	15.18	0.73	0.00	0.16	0.75	5.28	5.23	0.00	0.52	99.81	4.53	57.81	37.66
	625	61.66	0.01	22.02	0.23	0.00	0.17	4.18	8.76	1.44	0.01	0.43	98.89	19.24	72.90	7.87
	630	60.90	0.01	21.66	0.24	0.00	0.15	4.03	8.64	1.52	0.01	0.43	97.60	18.77	72.80	8.43
	665	61.17	0.00	22.83	0.25	0.01	0.09	4.54	8.60	0.93	0.00	0.43	98.86	21.40	73.38	5.22
	670	61.86	0.02	23.01	0.24	0.00	0.12	4.63	8.74	0.90	0.00	0.42	99.94	21.52	73.51	4.97
	690	65.94	0.05	18.15	0.56	0.00	0.33	0.71	6.62	5.87	0.00	0.49	98.72	3.62	60.87	35.51
	695	62.54	0.00	22.66	0.24	0.01	0.12	4.13	8.77	1.42	0.04	0.43	100.35	19.03	73.15	7.82
	700	61.74	0.00	22.97	0.22	0.00	0.13	4.36	8.73	1.38	0.00	0.44	99.96	19.99	72.47	7.54

Appendix B. Electron Microprobe Analyses of Feldspar (continued).

		Line Analyses														
Sample	Dist. μ	SiO_2	TiO_2	Al_2O_3	FeO	MgO	BaO	CaO	Na_2O	K_2O	MnO	SrO	Total	An	Ab	Or
RC12-14	705	60.67	0.00	22.92	0.23	0.00	0.10	4.45	8.52	1.38	0.03	0.44	98.73	20.67	71.71	7.62
	710	60.00	0.00	22.68	0.25	0.01	0.09	4.26	8.54	1.44	0.00	0.42	97.69	19.88	72.14	7.98
	720	59.83	0.00	22.65	0.27	0.01	0.17	4.18	8.67	1.39	0.00	0.43	97.59	19.41	72.92	7.67
	725	62.05	0.03	22.91	0.22	0.00	0.08	4.34	8.69	1.33	0.00	0.44	100.08	20.05	72.66	7.30
	730	62.09	0.01	23.24	0.23	0.01	0.18	4.51	8.74	1.32	0.02	0.43	100.76	20.59	72.24	7.17
	735	62.22	0.02	23.30	0.27	0.01	0.14	4.66	8.72	1.30	0.03	0.43	101.10	21.21	71.75	7.04
	740	62.21	0.01	23.21	0.25	0.00	0.14	4.52	8.81	1.29	0.02	0.42	100.88	20.53	72.47	7.00
	780	61.19	0.01	22.88	0.20	0.01	0.18	4.02	8.64	1.42	0.00	0.45	98.99	18.83	73.27	7.90
	810	61.91	0.01	22.71	0.23	0.00	0.14	4.15	8.62	1.42	0.01	0.44	99.63	19.37	72.76	7.87
	815	62.05	0.06	22.55	0.23	0.00	0.10	4.38	8.78	1.43	0.02	0.44	100.04	19.92	72.31	7.76
	820	62.19	0.00	22.82	0.21	0.00	0.13	4.34	8.75	1.44	0.00	0.44	100.30	19.83	72.35	7.83
	825	62.40	0.02	22.91	0.22	0.01	0.13	4.17	8.85	1.45	0.00	0.45	100.60	19.03	73.09	7.89
	830	62.56	0.00	22.86	0.26	0.00	0.12	4.22	8.77	1.47	0.01	0.44	100.70	19.34	72.64	8.03
	835	62.23	0.01	22.85	0.26	0.01	0.10	4.21	8.71	1.44	0.00	0.43	100.24	19.40	72.72	7.89
	840	62.55	0.00	22.70	0.24	0.01	0.15	4.05	8.57	1.62	0.03	0.42	100.33	18.86	72.16	8.99
	880	60.53	0.00	22.44	0.19	0.01	0.08	4.75	8.47	1.22	0.00	0.43	98.11	22.08	71.19	6.73
	885	64.74	0.03	21.60	0.23	0.00	0.07	3.55	8.89	0.98	0.00	0.44	100.52	17.06	77.33	5.61
	980	62.19	0.00	22.93	0.20	0.01	0.13	4.33	8.63	1.33	0.00	0.44	100.18	20.10	72.57	7.33
	985	61.06	0.01	22.38	0.40	0.03	0.05	4.32	8.05	1.27	0.00	0.43	97.99	21.18	71.41	7.41
	990	62.99	0.00	22.64	0.18	0.01	0.07	3.92	8.51	1.13	0.00	0.43	99.87	18.99	74.52	6.49
	1040	62.12	0.03	23.00	0.20	0.01	0.07	4.32	8.74	1.37	0.01	0.43	100.30	19.86	72.67	7.47
	1050	61.82	0.00	22.53	0.18	0.00	0.06	4.21	8.71	1.42	0.01	0.43	99.37	19.44	72.74	7.82
	1060	61.88	0.03	22.47	0.21	0.00	0.14	4.06	8.58	1.41	0.00	0.42	99.19	19.08	73.02	7.90
	1065	61.38	0.01	22.51	0.19	0.00	0.09	4.25	8.36	1.39	0.00	0.43	98.60	20.21	71.93	7.85
	1085	60.58	0.02	22.68	0.23	0.00	0.17	4.51	8.54	1.34	0.01	0.41	98.49	20.90	71.70	7.40
	1090	61.74	0.02	22.37	0.20	0.01	0.09	4.05	8.69	1.41	0.02	0.43	99.02	18.88	73.30	7.83
	1105	62.22	0.02	21.60	0.18	0.00	0.14	3.60	8.78	1.72	0.00	0.42	98.68	16.72	73.78	9.50
	1215	63.59	0.00	19.35	0.16	0.00	0.97	0.45	4.92	9.18	0.00	0.52	99.15	2.23	43.89	53.88
	1220	64.24	0.04	19.53	0.16	0.00	1.05	0.46	5.12	9.10	0.00	0.53	100.22	2.23	45.05	52.72
	1225	64.12	0.05	19.54	0.13	0.00	1.03	0.53	5.22	8.93	0.00	0.52	100.07	2.59	45.84	51.56
	1230	63.74	0.00	19.60	0.15	0.00	1.09	0.54	5.29	8.98	0.00	0.54	99.93	2.59	46.04	51.37

Appendix B. Electron Microprobe Analyses of Feldspar (continued).

		Line Analyses														
Sample	Dist. μ	SiO_2	TiO_2	Al_2O_3	FeO	MgO	BaO	CaO	Na_2O	K_2O	MnO	SrO	Total	An	Ab	Or
RC12-14	1235	63.53	0.02	19.60	0.20	0.00	1.11	0.55	5.21	8.89	0.00	0.54	99.65	2.69	45.86	51.45
	1240	64.21	0.02	19.60	0.16	0.00	1.19	0.54	5.17	8.89	0.00	0.55	100.33	2.66	45.66	51.68
	1245	64.14	0.04	19.81	0.15	0.00	1.27	0.52	5.17	8.75	0.01	0.53	100.38	2.55	46.10	51.35
	1250	64.28	0.03	19.76	0.15	0.00	1.32	0.48	5.18	8.90	0.01	0.53	100.64	2.36	45.86	51.79
	1255	63.68	0.02	19.63	0.16	0.00	1.36	0.50	5.05	9.17	0.00	0.54	100.11	2.44	44.43	53.13
	1260	64.26	0.03	19.93	0.16	0.00	1.28	0.48	4.06	8.42	0.03	0.52	99.15	2.67	41.15	56.18
DM2-10-2		63.62	0.02	20.04	0.22	0.00	0.01	1.29	8.31	3.48	0.02	0.46	97.46	6.29	73.44	20.27
		64.77	0.00	20.53	0.20	0.00	0.00	1.42	8.16	3.86	0.00	0.45	99.38	6.81	71.04	22.15
	0	64.44	0.00	19.80	0.19	0.00	0.05	1.24	7.86	3.88	0.00	0.77	98.23	6.18	70.83	23.00
	20	64.69	0.03	20.03	0.19	0.00	0.00	1.31	7.92	3.71	0.00	0.76	98.64	6.53	71.44	22.03
	40	64.78	0.00	19.82	0.19	0.01	0.03	1.24	7.80	4.11	0.00	0.79	98.78	6.12	69.72	24.16
	60	65.20	0.02	20.41	0.18	0.00	0.00	1.17	8.14	4.21	0.00	0.79	100.13	5.58	70.44	23.98
	80	64.42	0.00	19.93	0.20	0.01	0.01	1.23	8.07	4.01	0.01	0.74	98.64	5.94	70.88	23.17
	100	64.67	0.01	20.03	0.18	0.00	0.05	1.24	8.25	3.95	0.00	0.76	99.12	5.96	71.52	22.52
	140	64.57	0.00	20.37	0.21	0.00	0.02	1.40	8.14	3.75	0.00	0.77	99.23	6.79	71.54	21.67
	160	64.51	0.00	20.24	0.19	0.00	0.04	1.44	8.17	3.66	0.00	0.78	99.03	7.00	71.82	21.18
	180	64.53	0.00	20.14	0.19	0.00	0.00	1.39	8.27	3.76	0.00	0.78	99.05	6.65	71.87	21.47
	200	64.65	0.01	19.71	0.19	0.00	0.05	1.04	7.94	4.44	0.01	0.78	98.82	5.04	69.41	25.55
	220	64.59	0.00	20.08	0.18	0.00	0.02	0.97	8.05	4.34	0.03	0.79	99.05	4.69	70.34	24.96
	240	64.54	0.00	20.09	0.18	0.00	0.04	1.04	8.14	4.18	0.00	0.76	98.96	5.01	71.00	23.99
	260	64.60	0.01	19.82	0.20	0.00	0.00	0.88	8.01	4.43	0.00	0.79	98.74	4.25	70.21	25.54
	280	64.83	0.00	19.81	0.20	0.00	0.04	0.84	8.02	4.56	0.00	0.79	99.09	4.05	69.82	26.13
	300	65.68	0.02	20.21	0.21	0.00	0.01	1.04	7.98	4.53	0.01	0.82	100.52	5.00	69.17	25.83
	320	65.35	0.00	19.82	0.23	0.00	0.09	1.02	7.75	4.76	0.01	0.80	99.81	4.93	67.70	27.37
	340	65.38	0.02	20.06	0.22	0.00	0.03	1.10	8.04	4.54	0.02	0.78	100.17	5.21	69.10	25.69
	360	65.09	0.00	20.26	0.19	0.00	0.00	1.42	8.14	4.02	0.00	0.79	99.91	6.77	70.35	22.88
	380	65.00	0.01	20.50	0.20	0.00	0.00	1.34	8.20	3.90	0.00	0.78	99.93	6.42	71.31	22.28
	400	64.81	0.01	20.12	0.20	0.00	0.00	1.27	8.15	3.86	0.03	0.77	99.21	6.16	71.55	22.29
	420	63.96	0.02	19.88	0.22	0.00	0.04	1.31	8.17	3.83	0.00	0.76	98.18	6.34	71.60	22.06
	440	64.67	0.00	20.13	0.19	0.00	0.06	1.31	8.14	3.68	0.00	0.79	98.97	6.41	72.13	21.46

Appendix B. Electron Microprobe Analyses of Feldspar (continued).

								Line Analyses								
Sample	Dist. μ	SiO_2	TiO_2	Al_2O_3	FeO	MgO	BaO	CaO	Na_2O	K_2O	MnO	SrO	Total	An	Ab	Or
DM2-10-2	460	64.76	0.00	20.47	0.17	0.00	0.04	1.41	8.33	3.86	0.00	0.81	99.86	6.69	71.51	21.81
	480	64.27	0.01	20.17	0.20	0.00	0.01	1.40	8.27	3.66	0.00	0.75	98.74	6.77	72.21	21.03
	500	60.90	0.03	22.17	0.20	0.04	0.07	1.54	7.79	3.38	0.00	0.74	96.86	7.83	71.69	20.48
	520	64.71	0.01	20.25	0.19	0.00	0.01	1.54	8.45	3.54	0.00	0.79	99.47	7.31	72.67	20.01
	540	64.49	0.02	20.64	0.20	0.00	0.04	1.39	8.37	3.68	0.00	0.80	99.62	6.64	72.41	20.95
	560	64.75	0.01	20.08	0.19	0.00	0.01	1.41	8.37	3.73	0.00	0.80	99.34	6.70	72.14	21.15
	620	65.05	0.00	20.49	0.20	0.00	0.02	1.41	8.32	3.65	0.01	0.82	99.97	6.80	72.33	20.88
	640	64.71	0.07	20.13	0.17	0.00	0.01	1.41	8.53	3.45	0.00	0.79	99.28	6.73	73.66	19.61
	660	64.67	0.00	20.00	0.17	0.00	0.04	1.41	8.43	3.38	0.02	0.76	98.87	6.83	73.71	19.46
	680	64.91	0.01	20.00	0.23	0.00	0.07	1.33	8.52	3.59	0.02	0.78	99.45	6.32	73.38	20.31
DM2-10-3	rim	65.70	0.00	19.25	0.18	0.00	0.04	0.37	5.95	7.57	0.00	0.50	99.57	1.84	53.42	44.74
	rim	63.60	0.00	19.88	0.19	0.02	0.00	1.08	8.00	4.39	0.00	0.47	97.64	5.21	69.65	25.14
	core	64.99	0.05	20.10	0.20	0.00	0.02	1.33	8.28	3.81	0.00	0.45	99.23	6.37	71.88	21.75
	0	64.58	0.00	19.96	0.21	0.00	0.02	1.36	8.09	4.16	0.01	0.01	98.39	6.47	69.91	23.62
	60	64.87	0.00	20.02	0.23	0.00	0.01	1.20	8.01	4.16	0.01	0.11	98.61	5.79	70.22	23.99
	90	64.82	0.02	19.72	0.20	0.00	0.10	1.03	7.51	4.84	0.01	0.71	98.96	5.06	66.68	28.26
	210	52.29	0.01	14.19	0.16	0.02	0.07	1.18	8.20	4.32	0.01	20.12	100.55	5.59	70.10	24.31
	300	65.23	0.02	20.42	0.19	0.00	0.06	1.25	8.09	4.23	0.00	0.79	100.26	5.95	69.99	24.06
	330	65.26	0.03	20.13	0.20	0.00	0.02	1.34	8.16	4.09	0.00	0.78	100.01	6.38	70.38	23.24
	360	64.74	0.00	20.07	0.19	0.00	0.00	1.40	8.08	4.10	0.00	0.78	99.36	6.70	69.94	23.36
	390	63.52	0.00	19.61	0.19	0.00	0.03	1.30	8.37	4.15	0.00	0.76	97.94	6.09	70.82	23.09
	450	64.17	0.00	19.84	0.19	0.01	0.05	1.16	7.78	4.23	0.00	0.77	98.20	5.71	69.45	24.84
	480	65.19	0.00	19.13	0.21	0.00	0.02	0.45	6.08	7.33	0.00	0.75	99.17	2.24	54.54	43.22
	510	65.18	0.00	19.13	0.19	0.00	0.01	0.49	6.22	7.21	0.00	0.75	99.18	2.43	55.36	42.21
	630	67.22	0.00	19.67	0.17	0.00	0.04	0.49	6.40	7.05	0.00	0.78	101.81	2.38	56.58	41.04
	660	65.27	0.00	18.98	0.22	0.00	0.01	0.38	6.00	7.50	0.00	0.76	99.11	1.88	53.85	44.27
DM2-10	120	65.76	0.02	20.01	0.16	0.00	-	0.37	6.34	7.33	-	-	99.98	1.78	55.79	42.43
	125	65.15	0.02	19.29	0.16	0.00	-	0.37	6.36	7.30	-	-	98.65	1.80	55.97	42.23

Appendix B. Electron Microprobe Analyses of Feldspar (continued).

		Line Analyses														
Sample	Dist. μ	SiO_2	TiO_2	Al_2O_3	FeO	MgO	BaO	CaO	Na_2O	K_2O	MnO	SrO	Total	An	Ab	Or
DM2-10	150	66.77	0.00	20.33	0.19	0.00	-	0.43	6.63	6.98	-	-	101.36	2.09	57.85	40.06
	160	65.90	0.02	22.04	0.17	0.00	-	0.65	6.77	6.26	-	-	101.80	3.18	60.19	36.63
	165	63.43	0.01	20.34	0.16	0.00	-	1.02	7.50	4.73	-	-	97.19	5.04	67.13	27.82
	170	64.18	0.00	22.51	0.19	0.01	-	1.00	7.42	4.36	-	-	99.68	5.12	68.41	26.47
	185	65.76	0.00	20.53	0.20	0.01	-	1.22	7.52	4.41	-	-	99.64	6.09	67.78	26.13
	195	64.93	0.02	19.94	0.19	0.00	-	1.17	7.94	4.24	-	-	98.42	5.68	69.79	24.53
	200	65.22	0.02	20.42	0.20	0.00	-	1.29	7.98	4.12	-	-	99.24	6.25	69.99	23.75
	205	64.27	0.00	19.99	0.19	0.00	-	1.27	7.95	4.07	-	-	97.74	6.18	70.20	23.62
	210	64.41	0.02	19.71	0.18	0.00	-	1.11	7.79	4.14	-	-	97.37	5.50	70.02	24.48
	215	65.32	0.01	20.30	0.19	0.00	-	1.29	8.08	4.14	-	-	99.34	6.21	70.14	23.65
	220	65.51	0.01	20.49	0.21	0.00	-	1.08	8.02	4.44	-	-	99.77	5.19	69.51	25.30
	235	64.89	0.00	19.76	0.21	0.00	-	0.94	7.43	5.36	-	-	98.60	4.50	64.76	30.74
	240	65.86	0.02	20.91	0.19	0.00	-	0.87	7.18	5.81	-	-	100.86	4.18	62.53	33.29
	245	65.47	0.01	20.21	0.22	0.00	-	1.10	7.88	4.77	-	-	99.70	5.24	67.75	27.00
	250	65.26	0.00	20.00	0.15	0.00	-	0.87	7.33	5.75	-	-	99.36	4.12	63.25	32.63
	255	65.42	0.01	20.34	0.17	0.00	-	1.19	7.82	4.70	-	-	99.67	5.70	67.57	26.73
	260	66.32	0.03	21.50	0.19	0.00	-	1.06	7.69	4.65	-	-	101.44	5.19	67.81	27.01
	265	63.93	0.00	19.82	0.19	0.00	-	0.91	7.84	5.12	-	-	97.80	4.29	66.93	28.78
	270	65.14	0.00	19.96	0.20	0.00	-	0.80	7.33	5.31	-	-	98.75	3.92	65.05	31.02
	275	63.99	0.02	20.52	0.19	0.00	-	0.90	7.65	4.87	-	-	98.15	4.38	67.38	28.24
	280	66.62	0.02	20.98	0.19	0.00	-	0.89	7.15	5.35	-	-	101.21	4.41	64.06	31.54
	285	65.32	0.00	20.00	0.18	0.00	-	0.99	7.55	5.11	-	-	99.20	4.78	65.87	29.35
	290	65.20	0.00	20.15	0.19	0.00	-	1.07	7.60	5.03	-	-	99.26	5.13	66.09	28.79
	295	64.93	0.00	20.32	0.20	0.00	-	1.30	7.91	4.51	-	-	99.18	6.20	68.19	25.60
	345	64.37	0.00	20.10	0.22	0.01	-	1.28	7.29	4.27	-	-	97.55	6.57	67.43	26.00
	350	65.18	0.00	20.21	0.14	0.00	-	1.34	7.93	4.36	-	-	99.17	6.44	68.73	24.84
	355	65.07	0.00	20.09	0.16	0.00	-	1.34	7.83	4.27	-	-	98.77	6.52	68.77	24.70
	360	66.47	0.00	21.48	0.19	0.00	-	1.29	7.65	4.23	-	-	101.32	6.38	68.64	24.98
	365	65.10	0.00	20.27	0.18	0.00	-	1.29	8.14	4.28	-	-	99.27	6.11	69.75	24.14
	395	66.26	0.00	20.83	0.18	0.00	-	1.23	7.90	4.40	-	-	100.80	5.90	68.86	25.23
	400	65.73	0.00	21.07	0.20	0.01	-	1.27	7.44	4.30	-	-	100.03	6.39	67.81	25.79

Appendix B. Electron Microprobe Analyses of Feldspar (continued).

	Line Analyses															
Sample	Dist. μ	SiO_2	TiO_2	Al_2O_3	FeO	MgO	BaO	CaO	Na_2O	K_2O	MnO	SrO	Total	An	Ab	Or
DM2-10	410	64.56	0.02	19.55	0.17	0.00	-	1.14	7.74	4.73	-	-	97.92	5.48	67.43	27.08
	420	66.69	0.02	21.31	0.20	0.00	-	1.11	7.04	5.00	-	-	101.38	5.59	64.34	30.07
	425	65.45	0.01	20.09	0.21	0.00	-	1.07	7.41	5.12	-	-	99.36	5.18	65.20	29.62
	450	64.81	0.01	19.76	0.17	0.00	-	0.86	6.94	5.23	-	-	97.78	4.39	63.90	31.71
	455	64.84	0.00	19.80	0.19	0.00	-	0.91	6.80	5.19	-	-	97.73	4.67	63.45	31.88
	460	66.12	0.01	20.92	0.18	0.00	-	0.90	7.20	5.41	-	-	100.76	4.39	63.97	31.63
	465	65.77	0.02	19.77	0.16	0.00	-	0.85	7.36	5.59	-	-	99.52	4.09	63.96	31.95
	470	65.70	0.00	19.91	0.19	0.00	-	0.88	7.31	5.65	-	-	99.67	4.22	63.50	32.28
	480	65.99	0.00	21.00	0.17	0.00	-	1.00	7.21	4.92	-	-	100.29	5.01	65.56	29.43
	485	65.62	0.00	20.48	0.18	0.00	-	1.19	8.12	4.20	-	-	99.78	5.70	70.34	23.96
	490	65.55	0.00	20.35	0.18	0.00	-	1.19	8.12	4.27	-	-	99.64	5.67	70.09	24.24
	495	65.54	0.00	19.85	0.19	0.00	-	0.79	7.49	5.22	-	-	99.07	3.83	65.95	30.22
	500	66.10	0.03	20.57	0.17	0.00	-	0.77	6.49	6.16	-	-	100.29	3.85	59.19	36.96
	505	65.26	0.00	19.62	0.16	0.00	-	0.68	6.63	6.22	-	-	98.57	3.36	59.75	36.89
	515	65.56	0.00	19.95	0.17	0.00	-	0.80	6.55	5.80	-	-	98.83	4.11	60.56	35.32
	520	65.97	0.00	21.69	0.18	0.00	-	1.32	7.95	3.61	-	-	100.76	6.62	71.88	21.51
	530	64.76	0.00	21.16	0.19	0.00	-	1.96	8.93	2.10	-	-	99.12	9.52	78.35	12.13
	535	64.92	0.01	20.61	0.20	0.00	-	1.57	8.42	3.16	-	-	98.92	7.61	74.11	18.28
	540	66.05	0.01	21.57	0.18	0.00	-	1.46	7.75	3.74	-	-	100.76	7.33	70.31	22.36
	545	64.93	0.00	20.66	0.21	0.00	-	1.37	8.24	3.96	-	-	99.37	6.50	71.02	22.47
	550	68.22	0.00	21.70	0.19	0.01	-	1.30	8.36	4.40	-	-	104.18	6.01	69.82	24.17
	555	70.10	0.00	22.14	0.20	0.01	-	1.19	8.59	4.48	-	-	106.69	5.38	70.46	24.16
	560	70.36	0.00	22.85	0.17	0.00	-	1.12	8.70	4.53	-	-	107.75	5.02	70.74	24.24
	570	65.47	0.03	20.10	0.20	0.00	-	1.08	7.77	4.44	-	-	99.09	5.29	68.82	25.89
	575	65.39	0.00	20.33	0.17	0.00	-	1.27	8.11	4.10	-	-	99.41	6.09	70.46	23.45
	580	58.77	0.00	27.75	0.15	0.03	-	1.18	6.34	3.72	-	-	97.94	6.89	67.15	25.97
	600	66.53	0.02	21.41	0.24	0.00	-	1.22	7.51	4.60	-	-	101.52	6.03	66.97	27.00
	605	65.22	0.00	20.46	0.19	0.00	-	1.37	8.16	3.94	-	-	99.33	6.60	70.89	22.51
	610	65.48	0.01	20.89	0.19	0.00	-	1.50	8.39	3.66	-	-	100.12	7.12	72.16	20.72
	615	65.27	0.01	21.04	0.16	0.00	-	1.81	8.66	3.18	-	-	100.11	8.51	73.69	17.80
	620	66.62	0.03	21.96	0.21	0.00	-	1.53	7.97	3.70	-	-	102.02	7.50	70.85	21.66

Appendix B. Electron Microprobe Analyses of Feldspar (continued).

		Line Analyses														
Sample	Dist. μ	SiO_2	TiO_2	Al_2O_3	FeO	MgO	BaO	CaO	Na_2O	K_2O	MnO	SrO	Total	An	Ab	Or
DM2-10	625	65.37	0.02	20.93	0.19	0.00	-	1.50	8.02	3.60	-	-	99.62	7.40	71.51	21.10
	630	64.97	0.01	20.65	0.19	0.00	-	1.46	8.01	3.65	-	-	98.96	7.18	71.41	21.41
	635	64.81	0.01	20.68	0.18	0.00	-	1.48	7.67	3.71	-	-	98.55	7.49	70.19	22.31
	640	65.55	0.00	21.00	0.21	0.00	-	1.47	7.79	3.96	-	-	99.99	7.24	69.53	23.23
	645	65.33	0.00	20.49	0.17	0.00	-	1.39	8.12	4.06	-	-	99.58	6.66	70.26	23.08
	650	65.32	0.01	20.46	0.20	0.00	-	1.31	8.06	4.13	-	-	99.49	6.29	70.06	23.64
	655	65.33	0.01	20.34	0.20	0.00	-	1.24	8.02	4.37	-	-	99.54	5.93	69.25	24.83
	660	66.86	0.00	21.47	0.19	0.00	-	1.18	7.57	4.37	-	-	101.64	5.87	68.22	25.91
	665	65.05	0.02	20.75	0.18	0.00	-	1.53	8.35	3.67	-	-	99.58	7.27	71.93	20.81
	670	64.64	0.00	20.11	0.18	0.00	-	1.32	7.79	4.51	-	-	98.54	6.33	67.80	25.87
	675	65.14	0.02	20.11	0.21	0.00	-	1.16	7.71	4.61	-	-	98.96	5.63	67.73	26.64
	680	66.18	0.01	21.56	0.17	0.00	-	1.15	7.72	4.74	-	-	101.53	5.55	67.29	27.16
	685	65.71	0.02	19.72	0.15	0.00	-	0.78	7.24	5.86	-	-	99.48	3.74	62.81	33.45
	690	65.21	0.01	20.00	0.19	0.00	-	0.99	7.69	4.92	-	-	99.03	4.78	67.01	28.22
	695	64.91	0.03	19.95	0.17	0.00	-	1.09	7.78	4.75	-	-	98.67	5.22	67.60	27.18
	700	65.95	0.01	21.25	0.18	0.00	-	1.23	7.81	4.65	-	-	101.09	5.88	67.65	26.47
	705	64.90	0.00	20.12	0.18	0.00	-	1.18	7.95	4.52	-	-	98.87	5.64	68.67	25.69
	710	62.74	0.00	19.80	0.21	0.00	-	1.18	8.13	4.37	-	-	96.43	5.60	69.74	24.66
	715	65.34	0.00	20.26	0.21	0.00	-	1.19	7.88	4.44	-	-	99.34	5.75	68.78	25.47
	720	64.86	0.00	21.69	0.21	0.03	-	1.28	7.41	4.21	-	-	99.69	6.48	68.04	25.48
	725	64.98	0.01	20.48	0.19	0.00	-	1.22	8.54	4.31	-	-	99.73	5.59	70.86	23.54
	730	65.32	0.00	20.37	0.21	0.00	-	1.25	8.07	4.19	-	-	99.43	5.98	70.08	23.94
	735	65.03	0.03	20.51	0.22	0.00	-	1.32	8.24	4.13	-	-	99.49	6.24	70.51	23.25
	740	66.51	0.01	21.51	0.22	0.00	-	1.32	7.97	4.16	-	-	101.72	6.39	69.67	23.94
	745	65.40	0.00	20.57	0.19	0.00	-	1.37	8.21	4.05	-	-	99.81	6.52	70.58	22.91
	750	65.32	0.01	20.51	0.21	0.00	-	1.35	8.26	4.06	-	-	99.73	6.36	70.76	22.88
	755	65.50	0.00	20.49	0.19	0.00	-	1.32	8.38	4.05	-	-	99.92	6.22	71.17	22.61
	760	66.64	0.00	21.58	0.18	0.00	-	1.45	7.83	3.93	-	-	101.62	7.15	69.82	23.03
	765	65.32	0.00	20.31	0.18	0.00	-	1.39	8.14	3.84	-	-	99.19	6.72	71.16	22.12
	770	65.25	0.00	20.33	0.17	0.00	-	1.43	8.11	3.80	-	-	99.08	6.93	71.14	21.93
	775	64.90	0.02	20.23	0.21	0.00	-	1.36	8.19	3.82	-	-	98.72	6.56	71.48	21.96

Appendix B. Electron Microprobe Analyses of Feldspar (continued).

		Line Analyses														
Sample	Dist. μ	SiO_2	TiO_2	Al_2O_3	FeO	MgO	BaO	CaO	Na_2O	K_2O	MnO	SrO	Total	An	Ab	Or
DM2-10	780	66.06	0.00	21.40	0.20	0.00	-	1.42	8.06	3.85	-	-	100.98	6.88	70.85	22.27
	785	65.45	0.00	20.56	0.18	0.00	-	1.37	8.32	3.89	-	-	99.78	6.53	71.49	21.98
	790	65.37	0.00	20.55	0.17	0.00	-	1.45	8.54	3.83	-	-	99.91	6.74	72.01	21.25
	795	65.06	0.00	20.41	0.18	0.00	-	1.45	8.61	3.82	-	-	99.55	6.71	72.24	21.05
	810	63.83	0.01	20.56	0.22	0.00	-	1.37	8.46	3.81	-	-	98.27	6.43	72.16	21.40
	820	66.82	0.01	21.59	0.19	0.00	-	1.38	7.56	3.68	-	-	101.23	7.11	70.35	22.54
	825	65.27	0.00	20.44	0.19	0.00	-	1.35	8.31	3.85	-	-	99.41	6.46	71.71	21.83
	830	64.96	0.00	20.36	0.16	0.00	-	1.31	8.30	3.80	-	-	98.91	6.30	72.01	21.69
	835	64.91	0.00	20.41	0.16	0.00	-	1.35	8.27	3.82	-	-	98.92	6.48	71.73	21.79
	840	65.72	0.00	21.32	0.17	0.00	-	1.41	8.08	3.84	-	-	100.54	6.84	70.97	22.19
	845	64.87	0.00	20.36	0.22	0.00	-	1.40	8.37	3.83	-	-	99.04	6.63	71.78	21.59
	850	64.96	0.03	20.46	0.22	0.00	-	1.42	8.37	3.83	-	-	99.30	6.74	71.68	21.58
	855	64.72	0.00	20.31	0.20	0.00	-	1.44	8.38	3.78	-	-	98.82	6.80	71.85	21.35
	860	66.18	0.00	21.65	0.19	0.01	-	1.41	8.19	3.66	-	-	101.32	6.86	71.96	21.18
	865	65.06	0.00	20.57	0.21	0.00	-	1.42	8.40	3.73	-	-	99.42	6.72	72.18	21.10
	870	64.98	0.00	20.52	0.19	0.00	-	1.40	8.34	3.73	-	-	99.16	6.69	72.10	21.21
	875	65.05	0.02	20.46	0.18	0.00	-	1.40	8.27	3.90	-	-	99.30	6.67	71.23	22.10
	880	66.13	0.00	21.68	0.18	0.00	-	1.39	8.01	3.74	-	-	101.16	6.85	71.25	21.90
	885	64.93	0.02	20.18	0.17	0.00	-	1.31	8.20	4.11	-	-	98.91	6.21	70.54	23.25
	890	65.14	0.00	20.19	0.19	0.00	-	1.22	8.09	4.18	-	-	99.02	5.86	70.26	23.88
	895	64.60	0.01	20.18	0.21	0.00	-	1.35	8.21	3.90	-	-	98.46	6.46	71.28	22.26
	900	66.16	0.00	21.40	0.20	0.00	-	1.29	7.70	4.13	-	-	100.89	6.41	69.15	24.44
	905	65.67	0.02	20.00	0.18	0.00	-	0.85	7.85	4.97	-	-	99.53	4.06	67.74	28.21
	910	65.45	0.01	19.67	0.19	0.00	-	0.73	7.36	5.67	-	-	99.08	3.50	64.04	32.46
	915	65.74	0.00	19.88	0.15	0.00	-	0.89	7.53	5.32	-	-	99.52	4.27	65.34	30.38
	920	66.73	0.03	21.21	0.19	0.00	-	1.02	7.77	4.85	-	-	101.79	4.87	67.44	27.69
	925	66.26	0.01	20.61	0.18	0.00	-	1.05	8.65	4.88	-	-	101.62	4.65	69.55	25.79
	940	66.50	0.02	21.37	0.20	0.00	-	1.22	8.07	4.11	-	-	101.48	5.89	70.47	23.64
	945	64.07	0.01	19.83	0.19	0.02	-	1.33	7.84	3.88	-	-	97.17	6.62	70.45	22.93
	950	65.46	0.00	20.41	0.19	0.00	-	1.32	8.37	3.83	-	-	99.57	6.29	72.04	21.67
	955	65.30	0.00	20.22	0.18	0.00	-	1.24	8.28	3.79	-	-	99.03	5.96	72.28	21.76

Appendix B. Electron Microprobe Analyses of Feldspar (continued).

	Line Analyses															
Sample	Dist. μ	SiO_2	TiO_2	Al_2O_3	FeO	MgO	BaO	CaO	Na_2O	K_2O	MnO	SrO	Total	An	Ab	Or
	960	66.52	0.01	21.51	0.19	0.00	–	1.28	7.90	3.75	–	–	101.16	6.38	71.34	22.28
	965	65.40	0.00	20.60	0.18	0.00	–	1.27	8.46	3.75	–	–	99.66	6.01	72.76	21.23
	970	65.47	0.00	20.47	0.20	0.00	–	1.32	8.31	3.65	–	–	99.43	6.38	72.63	20.98
	975	65.40	0.01	20.38	0.17	0.00	–	1.41	8.30	3.68	–	–	99.33	6.76	72.19	21.05
	980	66.73	0.01	21.35	0.20	0.00	–	1.31	7.72	3.82	–	–	101.14	6.60	70.44	22.96
	985	64.80	0.00	20.28	0.20	0.00	–	1.34	8.17	3.94	–	–	98.73	6.46	71.00	22.55
	990	65.01	0.00	20.50	0.20	0.00	–	1.41	8.17	3.57	–	–	98.87	6.89	72.32	20.78
	995	64.80	0.00	20.38	0.23	0.00	–	1.34	8.35	3.65	–	–	98.75	6.43	72.70	20.87
	1000	66.04	0.00	21.29	0.19	0.00	–	1.34	7.96	3.73	–	–	100.57	6.62	71.37	22.01
	1005	64.76	0.02	20.25	0.19	0.00	–	1.24	8.17	3.88	–	–	98.52	6.02	71.61	22.37
	1010	65.03	0.02	20.24	0.18	0.00	–	1.33	8.34	3.68	–	–	98.83	6.40	72.53	21.08
	1015	65.00	0.00	20.34	0.17	0.00	–	1.39	8.31	3.68	–	–	98.90	6.67	72.27	21.06
	1020	66.17	0.00	21.79	0.21	0.00	–	1.34	7.95	3.75	–	–	101.20	6.62	71.25	22.13
	1025	64.95	0.00	20.28	0.18	0.00	–	1.30	8.07	3.64	–	–	98.41	6.41	72.15	21.44
	1030	64.89	0.01	20.36	0.20	0.00	–	1.31	8.12	3.60	–	–	98.49	6.45	72.43	21.12
	1035	64.68	0.00	20.39	0.18	0.00	–	1.39	7.99	3.57	–	–	98.23	6.90	71.97	21.13

APPENDIX C

ELECTRON MICROPROBE ANALYSES

OF

BIOTITE

Appendix C. Electron Microprobe Analyses of Biotite.

		Point Analyses										
Sample	Dist. μ	SiO_2	TiO_2	Al_2O_3	FeO	MnO	MgO	CaO	Na_2O	K_2O	F	Total
RC07	-	38.79	5.21	14.49	17.66	0.29	12.09	0.06	0.64	8.62	-	97.85
RC07	-	36.69	5.19	13.47	18.05	0.26	12.62	0.00	0.68	8.96	-	95.93
RC07	-	35.44	5.29	13.37	17.37	0.22	12.25	0.03	0.64	8.45	-	93.05
RC07	-	37.81	4.83	13.76	16.98	0.28	11.97	0.05	0.65	8.40	-	94.72
RC07	-	37.25	5.17	13.44	17.46	0.23	12.72	0.00	0.72	9.06	-	96.06
RC07	-	38.06	4.81	13.68	17.38	0.27	12.81	0.04	0.69	8.91	-	96.66
RC07	-	37.01	5.00	13.20	17.94	0.29	12.80	0.04	0.68	8.78	-	95.75
RC07	-	36.30	5.31	13.23	17.66	0.25	13.11	0.00	0.70	8.63	-	95.20
	-											
RC07-15	-	37.37	5.08	13.33	17.36	0.26	11.74	0.00	0.71	8.75	0.00	94.59
	-	37.72	4.94	13.30	16.88	0.23	11.72	0.00	0.72	8.67	0.00	94.19
	-	37.61	5.01	13.23	16.84	0.26	11.68	0.02	0.72	8.69	0.00	94.04
	-											
RC07-17	-	37.78	5.01	13.41	17.06	0.26	11.75	0.01	0.72	8.62	0.00	94.61
	-	37.93	5.10	13.45	16.68	0.19	11.51	0.04	0.72	8.49	0.00	94.09
	-	37.61	4.90	13.38	17.06	0.24	11.79	0.00	0.76	8.93	0.00	94.67
	-											
RC12	-	36.94	5.15	13.32	17.23	0.26	13.31	0.01	0.73	8.99	-	95.94
RC12	-	36.96	5.21	13.63	17.11	0.23	13.04	0.01	0.72	8.94	-	95.84
RC12	-	36.85	5.19	13.37	17.15	0.24	12.77	0.01	0.65	8.96	-	95.20
RC12	-	37.57	4.99	13.41	16.96	0.23	12.90	0.00	0.62	8.74	-	95.43
RC12	-	36.97	5.05	13.55	17.16	0.22	13.01	0.00	0.69	8.68	-	95.34
RC12	-	36.93	4.99	13.34	16.76	0.21	13.21	0.01	0.71	8.99	-	95.14
RC12	-	37.01	5.21	13.36	17.66	0.25	12.91	0.00	0.74	8.87	-	95.99

Appendix C. Electron Microprobe Analyses of Biotite.

		Line Analyses										
Sample	Dist. μ	SiO_2	TiO_2	Al_2O_3	FeO	MnO	MgO	CaO	Na_2O	K_2O	F	Total
RC07	0	36.91	5.01	13.39	17.59	0.28	12.62	0.02	0.64	8.81	-	95.27
	5	36.76	5.08	13.36	17.53	0.27	12.71	0.03	0.67	8.75	-	95.15
	10	36.61	5.14	13.23	17.70	0.24	12.77	0.02	0.66	8.84	-	95.19
	15	36.75	5.13	13.24	17.72	0.28	12.69	0.03	0.66	8.90	-	95.40
	20	36.82	5.03	13.12	17.67	0.25	12.78	0.00	0.65	9.00	-	95.31
	25	36.73	5.09	13.21	17.93	0.27	12.94	0.03	0.72	9.03	-	95.95
	30	36.76	5.14	13.14	18.00	0.29	12.79	0.00	0.66	8.89	-	95.67
	35	36.55	5.11	13.11	17.82	0.29	12.80	0.00	0.65	8.84	-	95.20
	40	36.78	5.08	13.32	17.78	0.24	12.77	0.03	0.68	9.03	-	95.71
	45	36.74	5.04	13.33	17.76	0.28	12.72	0.00	0.64	8.92	-	95.42
	70	36.76	5.17	13.40	18.02	0.23	12.64	0.00	0.68	8.98	-	95.87
	80	37.04	5.11	13.52	17.97	0.23	12.54	0.03	0.67	8.90	-	95.99
	85	36.79	5.15	13.50	18.08	0.27	12.55	0.01	0.67	8.96	-	95.98
	90	36.89	5.06	13.71	17.93	0.23	12.46	0.00	0.62	8.87	-	95.77
	95	37.15	5.17	13.76	18.02	0.26	12.45	0.01	0.66	8.80	-	96.28
	100	37.60	5.02	13.37	17.70	0.24	12.14	0.03	0.65	8.66	-	95.43
	125	36.85	5.24	13.43	17.76	0.25	12.77	0.02	0.63	8.96	-	95.91
	130	36.71	5.18	13.46	17.90	0.24	12.27	0.08	0.63	8.73	-	95.19
	135	36.28	5.20	13.34	18.01	0.28	12.49	0.08	0.67	8.71	-	95.04
	140	36.70	5.25	13.54	18.03	0.29	12.77	0.03	0.66	8.91	-	96.19
	145	36.63	5.21	13.54	17.97	0.27	12.67	0.01	0.68	8.96	-	95.95
	150	36.35	5.16	13.53	18.00	0.29	12.64	0.02	0.66	8.85	-	95.52
	155	36.82	5.24	13.48	18.12	0.24	12.66	0.05	0.68	8.86	-	96.14
	160	36.89	5.16	13.33	18.06	0.23	12.54	0.03	0.66	8.88	-	95.79
	165	36.94	5.12	13.40	18.17	0.26	12.76	0.00	0.64	8.94	-	96.25
	170	36.76	5.13	13.40	18.23	0.28	12.82	0.02	0.65	8.99	-	96.26
	175	36.75	5.16	13.31	18.07	0.24	12.52	0.03	0.67	8.83	-	95.60
	180	36.68	5.16	13.29	17.91	0.26	12.28	0.04	0.61	8.94	-	95.19

Appendix C. Electron Microprobe Analyses of Biotite.

Line Analyses												
Sample	Dist. μ	SiO_2	TiO_2	Al_2O_3	FeO	MnO	MgO	CaO	Na_2O	K_2O	F	Total
RC12-15	-	37.74	5.38	13.44	16.73	0.24	11.90	0.00	0.72	8.87	0.00	95.02
	100	37.76	5.04	13.07	16.91	0.24	11.98	0.03	0.92	9.19	0.00	95.13
	120	37.55	5.10	13.37	17.14	0.22	11.74	0.04	0.87	8.88	0.00	94.89
	160	38.25	4.89	13.36	16.96	0.27	11.95	0.02	0.76	8.87	0.00	95.32
	180	37.91	4.81	13.25	16.92	0.22	11.65	0.06	0.71	8.60	0.00	94.11
	200	37.93	4.99	13.38	17.08	0.22	12.01	0.00	0.67	8.86	0.00	95.14
RC12-5	core	37.75	5.16	13.47	17.33	0.26	11.79	0.00	0.77	8.76	0.00	95.29
	rim	42.11	4.59	13.27	14.96	0.23	10.51	0.08	0.84	8.24	0.00	94.82
	0	37.80	4.87	13.18	17.06	0.27	11.71	0.00	0.77	8.80	0.00	94.46
	20	37.72	5.06	13.37	17.21	0.22	11.67	0.00	0.76	8.71	0.00	94.72
	40	37.88	4.98	13.39	17.33	0.24	11.55	0.00	0.76	8.73	0.00	94.85
	60	38.51	4.93	13.57	17.34	0.21	11.33	0.02	0.77	8.68	0.00	95.35
	80	37.64	5.04	13.42	17.36	0.23	11.79	0.01	0.67	8.64	0.00	94.79
	100	38.05	4.99	13.46	17.18	0.20	11.68	0.03	0.76	8.56	0.00	94.90
	120	37.81	4.95	13.35	16.89	0.23	11.68	0.04	0.69	8.43	0.00	94.06
	140	37.72	4.99	13.43	16.97	0.17	11.61	0.04	0.75	8.46	0.00	94.14
RC12-16	20	37.99	4.90	13.33	17.44	0.25	11.59	0.01	0.72	8.82	0.00	95.05
	40	37.87	4.92	13.25	17.31	0.24	11.47	0.01	0.70	8.70	0.00	94.48
	60	38.25	4.73	13.24	17.29	0.21	11.31	0.02	0.77	8.62	0.00	94.43
	80	37.63	5.11	13.49	17.54	0.22	11.90	0.00	0.74	8.90	0.00	95.53
	100	37.37	5.17	13.43	17.22	0.29	11.65	0.00	0.70	8.83	0.00	94.67
	120	37.69	5.18	13.42	17.23	0.22	11.47	0.10	0.71	8.81	0.00	94.82
	140	37.50	5.02	13.34	17.13	0.24	11.53	0.10	0.73	8.78	0.00	94.36
	160	37.86	4.98	13.14	16.78	0.27	11.77	0.05	0.68	8.79	0.00	94.32
RC07-9	core	37.86	4.97	13.45	16.60	0.23	11.52	0.00	0.78	8.75	0.00	94.16
	20	37.69	4.89	13.34	16.84	0.20	11.67	0.03	0.73	8.80	0.00	94.19
	40	37.67	4.98	12.95	17.17	0.27	11.80	0.01	0.72	8.69	0.00	94.24

Appendix C. Electron Microprobe Analyses of Biotite.

		Line Analyses										
Sample	Dist. μ	SiO_2	TiO_2	Al_2O_3	FeO	MnO	MgO	CaO	Na_2O	K_2O	F	Total
RC07-9	100	37.44	5.03	13.25	17.12	0.23	11.65	0.00	0.69	8.75	0.00	94.15
	120	37.66	5.01	13.43	16.90	0.23	11.73	0.03	0.70	8.71	0.00	94.39
	240	37.76	4.92	13.47	17.05	0.27	11.76	0.02	0.72	8.58	0.00	94.55
	260	37.71	4.94	13.41	16.73	0.21	11.50	0.06	0.70	8.44	0.00	93.70
	280	37.94	4.88	13.40	16.96	0.23	11.41	0.06	0.83	8.63	0.00	94.33
	300	37.95	4.89	13.56	16.70	0.23	11.35	0.05	0.77	8.64	0.00	94.13
	320	37.88	5.00	13.45	16.79	0.29	11.46	0.04	0.72	8.57	0.00	94.20
	340	37.82	4.87	13.57	16.68	0.24	11.41	0.05	0.76	8.70	0.00	94.09
	360	37.69	4.89	13.31	17.14	0.21	11.42	0.07	0.75	8.61	0.00	94.09
	400	38.09	4.96	13.18	16.89	0.26	11.57	0.12	0.69	8.45	0.00	94.22
RC07-18	20	37.33	4.91	13.29	16.95	0.25	11.88	0.00	0.80	8.90	0.00	94.30
	40	38.12	4.94	13.27	16.70	0.24	11.81	0.04	0.70	8.83	0.00	94.65
	80	37.91	4.79	13.17	16.82	0.21	11.91	0.00	0.78	8.89	0.00	94.48
	100	38.44	4.53	13.51	16.69	0.27	11.73	0.06	0.75	8.53	0.00	94.51

APPENDIX D

ELECTRON MICROPROBE ANALYSES

OF

PYROXENE

Appendix D. Electron Microprobe Analyses of Clinopyroxene.

		Point Analyses														
Sample	Dist. μ	SiO_2	TiO_2	Al_2O_3	Cr_2O_3	FeO	MnO	MgO	CaO	Na_2O	K_2O	Total	Wo	En	Fs	Ac
RC07-p1	-	52.11	0.14	0.57	0.00	10.86	1.06	13.26	21.20	0.43	0.01	99.64	42.66	37.13	18.62	1.58
RC07-p2	-	51.33	0.13	0.52	0.00	12.91	0.95	11.75	20.84	0.50	0.01	98.94	42.66	33.47	22.03	1.84
RC07-p3	-	50.66	0.24	1.03	0.00	10.84	0.81	11.78	20.56	0.56	0.00	96.48	43.70	34.83	19.30	2.17
RC07-p4	-	49.71	0.15	0.60	0.00	11.11	0.78	12.57	21.00	0.54	0.01	96.46	43.17	35.97	18.87	1.99
RC07-p5	-	51.31	0.15	0.61	0.00	13.17	0.94	11.76	20.70	0.53	0.02	99.18	42.26	33.42	22.37	1.95
RC07-p6	-	52.05	0.16	0.70	0.01	10.48	0.82	13.41	21.43	0.46	0.00	99.51	43.12	37.54	17.66	1.69
RC07-21-p1	-	50.80	0.15	0.65	n.a	10.23	0.82	14.09	21.79	0.50	0.03	99.04	42.89	38.58	16.76	1.77
RC07-21-p2	-	49.94	0.15	0.71	n.a	9.91	0.77	13.83	21.62	0.46	0.01	97.39	43.30	38.54	16.48	1.68
RC07-22 -p1	-	49.87	0.10	0.49	n.a	10.95	0.95	13.13	21.26	0.78	0.33	97.86	42.45	36.49	18.23	2.83
RC07-22 -p2	-	49.79	0.09	0.50	n.a	12.65	0.88	12.37	21.23	0.49	0.02	98.03	42.67	34.61	20.96	1.76
RC07-22 -p3	-	50.04	0.12	0.65	n.a	9.81	0.75	14.13	21.51	0.52	0.07	97.58	42.82	39.13	16.17	1.88
DM2-10-p1	-	49.41	0.08	1.12	0.00	10.93	1.70	12.05	21.38	0.51	0.03	97.21	43.78	34.33	19.98	1.90
DM2-10-p2	-	51.96	0.07	0.52	0.02	11.00	1.74	12.03	22.22	0.55	0.01	100.12	44.57	33.59	19.84	2.00
DM2-10-p3	-	51.99	0.12	0.64	0.00	11.35	1.81	11.90	21.53	0.58	0.01	99.93	43.61	33.53	20.73	2.14
DM2-10-p4	-	51.32	0.10	0.55	0.00	11.15	1.72	11.84	21.41	0.55	0.01	98.65	43.80	33.70	20.46	2.04
DM2-10-p5	-	50.79	0.13	0.66	0.01	11.55	1.68	11.44	21.53	0.62	0.01	98.43	44.08	32.60	21.02	2.31
DM2-10-p6	-	52.01	0.09	0.54	0.01	11.00	1.74	11.66	21.57	0.63	0.00	99.23	44.16	33.22	20.29	2.33
DM2-10-p7	-	51.73	0.09	0.52	0.00	11.09	1.69	12.24	21.22	0.61	0.00	99.18	43.05	34.56	20.14	2.25
DM2-10-p8	-	52.35	0.11	0.46	0.00	11.23	1.69	12.17	21.90	0.63	0.00	100.55	43.78	33.87	20.06	2.29
DM2-10-p9	-	49.61	0.19	0.97	0.02	12.60	1.91	11.65	20.76	0.79	0.01	98.49	41.86	32.69	22.56	2.89
DM2-10-p10	-	50.55	0.11	0.53	0.00	11.25	1.79	12.32	21.46	0.67	0.00	98.68	43.00	34.36	20.19	2.44
DM2-10-p11	-	51.51	0.11	0.45	0.01	11.09	1.86	11.98	21.42	0.65	0.00	99.07	43.44	33.80	20.39	2.37

Appendix D. Electron Microprobe Analyses of Clinopyroxene.

						Line Analyses										
Sample	Dist. μ	SiO_2	TiO_2	Al_2O_3	Cr_2O_3	FeO	MnO	MgO	CaO	Na_2O	K_2O	Total	Wo	En	Fs	Ac
RC07-20-p1	core	50.71	0.21	0.95	n.a	8.25	0.76	15.13	21.45	0.59	0.01	98.06	42.46	41.68	13.75	2.12
RC07-20-l1	0	50.88	0.14	0.68	n.a	9.69	0.80	14.15	21.46	0.50	0.01	98.31	42.78	39.24	16.16	1.82
RC07-20-l2	20	48.79	0.14	2.25	n.a	9.57	0.76	13.45	20.64	0.57	0.07	96.24	42.69	38.70	16.48	2.13
RC07-20-l3	40	50.43	0.22	0.97	n.a	8.78	0.78	14.74	21.35	0.60	0.01	97.87	42.43	40.77	14.64	2.15
RC07-20-l4	60	49.83	0.34	1.42	n.a	8.70	0.80	14.54	21.41	0.61	0.02	97.67	42.76	40.42	14.61	2.21
RC07-20-l5	80	49.97	0.21	1.07	n.a	8.34	0.71	14.86	21.41	0.62	0.05	97.24	42.67	41.21	13.88	2.23
RC07-20-l6	100	48.41	0.29	3.79	n.a	8.19	0.70	14.86	20.41	0.65	0.10	97.39	41.58	42.13	13.91	2.38
RC07-20-l7	160	48.67	0.23	1.27	n.a	7.99	0.69	14.40	21.14	0.60	0.11	95.09	43.21	40.94	13.64	2.20
RC07-20-l8	180	50.20	0.30	1.35	n.a	8.27	0.72	14.70	21.75	0.55	0.04	97.87	43.40	40.81	13.82	1.97
RC07-20-l9	200	50.46	0.32	1.18	n.a	8.36	0.68	14.85	21.76	0.58	0.02	98.21	43.14	40.96	13.81	2.10
RC07-20-l10	240	49.77	0.45	1.68	n.a	8.57	0.67	14.12	21.71	0.63	0.03	97.62	43.75	39.59	14.36	2.30
RC07-20-l11	340	50.42	0.24	1.03	n.a	8.37	0.76	14.90	21.64	0.54	0.05	97.96	42.94	41.14	13.97	1.95
RC07-20-l12	380	51.09	0.20	0.90	n.a	8.25	0.81	15.14	21.78	0.52	0.01	98.68	42.89	41.51	13.76	1.84
DM2-10-1p1	core	50.10	0.12	0.69	n.a	11.89	1.75	11.94	21.77	0.75	0.05	99.05	43.32	33.07	20.91	2.70
DM2-10-1p2	rim	50.40	0.11	0.54	n.a	10.88	1.66	12.77	22.38	0.62	0.01	99.37	43.94	34.88	18.96	2.22
DM2-10-1l1	20	50.06	0.10	0.82	n.a	10.93	1.61	12.41	21.98	0.64	0.01	98.56	43.89	34.47	19.31	2.33
DM2-10-1l2	80	50.96	0.13	0.63	n.a	11.37	1.72	12.67	22.31	0.70	0.01	100.50	43.50	34.39	19.66	2.46
DM2-10-1l3	100	50.79	0.08	0.56	n.a	10.90	1.67	12.86	22.29	0.65	0.00	99.81	43.66	35.05	18.99	2.30
DM2-10-1l4	140	50.76	0.15	0.58	n.a	11.47	1.72	12.59	22.09	0.69	0.00	100.05	43.29	34.34	19.92	2.45
DM2-10-1l5	160	50.47	0.09	0.59	n.a	11.07	1.63	12.60	22.42	0.62	0.01	99.51	44.08	34.46	19.24	2.21
DM2-10-1l6	180	50.72	0.13	0.52	n.a	11.22	1.67	12.72	22.31	0.62	0.01	99.93	43.69	34.67	19.46	2.18
DM2-10-1l7	200	49.76	0.18	1.61	n.a	11.87	1.88	11.77	21.11	0.67	0.02	98.86	42.80	33.20	21.53	2.47
DM2-10-1l8	240	49.51	0.16	1.11	n.a	12.44	1.85	11.75	21.42	0.78	0.01	99.03	42.69	32.58	21.90	2.83
DM2-10-1l9	260	50.10	0.18	0.82	n.a	12.28	1.86	11.97	21.91	0.74	0.03	99.89	43.13	32.81	21.41	2.65
DM2-10-1l10	280	50.23	0.17	0.75	n.a	12.14	1.88	11.68	21.57	0.73	0.01	99.15	43.17	32.53	21.66	2.64
DM2-10-1l11	320	50.51	0.16	0.63	n.a	11.77	1.83	11.73	22.13	0.67	0.02	99.45	44.12	32.55	20.93	2.40
DM2-10-1l12	340	50.36	0.14	0.72	n.a	12.34	1.87	11.48	21.86	0.76	0.06	99.59	43.57	31.85	21.85	2.73
DM2-10-1l13	300	50.34	0.16	0.75	n.a	11.92	1.84	11.68	21.83	0.75	0.01	99.28	43.60	32.47	21.20	2.72

Appendix D. Electron Microprobe Analyses of Clinopyroxene (continued).

		Line Analyses														
Sample	Dist. μ	SiO_2	TiO_2	Al_2O_3	Cr_2O_3	FeO	MnO	MgO	CaO	Na_2O	K_2O	Total	Wo	En	Fs	Ac
DM2-10-1I14	360	51.17	0.12	0.53	n.a	11.03	1.48	12.72	22.28	0.65	0.04	100.01	43.85	34.84	18.99	2.32
DM2-10-1I15	380	50.60	0.08	0.60	n.a	10.95	1.38	12.69	22.25	0.64	0.02	99.21	43.99	34.92	18.80	2.29
DM2-10-1I16	400	50.82	0.12	0.63	n.a	11.20	1.45	12.69	22.27	0.70	0.02	99.90	43.70	34.66	19.14	2.49
DM2-10-2L1	20	51.40	0.09	0.66	0.00	11.01	1.71	12.03	21.34	0.64	0.06	98.94	43.45	34.09	20.09	2.37
DM2-10-2L2	60	51.72	0.13	0.61	0.01	11.02	1.65	12.10	21.66	0.60	0.02	99.52	43.83	34.08	19.91	2.18
DM2-10-2L3	80	50.74	0.07	1.15	0.00	10.23	1.60	11.09	21.44	0.53	0.02	96.87	45.55	32.80	19.61	2.05
DM2-10-2L4	100	49.64	0.14	1.34	0.00	10.48	1.61	11.19	21.17	0.61	0.01	96.19	44.81	32.96	19.89	2.34
DM2-10-2L5	120	50.48	0.09	0.64	0.00	10.86	1.65	11.48	21.44	0.63	0.00	97.27	44.41	33.09	20.12	2.37
DM2-10-2L6	140	51.09	0.09	0.87	0.00	10.51	1.60	11.75	21.35	0.59	0.01	97.84	44.31	33.93	19.55	2.22
DM2-10-2L7	160	52.81	0.12	1.78	0.02	10.10	1.64	12.38	21.52	0.64	0.02	101.01	43.86	35.12	18.66	2.35
DM2-10-2L8	180	50.93	0.08	0.97	0.01	10.46	1.63	11.53	21.59	0.55	0.01	97.75	44.94	33.40	19.57	2.08
DM2-10-2L9	200	51.29	0.08	0.54	0.00	10.63	1.72	12.08	21.72	0.64	0.00	98.69	44.09	34.11	19.44	2.35
DM2-10-2L10	240	50.22	0.13	0.64	0.01	11.56	1.75	11.54	20.94	0.68	0.01	97.48	43.14	33.08	21.25	2.52
DM2-10-2L11	280	50.68	0.10	0.72	0.00	11.46	1.69	11.74	21.37	0.65	0.01	98.42	43.55	33.29	20.76	2.40
DM2-10-2L12	300	51.01	0.15	0.69	0.00	11.73	1.56	11.41	21.42	0.68	0.00	98.65	43.85	32.51	21.11	2.52
DM2-10-2L13	320	50.53	0.14	0.65	0.00	11.50	1.53	11.65	21.42	0.67	0.01	98.09	43.78	33.13	20.62	2.47
DM2-10-2L14	340	50.24	0.14	0.59	0.00	11.62	1.63	11.77	21.42	0.66	0.01	98.06	43.52	33.26	20.81	2.41
DM2-10-2L15	360	50.51	0.16	0.60	0.00	11.55	1.66	11.89	21.31	0.63	0.00	98.30	43.29	33.63	20.77	2.31
DM2-10-2L16	380	51.22	0.14	0.60	0.02	11.60	1.78	12.10	21.18	0.68	0.00	99.31	42.70	33.94	20.89	2.47
DM2-10-2L17	440	51.63	0.13	0.70	0.01	12.18	1.94	11.88	20.50	0.72	0.01	99.69	41.59	33.54	22.23	2.65
DM2-10-2L18	560	50.81	0.11	1.11	0.00	11.61	1.90	11.78	20.95	0.66	0.00	98.93	42.73	33.44	21.38	2.45
DM2-10-2L19	620	50.87	0.13	2.45	0.00	11.33	1.88	11.68	20.39	0.70	0.01	99.43	42.33	33.72	21.31	2.64
DM2-10-2L20	760	51.68	0.09	2.42	0.00	11.35	1.82	11.96	21.00	0.69	0.01	101.03	42.74	33.89	20.83	2.54
DM2-10-2L1	0	50.99	0.13	0.60	0.01	11.68	1.87	11.73	21.30	0.66	0.00	98.96	43.19	33.09	21.30	2.42
DM2-10-2L2	20	51.07	0.11	0.55	0.00	11.24	1.81	11.88	21.50	0.59	0.00	98.75	43.67	33.60	20.58	2.15
DM2-10-2L3	40	51.04	0.09	0.58	0.00	11.57	1.94	11.77	21.45	0.66	0.00	99.10	43.34	33.11	21.14	2.40
DM2-10-2L4	60	51.32	0.09	0.51	0.02	11.36	1.79	12.08	21.45	0.65	0.00	99.26	43.22	33.87	20.53	2.37
DM2-10-2L5	80	51.39	0.10	0.50	0.00	11.17	1.75	12.09	21.66	0.61	0.00	99.26	43.66	33.91	20.20	2.23

APPENDIX E

XRF/ICPMS ANALYSES

Appendix E. XRF major and trace element analyses.

Sample	DC01	DC03	DC08	DC12	RC02	RC03	RC07
SiO_2	76.68	73.69	78.86	77.79	70.77	71.02	69.67
TiO_2	0.10	0.30	0.11	0.06	0.32	0.31	0.35
Al_2O_3	12.55	13.81	10.86	10.27	13.56	13.32	13.59
FeO	1.06	1.64	1.03	0.88	1.63	1.77	1.82
MnO	0.04	0.01	0.01	0.01	0.04	0.04	0.05
MgO	0.01	0.12	0.00	0.05	0.25	0.27	0.34
CaO	0.26	1.12	0.15	0.22	0.76	0.82	1.06
Na_2O	4.05	3.45	3.57	2.66	2.73	3.08	3.42
K_2O	4.68	4.35	4.30	3.78	5.24	5.15	4.83
P_2O_5	0.02	0.04	0.02	0.02	0.02	0.05	0.08
LOI	0.69	1.34	0.53	1.73	4.27	3.70	4.31
Total	100.14	99.86	99.44	97.47	99.59	99.53	99.53
Ni	5.40	17.30	5.80	7.80	6.90	6.40	7.40
Cr	1.40	18.80	0.00	2.20	2.60	0.90	3.60
Sc	2.20	4.50	2.80	2.20	3.90	3.60	3.80
V	0.00	21.20	0.90	1.50	10.70	10.80	14.10
Ba	37.30	554.70	111.70	34.40	689.80	679.60	722.60
Rb	156.40	134.70	102.50	189.10	120.70	115.70	108.40
Sr	4.60	197.80	22.20	13.70	103.20	99.60	133.40
Zr	161.90	125.10	225.00	142.00	264.70	260.80	277.00
Y	31.80	15.30	31.00	49.50	23.90	26.50	26.70
Nb	48.50	31.70	44.00	82.70	31.60	31.20	29.80
Ga	21.60	17.00	21.10	21.40	19.00	19.60	21.00
Cu	0.20	4.40	0.10	1.60	2.60	1.40	2.50
Zn	41.00	25.20	50.60	38.50	51.90	48.40	55.00
Pb	23.80	19.20	15.70	13.90	27.20	22.50	22.30
La	38.90	38.60	51.90	35.20	51.20	55.70	58.70
Ce	78.10	60.80	79.00	69.00	96.20	103.20	101.20
Th	16.80	20.40	13.10	23.80	17.40	14.00	13.10
Nd	28.30	18.20	33.80	30.90	31.40	38.20	38.80

Major elements are unnormalized in wt.%. Total = the sum of major element analysis including LOI values. Trace elements in ppm.

Appendix E. XRF major and trace element analyses continued.

Sample	RC09	RC10	RC12	RC18	DM1-01	DM1-04	DM2-02
SiO_2	69.75	68.95	69.75	69.99	73.80	74.06	74.01
TiO_2	0.35	0.36	0.36	0.34	0.09	0.09	0.09
Al_2O_3	13.47	13.57	14.17	13.82	12.01	12.09	12.32
FeO	1.73	2.00	1.58	1.55	0.96	0.95	1.01
MnO	0.05	0.04	0.04	0.04	0.05	0.06	0.05
MgO	0.29	0.32	0.26	0.25	0.03	0.03	0.03
CaO	0.88	1.03	1.20	1.03	0.36	0.35	0.35
Na_2O	3.08	3.57	3.57	3.59	3.79	3.87	3.75
K_2O	5.10	4.84	5.08	4.96	4.73	4.54	4.73
P_2O_5	0.06	0.08	0.09	0.07	0.01	0.01	0.01
LOI	4.32	3.36	3.17	3.69	3.47	3.56	3.46
Total	99.09	98.12	99.25	99.32	99.30	99.62	99.81
Ni	6.90	6.70	7.10	7.60	4.90	7.20	6.00
Cr	2.40	3.50	2.10	1.30	1.20	1.80	1.50
Sc	4.20	3.60	4.20	3.40	3.20	2.40	2.10
V	13.30	14.00	16.00	14.40	0.00	0.10	0.00
Ba	730.60	736.80	789.40	708.80	25.20	52.80	60.40
Rb	118.40	106.60	107.50	109.70	154.30	151.40	155.10
Sr	126.10	129.60	167.90	144.80	3.50	4.70	4.30
Zr	281.00	289.30	291.00	279.80	154.30	156.30	162.60
Y	28.10	25.80	27.10	24.70	36.70	37.70	36.60
Nb	30.20	30.50	29.90	30.50	46.80	46.50	48.10
Ga	19.80	19.10	20.00	19.50	19.10	20.90	22.70
Cu	1.40	3.10	2.70	1.50	0.10	1.10	2.20
Zn	48.00	48.90	53.10	46.10	55.20	58.40	55.90
Pb	22.60	21.30	22.50	24.30	28.90	29.50	30.40
La	54.90	52.00	53.00	56.30	43.60	43.90	46.10
Ce	95.70	100.10	95.50	96.80	83.60	82.80	88.00
Th	14.50	13.10	13.00	13.80	18.80	18.00	18.10
Nd	40.00	40.60	37.30	35.70	32.90	31.20	31.60

Appendix E. XRF major and trace element analysis continued.

Sample	DM2-07	DM2-09	DM2-10	DM2-11	DM3-01	DM3-03	DM3-05
SiO_2	73.52	74.35	73.26	76.42	74.25	73.14	73.14
TiO_2	0.10	0.09	0.12	0.09	0.12	0.12	0.12
Al_2O_3	12.54	12.15	12.67	12.53	12.67	12.68	12.79
FeO	1.02	0.97	0.97	1.00	0.97	0.95	0.98
MnO	0.06	0.05	0.06	0.03	0.06	0.06	0.07
MgO	0.04	0.01	0.03	0.03	0.04	0.03	0.03
CaO	0.36	0.35	0.37	0.22	0.38	0.38	0.38
Na_2O	3.89	3.85	3.85	4.03	4.05	3.95	4.00
K_2O	4.51	4.70	4.78	4.61	4.81	4.84	4.77
P_2O_5	0.01	0.01	0.02	0.02	0.01	0.01	0.01
LOI	3.84	3.68	3.82	0.71	3.00	3.64	3.59
Total	99.88	100.21	99.95	99.69	100.36	99.81	99.88
Ni	7.20	6.20	6.90	4.80	5.80	6.90	7.30
Cr	1.80	1.90	1.30	0.20	1.00	2.00	1.10
Sc	2.10	2.20	1.80	2.70	2.00	2.50	3.10
V	1.80	0.00	2.00	2.00	0.80	0.00	0.90
Ba	60.10	26.40	78.60	36.00	28.70	61.10	66.00
Rb	151.70	155.20	141.00	160.30	144.20	140.40	140.80
Sr	5.10	4.30	5.50	5.80	4.20	6.00	5.80
Zr	159.70	156.50	182.20	153.90	182.70	180.10	184.50
Y	35.60	36.60	34.30	20.50	35.20	34.10	34.90
Nb	47.70	47.30	47.40	48.10	48.00	47.70	48.90
Ga	21.30	19.60	20.20	21.70	21.00	19.90	20.10
Cu	1.10	1.50	0.00	0.50	0.10	1.10	0.30
Zn	57.10	55.30	55.50	33.40	54.50	52.60	54.50
Pb	29.90	29.50	27.40	37.60	27.90	29.10	28.10
La	45.20	44.80	46.10	31.60	44.00	47.10	45.50
Ce	83.50	86.10	88.00	61.60	88.60	83.00	89.00
Th	21.40	18.90	19.00	17.70	18.70	19.90	17.90
Nd	30.30	32.10	31.00	20.00	33.40	29.80	30.20

Appendix E. XRF Major and Trace element instrumental precision

Unnormalized Major	CaO	Al_2O_3	TiO_2	FeO	MnO	CaO	MgO	K_2O	Na_2O	P_2O_5	Total
Element Results	68.45	15.35	0.667	3.86	0.038	2.02	1.1	5.56	2.91	0.287	100.24
wt. %	0.18	0.11	0.004	0.01	0.001	0.01	0.1	0.09	0.05	0.003	0.36

Normalized Major	CaO	Al_2O_3	TiO_2	FeO	MnO	CaO	MgO	K_2O	Na_2O	P_2O_5
Element Results	68.59	15.31	0.666	3.85	0.37	2.01	1.09	5.55	2.9	0.286
wt. %	0.09	0.07	0.004	0.01	0.001	0.01	0.1	0.07	0.05	0.002

Trace Element	Ni	Cr	Sc	V	Ba	Rb	Sr	Zr	Y	Nb	Ga
Results	16	16	4	54	1294	253	233	527	30	27.4	23
ppm	1	2	2	5	9	1	1	1	1	0.5	1
	Cu	Zn	Pb	La	Ce	Th					
	31	103	53	184	399	106					
	2	2	2	10	10	2					

Instrumental precision is based on Washington State University GSP-1standard measured over an 8 month period (Johnson et al., 1999).

Appendix E. ICP-MS trace element analyses.

Sample	DC-01	DC-03	DC-08	DC-12	RC-02	RC-03	RC-07
La	40.32	37.33	49.75	35.62	51.91	57.73	60.00
Ce	78.90	62.84	85.81	74.42	93.42	104.63	107.17
Pr	8.80	6.13	10.57	9.13	9.70	11.15	11.77
Nd	29.31	19.03	35.32	33.21	31.57	37.04	39.93
Sm	6.27	3.28	7.13	8.89	5.67	6.73	7.22
Eu	0.23	0.63	0.24	0.11	0.83	0.84	1.03
Gd	5.61	2.62	6.11	8.81	4.65	5.55	6.03
Tb	1.05	0.44	1.06	1.68	0.79	0.92	0.97
Dy	6.50	2.80	6.52	10.54	4.80	5.51	5.82
Ho	1.31	0.59	1.33	2.18	1.00	1.13	1.17
Er	3.77	1.74	3.76	5.97	2.83	3.08	3.19
Tm	0.58	0.29	0.56	0.89	0.43	0.47	0.47
Yb	3.79	2.05	3.63	5.63	2.85	3.08	3.10
Lu	0.58	0.33	0.57	0.85	0.46	0.49	0.49
Ba	40.00	563.00	113.00	33.00	700.00	691.00	746.00
Th	16.97	21.61	13.29	23.26	14.50	14.24	13.43
Nb	48.56	33.56	45.90	89.97	33.61	33.02	32.59
Y	35.26	17.23	34.47	58.23	26.28	29.08	30.10
Hf	6.24	4.06	6.93	6.66	7.12	7.01	7.46
Ta	3.54	3.39	3.16	7.04	2.68	2.52	2.48
U	4.47	6.61	3.10	7.89	3.72	3.65	3.55
Pb	21.95	19.70	14.18	13.66	25.20	22.08	20.83
Rb	148.00	131.10	99.80	187.60	118.20	112.20	107.60
Cs	3.24	2.95	7.58	2.34	4.28	3.49	3.31
Sr	7.00	189.00	22.00	14.00	101.00	96.00	131.00
Sc	1.60	4.90	1.90	1.00	3.60	3.60	4.20
Zr	153.00	120.00	218.00	144.00	252.00	248.00	275.00
W	321.00	217.10	887.00	999.40	218.40	315.60	580.10

Appendix E. ICP-MS trace element analyses continued.

Sample	RC-09	RC-10	RC-12	RC-18	DM1-01	DM1-04	DM2-02
La	59.56	58.07	56.47	56.99	46.20	46.81	46.18
Ce	106.00	107.26	102.68	103.63	89.89	89.68	93.78
Pr	11.93	11.68	11.24	11.10	9.82	9.96	9.86
Nd	41.46	39.62	38.22	36.83	33.18	33.77	33.06
Sm	7.94	7.27	6.97	6.69	6.99	7.14	7.14
Eu	1.11	1.00	1.12	1.01	0.20	0.21	0.19
Gd	6.62	5.93	5.90	5.51	6.38	6.57	6.29
Tb	1.11	0.96	0.95	0.88	1.20	1.22	1.19
Dy	6.58	5.68	5.66	5.31	7.53	7.62	7.51
Ho	1.28	1.13	1.16	1.07	1.53	1.57	1.52
Er	3.53	3.16	3.13	2.92	4.42	4.36	4.34
Tm	0.52	0.46	0.46	0.45	0.66	0.67	0.66
Yb	3.33	3.01	3.03	2.90	4.26	4.22	4.22
Lu	0.54	0.48	0.48	0.46	0.65	0.66	0.65
Ba	762.00	758.00	800.00	733.00	28.00	51.00	60.00
Th	13.47	13.14	12.34	13.27	17.13	17.19	18.16
Nb	33.10	32.76	31.28	32.67	48.98	47.60	51.03
Y	32.73	29.51	29.58	27.81	41.10	41.42	40.88
Hf	7.58	7.63	7.43	7.51	6.33	6.27	6.60
Ta	2.59	2.56	2.34	2.49	3.52	3.52	3.66
U	3.50	3.39	3.31	3.46	4.70	4.76	4.85
Pb	20.86	20.37	21.25	23.62	26.88	27.12	28.02
Rb	118.80	106.80	105.50	108.00	149.10	145.40	148.50
Cs	3.64	3.33	3.88	3.43	4.86	4.81	4.90
Sr	125.00	129.00	162.00	143.00	4.00	5.00	5.00
Sc	4.40	4.20	4.40	3.50	1.80	1.80	2.00
Zr	284.00	284.00	279.00	278.00	152.00	150.00	158.00
W	1032.10	1118.40	602.20	703.40	449.60	334.00	344.50

Appendix E. ICP-MS trace element analyses continued.

Sample	DM2-07	DM2-09	DM2-10	DM2-11	DM3-01	DM3-03	DM3-05
La	45.74	47.02	46.34	31.10	47.13	45.50	46.00
Ce	92.68	90.26	91.27	60.00	92.53	89.96	91.73
Pr	9.76	10.04	9.85	5.90	10.04	9.75	9.87
Nd	32.65	33.80	33.04	19.28	34.10	32.73	32.95
Sm	6.94	7.19	6.91	4.07	7.15	6.92	7.05
Eu	0.21	0.20	0.28	0.22	0.26	0.30	0.28
Gd	6.33	6.46	6.15	3.59	6.36	6.29	6.30
Tb	1.19	1.21	1.14	0.67	1.18	1.15	1.16
Dy	7.43	7.60	7.05	4.21	7.33	7.15	7.14
Ho	1.51	1.55	1.44	0.87	1.50	1.48	1.48
Er	4.30	4.39	4.01	2.49	4.17	4.13	4.08
Tm	0.65	0.66	0.62	0.38	0.64	0.63	0.62
Yb	4.13	4.25	3.92	2.59	4.07	4.00	3.98
Lu	0.64	0.65	0.61	0.39	0.63	0.61	0.61
Ba	60.00	28.00	83.00	37.00	31.00	56.00	64.00
Th	17.68	17.29	17.14	17.09	17.38	17.12	17.26
Nb	50.50	48.84	49.73	49.82	50.48	50.40	49.84
Y	40.77	41.47	38.65	22.54	39.37	39.11	39.14
Hf	6.56	6.34	6.71	6.29	6.85	6.69	6.91
Ta	3.63	3.51	3.47	3.59	3.50	3.49	3.47
U	4.71	4.75	4.45	4.23	4.57	4.51	4.49
Pb	28.61	27.36	26.66	35.89	26.89	26.88	26.84
Rb	146.20	148.80	135.40	150.70	138.10	135.60	135.20
Cs	4.87	4.80	4.36	3.76	4.49	4.38	4.37
Sr	6.00	4.00	7.00	6.00	5.00	6.00	6.00
Sc	2.00	1.90	2.10	1.80	2.20	2.20	2.20
Zr	158.00	154.00	178.00	146.00	179.00	178.00	179.00
W	324.30	320.90	343.50	370.70	320.40	320.10	291.80

Appendix E. ICP-MS trace element instrumental precision.

Element	La	Ce	Nd	Sm	Eu	Gd	Tb	Dy	Ho	Er	Tm	Yb	Lu
	0.98	1.24	0.96	0.3	0.08	0.16	0.02	0.2	0.04	0.12	0.02	0.06	0.02

Element	Ba	Th	Yb	Hf	Ta	U	Pb	Rb	Cs	Sr	Sc	Zr
	25.36	0.98	0.58	0.14	0.04	0.22	0.58	1.34	0.06	n.d.	n.d.	n.d.

The reproducibility (total of sample preparation plus instrumental precision) is based on Washinton State Univeristy Geoanalytical lab BCR-P standard in 12 separate runs between September 1994 and December 1994.

APPENDIX F

$^{238}U/^{206}PB$

ION MICROPROBE DATA

Appendix F. U-Pb ion microprobe results for zircons from Deer Canyon rhyolite.

Sample	Grain	Spot	Location	$^{206}Pb/^{238}U$	$^{206}Pb/^{238}U$ 1σ	$^{207}Pb/^{235}U$	$^{207}Pb/^{235}U$ 1σ	$^{207}Pb/^{206}Pb$	$^{207}Pb/^{206}Pb$ 1σ	% rad ^{206}Pb	Age (ka)	± (ka) 1σ
DC03	1	1	core	0.000851	0.000023	0.009164	0.000766	0.078	0.006	96	5345	156
DC03	1	2	rim	0.000858	0.000023	0.011340	0.000713	0.096	0.006	94	5259	153
DC03	2	1	rim	0.000870	0.000018	0.007248	0.000422	0.060	0.003	98	5579	118
DC03	3	1	rim	0.000871	0.000020	0.007231	0.000320	0.060	0.002	98	5590	131
DC03	4	1	core	0.000905	0.000020	0.007755	0.000518	0.062	0.004	98	5790	132
DC03	5	1	core	0.000779	0.000020	0.006741	0.000453	0.063	0.004	98	4981	134
DC03	6	1	rim	0.000804	0.000024	0.010130	0.000970	0.091	0.008	94	4952	164
DC03	7	1	rim	0.000960	0.000049	0.021560	0.003300	0.003	0.163	85	5343	371
DC03	8	1	core	0.000853	0.000032	0.012750	0.001630	0.108	0.012	92	5144	229
DC03	9	1	core	0.000808	0.000021	0.006766	0.000353	0.061	0.003	98	5196	142
DC03	10	1	core	0.000886	0.000026	0.007603	0.000471	0.062	0.003	98	5678	172
DC03	10	2	rim	0.000845	0.000024	0.010880	0.000835	0.093	0.007	94	5222	166
DC03	11	1	core	0.000816	0.000023	0.007445	0.000481	0.066	0.004	97	5227	156
DC03	12	1	core	0.000972	0.000024	0.023190	0.000868	0.173	0.006	84	5344	166
DC03	13	1	rim	0.000778	0.000022	0.009722	0.001190	0.091	0.010	94	4830	161
DC03	14	1	core	0.000876	0.000022	0.007004	0.000307	0.058	0.002	98	5636	143
DC03	15	1	core	0.000842	0.000027	0.007953	0.000435	0.069	0.003	97	5343	181
DC03	16	1	core	0.000760	0.000020	0.006180	0.000283	0.059	0.002	98	4896	133
DC03	17	1	core	0.000826	0.000028	0.007240	0.000490	0.064	0.004	98	5274	185
DC03	18	1	core	0.000771	0.000024	0.007720	0.000772	0.073	0.007	97	4880	163
DC03	19	1	rim	0.000803	0.000025	0.007440	0.000536	0.067	0.004	97	5119	166
DC03	20	1	core	0.000817	0.000033	0.009900	0.000840	0.088	0.008	95	5063	219
DC03	21	1	core	0.000918	0.000043	0.015900	0.001930	0.125	0.013	90	5401	304
DC03	22	1	rim	0.000932	0.000042	0.016900	0.002170	0.132	0.014	89	5426	300
DC03	23	1	core	0.000793	0.000024	0.007120	0.000471	0.065	0.004	98	5068	159
DC03	24	1	rim	0.000813	0.000023	0.006240	0.000318	0.056	0.002	99	5239	153
DC03	25	1	rim	0.000843	0.000025	0.006210	0.000278	0.053	0.002	99	5450	166

Appendix F. U-Pb ion microprobe results for zircons from Redondo Creek rhyolite.

Sample	Grain	Spot	Location	$^{206}Pb/^{238}U$	$^{206}Pb/^{238}U$ 1σ	$^{207}Pb/^{235}U$	$^{207}Pb/^{235}U$ 1σ	$^{207}Pb/^{206}Pb$	$^{207}Pb/^{206}Pb$ 1σ	% rad ^{206}Pb	Age (ka)	± Age (ka) 1σ
RC07	1	1	core	0.003682	0.000206	0.034080	0.001770	0.067	0.005	97	23165	1335
RC07	2	1	rim	0.000263	0.000017	0.010550	0.001640	0.292	0.033	69	1240	153
RC07	4	1	rim	0.000302	0.000020	0.016110	0.002580	0.386	0.045	56	1188	209
RC07	5	1	rim	0.000416	0.000038	0.022070	0.004170	0.385	0.049	57	1600	354
RC07	6	1	rim	0.000203	0.000006	0.002525	0.000216	0.090	0.007	89	1250	43
RC07	7	1	rim	0.000323	0.000024	0.014570	0.002370	0.328	0.038	64	1413	216
RC07	8	1	rim	0.000342	0.000041	0.020750	0.003800	0.440	0.066	50	1154	356
RC07	9	1	rim	0.000209	0.000008	0.003281	0.000446	0.114	0.015	91	1322	61
RC07	10	1	core	0.000249	0.000010	0.007034	0.000305	0.205	0.012	80	1363	70
RC07	11	1	core	0.000225	0.000006	0.005130	0.000226	0.165	0.007	85	1315	42
RC07	12	1	core	0.000348	0.000019	0.019850	0.001990	0.414	0.034	53	1248	174
RC07	14	1	rim	0.000339	0.000020	0.021680	0.001630	0.464	0.036	47	1094	170
RC07	17	1	core	0.000463	0.000017	0.031000	0.001450	0.485	0.015	44	1351	141
RC07	18	1	core	0.000318	0.000024	0.015600	0.002870	0.356	0.059	60	1324	241
RC07	19	1	core	0.000217	0.000008	0.004370	0.000452	0.146	0.012	87	1311	64
RC07	20	1	rim	0.000337	0.000030	0.017000	0.002500	0.365	0.035	59	1365	253
RC07	21	1	rim	0.000560	0.000026	0.049200	0.002510	0.637	0.026	24	965	239
RC07	22	1	core	0.000202	0.000008	0.003680	0.000333	0.132	0.011	89	1236	57
RC07	23	1	rim	0.000376	0.000035	0.023200	0.003340	0.447	0.037	49	1251	309
RC07	24	1	rim	0.000631	0.000043	0.047500	0.005230	0.546	0.038	36	1551	425

Appendix F. U-Pb ion microprobe standards.

Name	Blk Size	Rejections /Cycles	Age	Common Pb corr.	206Pb/ 204Pb	207Pb/ 204Pb	208Pb/ 204Pb
2006_09_09Sep\ as3@1.ais		0 [/12]	1099.1 Ma	(204Pb)	18.86	15.62	38.34
2006_09_09Sep\ as3@2.ais		0 [/12]	1099.1 Ma	(204Pb)	18.86	15.62	38.34
2006_09_09Sep\ as3@3.ais		0 [/12]	1099.1 Ma	(204Pb)	18.86	15.62	38.34
2006_09_09Sep\ as3@4.ais		0 [/12]	1099.1 Ma	(204Pb)	18.86	15.62	38.34
2006_09_09Sep\ as3@5.ais		0 [/12]	1099.1 Ma	(204Pb)	18.86	15.62	38.34
2006_09_09Sep\ as3@6.ais		0 [/12]	1099.1 Ma	(204Pb)	18.86	15.62	38.34
2006_09_09Sep\ as3@7.ais		0 [/12]	1099.1 Ma	(204Pb)	18.86	15.62	38.34
2006_09_09Sep\ as3@8.ais		0 [/12]	1099.1 Ma	(204Pb)	18.86	15.62	38.34
2006_09_09Sep\ as3@9.ais		0 [/12]	1099.1 Ma	(204Pb)	18.86	15.62	38.34
2006_09_09Sep\ as3@10.ais		0 [/12]	1099.1 Ma	(204Pb)	18.86	15.62	38.34
2006_09_09Sep\ as3@15.ais		0 [/12]	1099.1 Ma	(204Pb)	18.86	15.62	38.34
2006_09_09Sep\ as3@11.ais		0 [/12]	1099.1 Ma	(204Pb)	18.86	15.62	38.34
2006_09_09Sep\ as3@12.ais		0 [/12]	1099.1 Ma	(204Pb)	18.86	15.62	38.34
2006_09_09Sep\ as3@13.ais		0 [/12]	1099.1 Ma	(204Pb)	18.86	15.62	38.34
2006_09_09Sep\ as3@14.ais		0 [/12]	1099.1 Ma	(204Pb)	18.86	15.62	38.34

APPENDIX G

PARTITION COEFFICIENTS

Appendix G. Partition Coefficients for Rhyolite Petrogenetic Modeling

Element	Sanidine	Plagioclase	Biotite	Cpx	Opx	Zircon	Alianite	Magnetite	Apatite
Sc	0.04	0.17	15.50	131.00	22.00	68.65	55.85	8.81	0.00
Rb	0.48	0.25	4.20	0.00	0.01	0.00	0.19	0.04	0.00
Sr	4.00	11.80	7.20	0.00	0.17	0.00	1.80	0.09	2.00
Y	0.04	0.05	2.40	0.00	1.10	60.00	95.50	3.21	40.00
Zr	0.10	0.09	0.50	2.31	0.05	6400.00	0.29	0.62	0.10
Nb	0.09	0.14	9.10	0.00	0.31	50.00	1.70	2.50	0.10
Cs	0.01	0.05	2.30	0.00	0.00	0.00	0.00	0.00	0.00
Ba	4.70	13.50	5.37	0.00	0.90	0.00	0.00	0.00	2.00
La	0.06	0.10	3.18	17.60	14.40	16.90	2595.00	21.50	20.00
Ce	0.02	0.06	2.80	10.25	12.30	16.75	2279.00	17.85	35.00
Sm	0.01	0.01	1.55	10.36	7.87	14.40	867.00	8.14	63.00
Eu	4.04	4.75	0.87	7.47	2.85	16.00	111.00	4.05	30.00
Tb	0.01	0.02	1.05	5.50	5.50	37.00	273.00	4.75	20.00
Yb	0.00	0.02	0.61	7.08	2.70	641.00	33.00	1.40	25.00
Lu	0.03	0.02	0.61	7.08	2.70	641.00	33.00	1.40	25.00
Hf	0.02	0.04	0.60	1.51	0.00	3193.00	18.90	4.41	0.10
Ta	0.02	0.05	1.34	0.91	1.13	47.50	3.15	0.87	0.00
Th	0.00	0.03	1.23	2.34	6.53	76.00	538.00	7.36	2.00
U	0.02	0.15	0.17	0.58	0.28	0.00	14.30	0.85	0.00
Pb	0.75	0.7	2.1	0	0	0	0	0.8	0

Higuchi and Nagasawa (1969); Schnetzler and Philpotts (1970); Nagsawa and Schnetzler (1971); Arth (1976); Mahood and Hildreth (1983); Michael (1983); Nash and Crecraft (1985); Stix and Gorton (1990); Ewart snd Griffen (1994); Streck and Grunder (1997).

REFERENCES

Aldrich, M.J., Jr., 1986, Tectonics of the Jemez lineament in the Jemez Mountains and Rio Grande rift: Journal of Geophysical Research, v. 91, p. 1779-1798.

Allègre, C.J., Provost, A., and Jaupart, C., 1981, Oscillatory zoning: a pathological case of crystal growth: Nature, v. 294, p. 223-228.

Anderson, A.T., Jr, 1983, Oscillatory zoning of plagioclase: Normarski inference contrast microscopy of etched polished sections: American Mineralogist, v. 68, p. 125-129.

Arth, J. G., 1976, Behavior of trace elements during magmatic processes; a summary of theoretical models and the applications: Journal of Research of the U.S. Geological Survey, v. 4, p. 41-47.

Bailey, R.A., Smith, R.L., and Ross, C.S., 1969, Stratigraphic nomenclature of volcanic rocks in the Jemez Mountains, New Mexico: U.S. Geological Survey Bulletin 1274-P, p. 1-19.

Bachmann, O., and Bergantz, G., 2004, On the origin of crystal-poor rhyolites: Extracted from batholithic crystal mushes: Journal of Petrology, v. 45, p. 1565-1582.

Bachmann, O., Dungan, M.A., and Lipman P. W., 2002, The Fish Canyon magma body, San Juan volcanic field, Colorado: rejuvenation and eruption of an upper crustal batholith: Journal of Petrology, v. 43, p. 1469-1503.

Baldridge, W.S., Olsen, K.H., and Callender, J.F., 1984, Rio Grande rift: problems and perspectives: New Mexico Geologic Society 35th Field Conference Guidebook, p 1-12.

Baldridge, W.S., Bartov, Y., and Kron, A., 1983, Geologic map of the Rio Grande rift and southeast Colorado plateau, New Mexico and Arizona, *in*, Tectonics and Magmatism, ed., Riecker, R.E.: American Geophysical Union, Washinton, D.C..

Balsley, S. D., 1986, The Petrology and Geochemistry of the Tshirege member of the Bandelier Tuff, Jemez Mountains Volcanic Field, New Mexico, U. S. A., [Masters Thesis]: University of Texas at Arlington, 188 p.

Bindeman I.N., Schmitt, A.K., and Valley, J.W., 2006, U-Pb zircon geochronology of silicic tuffs from Timber Mountains/Oasis Valley caldera complex, Nevada; rapid generation of large volume magmas by shallow level remelting: Contributions to Mineralogy and Petrology, v. 152, p. 649-665.

Bindeman I.N., and Valley, J.W., 2001, Low-$\delta^{18}O$ rhyolites from Yellowstone: Magmatic evolution based on analyses of zircons and individual phenocrysts: Journal of Petrology, v. 42, p. 1491-1517.

Cashman, K., and Blundy, J., 2000, Degassing and crystallization of andesite and dacite: Philosophical Transactions of the Royal Society of London, v. 358, p. 1487-1513.

Clarkson, G., and Reiter, M., 1984, Analysis of terrestrial heat-flow profiles across the Rio Grande rift and southern Rocky Mountains in northern New Mexico: New Mexico Geologic Society 35th Field Conference Guidebook, p 39-44.

Cole, D.R., Larson P.B., Riciputi, L.R., and Mora C. I., 2004, Oxygen isotope zoning profiles in hydrothermally altered feldspars: estimating the duration of water-rock interaction: Geology, v. 32, p. 29-32.

Davies G.R. and Halliday A.N., 1998, Development of the Long Valley rhyolitic magma system: strontium and neodymium isotope evidence from glasses and individual phenocrysts - New insights from eruptive stratigraphy: Geochimica et Cosmochimica Acta, v. 62, p. 3561-3574.

Davies G.R., and Stolz, A. J., 1989, Metasomatised lower crustal and upper mantle xenoliths from north Queensland: Chemical and isotopic evidence bearing on the composition and source of the fluid phase: Geochimica et Cosmochimica Acta, v. 53, p. 649-660.

Doell, R.R., Dalrymple, G.B., Smith, R.L., and Bailey, R.A., 1968, Paleomagnetism, potassium-argon ages, and geology of rhyolites and associated rocks of the Valles Caldera, New Mexico: *in* Coats, R.R., Hay, R.L., and Anderson, C.A., eds., Studies in Volcanology: Geological Society of America Memoir 116, p. 211-248.

Eichelberg, J. C., 1980, Vesiculation of mafic magmas during replenishment of silicic magma reservoirs: Nature, v. 288, p. 446-450.

Ewart, A. and Griffin, W.L., 1994, Application of Proton-Microprobe Data to Trace-Element Partitioning in Volcanic-Rocks: Chemical Geology, v. 117, p. 251-284.

Gardner, J.N., Goff, F., Garcia, S., and Hagan, R.C., 1986, Stratigraphic relations and lithologic variations in the Jemez Volcanic Field, New Mexico: Journal of Geophysical Research, v. 91, p. 1763-1778.

Gardner, J.N., 1985, Tectonic and petrologic evolution of the Keres Group: Implications for the development of the Jemez volcanic field, New Mexico [PhD Dissertation]: University of California, Davis, 292 p.

Gardner, J.N., and Goff, F., 1984, Potassium-argon dates from the Jemez volcanic field: Implications for tectonic activity in the north-central Rio Grande rift: New Mexico Geologic Society, Guidebook 35, p. 75-81.

Ginibre, C., Wörner, G., and Kronz, A., 2004, Structure and dynamics of the Laacher See magma chamber (Eifel Germany) from major and trace element zoning in sanidine: a cathodoluminescence and electron microprobe study: Journal of Petrology, v. 45, p 2197-2223.

Ginibre, C., Wörner, G., and Kronz, A., 2002, Minor and trace element zoning in plagioclase: implications for magma chamber processes at Parinacota volcano, northern Chile: Contributions to Mineralogy and Petrology, v. 143, p. 300-315.

Griggs, R.L., 1964, Geology and ground-water resources of the Los Alamos area, New Mexico: U.S. Geological Survey, Water-Supply Paper 1753, 104 p.

Halliday, A. N., 1990, Reply to comments of R. S. J. Sparks, H. E. Huppert, and C. J. N. Wilson on "Evidence for long residence times of rhyolitic magma in Long Valley magmatic system: the isotopic record in precaldera lavas of Glass Mountain": Earth and Planetary Science Letters, v. 99, p. 390-394.

Halliday, A. N, Mahood, G. A., Holden, P., Metz, J. M., Dempster, T. J., and Davidson, J. P., 1989, Evidence for long residence times of rhyolitic magma in the Long Valley magmatic system: the isotopic record in precaldera lavas of Glass Mountain: Earth and Planetary Science Letters, v. 94, p. 274-290.

Hasse, C. S., Chadam, J., Feinn, D. and Ortoleva, P. 1980, Oscillatory zoning in plagioclase feldspar: Science, v. 209, p. 272-274.

Hibbard, M.J., 1981, The magma mixing origin of mantled feldspars: Contributions to Mineralogy and Petrology, v. 76, p. 158-170.

Higuchi, H., and Nagasawa, H., 1969, Partition of trace elements between rock-forming minerals and their host volcanic rocks: Earth and Planetary Science Letters, v. 7, p. 281-287.

Hildreth W., and Wilson C., 2007, Compositional zoning of the Bishop Tuff: Journal of Petrology, v. 48, p. 951-999.

Hildreth, W., 1981, Gradients in silicic magma chambers: Implications for lithospheric magmatism: Journal of Geophysical Research, v. 86, p 10152-10192.

Huppert, and Sparks, 1988, The generation of granitic magmas by intrusion of basalt into continental crust: Journal of Petrology, v. 29, p. 599-624.

Johnson, D. M., Hooper, P.R., and Conrey R.M., 1999, XRF Analysis of rocks and minerals for major and trace elements on a single low dilution Li-tetraborate fused bead, JCPDS-International Center for Diffraction Data, p. 843-867.

Justet L., 2003, Effects of basalt intrusion on the multi-phase evolution of the Jemez volcanic field, NM, [PhD Dissertation], University of Nevada Las Vegas, 165 p.

Justet, L., and Spell T.L., 2001, Effusive eruptions form a large silicic magma chamber: the Bearhead Rhyolite, Jemez volcanic field, NM: Journal of Volcanology and Geothermal Research, v. 107, p 241-264.

Justet, L., 1999, The Geochronolgy and Geochemistry of the Bearhead rhyolite, Jemez Volcanic Field, New Mexico [Masters Thesis]: University of Nevada, Las Vegas, 152 p.

Knesel, K. M., Davidson, J. P., and Duffield, W. A., 1999, Evolution of silicic magma through assimilation and subsequent recharge: evidence from Sr isotopes in sanidine phenocrysts, Taylor Creek Rhyolite, NM: Journal of Petrology, v. 40, p. 773-786.

Knaack, C., Cornelius, S., and Hooper P., 1994, Trace element analysis of rocks and minerals by ICP-MS, GeoAnalytical Lab, Washington State University, (http://www.wsu.edu/~geolab/).

Koyaguchi, T., 1986, Textural and compositional evidence for magma mixing and its mechanism, Abu volcano group, Southwestern Japan: Contributions to Mineralogy and Petrology, v. 93, p. 33-45.

Lasaga, A.C., 1982, Toward a master equation in crystal growth: American Journal of Science, v. 282, p. 1264-1288.

Le Bas, M.J., Le Maitre, R. W., Streckeisen, A., and Zanettin, B.A., 1986, Chemical classification of volcanic rocks based on total alkali-silica diagram: Journal of Petrology, v. 27, p. 745-750.

L'Heureux, I., and Fowler, A. D., 1994, A nonlinear dynamic model of oscillatory zoning in plagioclase: American Mineralogist, v. 79, p. 885-891.

Lipman P.W., 2000, Calderas, In: Sigurdsson, H., (Ed.), Encyclopedia of Volcanoes, Academic Press, San Francisco, p. 643-662.

Lofgren, G. E., and Gooley, R., 1977, Simultaneous crystallization of feldspar intergrowths from the melt: American Journal of Science, v. 274, p. 243-273.

Lofgren, G. E., 1974, An experimental study of plagioclase crystal morphology; isothermal crystallization: American Journal of Science, v. 274, p. 243-273.

Loomis, T. P., 1982, Numerical simulations of crystallization processes of plagioclase in complex melts: the origin of major and oscillatory zoning in plagioclase: Contributions to Mineralogy and Petrology, v. 81, p. 219-229.

Mahood, G., 1990, Second reply to comment of Sparks, R. S. J., Huppert, H. E. and Wilson C. J. N., 1990, on 'Evidence for long residence times of rhyolitic magma in the Long Valley magmatic system: the isotopic record in precaldera lavas of Glass Mountain' by Halliday, A. N., Mahood, G. A., Holden, P., Metz, J. M., Dempster, T. J. & Davidson, J. P.: Earth and Planetary Science Letters, v. 99, p. 395-399.

Mahood, G., and Hildreth, W., 1983, Large Partition coefficients for trace elements in high-silica rhyolites: Geochimica et Cosmochimica Acta, v. 47, p. 11-30.

Michael, P.J., 1983, Chemical differentiation of the Bishop Tuff and other high-silica magmas through crystallization processes; Geology, v. 11, p. 31-34.

Morgan, P., and Golombeck, M.P, 1984, Factors controlling the phases and styles of extension in the northern Rio Grande rift: New Mexico Geologic Society 35th Field Conference Guidebook, p 13-19.

Miller, J.S., and Wooden J.L., 2004, Residence, resorption and recycling of zircons in Devils Kitchen rhyolite, Coso Volcanic filed, California: Journal of Petrology, v. 45, p. 2155 -2170.

Nash, W.P., and Crecraft, H.R., 1985, Partition coefficients for trace elements in silicic magmas: Geochimica et Cosmochimica Acta, v. 49, p. 2,309-2,322.

Nagawasa, H., and Schnetzler, C.C., 1971, Partitioning of rare earth, alkali and alkaline earth elements between phenocrysts and acidic igneous magma: Geochimica et Cosmochimica Acta, v. 35, p. 953-968.

Nekvasil, H., 1991, Ascent of felsic magma and formation of rapakivi: American Mineralogist, v. 76, p 1279-1290.

Nielson, D.L., and Hulen, J.B., 1984, Internal geology and evolution of the Redondo dome, Valles caldera, New Mexico, Journal of Geophysical Research, v. 89, p. 8695-8713.

Nixon, G. T., and Pearce, T. H., 1987, Laser-interferometry study of oscillatory zoning in plagioclase: the record of magma mixing and phenocryst recycling in calc-alkaline magma chamber, Iztlacíhuatl volcano, Mexico: American Mineralogist, v. 72, p. 1144-1162.

Paces, J.B., and Miller, J.D., 1993, Precise U-Pb ages of Duluth Complex and related mafic intrusions, Northeastern Minnesota: Geochronological insights to physical petrogenetic, paleomagnetic, and tectonomagnetic processes associated with the 1.1 Ga midcontinent rift system: Journal of Geophysical Research, v. 98, p. 13,997-14,013.

Pearce T.H., 1993, Recent work on oscillatory zoning in plagioclase. In: Parsons, I., (ed.) Feldspars and their reactions. Dordecht: Kluwer Academic, p. 313-349.

Pearce, T.H. and Kolisnik, A. M., 1990, Observations of plagioclase zoning using interference imaging: Earth-Science Reviews, no. 29, p. 9-26.

Pearce, T.H. and Clark, A. H., 1989, Nomarski interference contrast observations of textural details in volcanic rocks: Geology, v. 17, p. 757-759.

Pearce T. H., 1987, The theory of zoning patterns in magmatic minerals using olivine as an example: Contributions to Mineralogy and Petrology, no. 97, p. 451-459.

Phillips, E., 2004, Collapse and resurgence of the Valles caldera, Jemez Mountains, New Mexico: $^{40}Ar/^{39}Ar$ age constraints on the timing and duration of resurgence and ages of megabreccia blocks, [Masters Thesis], New Mexico Institute of Mining and Technology, 214 p.

Preston, 2002, Mineral chemistry spreadsheets for electron probe analyses: http://www.abdn.ac.uk/geology/profiles/analysis/software.htm: University of Aberdeen Department of Geology and Petroleum Geology.

Reid M.R., 2003, New ages for young rhyolites. Mono craters, California: Ion Microprobing into the Holocene: Geological Society of America Abstracts with Programs, v. 35, p. 183.

Reid, M.R., and Coath, C.D., 2000, In situ U-Pb ages of zircons from the Bishop Tuff: No evidence for long crystal residence times: Geology, v. 28, p. 443-446.

Reid M.R., Coath C.D., Harrison T.M., and McKeegan K.D., 1997, Prolonged residence times for the youngest rhyolites associated with Long Valley Caldera: ^{230}Th-^{238}U ion microprobe dating of young zircons Earth and Planetary Science Letters, v. 150, p. 27-39.

Reneau, S. L., Gardner, J. N., and Forman, S. L., 1996, New evidence for the age of the youngest eruptions in the Valles caldera, New Mexico, Geology, v. 24, p. 7-10

Schmitz, M.D., Bowring, S.A., and Ireland, T.R., 2003, Evaluation of Duluth Complex anothositic series (AS3) zircon as a U-Pb geochronological standard: New high-precision isotope dilution thermal ionization mass spectrometry results: Geochimica et Cosmochimica Acta, v. 67, p 3665-3672.

Schmitt, A.K., Lindsay, J.M., de Silva, S., and Trumbull, R. B., 2002, U-Pb zircon chronstratigraphy of early-Pliocene ignimbrites from La Pacana, north Chile: implications for the formation of stratified magma chambers: Journal of Volcanology and Geothermal Research, no. 120, p. 43-53.

Schnetzler, C.C., and Philpotts, J. A., 1970, Partition coefficients or rare-earth elements between igneous matrix and rock-forming mineral phenocrysts; II: Geochimica et Cosmochimica Acta, v. 34, p. 331-340.

Shaw C.A, and Karlstrom K. E., 1999, The Yavapai-Mazatzal crustal boundary in the Southern Rocky Mountains: Rocky Mountain Geology, v. 34, p. 37-52.

Simon J.I., and Reid, M.R., 2005, The pace of rhyolite differentiation and storage in an 'archetypical' silicic magma system, Long Valley, California: Earth and Planetary Science Letters, v. 235, p. 123-140.

Singer, B.S., Dungan, M.A. and Layne, G.D, 1995, Textures and Sr, Ba, Mg, Fe, K, and Ti compositional profiles in volcanic plagioclase: clues to the dynamics of calc-alkaline magmas chambers: American Mineralogist, v. 80, p. 776-798.

Sisson, T. W., and Bacon, C. R., 1999, Gas driven filter-pressing in magmas: Geology, v. 27, p. 613-616.

Smith R.L., and Bailey, R.A., 1979, Ash flow magmatism; Geologic Society of America Special Paper, v. 180, p. 5-27.

Smith, R.L., Bailey, R.A., and Ross, C.S., 1970 Geologic map of the Jemez Mountains New Mexico, Scale 1:25:000, U.S. Geological Survey , Misc Invest Map 1-571.

Smith R.L., and Bailey, R.A., 1968, Resurgent cauldrons, Geologic Society of America Memoir, no.116, p. 613-662.

Smith R.L., and Bailey, R.A., 1966, The Bandelier Tuff: a study of ash-flow eruption cycles from zoned magma chambers: Bulletin of Volcanology, v. 29, p. 83-103.

Smith R.L., Bailey, R.A., and Ross, C.S., 1961, Structural evolution of the Valles caldera, New Mexico, and its bearing on emplacement of ring dikes, U.S. Geological Survey Professional Paper 424-D, p. 145-149.

Smith, H.T.U, 1938, Tertiary geology of the Abiquiu quadrangle, New Mexico, Journal of Geology, v. 46, p. 933-965.

Sparks. R. S., Huppert, H. E., and Wilson C. J., 1990, Comment on "Evidence for long residence times of rhyolitic magma in the Long Valley magmatic system: the isotopic record in precaldera lavas of Glass Mountain" by A. N. Halliday, G. A. Mahood, P.

Holden, J. M Metz, T. J. Dempster, J. P. Davidson: Earth and Planetary Science Letters, v. 99, p. 387-389.

Spell T. L., Kyle, P.R., and Baker, J., 1996, Geochronology and geochemistry of the Cerro Toledo Rhyolite: New Mexico Geologic Society Guidebook, 47th Field Conference, p. 263-269.

Spell, T.L., Kyle, P.R., Thirlwall, M.F., and Campbell, A.R., 1993, Isotopic and geochemical constraints on the origin and evolution of postcollapse rhyolites in the Valles caldera, New Mexico, Journal of Geophysical Research, v. 98, p 19,723-19,739.

Spell, T. L. and Harrison, T.M., 1993, $^{40}Ar/^{39}Ar$ geochronology of post-Valles caldera rhyolites, Jemez Mountains volcanic field, New Mexico, Journal of Geophysical Research, v. 98, p. 8031-8051.

Spell, T.L., 1987, Geochemistry of the Valle Grande Member ring fracture rhyolites, Valles Caldera, New Mexico, [Masters Thesis]: N.M. Institute of Mining and Technology, Soccoro, 213 p.

Stix, J. and Gorton, M.P., 1990, Variations in trace element partition coefficients in sanidine in the Cerro Toledo Rhyolite, Jemez Mountains, New Mexico; effects of composition, temperature , and volatiles: Geochimica et Cosmochimica Acta, v. 54, p. 2,697-2,708.

Streck, M.J. and Grunder, A.L., 1997, Compositional gradients and gaps in high-silica rhyolites of the Rattlesnake Tuff, Oregon: Journal of Petrology , v. 38, p.133-163.

Tepley, F. J., III, Davidson, J. P., and Clyne, M. A., 1999, Magmatic interactions as recorded in plagioclase phenocrysts of Chaos Crags, Lassen Volcanic Center, California: Journal of Petrology, v. 40, p. 787-806.

Troll V. R., and Schminke, H. U., 2002, Magma Mixing and Crustal Recycling Recorded in Ternary Feldspar from Compositionally Zoned Peralkaline Ignimbrite 'A', Gran Canaria, Canary Islands: Journal of Petrology, v. 43, p. 243-270.

Tsuchiyama, A., 1985, Dissolution kinetics of plagioclase in the melt of the system diopside-albite-anorthite, and origin of dusty plagioclase in andesites: Contributions to Mineralogy and Petrology, v. 89, p. 1-16.

Vogel, T.A., Schuraytz, B. C., Eichelberger, J. C., Stockman, H.W., Westrich, H. R., Younker, L. W., and Horkowitz, J., P., 1989, Petrology and emplacement dynamics of intrusive and extrusive rhyolites of Obsidian Dome, Inyo Craters volcanic chain, Eastern California: Journal Geophysical Research, v. 94, p. 17,937-17,956.

Wallace, P.J., 2002, Volcanic SiO_2 emissions and the abundance and distribution of exsolved gas in magma bodies: Journal of Volcanology and Geothermal Research, v. 108, p. 85-106.

Wallace P.J., and Anderson A.T., 1999, Volatiles in Magmas. In: H. Sigurdsson et al. (Editors) Encyclopedia of Volcanoes, Academic Press, pp. 149-170.

Wallace, P.J., Anderson, A. T., and Davies, A. M., 1995, Quantification of pre-eruptive exsolved gas contents in silicic magmas: Nature, v. 377, p. 612-615.

Watson, B.E., and Harrison, M.T., 1983, Zircon saturation revisited; Temperature and composition effects in a variety of crustal magma types: Earth and Planetary Science Letters, v. 64, p. 295-304.

Wendt , I., and Carl, C., 1985, U/Pb dating of discordant 0.1Ma secondary U minerals: Earth and Planetary Science Letters, v. 73, p. 278-284.

Wolff, J. A., Rowe, M. C., Teasdale, R., Gardner, J. N., Ramos, F. C., and Heikoop, C. E., 2004, Petrogenesis of Pre-caldera Mafic Lavas, Jemez Mountains Volcanic Field (New Mexico, USA): Journal of Petrology, v. 46, p. 407-439.

Wolff, J. A., Balsley, S.D., and Gregory, R.T., 2001, Oxygen isotope disequilibrium between quartz and sanidine from the Bandelier Tuff, New Mexico, consistent with a short residence time of phenocrysts in rhyolitic magma: Journal of Volcanology and geothermal Research, v. 116, p 119-135.

Wolff, J. A, Ramos F. C., and Davidson, J. P., 1999, Sr isotope disequilibrium during differentiation of the Bandelier Tuff, New Mexico; Constraints on the crystallization of a large rhyolite magma chamber: Geology, v. 27, p. 495-498.

VITA

Graduate College
University of Nevada, Las Vegas

Kati I Gibler

Home Address:
824 Colina Alta Place
Las Vegas, Nevada 89138

Degrees:
Bachelor of Science, Natural Sciences, 2004
University of Alaska, Anchorage

Publications:

Naumann, Terry R., Gibler, Katherine, and Nelson Lisa K, (2003). Geology of Volcán Darwin, Isabela Island, Galápagos Archipelago. Geological Society of America, Abstracts with Programs 35, 324.

Special Honors and Awards:
GPSA Graduate student Grant, 2005
UNLV Lilly Fong Geoscience Department Scholarship 2005
Chugach Gem and Mineral Society Scholarship 2003, 2004
Phi Kappa Phi, 2003
National Honor Society Scholarship, 2002,
Deans list for Academic Honors, 2000, 2003
National Honor Society 2000-2007

Thesis Title: Postcollapse volcanism in the Valles Caldera, New Mexico: The Transition from Large Volume Explosive to Small Volume Effusive Eruptions

Thesis Examination Committee:
Chairperson, Dr. Andrew Hanson, Ph.D.
Committee Member, Dr. Rodney Metcalf, Ph.D.
Committee Member, Dr. Eugene Smith, Ph.D.
Graduate Faculty Representative, Dr. Stephan Lepp, Ph.D.